# DISSIPATIVITY AND PERFORMANCE ANALYSIS OF SEMIACTIVE SYSTEMS WITH SMART DAMPERS

by

Baris Erkus

---

A Dissertation Presented to the
FACULTY OF THE GRADUATE SCHOOL
UNIVERSITY OF SOUTHERN CALIFORNIA
In Partial Fulfillment of the
Requirements for the Degree
DOCTOR OF PHILOSOPHY
(CIVIL ENGINEERING)

May 2006

# SIGNATURE

# DEDICATION

Everything has reshaped when G found the *g*.

This work is dedicated to G.

# ACKNOWLEDGEMENTS

The author gratefully acknowledges the partial support of this research by the National Science Foundation under CAREER grant CMS 00-94030, and by the U. S. Department of Transportation through grant 03-17 from the National Center for Metropolitan Transportation Research.

I would like to thank Professor Erik A. Johnson for his continuous support and patience during this lengthy and complicated research. I also express my appreciation to my doctoral committee members Professor Sami F. Masri, Professor Robert Nigbor, Professor Edmund Jonckheere and Professor L. Carter Wellford for their guidance. I also would like to thank Professor Michael Safonov for his help and comments. I want to express my great respect to my former supervisors Professor Polat Gulkan, Professor Masato Abe and Professor Yozo Fujino. They have always been great mentors for me. Finally, I want to thank to my family and my girlfriend Ann for their continuous support and understanding during this study.

# TABLE OF CONTENTS

# LIST OF TABLES

# LIST OF FIGURES

# ABSTRACT

This research investigates the dissipativity and performance of semiactive systems with smart dampers. It is known that the dissipative nature of smart dampers has an important effect on the performance of semiactive systems; yet, frequently applied semiactive control strategies do not consider dissipativity in the design. To exploit the effects of dissipativity on the semiactive performance, two dissipativity indices are proposed and, then, used in the analysis and control design of structures with smart dampers. Two representative cases are considered: simple two-degree-of-freedom systems and more complex, realistic structures that can be encountered in a practical structural control problem.

For the 2-DOF structures, a dissipativity index is utilized to modify a standard linear quadratic regulator using linear matrix inequality techniques to achieve better semiactive performance. The first example is a shear building with an ideal damper attached in the first story. It is shown that the proposed control theory can be used not only to identify controllers that are suitable for a smart damper but also to improve the control force dissipativity and, thereby, the performance of the semiactive structure. In the second example, a highway bridge with a realistic magnetorheological damper model is analyzed; it is shown that smart dampers may further reduce the dissipativity of the primary controllers that already had low dissipativity levels, resulting in poor semiactive performance.

A recently-introduced three-dimensional base isolated benchmark building is used to investigate the benefits of a dissipativity analysis for a real-life problem. First, dissipativity performance-relations for the benchmark structure with a linear isolation layer are examined. A dissipativity analysis shows useful information about which controllers are more suitable for

semiactive application. In another example, an equivalent linearization technique is applied to implement a linear control strategy for the nonlinear structure, and a dissipativity analysis is shown to be an essential tool for faster solutions to this sophisticated problem, where a conventional semiactive design may be very impractical, time consuming and computationally intensive. In summary, a computationaly inexpensive dissipativity analysis as proposed herein can provide significant savings of time and computational resources in the semiactive control design process.

# CHAPTER 1

# INTRODUCTION

In the process of designing a civil structure, a structural engineer must address various safety and serviceability issues. In general, a structure should be safe enough to survive "most expected loads" that it will face during its lifetime. Moreover, it should be serviceable, *i.e.*, should perform satisfactorily so that it will not cause discomfort to the users of the structure. For example, consider a 100-story high-rise building: The structure must not fail under "most expected" loads including loads due to natural events such as earthquakes and wind and/or man-made loads such as heavy equipment used in the structure. Furthermore, it should be designed so that the vibration of the structure is small enough to not cause any discomfort to the occupants. In fact, if this structure is designed only for safety, it may not be serviceable; *i.e.*, although the structure will not fail, the magnitude of the vibration due to the everyday wind may be very large for an occupant, making the person feel unsafe.

In practical structural engineering, a standard design for safety and serviceability makes use of structural codes. Structural codes identify the external loads on a structure, provide methods to estimate the magnitudes of these loads and resistance of the structure against these loads. Using these well-defined procedures, a structural engineer estimates the loads that each structural member will be resisting and selects a proper dimension and characteristics for each member (Figure 1.1). The methods provided in structural codes are products of extensive research and statistical studies of decades and lessons learned from past structural failures. For example, the fundamental design philosophy of the codes used before 1960s were very different than their current versions in use. During the late 1960s and 1970s, various natural disasters occurred in the world that

caused extensive human casualties and economic damage, including earthquakes in San Fernando, California, in 1971, Managua, Nicaragua, in 1972, Miyagi-ken-oki, Japan, in 1978, the roof failure of the Hartford Civic Arena in Hartford, Connecticut, due to extreme snow load in 1978, Hurricane Camille on the Gulf Coast in 1969 and Hurricane Cyclone Tracy that devastated Darwin, Australia, in 1974. Due to these and other major disasters, the structural engineering community had to reevaluate the design procedures and philosophy of the design codes.

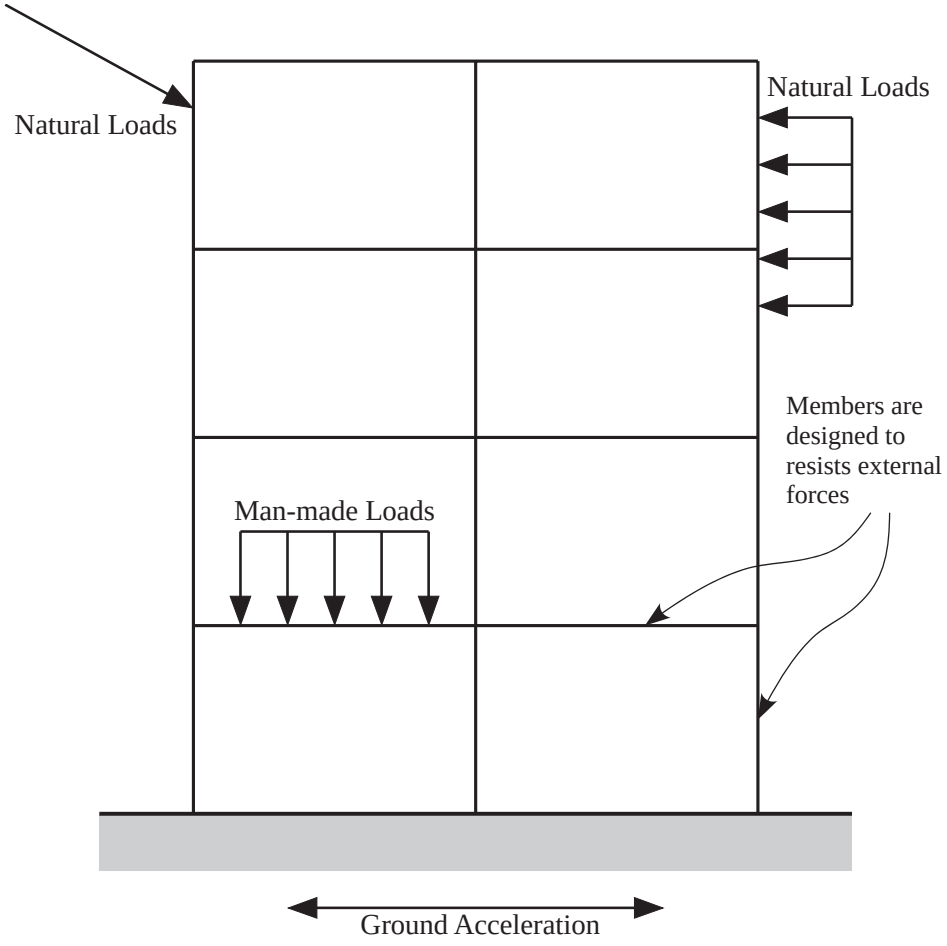


**Figure 1.1** A schematic representation of a conventional structure and its design

Another interesting side effect of the natural disasters mentioned above — especially earthquakes — was the investigation of new innovative structural design approaches to improve the safety of structures under extreme natural loads. Most of these ideas were already known in the conceptual sense, yet they had not yet been investigated and implemented scientifically and practically. One of the ideas for earthquake resistant design was to dissipate the energy, which is input by the earthquake, through special devices installed throughout the structure (Kelly *et al*. 1972). In a conventional design, energy is dissipated by the structural members. Installation of energy dissipation devices would reduce structural damage and improve the safety of the overall structure. Another idea proposed the concept of feedback control, where the structural responses are measured by sensors and fed into a computer that controls some type of actuators or similar devices placed throughout the structure (Yao 1972). Control of these devices is based on a control law and aims to modify the structural responses to address not only the safety but also serviceability issues. During the past three decades, these ideas have been shaped by extensive research, and various practical applications have been implemented. The study of these innovative approaches is now known to be structural control.

## 1.1 Structural Control

The main goal of structural control applications is to achieve safety and serviceability goals, which cannot be achieved by conventional structural design methods enforced by structural codes, by modifying structural characteristics or responses using innovative noncontrollable or controllable members or devices. Usually, the problems that structural control addresses are structural vibration problems. These can be special vibration issues that appear in the dynamic design of complex civil infrastructures such as wind induced vibration of high-rise buildings and vibration of long span bridges due to human walking. They can also be seismic performance

related issues of structures critical in economic and disaster management such as hospitals, schools and highway bridges.

In general, control strategies are classified into three main categories: active, passive and semiactive. A fourth category is hybrid control where two or more strategies are used in the same structure. Each control strategy and technology has its own advantages and disadvantages that are mostly determined by the nature of the problem, the complexity of the structure and the mechanical and economic properties of the technology used. In the following, a review of these strategies is given.

### 1.1.1 Active Control

In active control, externally powered devices such as hydraulic actuators or active tuned mass dampers apply forces to the structure to modify the motion of the structure. The forces that the devices apply are determined by a control law, which is generally the solution to a complex mathematical optimization problem. The sensors on the structure feed back the responses for the control law to estimate the optimal control force. A representation of an actively controlled structure is shown in Figure 1.2, and its feedback control diagram is shown in Figure 1.3. Active control has been mostly applied to mitigate wind-induced vibrations of high-rise buildings. One example is the Yokohama Landmark Tower in Japan, which is shown in Figure 1.4. Also, wind-induced vibration of large-size bridges during erection and service have been mitigated by active control technologies. There are several state-of-the-art papers that review these applications (Housner *et al*. 1997, Spencer and Sain 1997; Nishitani and Inoue 2001; Spencer and Nagarajaiah 2003).

The efficiency of an active system is related to the fact that an active device can apply a force that adds energy to the structure or a force that dissipates energy from the structure, which cannot

be achieved by other type of control devices. Therefore, an active system is always expected to have performance capabilities better than other strategies.

While active systems are efficient for wind-induced vibrations, there are concerns about their performance and robustness for earthquake loadings. These concerns are not due to the theoretical performance limitations of the control strategy or the devices used, but due to the practical issues, which can be summarized as follows. First, most structures, especially reinforced concrete buildings, experience extremely nonlinear behavior under earthquake excitation. In fact, a

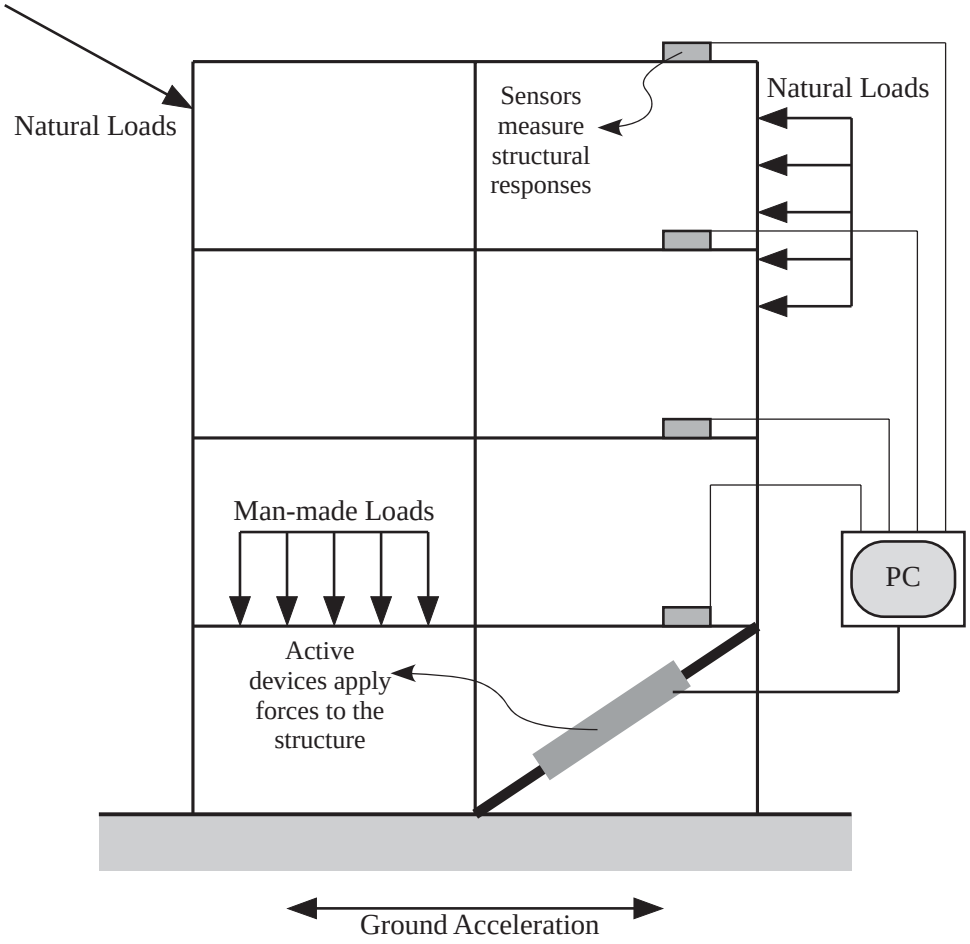


**Figure 1.2** A schematic representation of an actively controlled structure

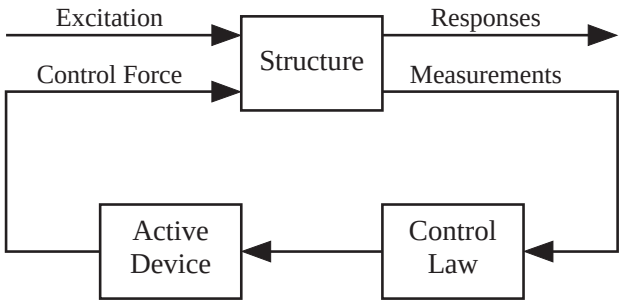


**Figure 1.3** Feedback control diagram of an active system

highly nonlinear behavior with high ductility and energy dissipation characteristics is more desirable than a linear and brittle behavior with high failure strengths in a seismic design, and this is the fundamental philosophy behind the current seismic design codes. Nonlinear behavior of civil structures cannot be modeled by analytic functions with an accuracy sufficient for active control theory. In general, approximate bilinear or trilinear models, which are not suitable for practical control theories, are utilized. Moreover, earthquake excitations have a very unpredictable random nature and may have a particular frequency content or magnitude that will intensify the nonlinear behavior of the structure. On the contrary, there is no efficient control strategy that guarantees good performance with a robust behavior for extremely nonlinear structures; in general, control strategies used in practice assume that the structure controlled is linear. Hence, it is very difficult to predict the performance and stability characteristics of an extremely nonlinear structure controlled with an active device even if it is very well designed.

In addition to robustness concerns, active devices require huge amounts of power to operate, and it is rarely guaranteed that the required amount of power will be available during a severe earthquake. To do so require expensive backup power supplies that make active control prohibitively costly.

Yokohama Landmark Tower

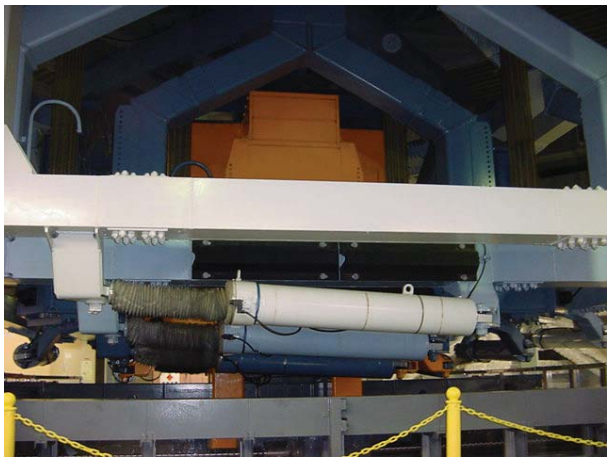

Active device in the top floor

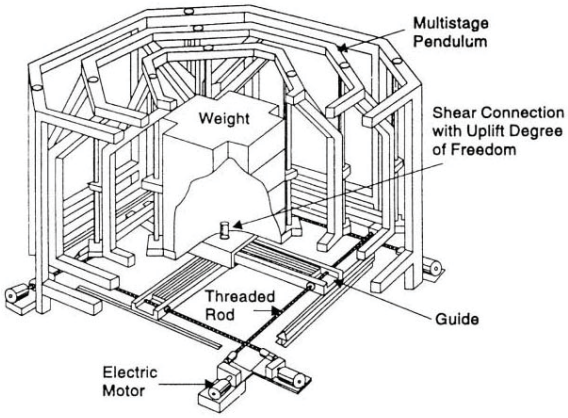


Schematic figure of the active device (Yamazaki *et al*. 1995)

**Figure 1.4** An example of actively controlled structure: Yokohama Landmark Tower (photos by Baris Erkus)

Moreover, active devices are, in general, expensive and have high maintenance costs. Installation of these devices requires special construction techniques and considerable labor time. Also, the structure should be designed and constructed accordingly. For example, consider the Yokohama tower in Figure 1.4. During construction of this building, the construction company had to use cranes that are specially designed to locate the active devices to the top floor. It would not be difficult to guess other challenges faced during the construction and overall cost of the system for this building. Therefore, only large construction companies tend to apply active control strategies.

In an overall sense, while active control technologies do have good performance characteristics, their robustness, reliability and cost characteristics limit their application to very special engineering problems, where other control approaches and conventional structural designs can not be utilized.

### 1.1.2 Passive Control

Passive devices, which are defined as devices that do not require an external power source to operate and that do not have controllable mechanical properties, are installed throughout the structure to serve two main purposes: energy dissipation and isolation (Figure 1.5). In dynamical terms, energy dissipation is achieved by converting the kinetic energy to heat and/or transferring the energy to less important vibration modes. Isolation is decoupling a structure from ground or from another structure to avoid the transfer of forces to the structure. From a practical point of view, passive devices can be classified into three categories: devices that dissipate energy by converting energy to heat, devices that transfer energy to less important modes, and devices that serve both isolation and energy dissipation purposes.

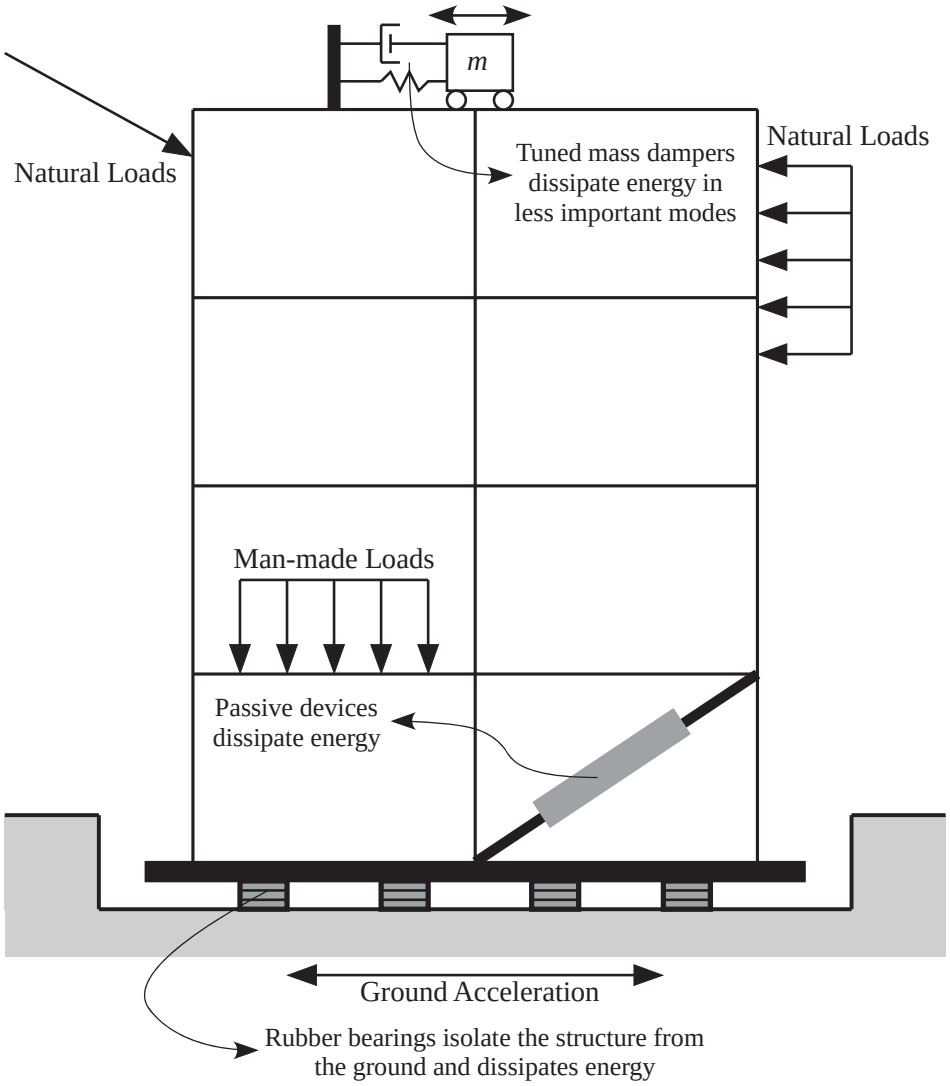


**Figure 1.5** Examples of passive devices and their utilizations

Passive devices that only dissipate energy by converting kinetic energy to heat have generally nonlinear stiffness and damping characteristics. When a large amount of energy is input to the structure, these devices dissipate energy in many ways such as damping, friction, yielding, and other types of nonlinear deformation of materials used in the device. In a structure, where passive devices are not installed, energy is dissipated by deformations of structural members.

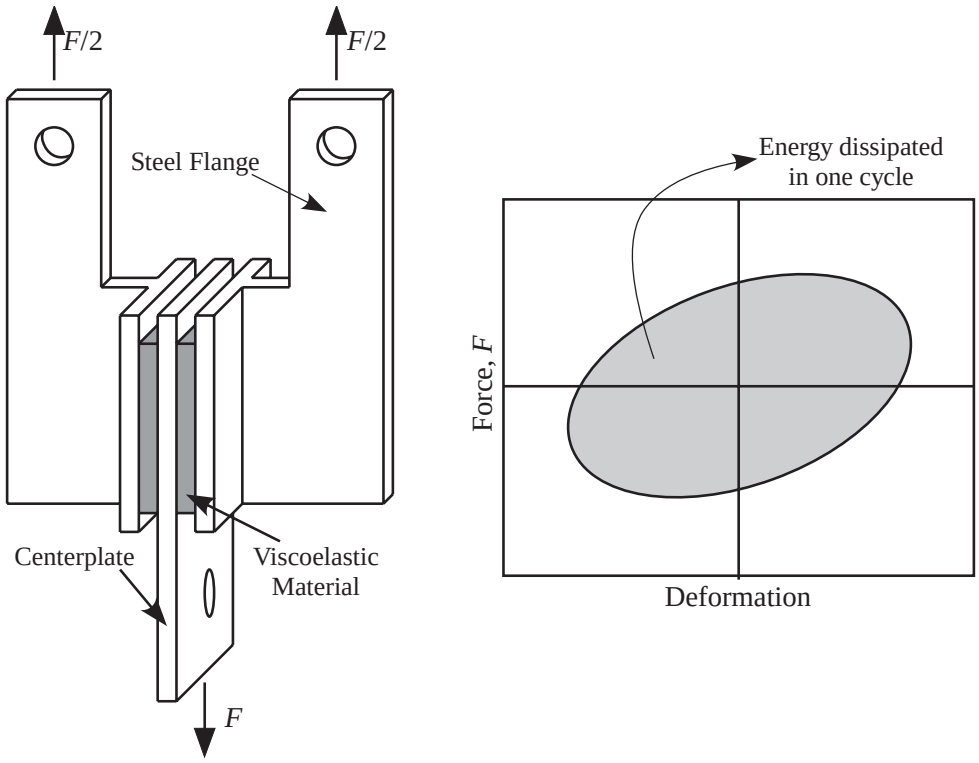


**Figure 1.6** A representative figure of a viscoelastic damper and its force-deformation relation (adapted from Shen and Soong, 1995)

Passive devices reduce the deformations of the structural members and, thereby, decrease the possibility of failure. Examples of these devices are metallic yielding dampers, friction dampers, viscoelastic dampers and viscous fluid dampers. These devices are mostly applied for earthquake protection of structures due to the energy characteristics of earthquakes. A representative figure of a viscoelastic damper and its force-displacement relation is given in Figure 1.6.

Passive devices that use less important vibration modes to dissipate energy operate on the dynamic vibration absorber concept, which has been heavily investigated, and a vast body of literature is available on the topic (*e.g.*, Ormondroyd and Den Hartog 1928; Den Hartog 1956). Tuned mass dampers (Figure 1.5) and tuned sloshing dampers are examples of these passive

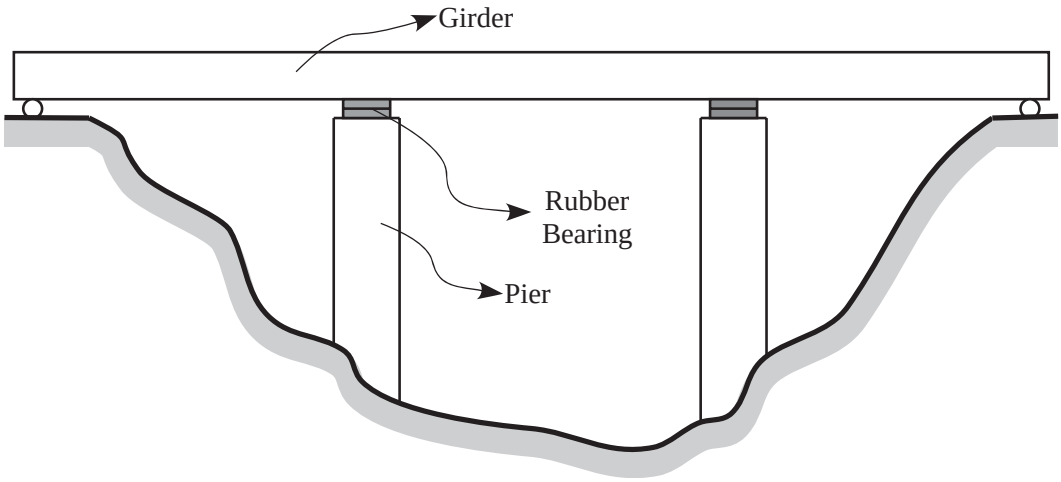


**Figure 1.7** A representative figure of an isolated bridge

devices. In a tuned mass damper (TMD), the mass of the damper is generally on the order of 1% of the structure mass. When the damping and stiffness of the TMD are properly designed, the TMD can considerably reduce the vibration of the structure for a class of excitations. Vibration absorbers are frequently used in buildings for earthquake and wind mitigation, as well as for other structures, such as bridges, that experience human/vehicle or wind-induced vibrations (*e.g*. Dallard *et al*. 2001; Carstairs *et al*. 2005).

The third class of passive devices are rubber bearings that isolate the structure from the ground as in isolated buildings (Figure 1.5) or isolate parts of the structure from each other as in isolated bridges (Figure 1.7). There are various kinds of rubber bearings, each of which has different behavior. In common, their force-deformation relations are nonlinear hysteresis. A rubber bearing and its representative behavior is shown in (Figure 1.8).

There are several advantages of passive devices and passive structures. First, performance and robustness characteristics of a passive structure can be predicted efficiently. A passive device can easily be tested in a laboratory environment, and its mechanical properties such as force-

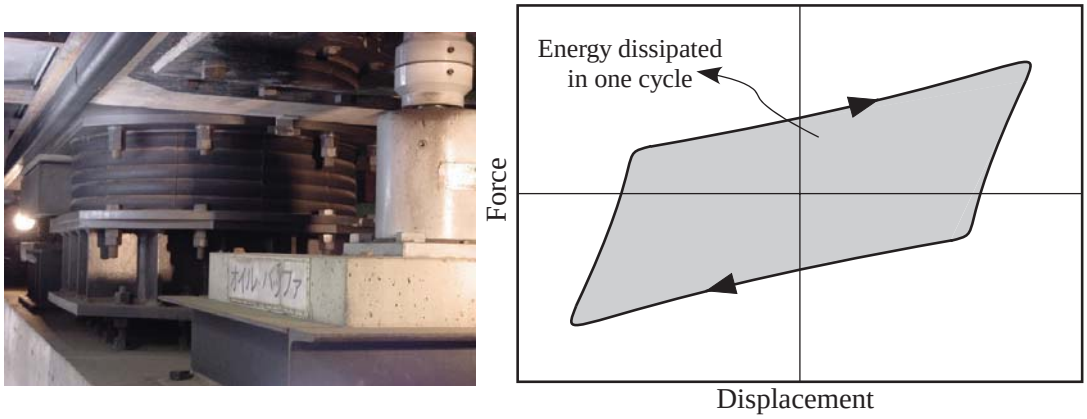


**Figure 1.8** A rubber bearing and its representative behavior (photo by Baris Erkus)

deformation and force-velocity relations, thermodynamic properties, and fatigue characteristics, can be modelled by efficient mathematical relations. Since a passive device is not a controllable device, the overall behavior of the structure can be predicted with an accuracy that is acceptable from a practical engineering point of view. Especially for extremely nonlinear structures, an engineer will have a better idea about the performance and robustness characteristics of a passive system than for an active system. This is very critical and important for a seismic design as discussed previously. Second, a passive device, by its nature, cannot inject energy into the system to which it is attached; therefore, they are more suitable for control problems where robustness is more important than the performance of the structure. Also, they do not require power to operate, which makes them reliable for events, such as earthquakes, where external power may not be available. Fourth, their initial and maintenance cost is lower than other control technologies.

The disadvantage of a passive system compared to an active system is its performance. Clearly, the performance of a passive systems is lower than a corresponding active system.

In summary, while passive systems are applied to various problems, they are more common in seismic protection than other control strategies since a system with a high likelihood of successful operation yet with a lower performance is more desirable in seismic design, instead of an active system with a very high performance but also very high risks of inoperation. Due to these and other reasons, passive control strategies have been applied for seismic protection throughout the world.

### 1.1.3 Semiactive Control

Semiactive systems combine the robustness characteristics of passive systems and performance characteristics of active systems. In general, semiactive devices are controllable passive devices (*i.e*, their stiffness and damping characteristics can be controlled dynamically) and, therefore, they cannot input energy into the system being controlled. The power requirements of semiactive devices are generally very small compared to active devices. Semiactive control is applied in a fashion similar to an active system as shown in Figure 1.2. Some examples of semiactive devices are variable-orifice dampers, variable-stiffness devices, variable-friction dampers, semiactive hydraulic dampers, and controllable-fluid dampers such as magnetorheological (MR) fluid and electrorheological (ER) fluid dampers. Variable-stiffness devices, as the name implies, provide a variable stiffness that can be tuned dynamically to change the natural frequencies of the structure to avoid resonance. Variable-damping devices — also called *smart dampers* — provide a variable damping that can be controlled to dissipative energy in an optimal manner.

The advantages and disadvantages of semiactive devices relative to active and passive devices can be summarized in several respects. First, semiactive devices are passive devices that cannot input energy into the system being controlled, yet, they can be controlled to have desired mechanical characteristics; thus, semiactive devices have robustness characteristics superior to

active devices, and performance characteristics superior to passive devices. These performance and robustness characteristics, in addition to their low operational energy requirements, make them very desirable and practical, especially from a seismic design point of view. Second, these devices have low initial and maintenance costs compared to active devices. On the other hand, there are some complex problems, where semiactive performance is limited.

In general, semiactive active systems are sound alternatives to active and passive systems. However, semiactive control did not receive considerable attention until experimental and numerical demonstrations showed that semiactive control with smart dampers can provide performance comparable to that of active control (Patten *et al*. 1994a, b; Dyke *et al.* 1996). After these results, semiactive control attracted the structural control community, and a vast body of research on various semiactive devices, particularly smart dampers, and their implementations on various control problems has been reported (Housner *et al*. 1997; Spencer and Sain 1997; Symans and Constantinou 1999; Spencer *et al*. 2000; Erkus *et al.* 2002; Ramallo *et al*. 2002; Soong and Spencer 2002; Johnson *et al.* 2006). These applications are in a wide spectrum from applications to building for seismic protection to cable vibration mitigation for cable-stayed and suspension bridges.

### 1.1.4 Significance of Semiactive Control for Performance and Robustness

It is very clear that the structural control field provides a wide variety of solutions to various structural engineering problems, addressing both safety and serviceability issues. In the previous sections, the energy dissipation and controllability of the devices are said to be the primary factors that effect the selection and applicability of the control strategy to a particular problem. If a control device has the ability to inject energy into the system to which it is attached, it may not be robust when the system exhibits extreme nonlinear behavior. On the other hand, if the device can

**Table 1.1:** A comparison of the control strategies from the point of view of performance and robustness

| Characteristics | Active | Semiactive | Passive |
|---|---|---|---|
| **Energy** | Can input energy<br>Can dissipate energy | Can only dissipate energy | Can only dissipate energy |
| **Ability to Control** | Fully active | Controllable damping and/or stiffness | Not controllable |
| **Robustness** | Critical for extremely nonlinear behavior | Good | Good |
| **Performance** | High | High to Low | Low |

only dissipate energy, it will have better robustness characteristics. Therefore, if the structural design goal is to achieve a high performance, the engineer sacrifice robustness characteristics, and vice versa. This can be put in a more formal way as follows: a structural control problem is typically a trade-off between performance and robustness. The structural engineer must clarify performance and robustness goals considering the safety and serviceability requirements, and select a control strategy that is most suitable to achieve these goals. In this respect, the control strategies discussed in the previous sections are summarized in Table 1.1. Clearly, semiactive devices are very promising in the applications where robustness is essential yet performance of alternate passive control approaches are not adequate.

## 1.2 Smart Dampers and Dissipativity

Smart dampers are nonlinear dampers with controllable damping characteristics. Therefore, they have the fundamental physical property of a simple mechanical damper (*e.g.*, a simple dash-pot element): they dissipate energy from the system to which they are attached. This section gives a review of smart dampers in the framework of energy dissipation. First, the operational

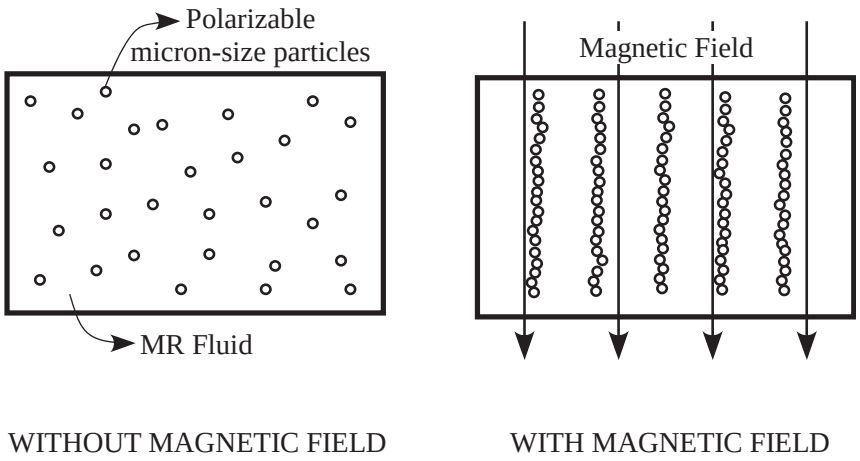


**Figure 1.9** MR fluid with and without a magnetic field

principle behind a smart damper is given considering an MR damper as an example. Then, methods used to control a smart damper and the effect of the dissipative nature of a smart damper on the efficiency of the control method are discussed in detail.

### 1.2.1 An Example of Smart Dampers: MR Dampers

An MR damper is composed of a special fluid, where micron-size particles that can be polarized by magnetic field are held in suspension. The fluid originally shows a Newtonian fluid behavior; however, when a magnetic field is applied to the fluid, the particles form a chain-like structure in the fluid, and change the fluid into a semi-solid form (Figure 1.9). The semi-solid form of the fluid has a yield strength; therefore, the damper can exert various levels of forces with various magnetic field magnitudes. Typical force-displacement and force-velocity relations for an MR damper are shown in Figure 1.10. When the magnetic field is removed, the fluid returns to its original form. This reversible action takes milliseconds, allowing the damper to be controlled efficiently. Recently, a commercial sized damper, which is shown is shown in Figure

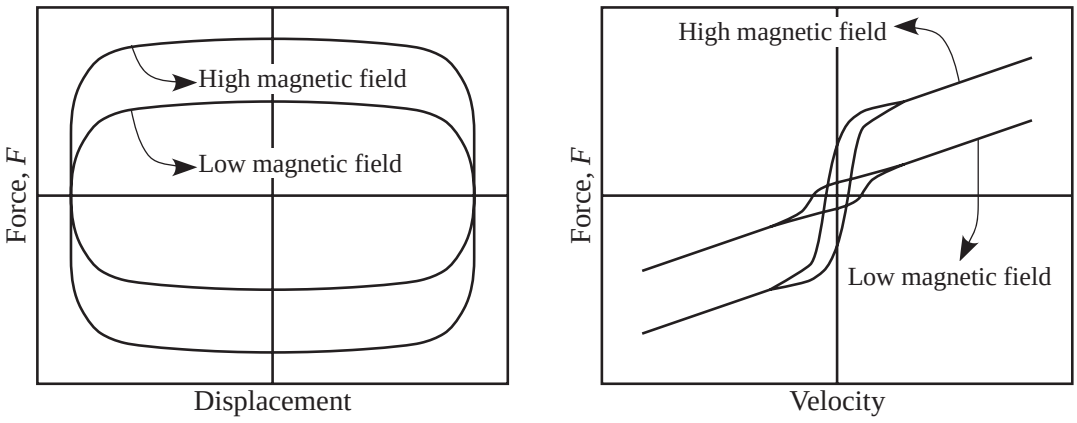


**Figure 1.10** A representative behavior of an MR damper

1.11, produced by the Lord Corporation, has been tested by Yang et al. (2002). MR dampers became very popular in the last decade, and various practical applications have been reported recently (Spencer and Nagarajaiah 2003).

### 1.2.2 Control of a Smart Damper

In general, the development of a theory that encompasses all of the challenges of controlling a smart damper is nontrivial. The challenges are mainly due to the extremely nonlinear behavior of smart dampers caused by their energy dissipation characteristics. In practice, methods employed to control smart dampers are based on well-defined active control theories. An often-employed semiactive control strategy for smart-dampers that makes use of active control theories is clipped optimal control (Dyke *et al.* 1996; Spencer *et al*. 2000; Erkus *et al.* 2002; Ramallo et al. 2002; Johnson *et al.* 2006). Clipped optimal control assumes that the structure is linear and the control device is fully active. It then employs a linear active control theory to design a primary controller, and a clipping algorithm is used as a secondary controller to make the damper mimic an active device and produce a force close to that commanded by the primary controller

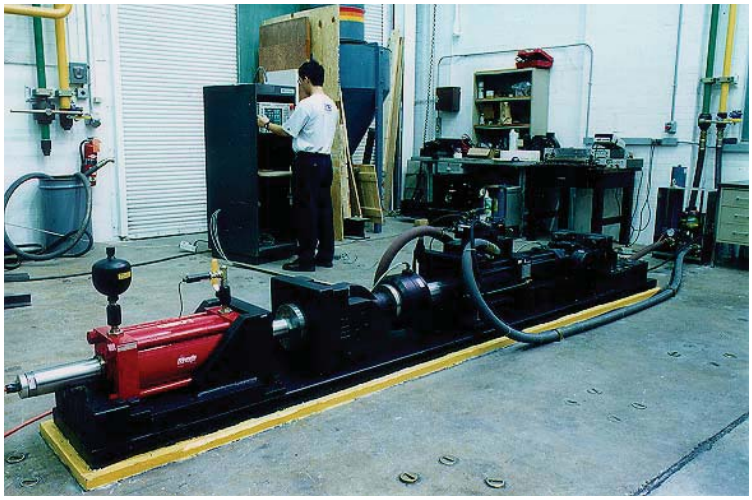

Testing of the commercial size MR damper

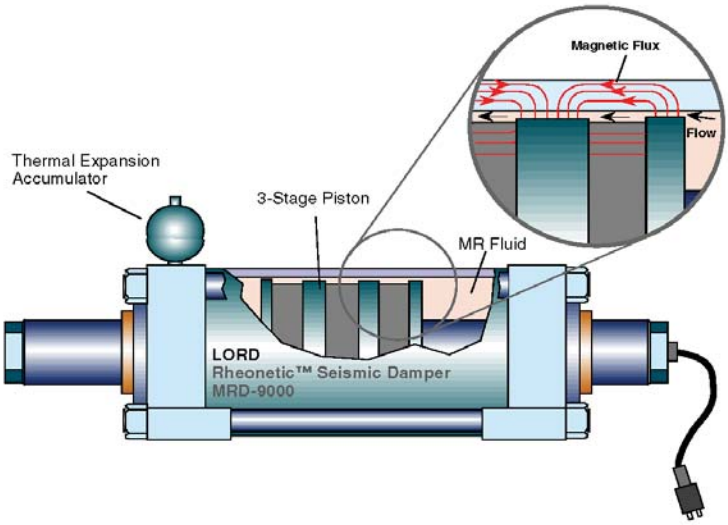


A schematic figure of the commercial size MR damper

**Figure 1.11** A commercial size MR damper (Yang *et al*. 2002)

(Figure 1.12). The primary controller is often a linear quadratic (LQ) optimal controller since this class of control theory is well-known and is widely applied in structural control. Consider an MR damper as an example. Assume that the damper is commanded by varying the voltage to an elec-

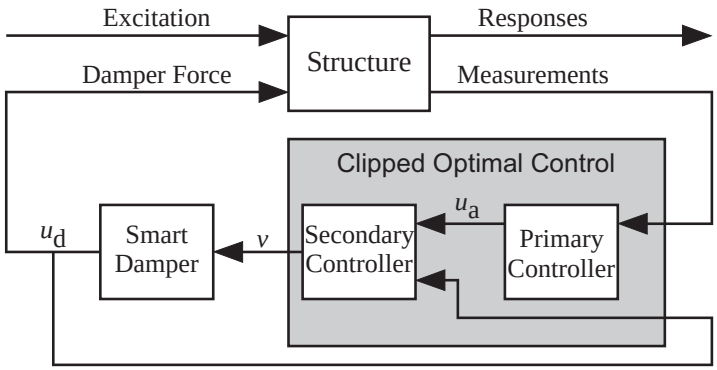


$u_a$: active control force, $v$: command parameter (*e.g.* voltage),
$u_d$: damper force

**Figure 1.12** A simplified representation of a clipped optimal control strategy

tromagnet that creates the desired magnetic field for operation. The damper achieves its minimum and maximum forces for minimum and maximum voltages, respectively. Hence, the damper can exhibit a wide variety of forces by varying the voltage. This behavior is illustrated in Figure 1.13. Clipped optimal control aims to reproduce the primary control force by varying the voltage to the damper. Considering the nonlinear behavior of a damper, clipped optimal control is a very practical and effective approach to command a smart damper.

### 1.2.3 Dissipativity and Semiactive Control

The effectiveness of a smart damper commanded by the clipped optimal control strategy can be explained by the primary control force being highly dissipative and, thus, suitable for the damper to mimic. In a narrow sense, the dissipative nature of a smart damper can be characterized by a simple nonlinear inequality given by $u_d v_d < 0$, where $u_d$ is the damper force and $v_d$ is the velocity across the damper. Similarly, a dissipative primary control force can be defined as $u_a v_d < 0$, where $u_a$ is the primary control force. This inequality simply states that the energy

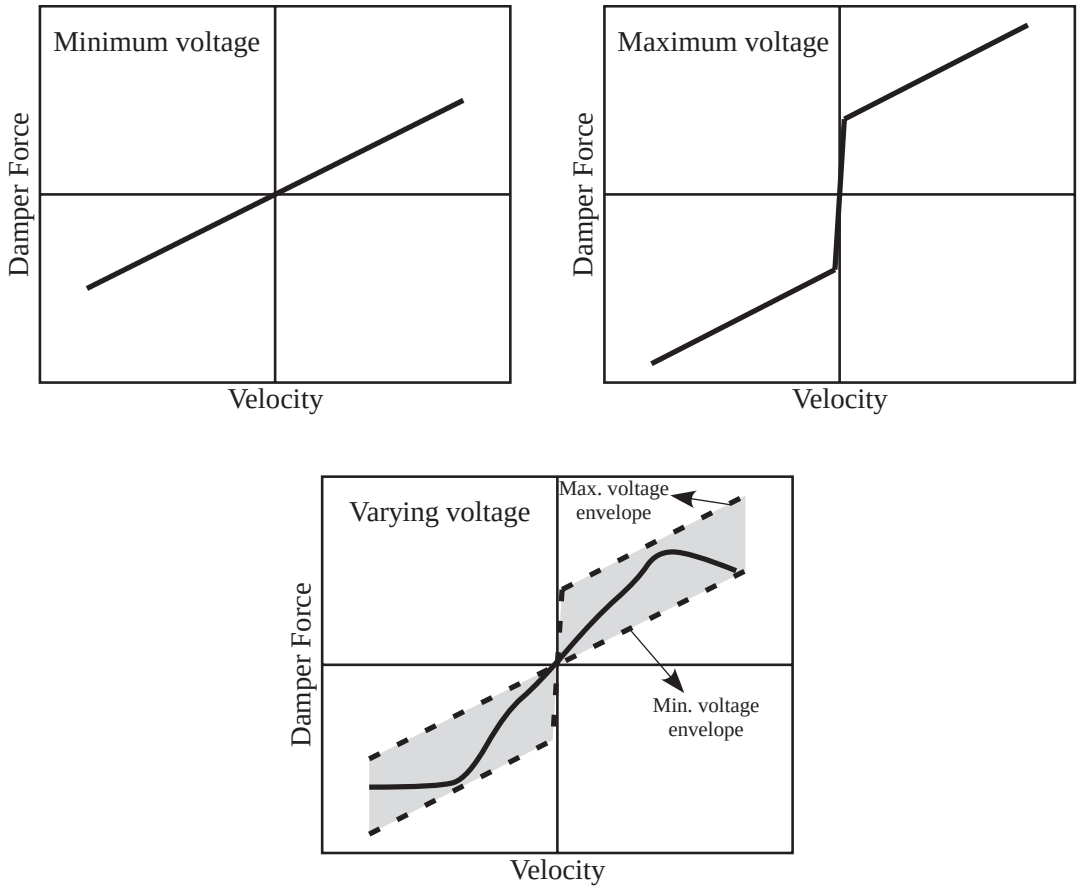


**Figure 1.13** MR damper behavior for varying voltages

flow rate of the primary control force is negative. Therefore, if a fully active device is commanded by a control force $u_a v_a < 0$ during a time period $\Delta t$ ($v_a$ being the velocity of the point where the device is exerting force), the device will dissipate energy from the structure during $\Delta t$. In general, one cannot enforce the condition $u_a v_d < 0$ on the primary controller of an LQ-based clipped optimal control strategy, and the dissipative nature of the controller is arbitrary. For example, the dissipativity condition is mostly satisfied for multistory buildings where the controller is placed in the first floor or in between the base and the ground (Dyke *et al*. 1996, 1998). There are other systems and control designs where the controller must add energy to the struc-

tural system to achieve a specific set of design objectives, and the primary controller may command highly nondissipative forces, *e.g.*, highway bridges and low-mass secondary systems (Inoudi 2000; Erkus *et al.* 2002). Both types of examples show that the dissipative nature of the primary controller is an important parameter that should be investigated to understand and predict the performance of a semiactive system with a smart damper commanded by a clipped optimal control algorithm. Insight into the concept of dissipativity may also help to develop methods to modify the primary controller so that designers can alter the dissipativity of the controller to get the uppermost performance from a smart damper.

In the literature, there is very little work that investigates the dissipative characteristics of the primary controller in a clipped optimal control strategy. This is particularly due to the absence of well defined indices that can measure the dissipativity of the primary control force. Inaudi (2000) proposed a stochastic index that estimates the probability of the primary control force being dissipative, *i.e.,* $P[u_a v_d < 0]$. Later, Christenson (2003, 2004) justified the correlation between $P[u_a v_d < 0]$ and the performance of the semiactive systems by implementing several numerical examples. Simple deterministic indices based on the dynamic time-history analyses are also used to observe the effect of the dissipative nature of the control force and the ability of the damper to mimic the control force (*e.g.*, Erkus *et al.* 2002).

From a practical point of view, a stochastic index gives a broader sense of the dissipativity of a controller in the design stage without time-consuming simulations, whereas a deterministic index is useful to investigate a specific controller for a specific excitation. A stochastic index, however, has a more crucial advantage over a deterministic index: it can be used in conjunction with special methods, such as convex multiobjective techniques, to obtain controllers with various dissipativity levels. These methods are quite popular in the control field, since they allow

numerical solution of multiobjective optimal control problems that do not have analytical solution. In fact, numerical solutions of these problems are straightforward if they can be represented as eigenvalue problems in terms of special matrix functions known as linear matrix inequalities (LMIs). On the other hand, for problems that cannot be represented in terms of LMIs, a solution is not always guaranteed, and more sophisticated methods should be employed. Whether they yield numerically solvable problems or not, convex multiobjective techniques are quite helpful for giving insight into very complex problems that cannot be investigated analytically, and can also be used to investigate dissipativity employing stochastic dissipativity indices.

The dissipativity concept can be investigated with two focuses. The first focus is given to simple structural systems such as two-degrees-of-freedom (2-DOF) structure models to explore the fundamental dissipativity concept. The second focus is on realistic structural control problems to investigate the theories used and results obtained for the simple models.

The first type of structural systems should be as simple as possible so that effects of other complexities are eliminated from the results to best understand dissipativity. Two structures are used herein for this goal. The first structure is a simple 2-DOF building where a damper is placed in the first story. This is a very typical example that has been used frequently by researchers. The second structure is a 2-DOF elevated highway bridge model. The uniqueness of this bridge model comes from the fact that the masses are distributed unevenly, resulting in interesting dynamic characteristics.

The second type of problem should include realistic structure and damper models and as many aspects of a real-life structural control problem as possible. A good example for this type of structure is the recently introduced base isolated benchmark structure (Narasimhan *et al*. 2006). The benchmark structure is a three-dimensional, L-shaped, eight-story building that is

typical in the Los Angeles area. The isolation in this benchmark study can have various isolation elements such as linear rubber bearings and bilinear lead-rubber bearings. This structure has many aspects that an engineer faces in a real-life structural control project and is very suitable to investigate the dissipativity concepts discussed previously.

The goal of this research is to give a detailed insight into the concept of dissipativity in semi-active control with smart dampers. Simple and complex structures are considered for numerical analysis. In the following, the objective and scope of this dissertation is explained in detail, and an agenda is provided.

## 1.3 Objective and Scope

The objectives of this study are

- to exploit the possibility of better semiactive system performance with smart dampers using dissipative-based control theories or control design methodologies that take into account dissipativity in contrast with conventional control design methods;
- to provide practical yet efficient indices for quantification of dissipative forces;
- to investigate the limits of semiactive performance for a wide variety of common structural systems;
- to provide generalized dissipativity-performance relations in semiactive systems with smart dampers.

The scope of this study is given as follows:

- Structural systems: Linear 2-DOF civil structures and a complex, high-order, linear, realistic base-isolated building with linear and bilinear isolators (base isolated benchmark problem).
- Semiactive devices: A theoretical ideal smart damper and a 20-ton MR damper.
- External loadings: White-noise and real-life earthquake ground accelerations.

- Active control theories: Linear quadratic (LQ) based optimal control theories.
- Semiactive control theories: A clipped optimal control theory.
- Modeling of earthquake ground accelerations: A Kanai-Tajimi filter
- State estimator: A Kalman filter.
- Software: MATLAB®, Simulink®, MATLAB® LMI Control Toolbox.

## 1.4 Organization of the Dissertation

The content of this dissertation is summarized as follows:

- Chapter 2, Literature Survey: This chapter summarizes the available literature on dissipativity in semiactive control in civil engineering. These papers are by Inaudi (2000), Christenson (2003, 2004), Erkus *et al*. (2002) and Johnson (2000).
- Chapter 3, Background: In this chapter, the mathematical and mechanical background information that is required for the dissertation is reviewed.
- Chapter 4, Dissipativity and Dissipativity Indices: In this chapter, the concept of dissipativity is formalized, and previous and proposed dissipativity indices are given.
- Chapter 5, Dissipativity-Based Control via LMI Synthesis: This chapter focuses on LMI techniques that are used to develop a LQ-based control theory with a dissipativity constraint. First, an linear quadratic regulator (LQR) problem is represented in terms of a LMI-based optimization problem. Then, the equivalency of the LMI-LQR and LQR problems is verified with a numerical study. Finally, dissipativity indices are used to obtain dissipativity constraints that are suitable for an LQ problem.
- Chapter 6, Dissipativity Analysis of Simple 2-DOF systems: In this chapter, advanced LMI-based techniques are utilized to investigate and improve the dissipativity characteristics of a standard clipped optimal control with an LQ-based primary controller for simple 2-DOF

structural systems. The LQR controller proposed in the previous chapter is implemented on two structures to observe the index–performance relations for several dissipativity levels and controller parameters for one dissipativity constraint: (1) a two-degree-of-freedom shear structure (2-DOF) with an ideal semiactive damper attached in the first story, and (2) a simplified 2-DOF highway bridge model given by Erkus *et al.* (2002) with an MR fluid damper (Yang *et al.*, 2002) in the isolation layer below the deck. For the other dissipativity constraint, an iterative method is proposed to implement the LMI-LQR. The results are presented in tabular and graphical forms. Herein, the base controller is a state-feedback LQR controller. The MATLAB® LMI Control Toolbox (Gahinet *et al.* 1995) is used as the LMI solver.

- Chapter 7, Dissipativity-Based Performance Analysis of the Smart Base Isolated Benchmark Building: This chapter is a numerical study of the dissipativity of the base isolated benchmark building and considers two types of isolation layers: linear and nonlinear. In the linear case, the structure has simple linear rubber bearings, while the nonlinear isolation has linear and bilinear bearings. This chapter also provides an equivalent linearization technique to utilize linear control theory for a nonlinear structure.
- Chapter 8, Conclusions and Directions for Future Research: In this chapter, major conclusions are listed, and suggested areas for future research are given.

# CHAPTER 2

# LITERATURE SURVEY

## 2.1 Introduction

Literature that focuses on dissipativity and its effects on the performance of semiactive control with smart dampers and clipped optimal control is very limited although researchers in the area of semiactive control have been long aware of the dissipativity concept. The reason for the lack of research on these topics is that semiactive control has only very recently become a sound alternative to other control strategies, and most of the smart damper applications in civil engineering already yielded satisfactory results. The author is aware of only four major works concerning the dissipativity concept in the semiactive control of civil structures. These papers are reviewed in this chapter.

## 2.2 Works by Inaudi (2000) and Christenson (2003, 2004)

The first important paper that investigated dissipativity in semiactive control with smart dampers and clipped optimal control is by Inaudi (2000). Although this paper's focus is not dissipativity and a very small section is provided on this topic, the results are significant. The section titled "*Can semiactive dampers realize an LQR controller with accuracy?*" starts with the statement that a semiactive damper can mimic an LQR control force only if the control force dissipates energy, *i.e.*, $u_a v_d < 0$. It should be noted that the term "*a semiactive damper*" in this statement represents a theoretical damper, which can apply any dissipative force. Then, he states that probability of the event $u_a v_d < 0$ for a closed-loop structure can be used as a measure for dissipativity, and derives this probability for a structure with an LQR controller and excited by a

zero-mean, stationary, Gaussian white noise process. This derivation requires the transformation of zero-mean joint Gaussian random variables $u_a$ and $v_d$ to two zero-mean, unit-variance, Gaussian, independent random variables, which is provided in detail by Christenson (2003). The probability of a control force being $u_a v_d < 0$ is then found to be

$$P[u_a v_d] = \frac{\text{acos}(\rho_{u_a v_d})}{\pi} \tag{2.1}$$

where $\rho_{u_a v_d}$ is the correlation coefficient between $u_a$ and $v_d$. Three examples are considered by Inaudi (2000), which are summarized in Figure 2.1. In all of the examples, LQR control is designed such that control force $u_a$ aims to reduce the interstory drifts (in the example (b), drift of the main structure). It is shown that the control force has high likelihood of being dissipative in the first example, while it has low likelihood in the second and third examples. Based on these results, Inaudi concluded that a semiactive damper would be successful in mimicking the control force in the first example and would not be efficient in the second and third example. Christenson (2003) further considered a multi-degree-of-freedom (MDOF) coupled structure and a cable vibration problem, where he concluded that $P[u_a v_d]$ can be used as a useful measure in a semiactive control design to avoid time consuming simulations. Also, Christenson (2004) suggested an approach for the design of semiactive structures with smart dampers based on the estimation of $P[u_a v_d]$.

## 2.3 Work by Erkus *et al*. (2002)

In this work, clipped optimal control of a 2-DOF highway bridge with an MR damper is considered. While a 2-DOF model is a very simple model for a bridge, it is very useful to understand the behavior of isolated bridges and, therefore, is used very extensively. Two LQR primary con-

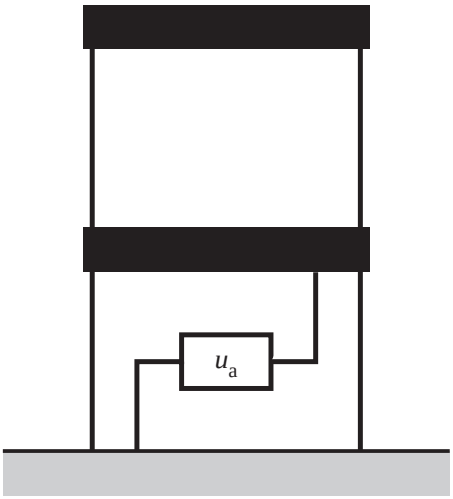


(a) A simple building

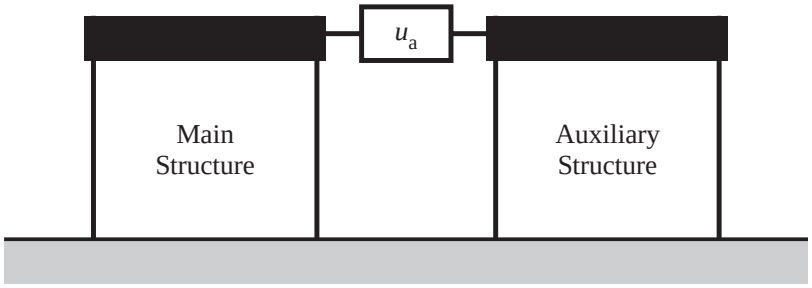


(b) A coupled building

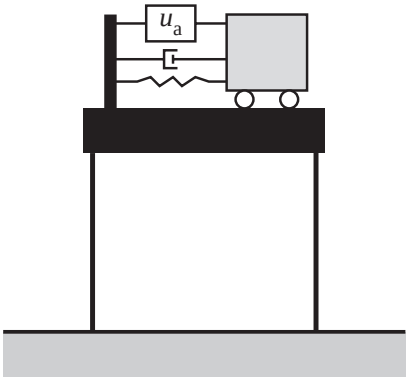


(c) A structure with an active TMD

**Figure 2.1** Examples considered by Inaudi (2000)

trollers are designed. In the first design, designated “D1”, the goal is to minimize the pier responses, mainly pier drift; in the second design, designated “D2”, the goal is to minimize the bearing responses, mainly bearing drift. Three different control approaches are considered: optimal passive, fully active, semiactive with an MR damper. Each of these designs uses linear stiffness and damping of both bearing and pier. It is shown by numerical simulations that an MR damper is successful in simulating the primary control force in an efficient manner for design

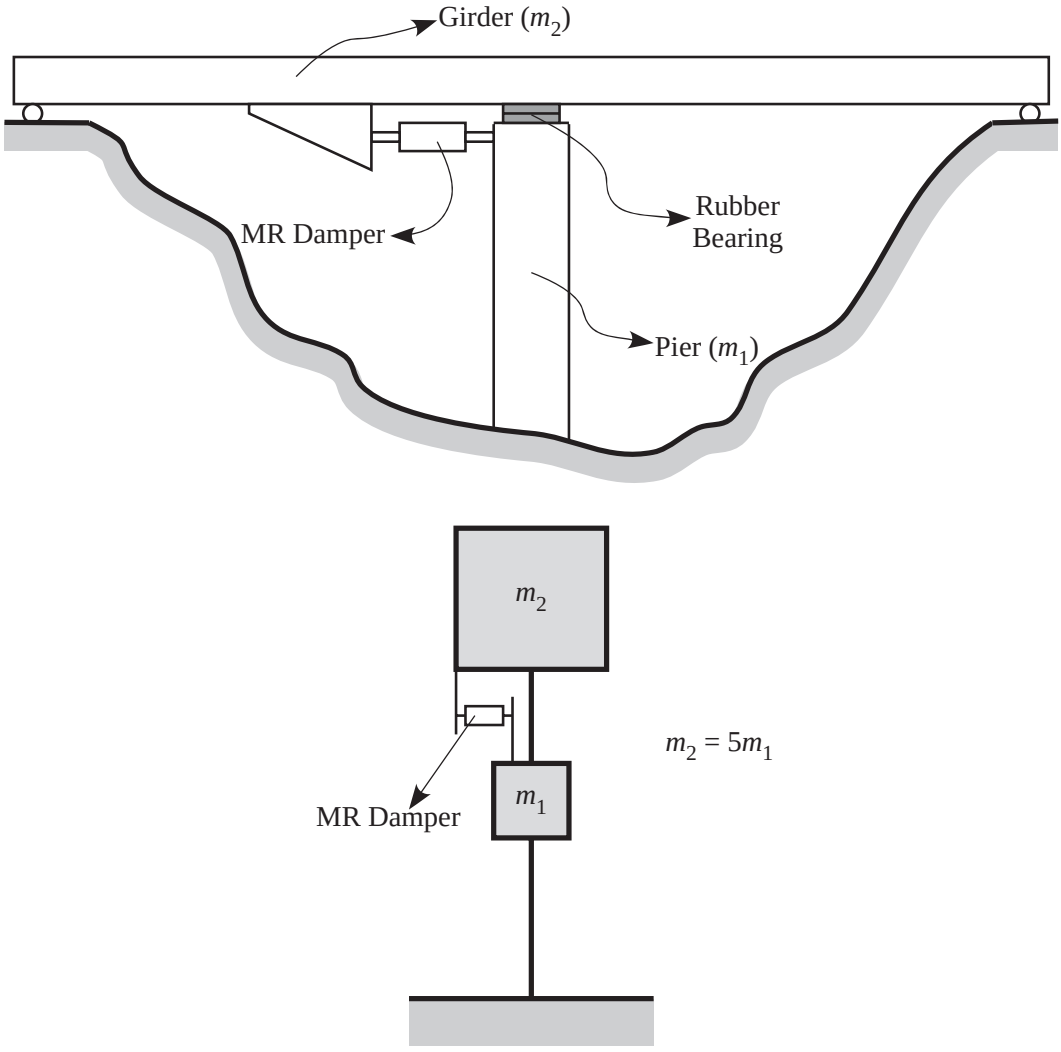


**Figure 2.2** Example considered by Erkus *et al*. (2002)

D2. On the other hand, for design D1, the damper is not able to mimic the primary control force; instead, the behavior of the semiactive system is very similar to the optimally designed passive system.

From Erkus *et al*. (2002), Figure 2.3 shows the primary control force vs. velocity and vs. damper drift curves. The dissipative regions in the primary control force versus damper velocity plots are shown by the shaded areas. Clearly, the control force is more dissipative using design D2 than using D1. This is also observed by the shape of the control force versus damper displacement curves, which are more elliptical in design D2. Also introduced is the percentage of direction coincidence, which is the percent of the time that the damper velocity is in the opposite direction of the primary control force (note that the sign convention used in the paper by Erkus *et*

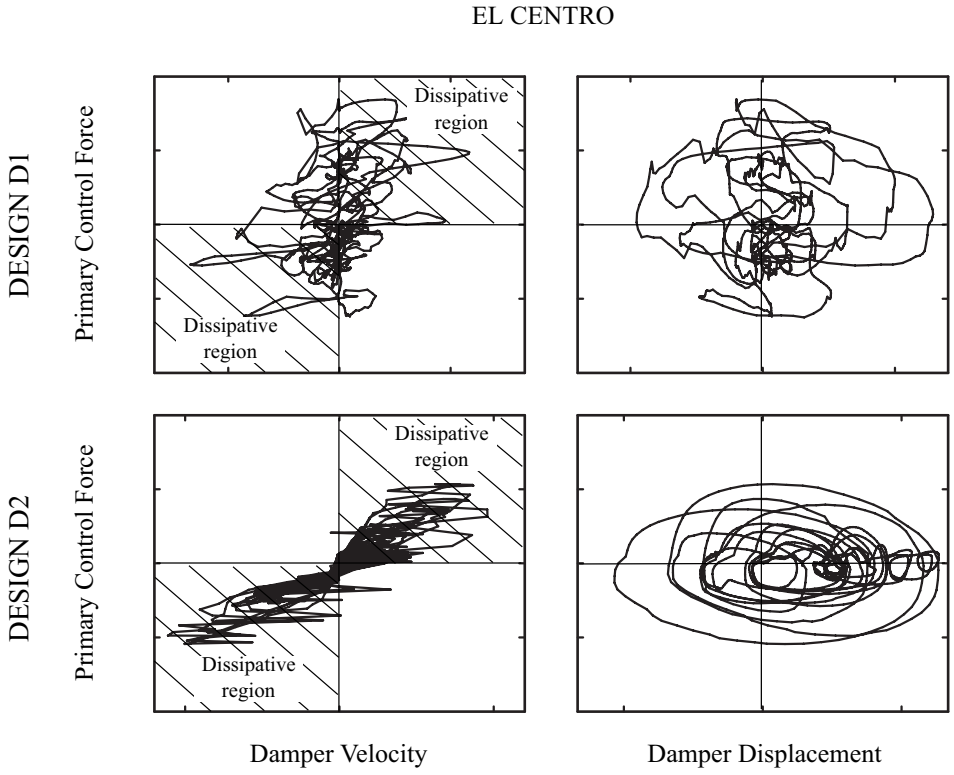


**Figure 2.3** Primary control force and damper displacement/velocity relations of the designs D1 and D2 for El Centro earthquake in Erkus *et al*. (2002)

*al*. (2002) is slightly different than the sign convention used herein; therefore, the dissipative regions in Erkus *et al*. (2002) correspond to $u_a v_d > 0$). This is, in fact, the percentage of the control forces that fall in the shaded areas in the control force versus damper velocity graphs It is also a deterministic index of percent dissipative forces. This index was computed for various control designs and earthquakes; the control designs that are suitable for a smart damper were identified. It is found that direction coincidence shows the same trend for all earthquakes. It is also observed that D1 is a control design that falls in a region with low direction coincidence values, and D2 falls in a region with high direction coincidence value.

## 2.4 Work by Johnson (2000)

The paper by Johnson (2000) concentrates on the LQR control theory. An LQR problem is essentially an optimization problem where a cost function is minimized subject to a dynamical equality constraint. In the original theory, the cost function includes a cross-term that corresponds to the multiplication of states and control force with a constant coefficient. In structural control, LQR is generally used ignoring this cross-term by using a zero coefficient. However, it is possible to select a coefficient such that the cross-term becomes $u_a v_d$; *i.e.*, the LQR also tries to minimize $u_a v_d$, which may result in controllers with better dissipativity characteristics. However, numerical simulations showed that this approach has a minor effect on the controller.

# CHAPTER 3

# BACKGROUND

## 3.1 Introduction

In this chapter, a review is given of the mathematical and mechanical background that is required to understand the concepts presented in this dissertation. It should be noted that most of the material given herein are well-known in the mathematical controls community, though they may be new to current structural control practice. Therefore, they are essential for the completeness of this dissertation.

The concepts given below are based on considerably complex mathematical theories which, in their original sources, may be very difficult to comprehend. Therefore, the author has tried to present the concepts in a simple manner so as to be accessible to the general structural engineering community without forfeiting their original mathematical meaning and strength. Readers are strongly recommended to refer to the articles and books cited herein for further and detailed information.

## 3.2 Mathematical Background

### 3.2.1 Definitions

**Definition 3.1** A function $f(x)$ is a *linear* function of $x$ if $f(\alpha x_1 + \beta x_2) = \alpha f(x_1) + \beta f(x_2)$ for all scalar $\alpha$ and $\beta$.

**Definition 3.2** A function $g(x)$ is an *affine* function of $x$ if it can be written as $g(x) = f(x) + a$ where $f(x)$ is a linear function and $a$ is a constant.

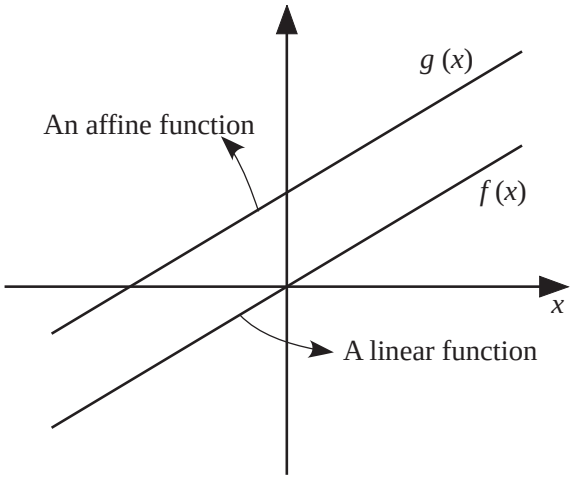


**Figure 3.1** Examples of linear and affine functions

To illustrate these concepts better, examples for a linear and an affine function are given in Figure 3.1.

**Definition 3.3** A set $C \subset \Re^n$ is *convex* if $\mu \mathbf{x}_1 + (1-\mu)\mathbf{x}_2 \in C$ for any $\mathbf{x}_1, \mathbf{x}_2 \in C$ and any $\mu \in [0, 1]$.

Figure 3.2 illustrates convex and nonconvex sets in a two-dimensional space, *i.e.*, $n = 2$.

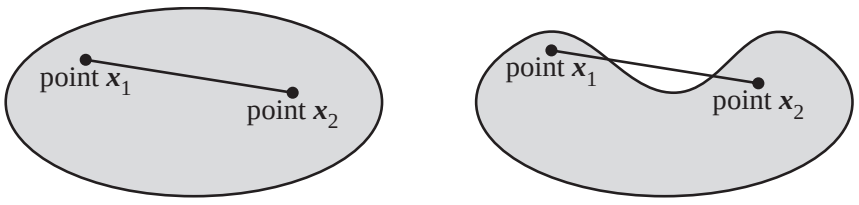


**Figure 3.2** Examples of convex and nonconvex sets

### 3.2.2 Linear Matrix Inequalities

The matrix inequality

$$\mathbf{F}(\mathbf{x}) = \mathbf{F}_0 + x_1\mathbf{F}_1 + \ldots + x_n\mathbf{F}_n > 0 \tag{3.1}$$

is called a *linear matrix inequality*, where $\mathbf{F}(\mathbf{x})$ is an affine function of the real vector $\mathbf{x} = [x_1 \;\; x_2 \;\ldots\; x_n]^{\mathrm{T}}$ and $\mathbf{F}_0$, $\mathbf{F}_1$, …, $\mathbf{F}_n$ are real symmetric matrices.

As mentioned before, control theories and problems that involve LMIs are quite involved and require a good understanding of the mathematical theory of LMIs. Herein, the major properties of LMIs are given.

- The inequality $\mathbf{F}(\mathbf{x}) > 0$ implies that $\mathbf{F}(\mathbf{x})$ is a positive definite matrix, *i.e.*, the real parts of all eigenvalues of $\mathbf{F}(\mathbf{x})$ are positive, and $\mathbf{u}^{\mathrm{T}}\mathbf{F}(\mathbf{x})\mathbf{u} > 0$ for any vector $\mathbf{u} \neq \mathbf{0}$.
- A vector $\mathbf{x}$ that satisfies the inequality (3.1) is known as a feasible solution of the LMI. The feasible solution set of the inequality (3.1), $\{\mathbf{x} \,|\, \mathbf{F}(\mathbf{x}) > 0\}$, is a convex set. Convexity is an important property since there are powerful numerical techniques for the solution of LMI problems with convex solution sets (Boyd *et al*. 1994; Nesterov and Nemirovskii 1994).
- Some inequalities not in the form of (3.1) can be converted to LMIs by some algebraic operations. Also, multiple LMIs can be represented with a single equivalent LMI by defining a new variable vector that includes the variables of the multiple LMIs. Further, the solution set of some nonconvex matrix inequalities can be mapped into a convex solution set of a corresponding LMI. Therefore, a problem that cannot be solved analytically or numerically, due to several types of inequalities, can be solved numerically if these inequalities can be converted into LMIs.
- Often encountered in control problems are inequalities with matrix variables instead of a vector as given in inequality (3.1). As an example, consider the Lyapunov inequality

$\mathbf{AP} + \mathbf{PA}^{\mathrm{T}} < 0$ where $\mathbf{A}$ is a given (known) matrix, and the symmetric real matrix $\mathbf{P}$ is the variable. This inequality can easily be reduced to the form given by inequality (3.1) (Boyd *et al*. 1994). In this dissertation, these types of LMIs will not be explicitly reduced to vector form (3.1); rather, they will be used as they are.

- According to the definitions given above, the function $\mathbf{F}(\mathbf{x})$ given in (3.1) is an affine function of $\mathbf{x}$, not linear. Some authors (*e.g.*, Dullerud and Paganini 2000) prefer to use the following for the definition of an LMI:

$$\mathbf{F}(\mathbf{x}) = x_1\mathbf{F}_1 + \ldots + x_n\mathbf{F}_n > -\mathbf{F}_0 \tag{3.2}$$

where $\mathbf{F}(\mathbf{x})$ is a linear function of $\mathbf{x}$.

**Definition 3.4** The inequality $\mathbf{F}(\mathbf{x}) > 0$ is a *strict* LMI while $\mathbf{F}(\mathbf{x}) \geq 0$ is a *nonstrict* LMI.

A note on strict and nonstrict LMIs regarding the numerical considerations is given in Appendix A.4.

### 3.2.3 Bilinear Matrix Inequalities

The inequality

$$\mathbf{F}(\mathbf{x}, \mathbf{y}) > 0 \tag{3.3}$$

is called a *bilinear matrix inequality* and the matrix valued function $\mathbf{F}(\mathbf{x}, \mathbf{y})$ is called bilinear if $\mathbf{F}(\mathbf{x}, \mathbf{y})$ is affine with respect to each of its arguments; *i.e.*, $\mathbf{F}(\mathbf{x}, \mathbf{y})$ is affine in $\mathbf{x}$ when $\mathbf{y}$ is fixed and vice versa.

BMIs are, in general, nonconvex and have an intractable computational complexity known as $\mathcal{NP}$-hardness (Toker and Özbay 1995). Therefore, there are no efficient algorithms for the numerical solution of problems involving BMIs (see Appendix A.3 for a note). However, by defining new variables, some BMIs can be converted to equivalent LMIs; *i.e.*, a new LMI is

defined whose solution set can be mapped into the solution set of the BMI. This property is important since BMIs are frequently encountered in control problems.

**Theorem 3.1** (*Schur complement formula*) The set of matrix inequalities

$$\mathbf{R} > 0 \quad \text{and} \quad \mathbf{Q} - \mathbf{S}\mathbf{R}^{-1}\mathbf{S}^{\mathrm{T}} > 0 \tag{3.4}$$

is equivalent to

$$\begin{bmatrix} \mathbf{Q} & \mathbf{S} \\ \mathbf{S}^{\mathrm{T}} & \mathbf{R} \end{bmatrix} > 0 \quad \text{and} \quad \mathbf{R} > 0 \tag{3.5}$$

where $\mathbf{Q}$, $\mathbf{R}$ and $\mathbf{S}$ are matrices, and $\mathbf{Q}$ and $\mathbf{R}$ are symmetric. See Dullerud and Paganini (2000) for a proof of this theorem.

The Schur complement formula is a tool used frequently in the control field to convert some BMIs into LMIs.

### 3.2.4 Stability and Lyapunov's Equality

There are various interpretations of stability in the general field of civil engineering. In this dissertation, stability will refer to bounded-input-bounded-output (BIBO) stability when dealing with control theories (see, *e.g.*, Chen (1999) for a definition and treatment of BIBO stability). This definition is summarized as follows.

A linear time-invariant system given by $\dot{\mathbf{q}} = \mathbf{A}\mathbf{q}$ is *stable* if every eigenvalue of $\mathbf{A}$ has a negative real part (Chen 1999). A matrix $\mathbf{A}$ satisfying this condition is called *Hurwitz*. A convenient way to check the eigenvalues of $\mathbf{A}$ is to employ a Lyapunov equation as follows: All eigenvalues of $\mathbf{A}$ have negative real parts if and only if, for any given matrix $\mathbf{Q} = \mathbf{Q}^{\mathrm{T}} > 0$, there exists a unique solution $\mathbf{S} = \mathbf{S}^{\mathrm{T}} > 0$ for the Lyapunov equation given by $\mathbf{A}\mathbf{S} + \mathbf{S}\mathbf{A}^{\mathrm{T}} = -\mathbf{Q}$ (or $\mathbf{A}^{\mathrm{T}}\mathbf{S} + \mathbf{S}\mathbf{A} = -\mathbf{Q}$). This condition can also be stated as follows: The system $\dot{\mathbf{q}} = \mathbf{A}\mathbf{q}$ is stable

(and $\mathbf{A}$ is Hurwitz) if the LMI $\mathbf{AS} + \mathbf{SA}^{\mathrm{T}} + \mathbf{Q} \leq 0$, or its strict version $\mathbf{AS} + \mathbf{SA}^{\mathrm{T}} + \mathbf{Q} < 0$, has a feasible solution $\mathbf{S} = \mathbf{S}^{\mathrm{T}} > 0$ (see, *e.g.*, Slotine and Li (1991) for a treatment of Lyapunov stability theory). Herein, $\mathbf{S}$ is called the Lyapunov matrix.

There are other useful properties of the Lyapunov equality. For example, the solution of the Lyapunov equation will simply give the controllability and observability grammians for a specific value of $\mathbf{Q} = \mathbf{Q}^{\mathrm{T}} > 0$ (see, *e.g.*, Dullerud and Paganini (2000) for the definitions and derivations). Similarly, for a given system $\dot{\mathbf{q}} = \mathbf{Aq} + \mathbf{Ew}$, where $\mathbf{w}$ is a white noise external disturbance with unit intensity $E[\mathbf{w}(t)\mathbf{w}^{\mathrm{T}}(t+\tau)] = \mathbf{I}\delta(\tau)$, the solution of the Lyapunov equation for $\mathbf{Q} = \mathbf{EE}^{\mathrm{T}}$ is simply the expected value of $\mathbf{qq}^{\mathrm{T}}$ (*i.e.*, the covariance matrix of the states $\mathbf{q}$).

### 3.2.5 LMI Characterization of Multivariable Feedback Control Systems

In a very broad sense, multivariable feedback control deals with problems with more than one design objective including time and frequency domain constraints (see, *e.g.*, Scherer *et al*. (1997) for a list of design objectives encountered frequently in the field of control). In most cases, an analytical solution for a controller that satisfies multiple constraints is not available. To obtain an LMI characterization for these types of problems, a method is given by Scherer *et al*. (1997) and is very briefly summarized here:

- Consider a closed-loop system $\dot{\mathbf{q}}_{\mathrm{c}} = \mathbf{A}_{\mathrm{c}}\mathbf{q}_{\mathrm{c}}$, where $\mathbf{A}_{\mathrm{c}}$ is Hurwitz and is a function of the controller. Let $\mathbf{S}$ be the Lyapunov matrix for this closed loop system satisfying the Lyapunov inequality. For each of the objectives, a matrix inequality condition in terms of a Lyapunov matrix is found. Inequality conditions are selected such that they are satisfied when the corresponding design specification is met. The final inequalities become a function of $\mathbf{A}_{\mathrm{c}}$, the controller and the Lyapunov matrix. Therefore, these inequalities are, in general, bilinear.

- Let the matrix inequality condition associated with the $i^{\text{th}}$ objective be $\mathbf{F}_i(\mathbf{K}, \mathbf{S}_i) > 0$, where $\mathbf{S}_i$ is the corresponding Lyapunov matrix and $\mathbf{K}$ is the controller. Then, to enforce a unique Lyapunov matrix for the system, all of the Lyapunov matrices are set to a single Lyapunov matrix as $\mathbf{S}_1 = \ldots = \mathbf{S}_N = \mathbf{S}$. Therefore, a problem with several BMIs, whose Lyapunov matrices are all $\mathbf{S}$, is obtained.
- The final step is to introduce new variables or to employ some algebraic manipulations to convert BMIs into LMIs. After obtaining an LMI for each constraint, all LMIs are cast into a single LMI. After these manipulations, the final problem will have a convex LMI constraint and can be solved numerically. It should be noted that the mapping between the BMIs and LMIs must be one-to-one.

### 3.2.6 Eigenvalue Problems

If the problem includes an optimization criteria, the LMI problem is generally in the form of an eigenvalue problem (Boyd *et al*. 1994). An eigenvalue problem has several representations. The representation that will be employed in this dissertation is as follows:

$$\begin{aligned} &\min_{\mathbf{x}} \ \mathbf{c}^{\mathrm{T}}\mathbf{x} \\ &\text{subject to } \mathbf{F}(\mathbf{x}) > 0 \end{aligned} \tag{3.6}$$

where $\mathbf{c}$ is a known vector, and $\mathbf{F}(\mathbf{x}) > 0$ is an LMI. Clearly, the object function $\mathbf{c}^{\mathrm{T}}\mathbf{x}$ is a linear function of $\mathbf{x}$, and the constraint $\mathbf{F}(\mathbf{x}) > 0$ is a convex inequality. Another form of the EVP has a matrix objective function in the form of $\mathbf{C}^{\mathrm{T}}\mathbf{X}$ where $\mathbf{C}$ and $\mathbf{X}$ are matrices of appropriate dimensions, which, in fact, can be represented by (3.6) with some algebraic manipulations (Boyd *et al*. 1994; Gahinet *et al*. 1995).

### 3.2.7 LQR Control Problem

Consider a linear time-invariant system:

$$\begin{aligned} \dot{\mathbf{q}} &= \mathbf{A}\mathbf{q} + \mathbf{B}\mathbf{u} + \mathbf{E}\mathbf{w} \\ \mathbf{z} &= \mathbf{C}_z\mathbf{q} + \mathbf{D}_z\mathbf{u} + \mathbf{F}_z\mathbf{w} \end{aligned} \tag{3.7}$$

where $\mathbf{q}$ is the state vector, $\mathbf{u}$ is a vector of control forces, $\mathbf{w}$ is a stationary zero-mean white noise stochastic vector process disturbance with unit intensity, and $\mathbf{z}$ is the vector of outputs to be minimized. In structural control, the excitation is generally earthquake ground acceleration or wind excitation modelled as filtered white noise, and the outputs are structural response quantities such as floor drifts or absolute accelerations that lead to a zero $\mathbf{F}_z$. The LQR problem is to find the control gain $\mathbf{K}$ that satisfies the optimization

$$\begin{aligned} &\min_{\mathbf{K}} E[\mathbf{z}^T\tilde{\mathbf{Q}}\mathbf{z} + \mathbf{u}^T\tilde{\mathbf{R}}\mathbf{u} + \mathbf{z}^T\tilde{\mathbf{N}}\mathbf{u} + \mathbf{u}^T\tilde{\mathbf{N}}^T\mathbf{z}] \\ &\text{subject to (3.7) and } \mathbf{u} = -\mathbf{K}\mathbf{q} \end{aligned} \tag{3.8}$$

where $\tilde{\mathbf{Q}} \geq 0$ and $\tilde{\mathbf{R}} > 0$ are symmetric weighting matrices, and $\mathbf{K}$ is a constant feedback gain matrix. Substituting the output equation in (3.7) into the optimization problem (3.8), one obtains another form of the LQR problem

$$\begin{aligned} &\min_{\mathbf{K}} E[\mathbf{q}^T\mathbf{Q}\mathbf{q} + \mathbf{u}^T\mathbf{R}\mathbf{u} + \mathbf{q}^T\mathbf{N}\mathbf{u} + \mathbf{u}^T\mathbf{N}^T\mathbf{q}] \\ &\text{subject to } \dot{\mathbf{q}} = \mathbf{A}\mathbf{q} + \mathbf{B}\mathbf{u} + \mathbf{E}\mathbf{w}, \quad \mathbf{u} = -\mathbf{K}\mathbf{q} \end{aligned} \tag{3.9}$$

where

$$\mathbf{Q} = \mathbf{C}_z^T\tilde{\mathbf{Q}}\mathbf{C}_z, \quad \mathbf{N} = \mathbf{C}_z^T\tilde{\mathbf{Q}}\mathbf{D}_z + \mathbf{C}_z^T\tilde{\mathbf{N}}, \quad \mathbf{R} = \tilde{\mathbf{R}} + \mathbf{D}_z^T\tilde{\mathbf{Q}}\mathbf{D}_z + \mathbf{D}_z^T\tilde{\mathbf{N}} + \tilde{\mathbf{N}}^T\mathbf{D}_z \tag{3.10}$$

For the problem defined by (3.9) and (3.10) to be well-posed, design parameters should satisfy the following inequalities (see the Appendix A.4 for a note on this condition):

$$\mathbf{W} = \begin{bmatrix} \mathbf{Q} & \mathbf{N} \\ \mathbf{N}^{\mathrm{T}} & \mathbf{R} \end{bmatrix} \geq 0 \text{ and } \mathbf{R} > 0 \tag{3.11}$$

## 3.3 Mechanical Background

### 3.3.1 Energy Flow Rate

Consider a continuous external force $f(x, t)$, which is applied to a system on a surface region $x \in \Omega$. Let $v(x, t)$ be the velocity of the surface (with positive velocity in the same direction as positive forces). The *rate of energy added* to the system by the force $f(x, t)$ is given by

$$\frac{\partial E}{\partial t} = \int_{\Omega} f(x, t) v(x, t) d\Omega \tag{3.12}$$

### 3.3.2 Ideal Smart Damper Model

An ideal smart damper can be considered to be an active device that can only apply dissipative forces. Therefore, an ideal smart damper can realize a control force when it is dissipative; otherwise, it produces no force. This behavior can be characterized as follows:

$$u_{\mathrm{d}} = \begin{cases} u_{\mathrm{a}}, & u_{\mathrm{a}} v_{\mathrm{d}} < 0 \\ 0, & u_{\mathrm{a}} v_{\mathrm{d}} \geq 0 \end{cases} \tag{3.13}$$

where $u_{\mathrm{d}}$ and $v_{\mathrm{d}}$ are the damper force and velocity, respectively, and $u_{\mathrm{a}}$ is the control force that is to be realized.

### 3.3.3 20-ton MR Damper Model

Recently, a 20-ton MR damper prototype was produced by the Lord Corporation, and an efficient mathematical model of this device was developed by Yang *et al*. (2002) (Figure 3.3). The

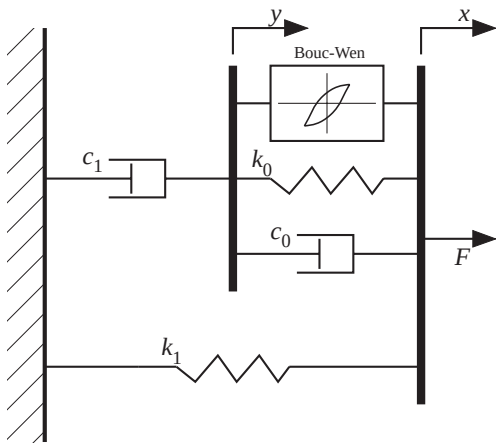


**Figure 3.3** Mechanical model of a 20-ton MR damper (Yang *et al*. 2002)

damper is idealized by simple spring and dashpot elements with a Bouc-Wen nonlinear model. The force is governed by the following equation:

$$F = \alpha z + c_0(\dot{x} - \dot{y}) + k_0(x - y) + k_1(x - x_0) = c_1\dot{y} + k_1(x - x_0) \tag{3.14}$$

where $z$ and $y$ are governed by the following differential equations:

$$\dot{z} = -\gamma|\dot{x} - \dot{y}|z|z|^{n-1} - \beta(\dot{x} - \dot{y})|z|^n + A(\dot{x} - \dot{y}) \tag{3.15}$$

$$\dot{y} = \frac{1}{c_0 + c_1}\{\alpha z + c_0\dot{x} + k_0(x - y)\} \tag{3.16}$$

The damping characteristics can be changed by modifying the current as follows:

$$\begin{aligned} \alpha(i) &= 16566i^3 - 87071i^2 + 168326i + 15114 \\ c_0(i) &= 437097i^3 - 1545407i^2 + 1641376i + 457741 \\ c_1(i) &= -9363108i^3 + 5334183i^2 + 48788640i - 2791630 \end{aligned} \tag{3.17}$$

where the currrent $i$ is in Amperes, $\alpha(i)$ is in N, and the damping constants $c_0(i)$ and $c_1(i)$ are in N·sec/m. Other parameters are $A = 2679\ \text{m}^{-1}$, $\gamma = \beta = 647.46\ \text{m}^{-1}$, $k_0 = 137810$ N/m,

$n = 10$, $x_0 = 0.18$ m, $k_1 = 617.31$ N/m. The maximum current that can be applied to the damper is $i_{max} = 2$ A. (It should be noted that the units of the MR damper parameters given herein are not consistent. However, these values are directly taken from Yang *et al*. (2002) without any modification.)

To illustrate the mathematical model given above, a numerical simulation is done for a 1 Hz frequency and 2 cm amplitude sinusoidal excitation, and the response characteristics of the model are given in Figure 3.4.

### 3.3.4 Clipped Optimal Control

The secondary controller in the clipped optimal control commands the damper current using the following law (Dyke *et al*. 1996):

$$i = i_{max} H[(u_a - u_d)u_d] \tag{3.18}$$

where $H[\cdot]$ is the Heaviside step function, $i_{max}$ is the maximum current that can be applied to the damper, $u_a$ is the primary control force and $u_d$ is the damper force. In discrete form, (3.18) can be written as

$$i^t = i_{max} H[(u_a^t - u_d^{t-1})u_d^{t-1}] \tag{3.19}$$

A graphical representation of the clipping algorithm is shown in Figure 3.5.

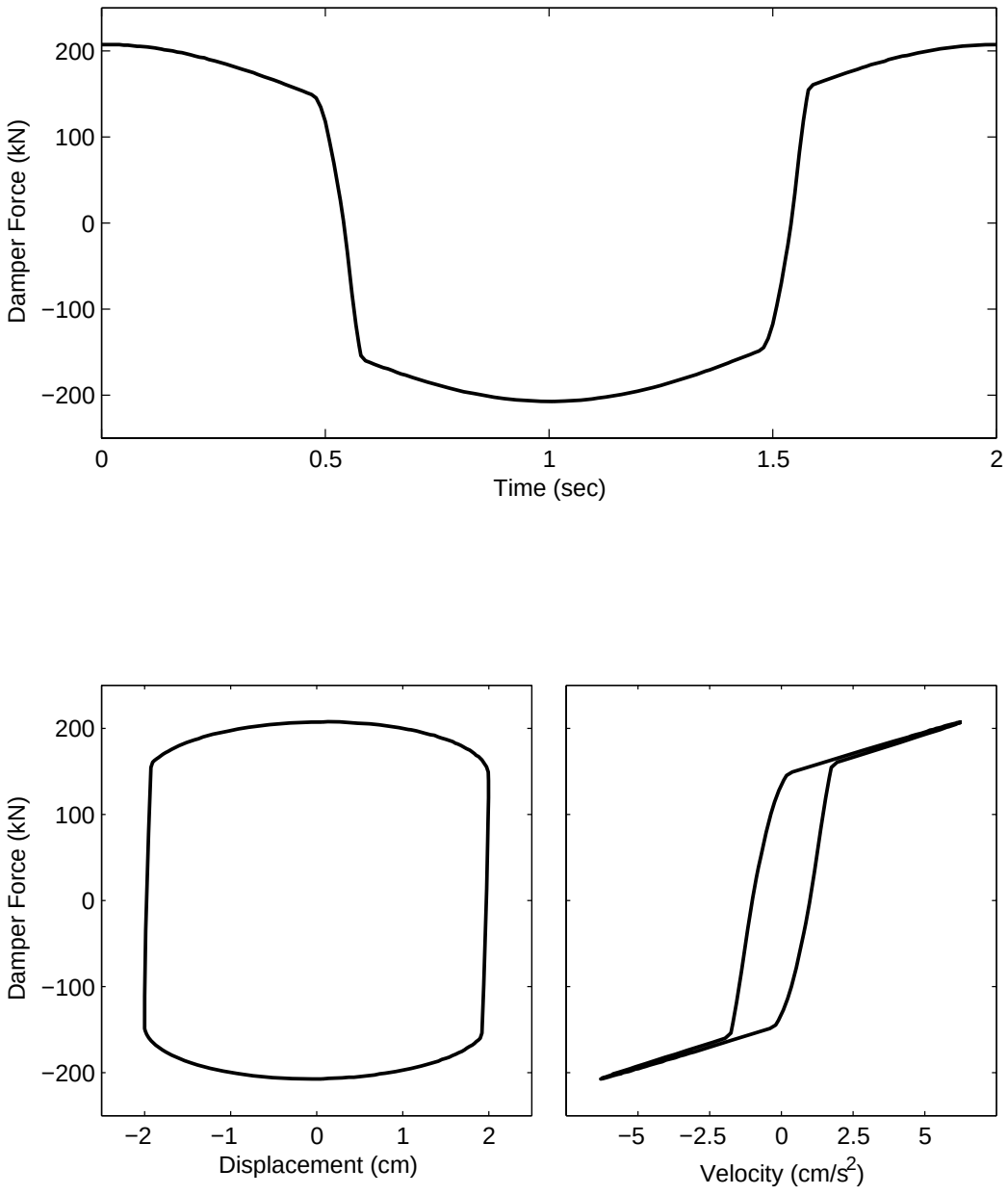


**Figure 3.4** Response characteristics of the mathematical model of the 20-ton MR damper under 1 Hz frequency and 2 cm amplitude sinusoidal excitation

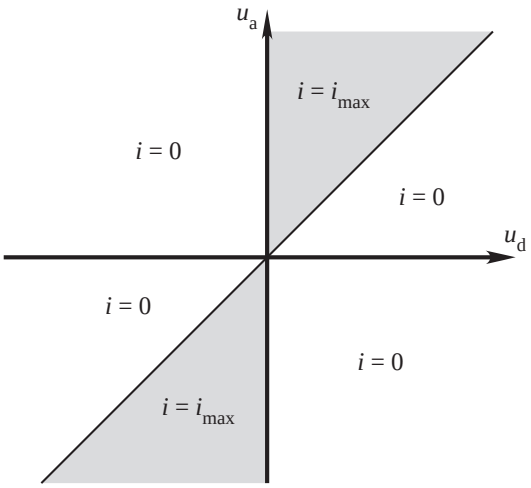


**Figure 3.5** Graphical representation of the secondary controller (Dyke *et al*. 1996)

# CHAPTER 4

# DISSIPATIVITY AND DISSIPATIVITY INDICES

## 4.1 Introduction

In this chapter, a review of the available dissipativity indices is given, and the proposed dissipativity indices are defined. For this purpose, a formal definition of a dissipative force is introduced.

## 4.2 Strictly Dissipative Force

Consider a continuous external force $f(x, t)$, which is applied to a system on a surface region $x \in \Omega$. Let $v(x, t)$ be the velocity of the surface (with positive velocity in the same direction as positive forces). The force $f(x, t)$ is called a *strictly dissipative force* if the rate of energy added is negative for all $t \geq 0$. Or, without loss of generality,

$$\int_{\Omega} f(x, t)v(x, t)d\Omega \leq \varepsilon(t) < 0, \quad \text{for all} \quad t \geq 0 \Leftrightarrow f(x, t) \text{ is strictly dissipative} \tag{4.1}$$

where $\varepsilon(t)$ is a strictly negative real function.

When the external force is a point load applied at point $x_0$ on the system, (4.1) simplifies to

$$f(t)v(t) \leq \varepsilon(t) < 0, \quad \text{for all} \quad t \geq 0 \Leftrightarrow f(t) \text{ is strictly dissipative}, \tag{4.2}$$

where $v(t)$ is the velocity of point $x_0$, and the location parameter $x_0$ is dropped for simplicity.

The definition given by (4.2) is more suitable for a control problem since the control force is generally modelled as a point load. This condition simply states that the directions of the force and the velocity are always opposite. In fact, this is the case for a damper. Therefore, a damper

force is a strictly dissipative force, and the rate it injects into the system is always negative (*i.e.*, it is always dissipating energy). In this dissertation, the term *dissipative force* is used instead of *strictly dissipative force* for convenience.

## 4.3 Previously Used Dissipativity Indices

### 4.3.1 Percentage of Dissipative Control Forces

The following deterministic index computes the percentage of the time that the primary control force commands dissipative forces:

$$D_{\%} = 1 - \frac{1}{T}\int_0^T H[u_{\mathrm{a}} v_{\mathrm{d}}]\,dt \tag{4.3}$$

where $H(\cdot)$ is the Heaviside unit step function. Since this index is deterministic, a discrete time representation is useful. For a time step $\Delta t = T/N$, $D_{\%}$ can be written as

$$D_{\%} = 1 - \frac{1}{N}\sum_{k=0}^{N-1} H[u_{\mathrm{a}}(k\Delta t) v_{\mathrm{d}}(k\Delta t)] \tag{4.4}$$

where $u_{\mathrm{a}}(k\Delta t)$ and $v_{\mathrm{d}}(k\Delta t)$ are the control force and the damper force at the time $k\Delta t$. The higher $D_{\%}$-value shows that the control force is more often dissipative.

### 4.3.2 Probability that the Control Force is Dissipative

For a linear system with stationary Gaussian responses, the probability that the control force is strictly dissipative is given by (Inaudi 2000)

$$D_{\mathrm{p}} = P[u_{\mathrm{a}} v_{\mathrm{d}} < 0] = \frac{\operatorname{acos}(\rho_{u_{\mathrm{a}} v_{\mathrm{d}}})}{\pi} \tag{4.5}$$

where $\rho_{u_a v_d}$ is the correlation coefficient between $u_a$ and $v_d$. For a linear system and a linear controller, $\rho_{u_a v_d}$ can be found by dividing the off-diagonal term to the square root of the product of the diagonal terms of the symmetric covariance matrix of the output $\mathbf{z} = [u_a \quad v_d]^T$.

## 4.4 Proposed Dissipativity Indices

### 4.4.1 Expected Value of the Energy Flow Rate

Since the dissipative force condition given by (4.2) is not stochastic, it cannot be directly used to examine a controller in a stochastic problem. Therefore, the expected value of this condition is given as follows:

$$E[u_a(t)v_d(t)] \le E[\varepsilon(t)] = \mu_\varepsilon(t) < 0 \Leftarrow u_a(t) \text{ is strictly dissipative} \tag{4.6}$$

Note that $E[u_a v_d] < 0$ does not necessarily mean that the control force is strictly dissipative or mostly strictly dissipative. However, it is clear that for values of $E[u_a v_d] \ll \mu_\varepsilon(t) < 0$, $u_a$ has a higher mean energy dissipation rate, which can be used as an indication of the dissipative nature of the control force. Therefore the following index is proposed:

$$D_e = E[u_a v_d] \tag{4.7}$$

$D_e$ is called the *mean energy flow rate* in this dissertation.

### 4.4.2 Normalized Mean Energy Flow Rate

One problem with $D_e$ is that it is not unitless; *i.e.*, a large magnitude of $D_e$ may be an indication of very large values of force $u_a$. To avoid this problem, a normalized index is also proposed as follows:

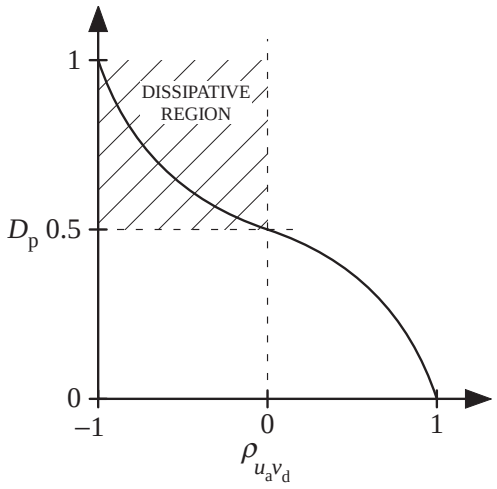


**Figure 4.1** Relation between $D_p$ and $\rho_{u_a v_d}$

$$D_{ne} = \frac{E[u_a v_d]}{\sqrt{E[u_a^2]}\sqrt{E[v_d^2]}} \tag{4.8}$$

$D_{ne}$ is called the *normalized mean energy flow rate* herein. Clearly, a negative value of $D_{ne}$ indicates the likelihood of the control force being strictly dissipative.

## 4.5 The Relation Between $D_p$ and $D_{ne}$ for an LQ Problem

In a standard LQ problem, all stochastic variables are zero-mean. Therefore, $D_{ne}$ is, in fact, the correlation coefficient between the force $u_a$ and the velocity $v_d$, *i.e.*, $D_{ne} = \rho_{u_a v_d}$. Therefore, $-1 \le D_{ne} \le 1$ holds. Moreover, since the denominator of $D_{ne}$ is always positive, then if $-1 \le D_{ne} < 0$ holds, the controller is more likely to produce strictly negative control forces. Also note that for $-1 \le D_{ne} < 0$, the probability index becomes $0.5 < D_p \le 1$ as shown in Figure 4.1. On the other hand, if $0 < D_{ne} \le 1$, the controller force is more likely to add energy to the system and $0 \le D_p < 0.5$.

## 4.6 Summary

In this chapter, a mathematical formalization of dissipativity in the context of semiactive control with smart dampers is provided. Two indices are introduced in addition to two previously used indices to quantify dissipativity. Also discussed is the relation between the indices $D_{\mathrm{p}}$ and $D_{\mathrm{ne}}$. These dissipativity indices will be used in the following chapters to obtain controllers that are better suited for smart dampers and to expose dissipativity-performance relations in semi-active structures.

# CHAPTER 5

# DISSIPATIVITY-BASED CONTROL VIA LMI SYNTHESIS

## 5.1 Introduction

In this chapter, an LMI-EVP that is equivalent to a standard LQR problem is derived. Then, two of the dissipativity indices are used to obtain so-called dissipativity constraints that can be appended to the EVP to obtain control forces with various dissipativity levels.

## 5.2 LMI-EVP Representation of an LQR Problem

A derivation of the LMI-EVP representation of an LQR problem is given utilizing the method summarized in Section 3.2.5. First, the LQR problem is redefined in a form suitable for LMI characterization as follows: consider the LQR problem given by (3.9) and (3.10). Let $\mathbf{Q}^{1/2}$ and $\mathbf{R}^{1/2}$ be real symmetric matrices that satisfy $\mathbf{Q}^{1/2}\mathbf{Q}^{1/2} = \mathbf{Q}$ and $\mathbf{R}^{1/2}\mathbf{R}^{1/2} = \mathbf{R}$. Using $\mathbf{u} = -\mathbf{K}\mathbf{q}$, optimization (3.9) can be written as

$$\begin{aligned} &\min_{\mathbf{K}} \; E[\mathbf{q}^{\mathrm{T}}\mathbf{Q}^{1/2}\mathbf{Q}^{1/2}\mathbf{q} + \mathbf{q}^{\mathrm{T}}\mathbf{K}^{\mathrm{T}}\mathbf{R}^{1/2}\mathbf{R}^{1/2}\mathbf{K}\mathbf{q} - \mathbf{q}^{\mathrm{T}}\mathbf{N}\mathbf{K}\mathbf{q} - \mathbf{q}^{\mathrm{T}}\mathbf{K}^{\mathrm{T}}\mathbf{N}^{\mathrm{T}}\mathbf{q}] \\ &\text{subject to} \;\; \dot{\mathbf{q}} = (\mathbf{A}-\mathbf{B}\mathbf{K})\mathbf{q} + \mathbf{E}\mathbf{w} \end{aligned} \tag{5.1}$$

Let $E[\mathbf{q}\mathbf{q}^{\mathrm{T}}] = \mathbf{P}$, which is the state covariance matrix; clearly, $\mathbf{P} = \mathbf{P}^{\mathrm{T}} > 0$ if $\mathbf{A} - \mathbf{B}\mathbf{K}$ is stable. Utilizing the trace operator $Tr(\cdot)$ and a Lyapunov equation, whose solution gives the state covariance matrix, to represent the stability of the system, optimization (5.1) can be written as

$$\begin{aligned} &\min_{\mathbf{K},\,\mathbf{P}} \; Tr(\mathbf{Q}^{1/2}\mathbf{P}\mathbf{Q}^{1/2}) + Tr(\mathbf{R}^{1/2}\mathbf{K}\mathbf{P}\mathbf{K}^{\mathrm{T}}\mathbf{R}^{1/2}) - Tr(\mathbf{K}\mathbf{P}\mathbf{N}) - Tr(\mathbf{N}^{\mathrm{T}}\mathbf{P}\mathbf{K}^{\mathrm{T}}) \\ &\text{subject to} \;\; (\mathbf{A}-\mathbf{B}\mathbf{K})\mathbf{P} + \mathbf{P}(\mathbf{A}-\mathbf{B}\mathbf{K})^{\mathrm{T}} + \mathbf{E}\mathbf{E}^{\mathrm{T}} = 0, \qquad \mathbf{P} = \mathbf{P}^{\mathrm{T}} > 0 \end{aligned} \tag{5.2}$$

Having redefined the LQR problem in a form suitable for LMI characterization, the LMI-EVP representation can be found using the first step of the aforementioned method (Scherer *et al*. 1997). For this purpose, the following optimization problem for the closed loop system $\dot{\mathbf{q}} = \mathbf{Aq} + \mathbf{Bu} + \mathbf{Ew}$ and $\mathbf{u} = -\mathbf{Fq}$ is defined:

$$\begin{aligned} &\min_{\mathbf{F},\,\mathbf{S}} \; Tr(\mathbf{Q}^{1/2}\mathbf{S}\mathbf{Q}^{1/2}) + Tr(\mathbf{R}^{1/2}\mathbf{F}\mathbf{S}\mathbf{F}^{\mathrm{T}}\mathbf{R}^{1/2}) - Tr(\mathbf{F}\mathbf{S}\mathbf{N}) - Tr(\mathbf{N}^{\mathrm{T}}\mathbf{S}\mathbf{F}^{\mathrm{T}}) \\ &\text{subject to} \;\; (\mathbf{A}-\mathbf{B}\mathbf{F})\mathbf{S} + \mathbf{S}(\mathbf{A}-\mathbf{B}\mathbf{F})^{\mathrm{T}} + \mathbf{E}\mathbf{E}^{\mathrm{T}} < 0, \qquad \mathbf{S} = \mathbf{S}^{\mathrm{T}} > 0 \end{aligned} \tag{5.3}$$

where $\mathbf{S}$ is the Lyapunov matrix. It is proposed that the solution of (5.2) is indeed equivalent to the solution of (5.3); *i.e.*, if $\mathbf{K}_0$ and $\mathbf{P}_0$ are the solutions to (5.2), and $\mathbf{F}_0$ and $\mathbf{S}_0$ are the solutions to (5.3), then $\mathbf{K}_0 = \mathbf{F}_0$ and $\mathbf{P}_0 = \mathbf{S}_0$. One should note that although $\mathbf{S}$ does not represent the state covariance matrix, the solution of (5.3), $\mathbf{S}_0$, is equal to the state covariance matrix. Proof of this proposition is given next. For this purpose, some useful corollaries are given first. In corollaries 5.1 to 5.5 and Lemma 5.6, it is assumed that $\mathbf{S} = \mathbf{S}^{\mathrm{T}} > 0$, $\mathbf{P} = \mathbf{P}^{\mathrm{T}} > 0$ and $\mathbf{A}$ is Hurwitz. Also, the following shorthand notations are used: $\mathbf{L}_\mathbf{S} \equiv \mathbf{AS} + \mathbf{SA}^{\mathrm{T}} + \Psi$ and $\mathbf{L}_\mathbf{P} \equiv \mathbf{AP} + \mathbf{PA}^{\mathrm{T}} + \Psi$ where $\Psi = \Psi^{\mathrm{T}} > 0$.

**Corollary 5.1** $\mathbf{S} > \mathbf{P} \Leftrightarrow \mathbf{L}_\mathbf{S} < \mathbf{L}_\mathbf{P}$.

*Proof:* $\mathbf{S} > \mathbf{P} \Leftrightarrow \mathbf{S} - \mathbf{P} > 0 \Leftrightarrow \mathbf{A}(\mathbf{S} - \mathbf{P}) + (\mathbf{S} - \mathbf{P})\mathbf{A}^{\mathrm{T}} < 0 \Leftrightarrow \mathbf{AS} + \mathbf{SA}^{\mathrm{T}} < \mathbf{AP} + \mathbf{PA}^{\mathrm{T}} \Leftrightarrow \mathbf{L}_\mathbf{S} < \mathbf{L}_\mathbf{P}$.

**Corollary 5.2** $\mathbf{L}_\mathbf{S} < 0$ and $\mathbf{L}_\mathbf{P} = \mathbf{0} \Rightarrow \mathbf{S} > \mathbf{P}$. This is a consequence of corollary 5.1.

**Corollary 5.3** $\Phi = \Phi^{\mathrm{T}} > 0 \Rightarrow Tr(\mathbf{C}\Phi\mathbf{C}^{\mathrm{T}}) > 0$.

*Proof:* Let $\mathbf{c}_i$ be the $i^{\text{th}}$ row of $\mathbf{C}$. Then, $\Phi > 0 \Leftrightarrow \mathbf{c}_i\Phi\mathbf{c}_i^{\mathrm{T}} > 0 \;\; \forall i \Rightarrow \sum_i \mathbf{c}_i\Phi\mathbf{c}_i^{\mathrm{T}} = Tr(\mathbf{C}\Phi\mathbf{C}^{\mathrm{T}}) > 0$.

**Corollary 5.4** $\mathbf{S} > \mathbf{P} \Rightarrow Tr(\mathbf{CSC}^{\mathrm{T}}) > Tr(\mathbf{CPC}^{\mathrm{T}})$.

*Proof:* $\mathbf{S} > \mathbf{P} \Leftrightarrow \mathbf{S} - \mathbf{P} > 0 \Rightarrow Tr[\mathbf{C}(\mathbf{S} - \mathbf{P})\mathbf{C}^{\mathrm{T}}] > 0 \Leftrightarrow Tr(\mathbf{CSC}^{\mathrm{T}} - \mathbf{CPC}^{\mathrm{T}}) > 0 \Leftrightarrow$ $Tr(\mathbf{CSC}^{\mathrm{T}}) - Tr(\mathbf{CPC}^{\mathrm{T}}) > 0 \Leftrightarrow Tr(\mathbf{CSC}^{\mathrm{T}}) > Tr(\mathbf{CPC}^{\mathrm{T}})$.

**Corollary 5.5** Let $S = \{\mathbf{S} | \mathbf{L}_{\mathbf{S}} < 0\}$. Then, there exists a unique matrix $\mathbf{P}_0$ such that $\mathbf{P}_0 = [\mathbf{P} | \mathbf{L}_{\mathbf{P}} = 0]$ and $\mathbf{P}_0 < \mathbf{S}$ for any $\mathbf{S} \in S$. Moreover, $Tr(\mathbf{CP}_0\mathbf{C}^{\mathrm{T}}) < Tr(\mathbf{CSC}^{\mathrm{T}})$ holds for any $\mathbf{S} \in S$.

*Proof:* See corollaries 5.2 and 5.4.

**Lemma 5.6** Let $\mathbf{P}_0 = [\mathbf{P} | \mathbf{L}_{\mathbf{P}} = 0]$

$$\begin{aligned} \mathbf{S}_0 = \arg \min_{\mathbf{S}} \quad & Tr(\mathbf{CSC}^{\mathrm{T}}) \\ \text{subject to} \quad & \mathbf{L}_{\mathbf{S}} \le 0 \end{aligned} \tag{5.4}$$

Then, $\mathbf{S}_0 = \mathbf{P}_0$ and $Tr(\mathbf{CS}_0\mathbf{C}^{\mathrm{T}}) = Tr(\mathbf{CP}_0\mathbf{C}^{\mathrm{T}})$. The proof is readily obtained using Corollary 5.5.

**Theorem 5.7** The problems given by (5.2) and (5.3) are equivalent.

*Proof:* It can be shown with some matrix algebra that the objective function in the LQR problem can be written as

$$\begin{aligned} Tr(\mathbf{Q}^{1/2}\mathbf{PQ}^{1/2}) + Tr(\mathbf{R}^{1/2}\mathbf{KPK}^{\mathrm{T}}\mathbf{R}^{1/2}) - Tr(\mathbf{KPN}) - Tr(\mathbf{N}^{\mathrm{T}}\mathbf{PK}^{\mathrm{T}}) \\ = Tr[\mathbf{C}_{\underset{\sim}{z}}(\mathbf{K})\mathbf{P}\mathbf{C}_{\underset{\sim}{z}}^{\mathrm{T}}(\mathbf{K})] \end{aligned} \tag{5.5}$$

where

$$\mathbf{C}_{\underset{\sim}{z}}(\mathbf{K}) = \begin{bmatrix} \mathbf{Q}^{1/2} - \Upsilon\mathbf{K} \\ \Upsilon^{\mathrm{T}} - \mathbf{R}^{1/2}\mathbf{K} \end{bmatrix} \tag{5.6}$$

for real symmetric matrices $\mathbf{Q}^{1/2}$ and $\mathbf{R}^{1/2}$. Note that there is not necessarily a unique $\Upsilon$ for a given $\mathbf{N}$ in (5.5). The gain in problem (5.2) can be found as

$$\mathbf{K}_0 = \arg \min_{\mathbf{K}} Tr[\mathbf{C}_{\underset{\sim}{z}}(\mathbf{K})\mathbf{P}_0(\mathbf{K})\mathbf{C}_{\underset{\sim}{z}}(\mathbf{K})] \tag{5.7}$$

where $\mathbf{A}_c(\mathbf{K}) = \mathbf{A} - \mathbf{B}\mathbf{K}$

$$\mathbf{P}_0(\mathbf{K}) = [\mathbf{P} \mid \mathbf{A}_c(\mathbf{K})\mathbf{P} + \mathbf{P}\mathbf{A}_c^{\mathrm{T}}(\mathbf{K}) + \mathbf{E}\mathbf{E}^{\mathrm{T}} = 0] \tag{5.8}$$

Similarly, the gain in problem (5.3) can be written as

$$\mathbf{F}_0 = \arg \min_{\mathbf{F}} Tr[\mathbf{C}_{\underset{\sim}{z}}(\mathbf{F})\mathbf{S}_0(\mathbf{F})\mathbf{C}_{\underset{\sim}{z}}(\mathbf{F})] \tag{5.9}$$

where

$$\mathbf{S}_0(\mathbf{K}) = \underset{\mathbf{S}}{\operatorname{argmin}}\ Tr[\mathbf{C}_{\underset{\sim}{z}}(\mathbf{K})\mathbf{S}\mathbf{C}_{\underset{\sim}{z}}^{\mathrm{T}}(\mathbf{K})] \quad \text{and} \quad \mathbf{A}_c(\mathbf{K}) = \mathbf{A} - \mathbf{B}\mathbf{K} \tag{5.10}$$
$$\text{subject to } \mathbf{A}_c(\mathbf{K})\mathbf{S} + \mathbf{S}\mathbf{A}_c^{\mathrm{T}}(\mathbf{K}) + \mathbf{E}\mathbf{E}^{\mathrm{T}} \le 0$$

Using Lemma 5.6, one can show that the matrix functions given by equations (5.8) and (5.10) are equal. Therefore, $\mathbf{K}_0 = \mathbf{F}_0$ and $\mathbf{P}_0(\mathbf{K}_0) = \mathbf{S}_0(\mathbf{F}_0)$. Note that a strict inequality is used in (5.3) while a (5.10) is a semidefinite problem. As discussed before, from a numerical point of view, the strict and nonstrict versions of the inequalities do not make a difference in the solutions.

The main difference between the problems (5.2) and (5.3) — *i.e.*, the inequality condition — allows one to add additional constraints to the LQR problem. It is clear that the addition of a new constraint will result in $\mathbf{S}_0 \ge \mathbf{P}_0$. Therefore, the solution of (5.3) with additional inequality constraints is expected to give larger states (though possibly a more robust controller) than a standard LQR. This concept can also be used to explain the difference between active and semiactive control. Let $\mathbf{S}_d$ and $\mathbf{P}_0$ be the Lyapunov matrices obtained from the LQR problem with the dissipativity constraint and without it. For $\mathbf{S}_d$ to be equal to $\mathbf{P}_0$, the Lyapunov dissipativity must be

equal to the mean closed-loop dissipativity, which is practically impossible if higher mean dissipativity is desired. A high dissipativity will result in $\mathbf{S}_d > \mathbf{P}_0$, *i.e.*, increased states and robustness.

The optimization problem (5.3) is not exactly in the form of the EVP (3.6) since it includes the multiplicative terms $\mathbf{FS}$ (*i.e.*, the objective function is not linear), and the first inequality constraint is a BMI (i.e, the constraint is not convex). To convert the BMI constraint into an LMI constraint, a new variable $\mathbf{Y} = \mathbf{FS}$ is introduced, and (5.3) becomes

$$\begin{aligned} &\min_{\mathbf{Y},\,\mathbf{S}} \; Tr(\mathbf{Q}^{1/2}\mathbf{S}\mathbf{Q}^{1/2}) + Tr(\mathbf{R}^{1/2}\mathbf{Y}\mathbf{S}^{-1}\mathbf{Y}^{\mathrm{T}}\mathbf{R}^{1/2}) - Tr(\mathbf{Y}\mathbf{N}) - Tr(\mathbf{N}^{\mathrm{T}}\mathbf{Y}^{\mathrm{T}}) \\ &\text{subject to} \;\; \mathbf{A}\mathbf{S} - \mathbf{B}\mathbf{Y} + \mathbf{S}\mathbf{A}^{\mathrm{T}} - \mathbf{Y}^{\mathrm{T}}\mathbf{B}^{\mathrm{T}} + \mathbf{E}\mathbf{E}^{\mathrm{T}} < 0, \qquad \mathbf{S} = \mathbf{S}^{\mathrm{T}} > 0 \end{aligned} \tag{5.11}$$

The nonlinear term in the objective function can be represented as the solution to an optimization

$$Tr(\mathbf{R}^{1/2}\mathbf{Y}\mathbf{S}^{-1}\mathbf{Y}^{\mathrm{T}}\mathbf{R}^{1/2}) \;=\; \begin{bmatrix} \min\limits_{\mathbf{X}} \; Tr(\mathbf{X}) \\ \text{subject to} \;\; \mathbf{X} > \mathbf{R}^{1/2}\mathbf{Y}\mathbf{S}^{-1}\mathbf{Y}^{\mathrm{T}}\mathbf{R}^{1/2} \end{bmatrix} \tag{5.12}$$

where $\mathbf{X}$ is an auxiliary parameter. The inequality in (5.12) can be rewritten using the Schur complement formula

$$\begin{bmatrix} \mathbf{X} & \mathbf{R}^{1/2}\mathbf{Y} \\ \mathbf{Y}^{\mathrm{T}}\mathbf{R}^{1/2} & \mathbf{S} \end{bmatrix} > 0 \tag{5.13}$$

Therefore the problem (5.11) can be written as

$$\begin{aligned} &\min_{\mathbf{Y},\,\mathbf{S},\,\mathbf{X}} \; Tr(\mathbf{Q}^{1/2}\mathbf{S}\mathbf{Q}^{1/2}) + Tr(\mathbf{X}) - Tr(\mathbf{Y}\mathbf{N}) - Tr(\mathbf{N}^{\mathrm{T}}\mathbf{Y}^{\mathrm{T}}) \\ &\text{subject to} \;\; \mathbf{A}\mathbf{S} - \mathbf{B}\mathbf{Y} + \mathbf{S}\mathbf{A}^{\mathrm{T}} - \mathbf{Y}^{\mathrm{T}}\mathbf{B}^{\mathrm{T}} + \mathbf{E}\mathbf{E}^{\mathrm{T}} < 0, \quad \begin{bmatrix} \mathbf{X} & \mathbf{R}^{1/2}\mathbf{Y} \\ \mathbf{Y}^{\mathrm{T}}\mathbf{R}^{1/2} & \mathbf{S} \end{bmatrix} > 0, \quad \mathbf{S} > 0 \end{aligned} \tag{5.14}$$

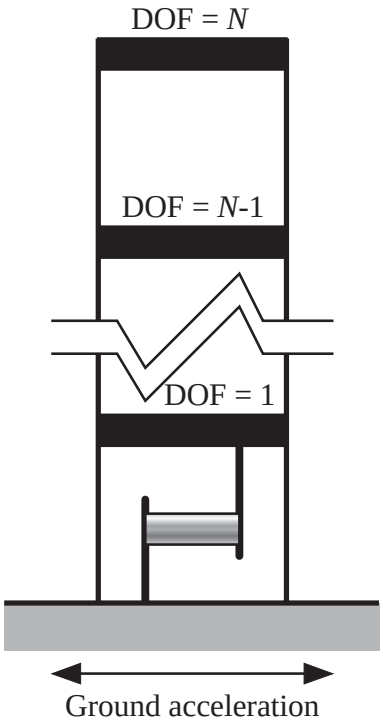


**Figure 5.1** A sample *N*-DOF structure

Problem (5.14) is equivalent to the standard LQR problem defined by (3.8), and the feedback gain is then given by $\mathbf{K}_0 = \mathbf{F}_0 = \mathbf{Y}_0\mathbf{S}_0^{-1}$.

A MATLAB® implementation of the EVP (5.14) using the MATLAB® LMI Control Toolbox is given in the Appendix.

## 5.3 Verification of LQR-EVP Equivalence

In this section, the equivalency of the LQR problem given by (3.9) and the EVP given by (5.14) is investigated through a simple numerical example. In this example, a general *N*-DOF structure is considered where a controller is located in the first story as shown in Figure 5.1. The mass of each story is taken as 100 tons, the stiffness of each story is selected such that the story

**Table 5.1:** Control gains and covariances matrices[a] from LMI-EVP and LQR approaches

| | LMI | | | | LQR | | | |
|---|---|---|---|---|---|---|---|---|
| **K** | 16440.77 | 8539.46 | 24199.28 | 14728.74 | 16440.77 | 8539.46 | 24199.28 | 14728.74 |
| **P** | $9.86\times10^{-3}$ | $1.57\times10^{-2}$ | $-3.94\times10^{-17}$ | $-4.08\times10^{-5}$ | $9.86\times10^{-3}$ | $1.57\times10^{-2}$ | $1.57\times10^{-16}$ | $-4.08\times10^{-5}$ |
| | $1.57\times10^{-2}$ | $2.56\times10^{-2}$ | $-4.08\times10^{-5}$ | $-5.33\times10^{-17}$ | $1.57\times10^{-2}$ | $2.56\times10^{-2}$ | $-4.08\times10^{-5}$ | $2.36\times10^{-16}$ |
| | $-3.94\times10^{-17}$ | $4.08\times10^{-5}$ | 0.631 | 0.929 | $1.57\times10^{-16}$ | $4.08\times10^{-5}$ | 0.631 | 0.929 |
| | $-4.08\times10^{-5}$ | $-5.33\times10^{-17}$ | 0.929 | 1.56 | $-4.08\times10^{-5}$ | $2.36\times10^{-16}$ | 0.929 | 1.56 |

a. with appropriate SI units

natural period corresponds to 0.5 sec, and a modal damping ratio of 2% of the critical damping is considered for all modes. A MATLAB® code is provided for generation of the model for this structure in the Appendix.

As an initial example, a 2-DOF structure is considered. The equivalency of the LQR problem and the LMI-EVP are verified for a set of design parameters given by

$$\mathbf{Q} = \begin{bmatrix} \mathbf{K} & \mathbf{0} \\ \mathbf{0} & \mathbf{M} \end{bmatrix} \qquad \mathbf{R} = 10^{-4}\ \text{m/N} \qquad \mathbf{N} = [1 \quad 1 \quad 1\text{s} \quad 1\text{s}]^{\mathrm{T}} \tag{5.15}$$

where $\mathbf{K}$ and $\mathbf{M}$ are the stiffness and mass matrices, respectively. This set of parameters satisfies the positive definite inequality (3.11). Table 5.1 shows that the gains and covariance matrices obtained from LQR and LMI approaches are identical within numerical round-off accuracy. Also, other weighting matrix sets that satisfy the positive definite inequality (3.11) are observed to give identical gains and covariances, whereas those not satisfying (3.11) give different results as the LQR optimization problem is then improper. It is also observed that the two approaches give different results for some control designs, even though inequality (3.11) is satisfied; for these designs, it is found that the smallest eigenvalue of $\mathbf{W}$ in (3.11) is very close to zero, *e.g.,* $o(10^{-10})$, which causes numerical problems in the solution.

To investigate the effects of more degrees-of-freedom on the efficiency of the EVP solver, the analysis explained for the 2-DOF structure above is applied to a shear building with various numbers of floors. Control design parameters similar to (5.15) are utilized for these structures. The difference in the LQR and LMI-EVP gains and covariance matrices are observed through several error indices:

$$E_1 = \frac{\min(\left|\mathbf{K}_{ij}^{\mathrm{LMI}}\right|) - \min(\left|\mathbf{K}_{ij}^{\mathrm{LQR}}\right|)}{\min(\left|\mathbf{K}_{ij}^{\mathrm{LQR}}\right|)} \qquad E_2 = \frac{\max(\left|\mathbf{K}_{ij}^{\mathrm{LMI}}\right|) - \max(\left|\mathbf{K}_{ij}^{\mathrm{LQR}}\right|)}{\max(\left|\mathbf{K}_{ij}^{\mathrm{LQR}}\right|)} \tag{5.16}$$

$$E_3 = \frac{\min(\left|\lambda_i^{\mathrm{LMI}}\right|) - \min(\left|\lambda_i^{\mathrm{LQR}}\right|)}{\min(\left|\lambda_i^{\mathrm{LQR}}\right|)} \qquad E_4 = \frac{\max(\left|\lambda_i^{\mathrm{LMI}}\right|) - \max(\left|\lambda_i^{\mathrm{LQR}}\right|)}{\max(\left|\lambda_i^{\mathrm{LQR}}\right|)} \tag{5.17}$$

Here, $\min(\left|\mathbf{K}_{ij}^{\mathrm{LMI}}\right|)$ and $\min(\left|\mathbf{K}_{ij}^{\mathrm{LQR}}\right|)$ are the element-wise minimum of absolute control gain vectors obtained from the EVP solution and LQR solution, respectively. Similarly, $\min(\left|\lambda_i^{\mathrm{LMI}}\right|)$ and $\min(\left|\lambda_i^{\mathrm{LQR}}\right|)$ are the smallest eigenvalues of the covariance matrices obtained from the EVP solution and LQR solution, respectively. The options vector is selected as [1e–30, 100, –1, 10, 1] (see the LMI Control Toolbox for details). The rest of the terms are self explanatory. A 2.4 GHz Pentium 4 personal computer with a 512 MB RAM is used for the simulations. The versions of the MATLAB® and LMI Control Toolbox used are 6.5.0.180913a and 1.0.8 (R13), respectively.

The error indices are shown in Figure 5.2, and the time required for the LMI solver to solve the EVP is shown in Figure 5.3. It is clear that the LMI solver is very efficient for degrees of freedom smaller than 10, which corresponds to 20 states. However, for larger problems, error and time efficiency is not adequate.

It is strongly emphasized that the results provided above are for the structure shown in Figure 5.1 and cannot be generalized to the LMI-solver software itself. In general, LMI solvers use

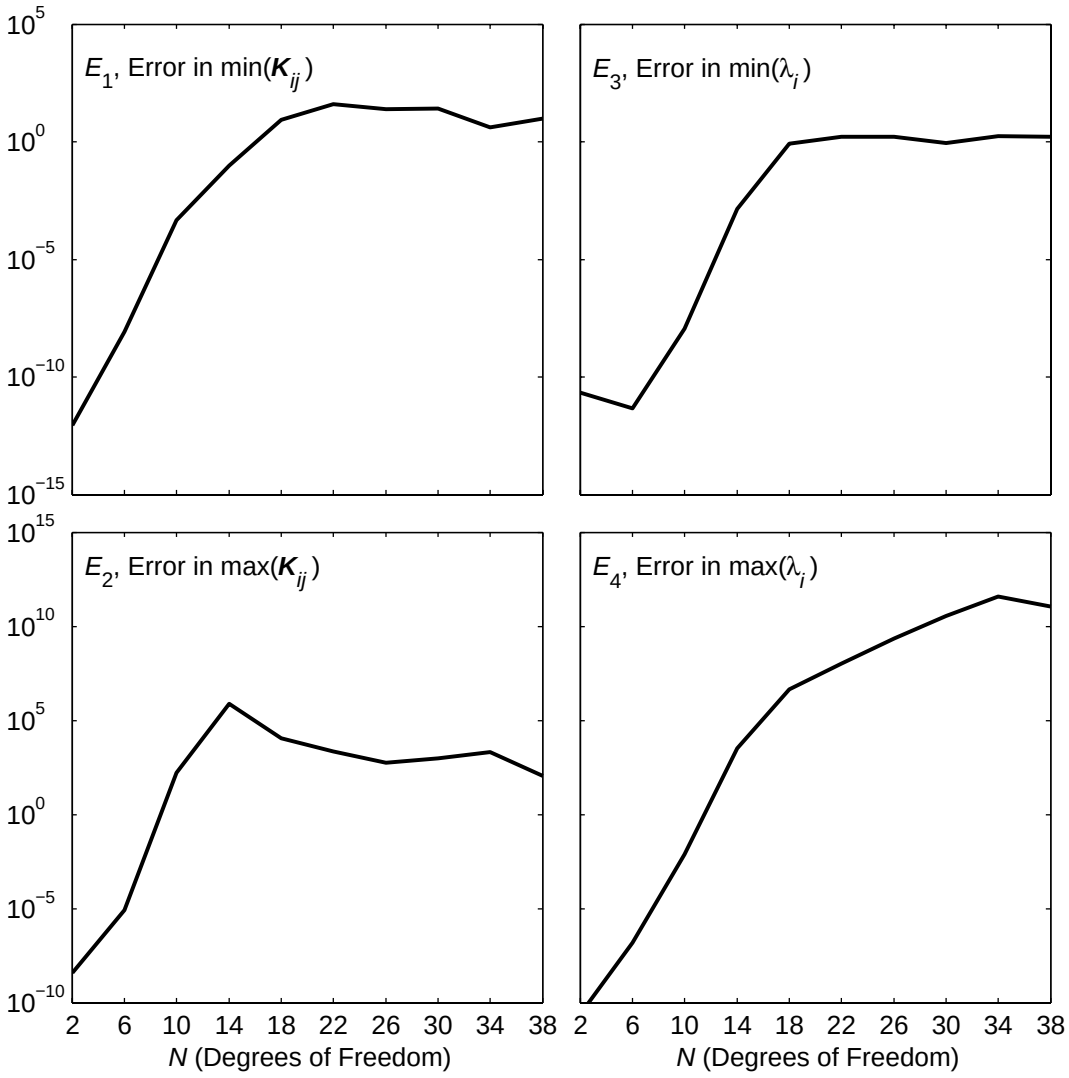


**Figure 5.2** Error indices $E_1$, $E_2$, $E_3$ and $E_4$ in the LQR-EVP equivalency study

very complex algorithms for the solution of EVPs, which makes it difficult to comment on the source of the error level and computational intensity of these results.

## 5.4 Dissipativity Constraints

In this section, the dissipativity indices are used to obtain dissipativity matrix inequality constraints that are suitable for the LMI-EVP. Among the indices given, $D_{\%}$ and $D_{\mathrm{d}}$ cannot be rep-

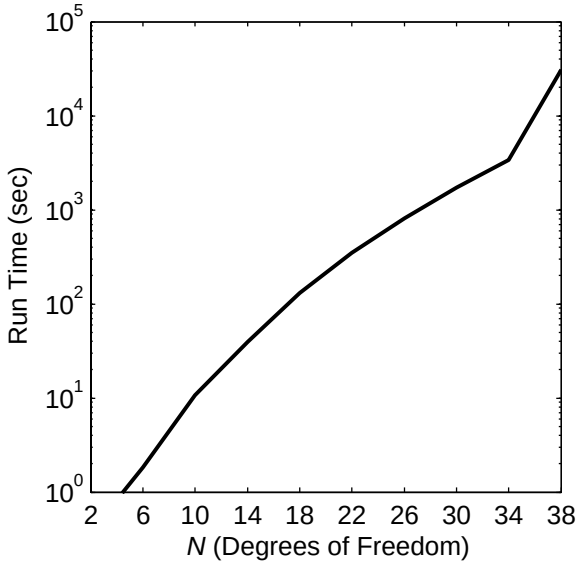


**Figure 5.3** Time required for the LMI solver to solve the EVP for various degrees of freedom

resented in a manner suitable for the LQR problem since they are deterministic. To find a constraint for $D_\mathrm{p}$, $\rho_{u_\mathrm{a}v_\mathrm{d}}$ is represented in a form suitable for the EVP first. Let the velocity of the system at the point where the damper exerts force be given by $v = \mathbf{C}_\mathrm{v}\mathbf{q}$. Since the LQR control force is a feedback force as $u_\mathrm{a} = -\mathbf{F}\mathbf{q}$, $\rho_{u_\mathrm{a}v_\mathrm{d}}$ can be written as

$$\rho_{u_\mathrm{a}v_\mathrm{d}} = \frac{E[-\mathbf{F}\mathbf{q}(\mathbf{C}_\mathrm{v}\mathbf{q})^\mathrm{T}]}{\sqrt{E[-\mathbf{F}\mathbf{q}(-\mathbf{F}\mathbf{q})^\mathrm{T}]}\sqrt{E[\mathbf{C}_\mathrm{v}\mathbf{q}(\mathbf{C}_\mathrm{v}\mathbf{q})^\mathrm{T}]}}. \tag{5.18}$$

Using the state covariance matrix $\mathbf{P} = E[\mathbf{q}\mathbf{q}^\mathrm{T}]$, a constraint for $D_\mathrm{p}$ is obtained as

$$\frac{1}{\pi}\mathrm{acos}\left(\frac{-\mathbf{F}\mathbf{P}\mathbf{C}_\mathrm{v}^\mathrm{T}}{\sqrt{\mathbf{F}\mathbf{P}\mathbf{F}^\mathrm{T}}\sqrt{\mathbf{C}_\mathrm{v}\mathbf{P}\mathbf{C}_\mathrm{v}^\mathrm{T}}}\right) > \gamma_\mathrm{p} \quad \text{where} \quad 0 \le \gamma_\mathrm{p} \le 1 \tag{5.19}$$

Using the same notation, a constraint for $D_\mathrm{e}$ is found as

$$-\mathbf{F}\mathbf{P}\mathbf{C}_\mathrm{v}^\mathrm{T} < \gamma_\mathrm{e}. \tag{5.20}$$

Similarly, a constraint for $D_{ne}$ is given by

$$\frac{-\mathbf{FPC}_v^T}{\sqrt{\mathbf{FPF}^T}\sqrt{\mathbf{C}_v\mathbf{PC}_v^T}} < \gamma_{ne} \quad \text{where} \quad -1 \le \gamma_{ne} \le 1 \tag{5.21}$$

Clearly, the conditions given by

$$0.5 \le \gamma_p \le 1, \qquad \gamma_e < 0, \qquad -1 \le \gamma_{ne} < 0 \tag{5.22}$$

are more desired as the primary control force is more likely to dissipate energy for these values.

The constraints given by (5.19), (5.20) and (5.21) should be represented in terms of Lyapunov matrices to be used in the EVP. In the following, (5.20) and (5.21) are represented in terms of Lyapunov matrices. The $D_p$-based constraint is not considered further since it includes a sinusoidal function and is not suitable for the EVP by nature.

### 5.4.1 $D_e$-Based Dissipativity Constraint

To find a $D_e$-based dissipativity constraint that can be appended to the EVP, (5.20) should be represented in terms of a Lyapunov matrix, which will be designated as $\mathbf{S}_e$ herein. The introduction of $\mathbf{S}_e$ requires the addition of the equality constraint given by

$$(\mathbf{A}-\mathbf{BF})\mathbf{S}_e + \mathbf{S}_e(\mathbf{A}-\mathbf{BF})^T + \mathbf{EE}^T = 0 \tag{5.23}$$

However, if the equality constraint (5.23) is enforced in the EVP, the EVP will no longer be an LMI problem and cannot be solved by available techniques. Therefore, the equality constraint is relaxed, and the following constraint is used:

$$-\mathbf{FSC}_v^T < \gamma_e^L \tag{5.24}$$

There are several advantages and disadvantages of this constraint. First of all, (5.24) does not fully represent the index $D_e$ since the equality constraint (5.23) is dropped. Also, the term

$-\mathbf{FSC}_v^T$ is not a normalized index. However, this constraint simply allows a numerical solution to this sophisticated multiobjective problem, which is actually the fundamental philosophy behind the LMI-EVP approach.

### 5.4.2 $D_{ne}$-Based Dissipativity Constraint

To find a $D_{ne}$-based dissipativity constraint that can be appended to the EVP, (5.21) has to be represented in terms of a Lyapunov matrix, which will be designated by $\mathbf{S}_{ne}$, and the following equality constraint has to be introduced:

$$(\mathbf{A}-\mathbf{BF})\mathbf{S}_{ne} + \mathbf{S}_{ne}(\mathbf{A}-\mathbf{BF})^T + \mathbf{EE}^T = 0 \tag{5.25}$$

Similar to the discussion given for the $D_e$-constraint, this equality constraint is relaxed to have a solvable EVP and the following constraint is obtained:

$$\frac{-\mathbf{FSC}_v^T}{\sqrt{\mathbf{FSF}^T}\sqrt{\mathbf{C}_v\mathbf{SC}_v^T}} < \gamma_{ne}^L \quad \text{where} \quad -1 \le \gamma_{ne}^L \le 1 \tag{5.26}$$

The constraint (5.26) is a nonlinear inequality constraint and, therefore, constitutes a very major challenge. Due to the complexity of this constraint, an equivalent LMI (or BMI) may not be available. Therefore, a numerical solution of the EVP with the constraint (5.26) is not guaranteed by the available solution techniques used for LMIs. In fact, substantial research may be required for the development of new techniques specific to (5.26) to obtain an at-least-local solution, which is out of the scope of this study. Instead, an iterative method is proposed to implement (5.26) with the EVP defined above. This method will be introduced in the following chapter.

## 5.5 Summary

In this chapter, an LMI-based EVP is derived to represent a standard LQR problem. The difference between these two representations is that the constraints are represented in terms of matrix inequalities in the EVP, while the LQR has equality constraints. Then, the equivalency of the proposed EVP to original LQR is shown by a numerical example. It is observed that for large-order systems, the LMI solution may not be efficient due to numerical errors and computational time cost. Finally, two of the dissipativity indices are represented in terms of matrix inequalities suitable for the LMI-EVP.

# CHAPTER 6

# DISSIPATIVITY ANALYSIS OF SIMPLE 2-DOF SYSTEMS

## 6.1 Introduction

This chapter consists of two main parts. In the first part, two numerical examples are investigated to understand how dissipativity characteristics of a semiactive system are related to the overall semiactive performance using the LMI-EVP with the $D_e$-dissipativity constraint. The first example is a simple two-degree-of-freedom shear structure where an ideal smart damper is placed in the first story. The second example is a simple highway bridge model with a rubber bearing and an MR damper between the superstructure and the substructure. For each example, a set of LQR controller parameters is defined, and the structural system is analyzed numerically for white noise excitations, with and without the $D_e$-dissipativity constraint (5.24). The performances and dissipativity characteristics are presented graphically. The control systems investigated for the 2-DOF building and bridge models are summarized in Table 6.1 and explained below.

- *Act-LQR*: This is a theoretical fully active system. A fictitious fully active actuator is used instead of a smart damper. Standard LQR is used to command the actuator.
- *Act-LMI*: This system is also a theoretical fully active system. A fictitious fully active actuator is used instead of a smart damper. The proposed LMI-EVP controller with the dissipativity constraint is utilized instead of the standard LQR to observe how the added dissipativity constraint changes the dissipative nature of the active control force.

**Table 6.1:** A summary of the systems analyzed in the numerical examples

| Systems | Control Device | Control Strategy | Primary Controller | $-\mathbf{F}\mathbf{S}\mathbf{C}_{\mathrm{v}}^{\mathrm{T}} < \gamma_{\mathrm{e}}^{\mathrm{L}}$ |
|---|---|---|---|---|
| Act | Fully Active | LQR | — | Not Incl. |
| Act-Dis | Fully Active | LMI-EVP | — | Included |
| SAct | Smart Damper | Clipped Opt. | LQR | Not Incl. |
| SAct-Dis | Smart Damper | Clipped Opt. | LMI-EVP | Included |

- *SAct-LQR*: This is a semiactive system where a smart damper is used. A two-stage clipped optimal control strategy is utilized to command the smart damper. The primary controller in the clipped optimal control is a standard LQR controller.
- *SAct-LMI*: This is also a semiactive system where a smart damper is used. A two-stage clipped optimal control strategy is utilized to command the smart damper. The primary controller in the clipped optimal control is the proposed LMI-EVP controller with the dissipativity constraint.

In the second part, an iterative method to solve the LMI-EVP with the $D_{\mathrm{ne}}$-dissipativity constraint is proposed, and the 2-DOF building is used to test the method. Graphical results are provided for this study.

## 6.2 LMI-EVP with the $D_{\mathrm{e}}$-Based Constraint

In this section, the LMI-EVP problem with the $D_{\mathrm{e}}$-based constraint is considered. The modified LQR is given by

$$\begin{aligned} \min_{\mathbf{Y},\,\mathbf{S},\,\mathbf{X}} \quad & Tr(\mathbf{Q}^{1/2}\mathbf{S}\mathbf{Q}^{1/2}) + Tr(\mathbf{X}) - Tr(\mathbf{Y}\mathbf{N}) - Tr(\mathbf{N}^{\mathrm{T}}\mathbf{Y}^{\mathrm{T}}) \\ \text{subject to} \quad & \mathbf{A}\mathbf{S} - \mathbf{B}\mathbf{Y} + \mathbf{S}\mathbf{A}^{\mathrm{T}} - \mathbf{Y}^{\mathrm{T}}\mathbf{B}^{\mathrm{T}} + \mathbf{E}\mathbf{E}^{\mathrm{T}} < 0, \quad \begin{bmatrix} \mathbf{X} & \mathbf{R}^{1/2}\mathbf{Y} \\ \mathbf{Y}^{\mathrm{T}}\mathbf{R}^{1/2} & \mathbf{S} \end{bmatrix} > 0, \quad \mathbf{S} > 0, \\ & \text{and} \qquad -\mathbf{Y}\mathbf{C}_{\mathrm{v}}^{\mathrm{T}} < \gamma_{\mathrm{e}}^{\mathrm{L}} \end{aligned} \tag{6.1}$$

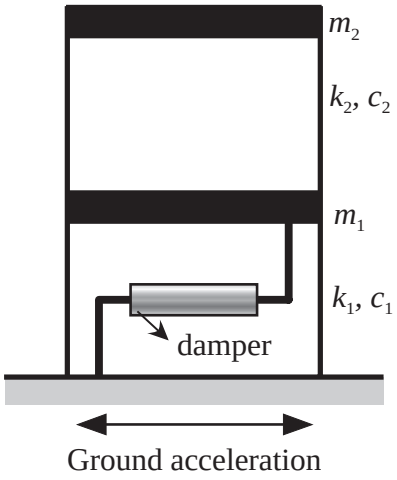


**Figure 6.1** A 2-DOF building

The feedback gain is then given by $\mathbf{K}_0 = \mathbf{F}_0 = \mathbf{Y}_0\mathbf{S}_0^{-1}$, where $\mathbf{Y}_0$, $\mathbf{S}_0$ and $\mathbf{X}_0$ are the solutions of the problem (6.1). The goal in the dissipativity analysis is to obtain controllers with various $\gamma_{\mathrm{e}}^{\mathrm{L}}$ values.

### 6.2.1 Numerical Example: A 2-DOF Building Structure

The 2-DOF shear building model shown in Figure 6.1 is considered as the first numerical example. The equation of motion and the state-space representation of the equation of motion are straightforward and will not be given here. The floor masses $m_1$ and $m_2$ are 100 tons. The stiffnesses $k_1$ and $k_2$ are selected such that the story periods are 0.5 secs. Similarly, the floor damping coefficients are found by setting the modal damping ratios to 2%. An ideal smart damper is attached between the first floor and the ground.

A control design to be used in the dissipativity analysis is defined as follows. The output vector to be minimized is selected to be the drifts of each story and the absolute accelerations of each floor, $\mathbf{z} = [x_1 \quad x_2 - x_1 \quad \ddot{x}_1^{\mathrm{abs}} \quad \ddot{x}_2^{\mathrm{abs}}]^{\mathrm{T}}$. The control design parameters are selected as

$$\tilde{\mathbf{Q}} = \begin{bmatrix} \alpha \mathbf{I}_{2\times 2} & \mathbf{0} \\ \mathbf{0} & \dfrac{\beta}{\omega_{\mathrm{n}}^4}\mathbf{I}_{2\times 2} \end{bmatrix} \qquad \tilde{\mathbf{R}} = \eta \qquad \tilde{\mathbf{N}} = \mathbf{0} \tag{6.2}$$

This set of parameters allows one to choose the relative importance of the drift and absolute acceleration responses. The normalization frequency $\omega_{\mathrm{n}}$ is taken as 10.5 rad/sec; this value is found such that the drift and absolute acceleration portions of the term $E[\mathbf{z}^{\mathrm{T}}\tilde{\mathbf{Q}}\mathbf{z}]$ give the same values for ($\alpha = 1$, $\beta = 1$) in active control.

As a first attempt, a MATLAB® code is written where the dissipativity constraint (5.24) with several values of $\gamma_{\mathrm{e}}^{\mathrm{L}}$ is simply appended to the LMI-EVP to obtain the smallest possible value of $D_{\mathrm{e}}$ for a given set of control design parameters. During this initial study, it is found that one of the parameters of the MATLAB® LMI solver, known as feasibility radius $R_{\mathrm{f}}$, affects the results considerably. $R_{\mathrm{f}}$ creates a limit for the Euclidian magnitude of the EVP parameter $\mathbf{x}$ (see inequality (4.8) above) for numerical efficiency. It is observed that for a given $\gamma_{\mathrm{e}}^{\mathrm{L}}$, different values of the feasibility radius yield different dissipativity levels. This is a natural consequence of the dissipativity constraint (5.24), which includes a term that is not normalized. Therefore, a parametric study is carried out to find the $(\gamma_{\mathrm{e}}^{\mathrm{L}}, R_{\mathrm{f}})$ pair that yields the smallest $D_{\mathrm{e}}$ for each control design. The resulting $(\gamma_{\mathrm{e}}^{\mathrm{L}}, R_{\mathrm{f}})$ values are then employed in the dynamic analysis of the 2-DOF structure excited by an artificial white noise signal for the corresponding control designs. The performance of the structure is investigated using three indices given by

$$J_{\mathrm{d}} = \sigma_{x_1}^2 + \sigma_{x_2 - x_1}^2, \quad J_{\mathrm{a}} = \frac{1}{\omega_{\mathrm{n}}^4}(\sigma_{\ddot{x}_1^{\mathrm{abs}}}^2 + \sigma_{\ddot{x}_2^{\mathrm{abs}}}^2) \quad \text{and} \quad J = J_{\mathrm{d}} + \frac{\beta}{\alpha} J_{\mathrm{a}} + \frac{\eta}{\alpha}\sigma_{\mathrm{u}}^2 \tag{6.3}$$

where, for a discrete time history $x(k\Delta t)$, $\sigma_x^2$ is defined by

$$\sigma_x^2 = \frac{1}{N}\sum_{k=1}^{N}[x(k\Delta t)]^2 \tag{6.4}$$

The following results are obtained for $\beta = 1000$ and several values of $\alpha$ ranging from $10^{-5}$ to $10^5$ as it is found that these sets of controllers yield the best performance after some test simulations.

Figure 6.2 shows the dissipativity characteristics of the controllers for the 2-DOF building structure, where the terms $D_{\mathrm{n}}$ and $D_{\mathrm{ne}}$ are obtained using stochastic analysis for a white noise

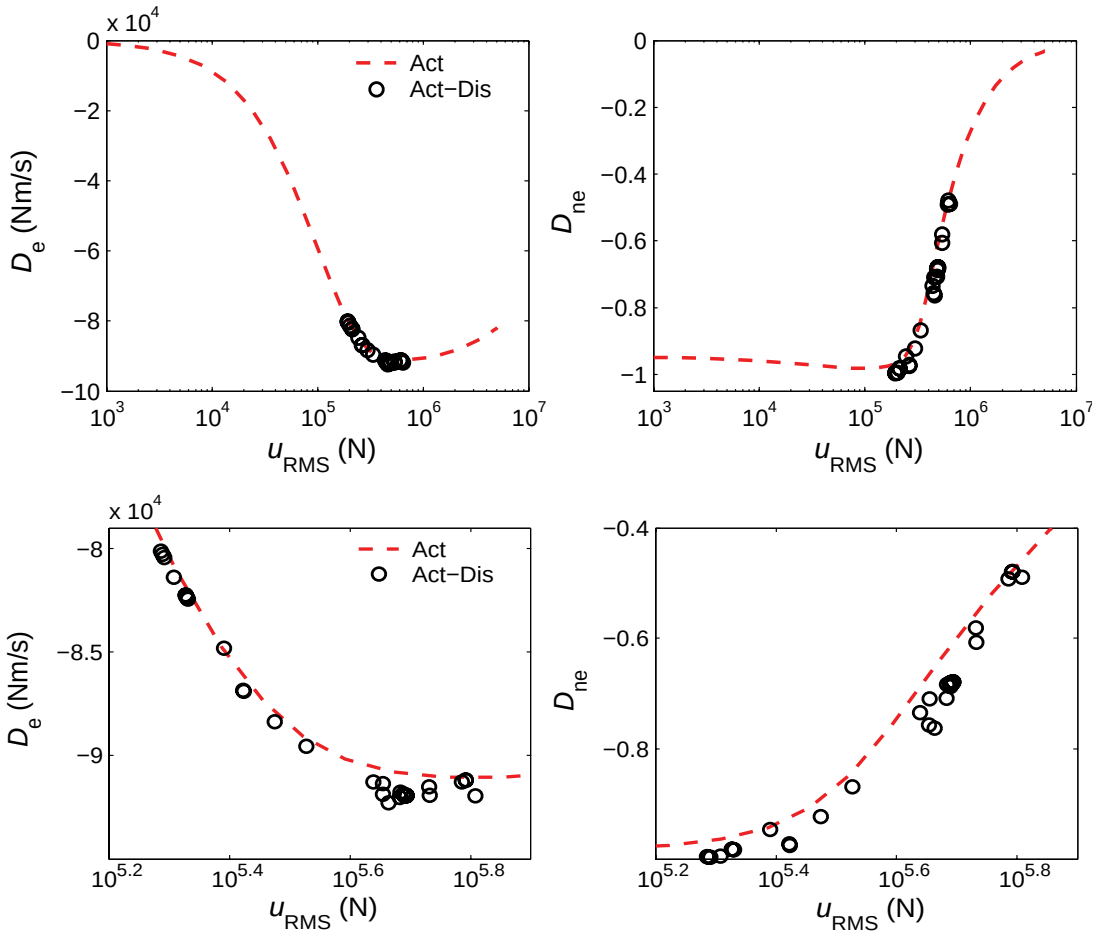


**Figure 6.2** $D_{\mathrm{e}}$ and $D_{\mathrm{ne}}$ plots for the 2-DOF building from the covariance analysis (overall in the top row and detailed in the bottom row)

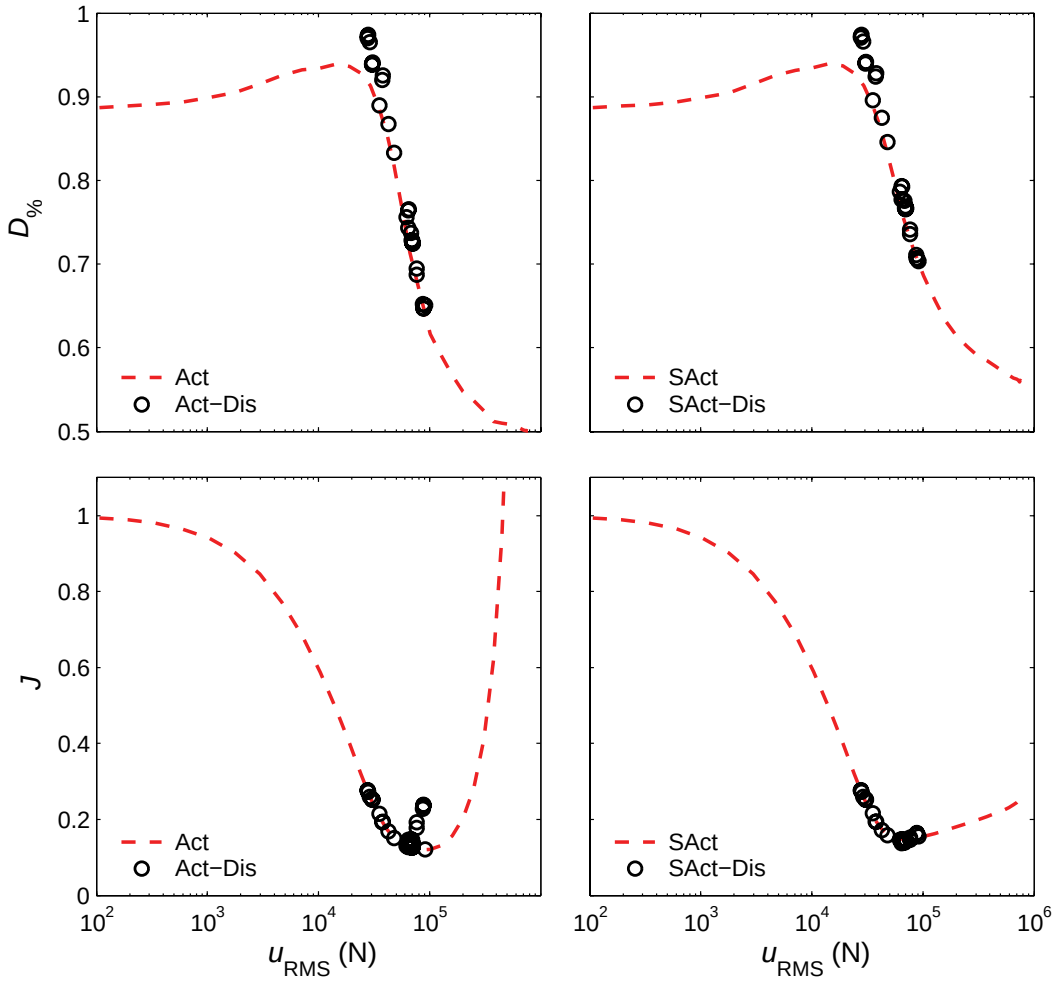


**Figure 6.3** $D_{\%}$ and normalized $J$ plots for the 2-DOF building from the simulations for a white noise excitation

excitation with unit intensity. Figure 6.3 shows $D_{\%}$ and $J$ plots where the structure is excited with a 50 sec white noise signal. The white noise is normalized by a factor of 1000 to have response magnitudes consistent with the structural properties. Figure 6.4 shows the displacement and acceleration indices for the semiactive systems. In all of the above plots, the performance indices are normalized with the corresponding uncontrolled system indices. The difference in the RMS control force scales in Figure 6.2 and Figure 6.3 is due to the normalization of the white

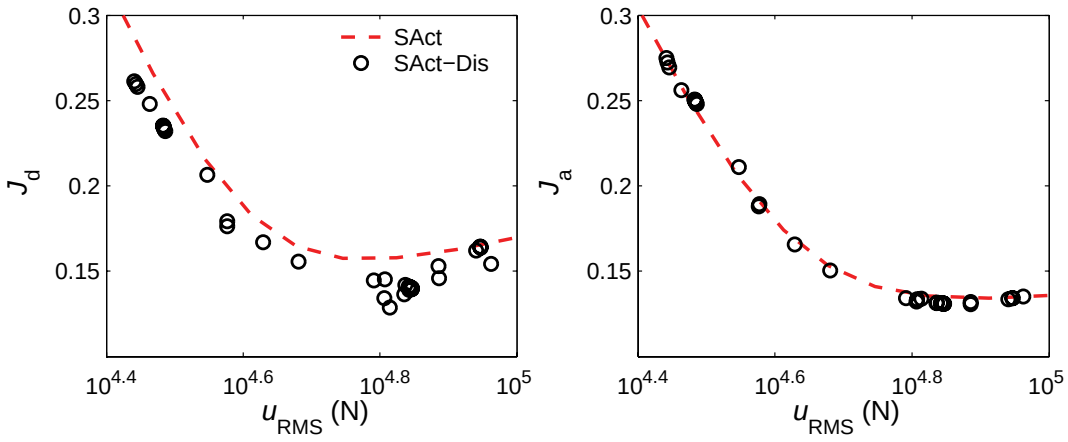


**Figure 6.4** Detailed plots of normalized $J_d$ and $J_a$ of the 2-DOF building from the simulations for a white noise excitation

noise. In the discussions below, the RMS control force scale of Figure 6.3 is used. Note that the control force term in the index $J$ is not used for the uncontrolled structure. The following observations are made:

- For practical control force levels ($[10^4, 10^5]$ N in Figure 6.3) the dissipativity of the controller is very high for this particular structure and control design.
- It is observed that the variation of $D_e$ is not similar to the variation of $D_{ne}$ for the active system (Act), *i.e.*, for small control force levels $D_e$ is low while $D_{ne}$ is high. This difference can be attributed to the magnitudes of the RMS control force and RMS velocity used as normalization coefficients in the computation of $D_{ne}$. Therefore, although a high value of $D_{ne}$ indicates highly dissipative control forces, the corresponding control design may not be suitable for practical purposes due to low control force levels.
- The LMI method improves $D_e$ and $D_{ne}$ for a given $u_{RMS}$. This is more clear for $u_{RMS} \approx 10^{4.8}$ N. However, the best improvement in $D_{\%}$ is for $u_{RMS} \approx 10^{4.2}$ N. Moreover, it

is observed that the LMI method improves the drift performance about 25% for $u_{\mathrm{RMS}} \approx 10^{4.8}$ N. This improvement is not clear on the overall performance index $J$.

- Another difference between $D_{\mathrm{e}}$ and $D_{\mathrm{ne}}$ is that the highest value of $D_{\mathrm{e}}$ corresponds to RMS control force levels of $[10^{4.7}, 10^{5}]$ N, while this range is $[10^{4.1}, 10^{4.3}]$ N for $D_{\mathrm{ne}}$. Also observed is the similarity between $D_{\mathrm{ne}}$ and $D_{\%}$ (note that the $D_{\%}$ plot should be flipped vertically to visualize this similarity).The LMI method narrows the range of possible $u_{\mathrm{RMS}}$ values for the control designs. This is a very useful property in the design process. In general, one must do a comprehensive parametric study, which may include computationaly expensive nonlinear analyses, to find the best $(\alpha, \beta)$ pair for a given $\eta$. The LMI method and the dissipativity indices may give a good sense of the achievable semiactive performance letting the designer to avoid simulations that will not yield better results.
- The plot of overall performance index shows a high similarity to the $D_{\mathrm{e}}$ plot. Therefore, for this example $D_{\mathrm{e}}$ is more useful to guess the best control design.
- The indices proposed in this dissertation are very helpful to understand the dissipative nature of the primary control force and the semiactive performance of this example. The LMI method is able to modify the dissipativity characteristics of the controller so that the semiactive performance is improved. Two critical designs are located. The first design corresponds to $u_{\mathrm{RMS}} \approx 10^{4.2}$ N, and the LMI method improves the indices $D_{\mathrm{ne}}$ and $D_{\%}$ though it is not the best semiactive design. The second design point is for $u_{\mathrm{RMS}} \approx 10^{4.8}$ N, which has the best semiactive performance and the highest improvement in $D_{\mathrm{e}}$. The results for these two designs are summarized in Tables 6.2 and 6.3. Therefore, each index exhibits a different characteristic of the control force and may be useful to understand different problems.

**Table 6.2:** Indices for design $u_{RMS} = 10^{4.2}$ N

| | $D_e$ (Nm/s) | $D_{ne}$ | $D_{\%}$ | $J_d$ | $J_a$ |
|---|---|---|---|---|---|
| **Act** | $-7.983\times10^4$ | –0.966 | 0.917 | - | - |
| **Act-Dis** | $-8.043\times10^4$ | –0.997[a] | 0.974[a] | - | - |
| **SAct** | - | - | 0.917 | 0.283 | 0.273 |
| **SAct-Dis** | - | - | 0.974[a] | 0.258 | 0.269 |

a. Highest dissipativity achieved.

**Table 6.3:** Indices for design $u_{RMS} = 10^{4.8}$ N

| | $D_e$ (Nm/s) | $D_{ne}$ | $D_{\%}$ | $J_d$ | $J_a$ |
|---|---|---|---|---|---|
| **Act** | $-9.073\times10^4$ | –0.652 | 0.721 | - | - |
| **Act-Dis** | $-9.229\times10^4$ [a] | –0.763 | 0.765 | - | - |
| **SAct** | - | - | 0.760 | 0.160 | 0.135 |
| **SAct-Dis** | - | - | 0.793 | 0.129[b] | 0.134 |

a. Highest dissipativity achieved.
b. Highest performance achieved.

### 6.2.2 Numerical Example: 2-DOF Highway Bridge Model

The bridge model, given by Erkus *et al*. (2002) and shown in Figure 6.5, is used as the second example. In this model, the mass ratio, damping ratio and natural period of the pier are $m_2/m_1 = 5$, $5\%$ and 0.5 sec, respectively. The mass of the pier is $m_1 = 100$ ton. The bearing stiffness is $7.685 \times 10^6$ N/m, which is computed using a formula for optimal stiffness (Erkus *et al*. 2002). For active control, the damping of the bearing is assumed to be zero and for the uncontrolled structure it is taken as 196 kN·sec/m. If the design goal is to reduce the pier response using a damper attached between the pier and the deck, a particular control design may yield low

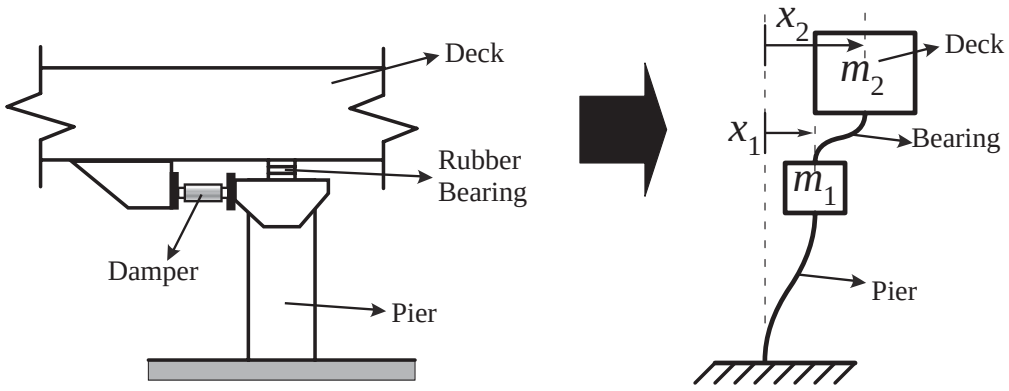


**Figure 6.5** 2-DOF modelling of the highway bridge (Erkus *et al*. 2002)

dissipativity levels, and the damper cannot mimic the primary control force efficiently (Erkus *et al*. 2002). Note that this dissipativity characteristic is also observed by Inaudi (2000) in an analytical study. The mathematical model is already given by Erkus *et al*. (2002) and will not be repeated here. The damper in the original paper (Erkus *et al*. 2002) is an MR fluid damper and the mathematical model of a prototype small-scale MR fluid damper is used in the analysis. This study, however uses a more realistic damper model, which is obtained for a 20-ton MR fluid damper (Yang *et al*. 2002). In the analysis, the damper force is amplified by a factor of 3 to be able to exert forces commanded by the primary control force (in a practical application a 60-ton damper would be used). The equivalency of the LMI-EVP and LQR problem is tested for this example using several control design parameters. It is found that the two methods yield identical results when the dissipativity constraint is not employed and condition (3.11) is satisfied.

In this example, $\mathbf{R} = 10^{-12}$ N·m and the control design parameter $\mathbf{Q}$ is selected such that the term $\mathbf{q}^{\mathrm{T}}\mathbf{Q}\mathbf{q}$ represents an energy quantity; *i.e.*,

$$\mathbf{q}^{\mathrm{T}}\mathbf{Q}\mathbf{q} = r\left(\frac{1}{2}k_1(x_1)^2 + \frac{1}{2}m_1(v_1)^2\right) + \left(\frac{1}{2}k_2(x_2 - x_1)^2 + \frac{1}{2}m_2(v_2 - v_1)^2\right) \tag{6.5}$$

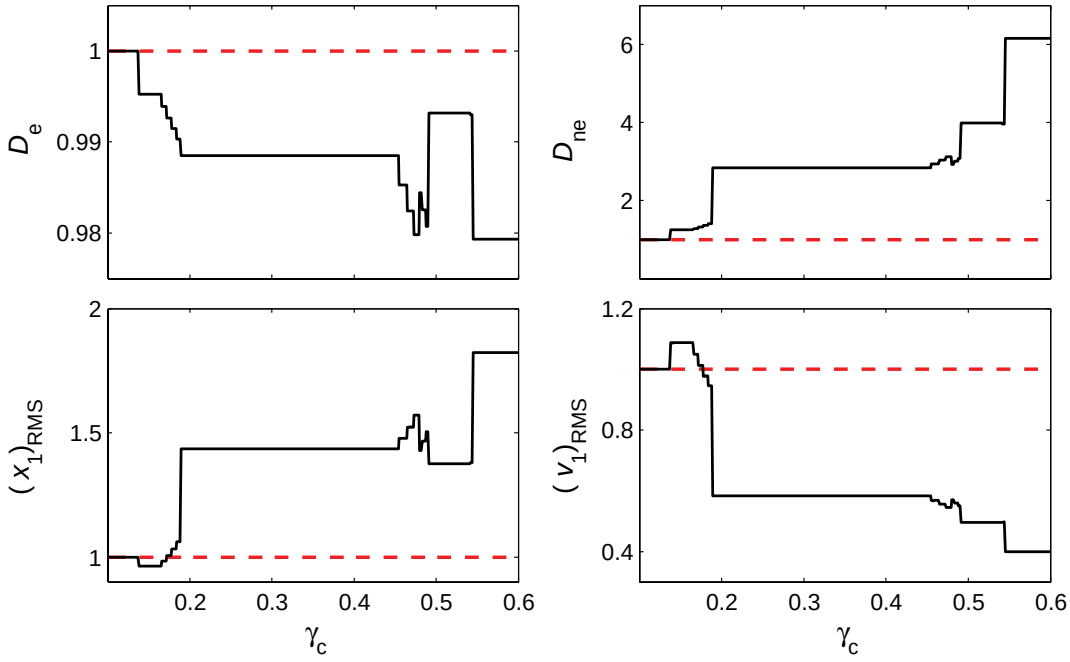


**Figure 6.6** Normalized $D_e$, $D_{ne}$ and performance plots of the LMI-EVP controller of the 2-DOF bridge structure for various $\gamma_e^L$ values (covariance analysis)

where $r$ determines the relative importance of the pier and the bearing responses. In this example, $r = 1000$ is selected, which results in LQR controllers with low dissipativity levels. Using this particular controller design, the LMI-EVP problem is solved for several values of $\gamma_e^L$ to increase the controller dissipativity. After some test simulations, $R_f = 1 \times 10^{30}$ is used. The results are graphed using a normalized dissipation rate $\gamma_c = -\gamma_e^L / R_f$.

Figure 6.6 shows the dissipativity and performance characteristics of the LMI-EVP controller for various values of $\gamma_e^L$, which is obtained by standard stochastic analysis. In these plots, the values are normalized by the corresponding standard LQR controller values. Figure 6.7 shows the dissipativity nature of the controllers and performance of the systems for both active and semiactive systems excited by the white noise signal used in the first example. In these plots, the

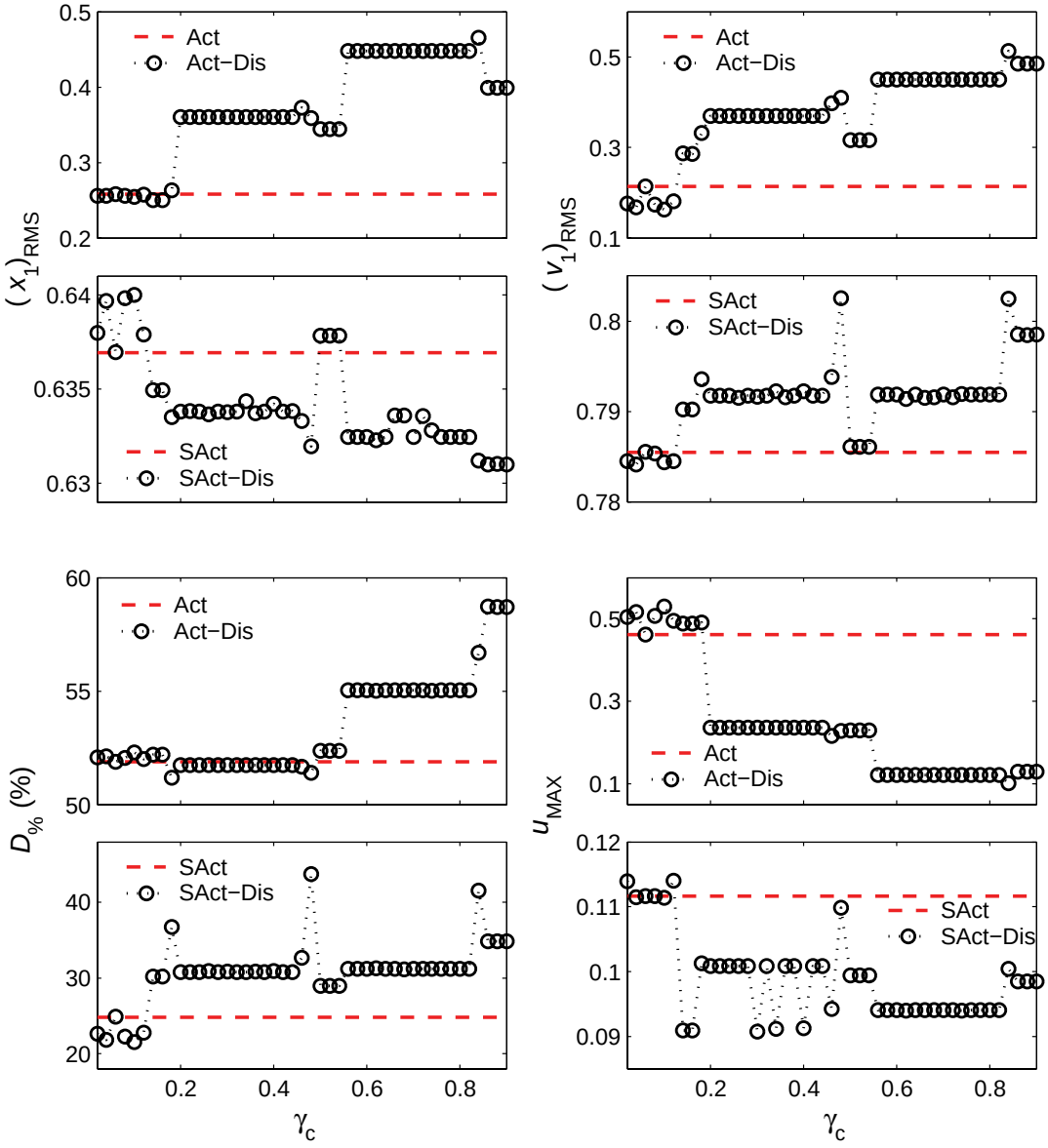


**Figure 6.7** Normalized $D_{\%}$ and normalized performance plots for the 2-DOF bridge structure from the simulations for a white noise excitation

RMS response values are normalized with the corresponding RMS values of an uncontrolled structure given by Erkus *et al*. (2002), and the maximum control force values are normalized by the total weight of the structure. The following points are observed:

- As seen in Figure 6.6, the LMI method improves the dissipativity index $D_{\text{ne}}$ even though a weak form of the dissipativity constraint is used. On the other hand, the index $D_{\text{e}}$ indicates a reduction in the mean energy flow rate. It is also observed that there is an improvement in the drift index for $\gamma_{\text{c}} \approx 0.15$ although this is not anticipated. In the design process, this point may be considered more suitable for a semiactive design.
- The simulation results given in Figure 6.7 show that improving dissipativity characteristics makes a very minor improvement on the semiactive drift performance. There are several reasons for this result. First, Act-Dis performance does not improve; indeed, $(x_1)_{\text{RMS}}$ increases considerably. Second, the damper is not an ideal smart damper and has very nonlinear dynamics. It is not as efficient as an ideal smart damper in applying the required force.
- A more interesting observation that effects the semiactive performance is that the dissipativity index $D_{\%} \approx 52\%$ of the active system reduces to $D_{\%} \approx 25\%$ for the semiactive system. The main reason for this reduction is inability of the MR damper to apply nondissipative forces. The active controller with $D_{\%} \approx 52\%$ requires nondissipative forces, probably ones that inject energy into the structural system. During the simulation, the damper will not be able to mimic the active control force since it cannot exert nondissipative forces. Therefore, the response of the semiactive system will be considerably different from a corresponding fully active system response. In this case, the primary controller (standard LQR) will command forces that inject even more energy than in the active case to push the semiactive response path back towards the fully active response path. This will yield control forces with lower dissipativity than expected. (Obviously, if an ideal smart damper model were used, this effect will not be as significant as in the MR fluid damper case.) Therefore, it can be concluded that the use of semiactive devices to implement very nondissipative control designs

may reduce the semiactive performance in two ways: first, performance reduction due to low dissipativity; second, additional dissipativity reduction due to the inability of the damper to mimic a nondissipative control force.

- Although the LMI approach improves the dissipativity, it cannot compensate for the severe reduction caused by the damper effect described above, and its benefits are not observed on the final semiactive performance.
- The benefit of improved dissipativity is the lowered control force levels implemented by the damper. About 20% reduction occurred on the maximum control force required for $\gamma_c \in (0.6, 0.8)$ to achieve the same drift performance. It should be noted that there may be other control design parameter sets that gives the same performance improvement, though a comprehensive and time consuming parametric study would be required to search for the existence of such sets. On the other hand, the proposed LMI method allows one to achieve the same performance without an extensive and time consuming study.

## 6.3 LMI-EVP with the $D_{ne}$-Based Dissipativity Constraint

In this section, an iterative method to solve the LMI-EVP with the $D_{ne}$-based dissipativity constraint is proposed:

$$\min_{\mathbf{Y},\,\mathbf{S},\,\mathbf{X}} \; Tr(\mathbf{Q}^{1/2}\mathbf{S}\mathbf{Q}^{1/2}) + Tr(\mathbf{X}) - Tr(\mathbf{Y}\mathbf{N}) - Tr(\mathbf{N}^{\mathrm{T}}\mathbf{Y}^{\mathrm{T}})$$

$$\text{subject to} \quad \mathbf{A}\mathbf{S} - \mathbf{B}\mathbf{Y} + \mathbf{S}\mathbf{A}^{\mathrm{T}} - \mathbf{Y}^{\mathrm{T}}\mathbf{B}^{\mathrm{T}} + \mathbf{E}\mathbf{E}^{\mathrm{T}} < 0, \qquad \begin{bmatrix} \mathbf{X} & \mathbf{R}^{1/2}\mathbf{Y} \\ \mathbf{Y}^{\mathrm{T}}\mathbf{R}^{1/2} & \mathbf{S} \end{bmatrix} > 0, \qquad \mathbf{S} > 0, \tag{6.6}$$

$$\text{and} \qquad \frac{-\mathbf{F}\mathbf{S}\mathbf{C}_{\mathrm{v}}^{\mathrm{T}}}{\sqrt{\mathbf{F}\mathbf{S}\mathbf{F}^{\mathrm{T}}}\sqrt{\mathbf{C}_{\mathrm{v}}\mathbf{S}\mathbf{C}_{\mathrm{v}}^{\mathrm{T}}}} < \gamma_{\mathrm{ne}}^{\mathrm{L}} \qquad \text{where} \qquad -1 \le \gamma_{\mathrm{e}}^{\mathrm{L}} \le 1$$

The iterative procedure starts with an initial guess of $\mathbf{F}$ and $\mathbf{S}$ for the dissipativity constraint. Lets denote these matrices by $\mathbf{F}^0$ and $\mathbf{S}^0$. Then, the following problem is solved:

$$\min_{\mathbf{Y},\,\mathbf{S},\,\mathbf{X}} \; Tr(\mathbf{Q}^{1/2}\mathbf{S}\mathbf{Q}^{1/2}) + Tr(\mathbf{X}) - Tr(\mathbf{Y}\mathbf{N}) - Tr(\mathbf{N}^{\mathrm{T}}\mathbf{Y}^{\mathrm{T}})$$

$$\text{subject to } \mathbf{A}\mathbf{S}-\mathbf{B}\mathbf{Y} + \mathbf{S}\mathbf{A}^{\mathrm{T}}-\mathbf{Y}^{\mathrm{T}}\mathbf{B}^{\mathrm{T}} + \mathbf{E}\mathbf{E}^{\mathrm{T}} < 0, \qquad \begin{bmatrix} \mathbf{X} & \mathbf{R}^{1/2}\mathbf{Y} \\ \mathbf{Y}^{\mathrm{T}}\mathbf{R}^{1/2} & \mathbf{S} \end{bmatrix} > 0, \qquad \mathbf{S} > 0, \tag{6.7}$$

$$\text{and} \qquad \frac{-\mathbf{Y}\mathbf{C}_{\mathrm{v}}^{\mathrm{T}}}{\sqrt{\mathbf{F}^0\mathbf{S}^0(\mathbf{F}^0)^{\mathrm{T}}}\sqrt{\mathbf{C}_{\mathrm{v}}\mathbf{S}^0\mathbf{C}_{\mathrm{v}}^{\mathrm{T}}}} < \gamma_{\mathrm{ne}}^{\mathrm{L}} \qquad \text{where} \qquad -1 \le \gamma_{\mathrm{e}}^{\mathrm{L}} \le 1$$

Problem (6.7) is a LMI-EVP and can be solved for $\mathbf{S}$ and $\mathbf{F} = \mathbf{Y}\mathbf{S}^{-1}$ for a given $\gamma_{\mathrm{ne}}^{\mathrm{L}}$. Lets denote this solution by $\mathbf{F}^1$ and $\mathbf{S}^1$. In the next step, the (6.7) is solved again, where $\mathbf{F}^0$ and $\mathbf{S}^0$ is replaced with $\mathbf{F}^1$ and $\mathbf{S}^1$. Therefore, the following problem is solved at the $i^{\mathrm{th}}$-iteration

$$\min_{\mathbf{Y},\,\mathbf{S},\,\mathbf{X}} \; Tr(\mathbf{Q}^{1/2}\mathbf{S}\mathbf{Q}^{1/2}) + Tr(\mathbf{X}) - Tr(\mathbf{Y}\mathbf{N}) - Tr(\mathbf{N}^{\mathrm{T}}\mathbf{Y}^{\mathrm{T}})$$

$$\text{subject to } \mathbf{A}\mathbf{S}-\mathbf{B}\mathbf{Y} + \mathbf{S}\mathbf{A}^{\mathrm{T}}-\mathbf{Y}^{\mathrm{T}}\mathbf{B}^{\mathrm{T}} + \mathbf{E}\mathbf{E}^{\mathrm{T}} < 0, \qquad \begin{bmatrix} \mathbf{X} & \mathbf{R}^{1/2}\mathbf{Y} \\ \mathbf{Y}^{\mathrm{T}}\mathbf{R}^{1/2} & \mathbf{S} \end{bmatrix} > 0, \qquad \mathbf{S} > 0, \tag{6.8}$$

$$\text{and} \qquad \frac{-\mathbf{Y}\mathbf{C}_{\mathrm{v}}^{\mathrm{T}}}{\sqrt{\mathbf{F}^{i-1}\mathbf{S}^{i-1}(\mathbf{F}^{i-1})^{\mathrm{T}}}\sqrt{\mathbf{C}_{\mathrm{v}}\mathbf{S}^{i-1}\mathbf{C}_{\mathrm{v}}^{\mathrm{T}}}} < \gamma_{\mathrm{ne}}^{\mathrm{L}} \qquad \text{where} \qquad -1 \le \gamma_{\mathrm{e}}^{\mathrm{L}} \le 1$$

and $\mathbf{F}^i$ and $\mathbf{S}^i$ are obtained.

It should be noted that the procedure defined above utilizes LMI procedures for a nonlinear matrix inequality problem and should not be considered as a sound alternative to the algorithms proposed for the solution of bilinear and/or nonlinear matrix inequality problems.

### 6.3.1 Numerical Example: A 2-DOF Building Structure

The 2-DOF building structure investigated in the previous section is used in this example also. LQR control parameters are selected to be the same as in Section 6.2.1. The iterative method is implemented for a wide set of control designs and dissipativity goals. The control designs are selected as $\beta = 1000$ and values of $\alpha$ ranging from $10^{-5}$ to $10^{5}$. Several values between $-1$ and 0 are considered for $\gamma_{\mathrm{ne}}^{\mathrm{L}}$. For each $((\alpha, \beta), \gamma_{\mathrm{ne}}^{\mathrm{L}})$ pair, the iterative method is

used to solve the EVP. Initial values of **F** and **S** are taken as **K** and **P**, respectively, *i.e.*, solution of the LQR problem without a dissipativity constraint. Similar to the previous section, the goal in the dissipativity analysis is to find controllers with various $D_{ne}$ values.

The numerical simulations show that the iterative method converges to a single solution for each control design and 10 iterations yield acceptable results for the 2-DOF system.

Figure 6.8 shows the $\gamma_e^L$ and $\gamma_{ne}^L$ values obtained from the iterative method. In this figure, $\gamma_{ne}^{iteration}$ is used to emphasize that this value is the value used in the iterative method, and $\gamma_e^L$ and $\gamma_{ne}^L$ are the dissipativity indices that are calculated with the converged Lyapunov matrices $\mathbf{S}_e$ and $\mathbf{S}_{ne}$, respectively, instead of the covariance matrices $\mathbf{P}_e$ and $\mathbf{P}_{ne}$. Also, the RMS control force is normalized with the weight of the structure, $W_{str}$. The $\gamma_e^L$ -surface shows that the iterative method successfully enforces high dissipativity levels in the Lyapunov sense, *i.e.*, as $\gamma_{ne}^{iteration}$ is moved closer to $-1$, which is a purely dissipative controller in the Lyapunov sense, $\gamma_e^L$ reaches negative values of very large magnitudes. The $\gamma_{ne}^L$ -surface provides two important observations. First, it shows that the iterative method successfully implements the nonlinear matrix inequality problem. To elaborate, consider a value for $\gamma_{ne}^{iteration}$, *e.g.*, –0.5. The value of $\gamma_{ne}^L$ that corresponds to $\gamma_{ne}^{iteration} = -0.5$ is very close to –0.5 for the normalized RMS control forces larger than 0.1. Second, the controllers with normalized RMS control forces smaller than 0.1 already have high dissipativity values in the Lyapunov sense. Figure 6.9 shows the actual values of the dissipativity indices of the controllers. It is evident that there is no change in the dissipativity indices $D_e$ and $D_{ne}$ for the values of $\gamma_{ne}^{iteration}$ that are close to $-1$.

In summary, the results presented in Figures 6.8 and 6.9 show that while the iterative method successfully modifies the Lyapunov dissipativity of the system, it does not effect actual dissipa-

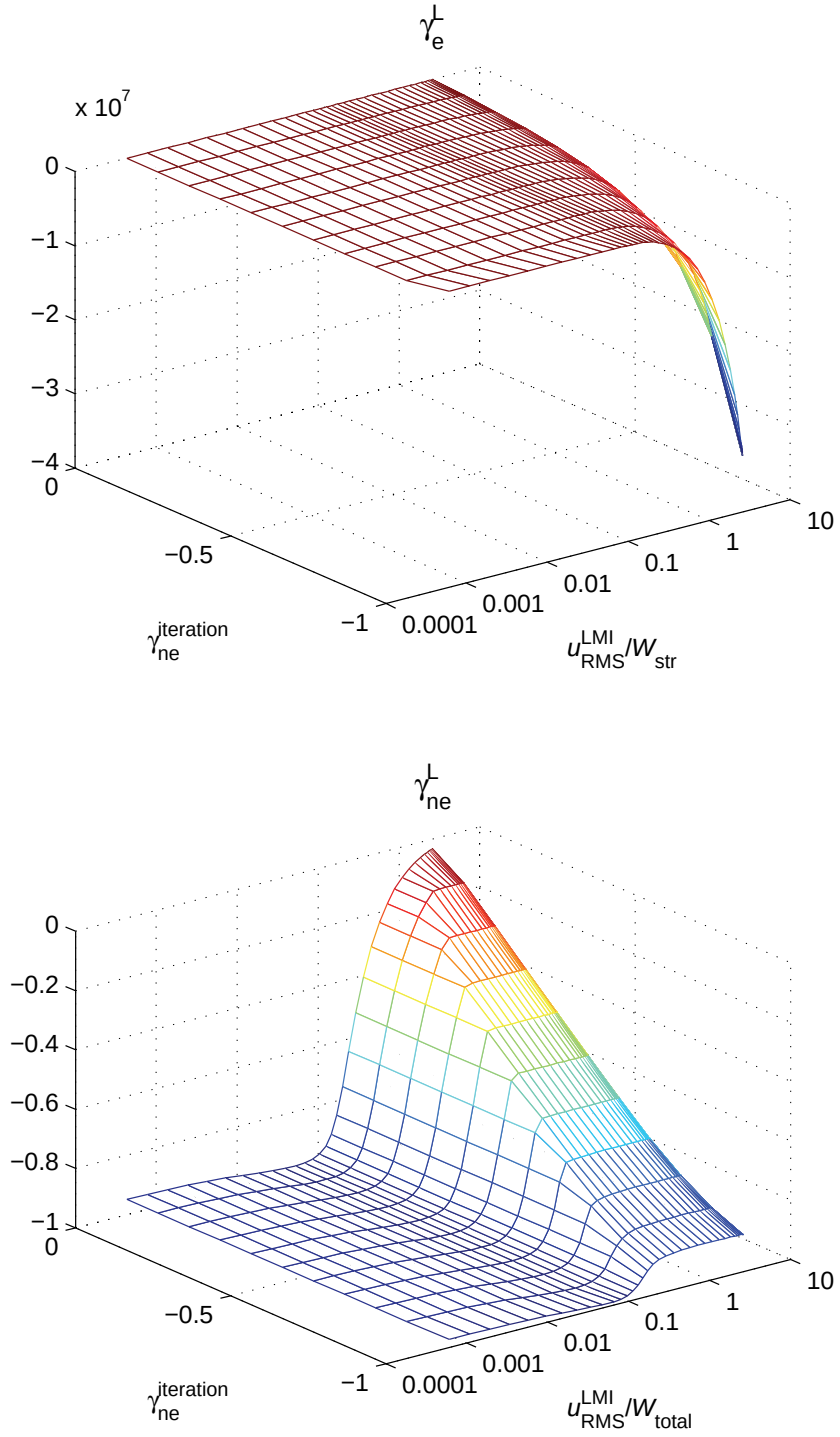


**Figure 6.8** $\gamma_e{}^L$ and $\gamma_{ne}{}^L$ values obtained from the iterative method for the 2-DOF structure

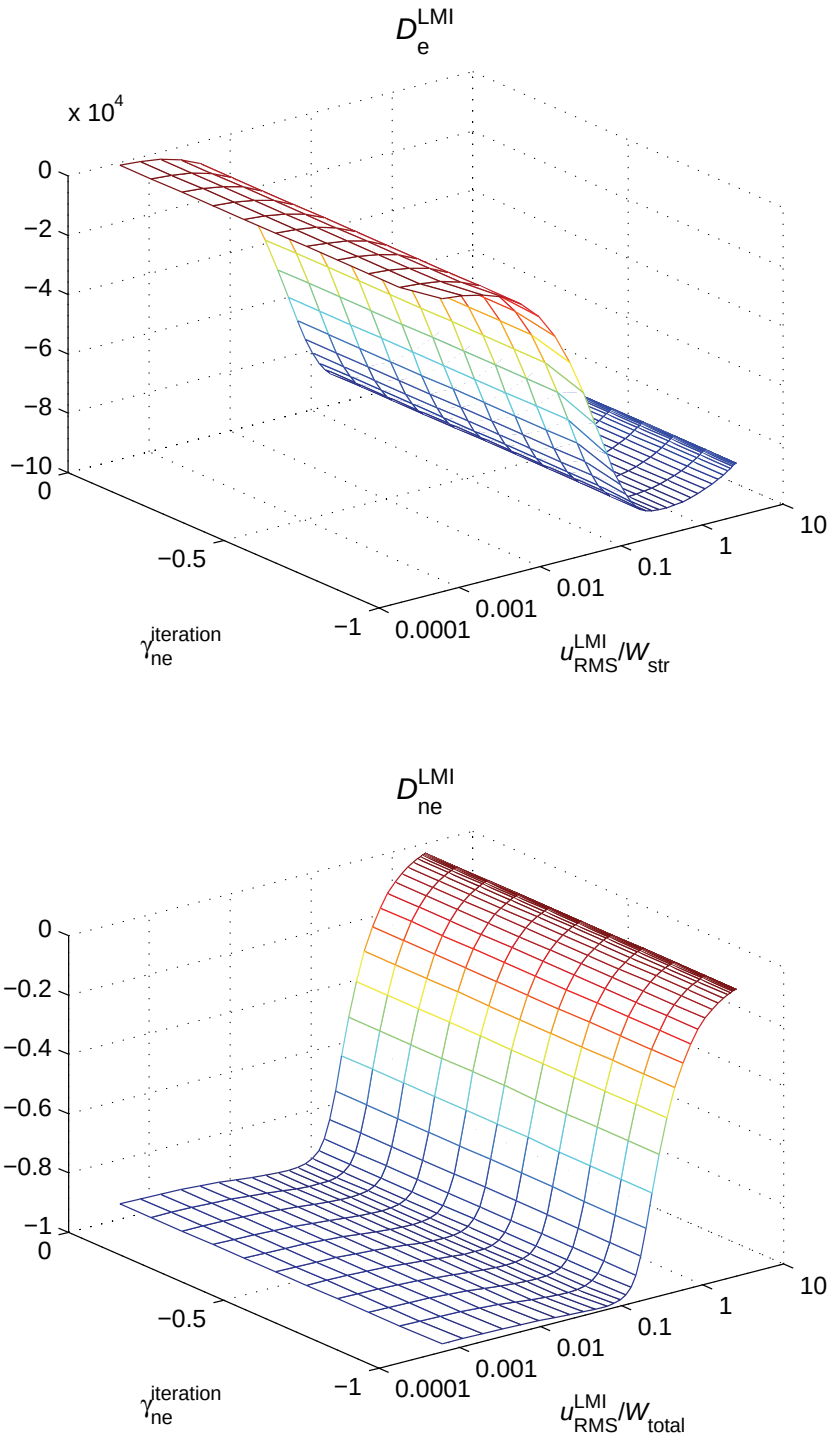


**Figure 6.9** $D_e$ and $D_{ne}$ values obtained from the iterative method for the 2-DOF structure

tivity of the system. One important reason for this result is that the optimization problem does not enforce the equality constraint

$$(\mathbf{A}-\mathbf{BF})\mathbf{S}_{ne} + \mathbf{S}_{ne}(\mathbf{A}-\mathbf{BF})^{T} + \mathbf{EE}^{T} = 0 \tag{6.9}$$

which was dropped to have a solvable LMI-EVP. It is also found that performance of the controllers with and without the $D_{ne}$-based constraint are same.

## 6.4 Summary

In the first part of this chapter, the proposed LMI-EVP and $D_e$-based dissipativity index are employed for two numerical examples: a highly dissipative control design for a 2DOF frame structure with an ideal damper and a minimally dissipativity control design for a 2DOF model of an highway bridge with a realistic MR fluid damper model. In the first example, the dissipativity indices were very useful for understanding different characteristics of the controller, and the proposed LMI approach was able to improve drift performance of the controller even though a weak form of the dissipativity constraint is employed. In the second example, although the LMI method was able to improve the dissipative nature of the primary controller, this improvement was not reflected in the final semiactive performance efficiently since the use of a realistic damper model with a nondissipative primary controller further lowers the original dissipativity.

In the second part of this chapter, the EVP with the $D_{ne}$-constraint is solved with an iterative method. While the method improves the Lyapunov dissipativity, it does not effect the actual dissipativity as the equality constraint that equalizes the Lyapunov matrix to the state covariance matrix is ignored in the solution.

# CHAPTER 7

# DISSIPATIVITY-BASED PERFORMANCE ANALYSIS OF THE SMART BASE ISOLATED BENCHMARK BUILDING

## 7.1 Introduction

In the previous chapters, several dissipativity indices are introduced to quantify the dissipative nature of a control force and employed to investigate dissipativity-performance relations in two simple 2-DOF structures. Moreover, a proposed LMI-based optimization method is shown to be successful in improving the dissipative nature of a 2-DOF semiactive system and to be helpful in selecting controllers well suited for a smart damper. From a theoretical point of view, the results are very helpful to understand the phenomena and identify performance issues due to the dissipative nature of smart dampers even though the examples are based on simple structural systems.

The next step in this study is to investigate dissipativity-performance relations in a realistic structural engineering control problem. A realistic problem consists of many challenges such as a complex mathematical model with a large number of degrees of freedom, three-dimensional behavior with torsional deformation, effects of sensor and observer dynamics, realistic damper models, possible nonlinear behavior of structural members and, the most important challenge, different earthquake characteristics. In fact, these are not only specific to a semiactive control problem, but are also encountered in any structural engineering problem. Addressing these issues separately requires a considerable amount of work; therefore, the scope of this study is kept in the boundaries of the applicability and efficiency of the proposed indices and methods for a complete and complex structural engineering problem defined above.

A good example of a realistic structural control problem is the smart base isolated benchmark building (Narasimhan *et al*., 2006), which was introduced by the ASCE Technical Committee on Structural Control. The goal in the base isolated benchmark building study is to evaluate control methods and technologies that are developed for base-isolated buildings. There are two-phases of this study, where the first phase concentrates on the benchmark structure with a linear isolation (Nagarajaiah and Narasimhan, 2006), and the second phase concentrates on the benchmark structure with a nonlinear isolation (Erkus and Johnson, 2006). Both of these phases possess various facets of a practical structural control problem that are discussed above and, therefore, are useful for this study.

In this chapter, first a review of the benchmark structure is given. Only, the mathematical model of the structure with a nonlinear isolation is provided since obtaining a model of the linear structure is straightforward from the nonlinear model. Then, both linear and nonlinear structures are investigated in the context of dissipativity-performance relationships. In this investigation, an LMI-EVP-based dissipativity analysis is not carried due to the time-inefficiency and accuracy issues associated with the LMI solver for large systems. Even in its simplified form, the benchmark structure model is very complex, and the LMI solver is not expected to be efficient for this problem.

## 7.2 Smart Base Isolated Benchmark Structure

In this section, a brief review of the benchmark structure and its mathematical modelling is given. For further information, the reader is referred to the problem definition paper (Narasimhan *et al*. 2006).

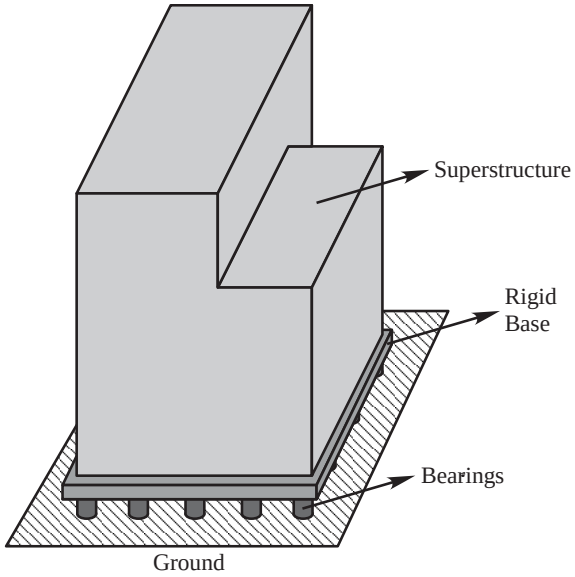


**Figure 7.1** A representative figure of the benchmark structure

### 7.2.1 Review

The benchmark structure is an eight-story frame building with steel braces. Stories one to six have an L-shaped plan while the higher floors have a rectangular plan. The superstructure rests on a rigid concrete base, which is isolated from the ground by an isolation layer, and consists of linear beam, column and bracing elements and rigid slabs (Figure 7.1). Below the base, the isolation layer consists of a variety of 92 isolation bearings. Benchmark participants are allowed to modify the properties of the isolation bearings, as well as add passive, active or semiactive devices between the ground and the base. The details of the isolation layer used in this study are given later in this section.

### 7.2.2 Mathematical Model

The mathematical model of the benchmark structure is complicated and cannot be used directly for control design. Therefore, the model is reviewed and developed here in a manner that

is somewhat more amenable for control design. The isolated building is modeled in two parts: (1) the superstructure, which consists of the eight-story structure above the base; and (2) the base, isolation bearings and any additional control devices.

The superstructure is linear, and the slabs are assumed to be rigid. The response of each story is characterized by three degrees-of-freedom (DOFs) — two horizontal DOFs and one rotational DOF — located at the center of mass of the corresponding floor. Thus, the superstructure finite element model is condensed to a 24 DOF model. The superstructure equation of motion can be written as

$$\mathbf{M}_s\ddot{\mathbf{x}}_s^b + \mathbf{C}_s\dot{\mathbf{x}}_s^b + \mathbf{K}_s\mathbf{x}_s^b = -\mathbf{M}_s\mathbf{R}_1\ddot{\mathbf{x}}_b^{abs} \tag{7.1}$$

In this equation, $\mathbf{x}_s^b = [x_8^b \quad y_8^b \quad \theta_8^b \ \ldots \ x_1^b \quad y_1^b \quad \theta_1^b]^T$ is the $24 \times 1$ displacement vector of the superstructure where $x_i^b$, $y_i^b$ and $\theta_i^b$ are the displacements in the horizontal $x$ and $y$–directions and the rotation of the mass-center of the $i^{th}$ floor with respect to the base, respectively; $\mathbf{M}_s$, $\mathbf{C}_s$ and $\mathbf{K}_s$ are the mass, proportional damping and stiffness matrices of the superstructure, respectively; $\ddot{\mathbf{x}}_b^{abs}$ is the $3 \times 1$ absolute acceleration of the base (acceleration in the $x$ and $y$–directions and the rotational acceleration), and $\mathbf{R}_1$ is the influence coefficient matrix. Let $\Phi_s$ be the mass-normalized eigenmatrix of the superstructure. The equation of motion can be written in modal form as

$$\ddot{\eta}_s^b + \tilde{\mathbf{C}}_s\dot{\eta}_s^b + \tilde{\mathbf{K}}_s\eta_s^b = -\Phi_s^T\mathbf{M}_s\mathbf{R}_1\ddot{\mathbf{x}}_b^{abs} \tag{7.2}$$

where $\eta_s^b$ is the modal response vector of the superstructure with respect to the base, and $\mathbf{x}_s^b = \Phi_s\eta_s^b$. Also,

$$\tilde{\mathbf{C}}_s = \Phi_s^T \mathbf{C}_s \Phi_s = \begin{bmatrix} 2\zeta_1\omega_1 & & \\ & \ddots & \\ & & 2\zeta_{24}\omega_{24} \end{bmatrix} \qquad \tilde{\mathbf{K}}_s = \Phi_s^T \mathbf{K}_s \Phi_s = \begin{bmatrix} \omega_1^2 & & \\ & \ddots & \\ & & \omega_{24}^2 \end{bmatrix} \tag{7.3}$$

where $\omega_i$ and $\zeta_i$ are the modal frequency and damping ratio of the $i^{\text{th}}$ mode, respectively.

The base is modelled with three degrees-of-freedom located at the center of mass of the base: displacement in the horizontal $x-$ and $y-$directions and the rotation about the vertical $z-$direction. There are four types of external forces exerted on the base: resultant isolator force, resultant controller force, shear force caused by the superstructure and inertia force induced by the ground acceleration.

The resultant isolator force is found by transferring the bearing forces to the center of mass of the base. The bearings apply forces only in the $x-$ and $y-$directions, possibly with biaxial interaction. Yet, when these forces are transferred to the center of mass of the base, they may have rotational effects. The bearings may have linear or nonlinear behavior. The linear bearings are represented with linear stiffness and damping. The nonlinear bearings, which are displacement and/or velocity-dependent, are represented in a nonlinear isolation force vector. The active and semiactive devices are assumed to apply forces either in the $x$ or $y-$direction and may cause rotational force effects when they are transferred to the center of mass of the base. The equation of motion of the base is then given by

$$\mathbf{M}_b \ddot{\mathbf{x}}_b^g + \mathbf{C}_b \dot{\mathbf{x}}_b^g + \mathbf{K}_b \mathbf{x}_b^g + \mathbf{F}_s = -\mathbf{M}_b \mathbf{R}_3 \ddot{\mathbf{x}}_g^{abs} + \mathbf{F}_c + \mathbf{F}_{is} \tag{7.4}$$

where $\mathbf{x}_b = [x_b^g \quad y_b^g \quad \theta_b^g]^T$ is the displacement vector of base mass-center with respect to the ground; $\mathbf{M}_b$, $\mathbf{C}_b$ and $\mathbf{K}_b$ are the $3 \times 3$ mass matrix of the base, and the damping and stiffness matrices of the linear isolators, respectively; $\mathbf{R}_3$ is the influence matrix; $\ddot{\mathbf{x}}_g^{abs}$ is the $2 \times 1$ absolute ground acceleration vector ($x-$ and $y-$directions); $\mathbf{F}_c$ and $\mathbf{F}_{is}$ are the $3 \times 1$ effective con-

troller and nonlinear isolator force vectors acting on the base-mass-center, respectively; and $\mathbf{F}_s$ is the superstructure shear force given by

$$\mathbf{F}_s = \mathbf{R}_1^T \mathbf{M}_s (\ddot{\mathbf{x}}_s^b + \mathbf{R}_1 \ddot{\mathbf{x}}_b^{abs}) \tag{7.5}$$

An equation of motion of the whole structure can be obtained by combining equations (7.2), (7.4) and (7.5) as

$$\mathbf{M}\ddot{\mathbf{x}} + \mathbf{C}\dot{\mathbf{x}} + \mathbf{K}\mathbf{x} = \mathbf{S}_1 \mathbf{F}_c + \mathbf{S}_2 \ddot{\mathbf{x}}_g^{abs} + \mathbf{S}_3 \mathbf{F}_{is} \tag{7.6}$$

where $\mathbf{x} = [(\eta_s^b)^T \quad (\mathbf{x}_b^g)^T]^T$ and the corresponding state-space form is given by

$$\dot{\mathbf{q}} = \mathbf{A}\mathbf{q} + \mathbf{B}\mathbf{u} + \mathbf{E}\ddot{\mathbf{x}}_g^{abs} + \mathbf{F}\mathbf{f} \tag{7.7}$$

where $\mathbf{u}$ is the $n_c \times 1$ controller force vector, and $\mathbf{f}$ is the $3n_b \times 1$ nonlinear isolation force vector. Here, $n_c$ and $n_b$ are the number of the controllers and the number of the nonlinear bearings, respectively.

The measurement and output equations used in the numerical simulations are given by

$$\begin{aligned} \mathbf{y}_v &= \mathbf{C}_y \mathbf{q} + \mathbf{D}_y \mathbf{u} + \mathbf{E}_y \ddot{\mathbf{x}}_g^{abs} + \mathbf{F}_y \mathbf{f} + \mathbf{v} \\ \mathbf{z} &= \mathbf{C}_z \mathbf{q} + \mathbf{D}_z \mathbf{u} + \mathbf{E}_z \ddot{\mathbf{x}}_g^{abs} + \mathbf{F}_z \mathbf{f} \end{aligned} \tag{7.8}$$

where $\mathbf{v}$ is the noise vector. In this dissertation, the measurements are absolute accelerations of the center of mass of each floor and base, absolute ground accelerations and controller displacements relative to the ground. All of the measurements are in the $x$– and $y$–directions. The outputs to be minimized are selected to be the drifts of the isolators in the corners and the absolute floor accelerations.

In the following, the details of the equations derived above are given. The state space matrices in equation (7.7) are given as

$$\mathbf{A} = \begin{bmatrix} \mathbf{0} & \mathbf{I} \\ -\mathbf{M}^{-1}\mathbf{K} & -\mathbf{M}^{-1}\mathbf{C} \end{bmatrix}, \qquad \mathbf{B} = \begin{bmatrix} \mathbf{0} \\ \mathbf{M}^{-1}\mathbf{S}_1\mathbf{R}_2^{\mathrm{c}} \end{bmatrix}, \qquad \mathbf{E} = \begin{bmatrix} \mathbf{0} \\ \mathbf{M}^{-1}\mathbf{S}_2 \end{bmatrix},$$
$$\mathbf{F} = \begin{bmatrix} \mathbf{0} \\ \mathbf{M}^{-1}\mathbf{S}_3\mathbf{R}_2^{\mathrm{is}} \end{bmatrix} \tag{7.9}$$

where

$$\mathbf{M} = \begin{bmatrix} \mathbf{I} & \Phi_{\mathrm{s}}^{\mathrm{T}}\mathbf{M}_{\mathrm{s}}\mathbf{R}_1 \\ \mathbf{R}_1^{\mathrm{T}}\mathbf{M}_{\mathrm{s}}\Phi_{\mathrm{s}} & \mathbf{R}_1^{\mathrm{T}}\mathbf{M}_{\mathrm{s}}\mathbf{R}_1 + \mathbf{M}_{\mathrm{b}} \end{bmatrix}, \qquad \mathbf{K} = \begin{bmatrix} \tilde{\mathbf{K}}_{\mathrm{s}} & \mathbf{0} \\ \mathbf{0} & \mathbf{K}_{\mathrm{b}} \end{bmatrix}, \qquad \mathbf{C} = \begin{bmatrix} \tilde{\mathbf{C}}_{\mathrm{s}} & \mathbf{0} \\ \mathbf{0} & \mathbf{C}_{\mathrm{b}} \end{bmatrix} \tag{7.10}$$

Here the superstructure mass matrix is $\mathbf{M}_{\mathrm{s}} = diag[m_x^8 \quad m_y^8 \quad m_\theta^8 \ \ldots \ m_x^1 \quad m_y^1 \quad m_\theta^1]$, and base mass matrix is $\mathbf{M}_b = diag[m_x^{\mathrm{b}} \quad m_y^{\mathrm{b}} \quad m_\theta^{\mathrm{b}}]$. The damping and stiffness matrices of the substructure are given by

$$\mathbf{C}_{\mathrm{b}} = \mathbf{R}_2^{\mathrm{is}}\mathbf{C}^{\mathrm{is}}(\mathbf{R}_2^{\mathrm{is}})^{\mathrm{T}}, \qquad \mathbf{K}_{\mathrm{b}} = \mathbf{R}_2^{\mathrm{is}}\mathbf{K}^{\mathrm{is}}(\mathbf{R}_2^{\mathrm{is}})^{\mathrm{T}},$$
$$\mathbf{C}^{\mathrm{is}} = \begin{bmatrix} \mathbf{C}_1^{\mathrm{is}} & & \\ & \ddots & \\ & & \mathbf{C}_{n_{\mathrm{b}}}^{\mathrm{is}} \end{bmatrix}, \qquad \mathbf{K}^{\mathrm{is}} = \begin{bmatrix} \mathbf{K}_1^{\mathrm{is}} & & \\ & \ddots & \\ & & \mathbf{K}_{n_{\mathrm{b}}}^{\mathrm{is}} \end{bmatrix} \tag{7.11}$$

where $\mathbf{C}_i^{\mathrm{is}}$ and $\mathbf{K}_i^{\mathrm{is}}$ are the $3 \times 3$ damping and stiffness matrices of the $i^{\mathrm{th}}$ bearing. In the benchmark problem, the bearings have only axial force components. Therefore the third column and row of each $\mathbf{C}_i^{\mathrm{is}}$ and of each $\mathbf{K}_i^{\mathrm{is}}$ are zero. Also note that, although the vector $\mathbf{f}$ in equation (7.7) is a $3n_{\mathrm{b}} \times 1$ vector, its rotational components are zero. The other matrices are given as

$$\mathbf{S}_1 = \mathbf{S}_3 = \begin{bmatrix} \mathbf{0}_{24\times 3} \\ \mathbf{I}_{3\times 3} \end{bmatrix} \qquad \mathbf{S}_2 = -\begin{bmatrix} \Phi_{\mathrm{s}}^{\mathrm{T}}\mathbf{M}_{\mathrm{s}}\mathbf{R}_1 \\ \mathbf{R}_1^{\mathrm{T}}\mathbf{M}_{\mathrm{s}}\mathbf{R}_1 + \mathbf{M}_{\mathrm{b}} \end{bmatrix}\mathbf{R}_3$$
$$\mathbf{R}_1 = \begin{bmatrix} \mathbf{I}_{3\times 3} \\ \vdots \\ \mathbf{I}_{3\times 3} \end{bmatrix}_{24\times 3} \qquad \mathbf{R}_2^{\mathrm{c}} = [\mathbf{r}_1^{\mathrm{c}} \ \ldots \ \mathbf{r}_{n_{\mathrm{c}}}^{\mathrm{c}}] \qquad \mathbf{R}_3 = \begin{bmatrix} 1 & 0 \\ 0 & 1 \\ 0 & 0 \end{bmatrix} \tag{7.12}$$
$$\mathbf{R}_2^{\mathrm{is}} = [\mathbf{r}_1^{\mathrm{is}} \ \ldots \ \mathbf{r}_{n_{\mathrm{b}}}^{\mathrm{is}}]$$

$$\mathbf{r}_i^{\mathrm{c}} = \begin{cases} [1 \quad 0 \quad -Y_i^{\mathrm{c}}]^{\mathrm{T}}, & \text{controller is in the } x-\text{direction} \\ [0 \quad 1 \quad X_i^{\mathrm{c}}]^{\mathrm{T}}, & \text{controller is in the } y-\text{direction} \end{cases} \qquad \mathbf{r}_i^{\mathrm{is}} = \begin{bmatrix} 1 & 0 & 0 \\ 0 & 1 & 0 \\ -Y_i^{\mathrm{is}} & X_i^{\mathrm{is}} & 1 \end{bmatrix} \tag{7.13}$$

where $(X_i^{\mathrm{c}}, Y_i^{\mathrm{c}})$ and $(X_i^{\mathrm{is}}, Y_i^{\mathrm{is}})$ are the coordinates of the $i^{\mathrm{th}}$ controller and bearing, respectively, relative to the center of mass of the base.

Consider the evaluation output equation in (7.8). The outputs considered are the corner isolator drifts and absolute floor accelerations, $\mathbf{z} = [(\mathbf{x}^{\mathrm{coriso}})^{\mathrm{T}} \quad (\ddot{\mathbf{x}}^{\mathrm{abs}})^{\mathrm{T}}]^{\mathrm{T}}$. Here, the corner isolator drifts are formed as follows:

$$\mathbf{x}^{\mathrm{coriso}} = [d\mathbf{X}_{\mathrm{b}}], \qquad d\mathbf{X}_i = \begin{bmatrix} d\mathbf{x}_i^1 \\ d\mathbf{x}_i^2 \\ \vdots \\ d\mathbf{x}_i^{n_{\mathrm{cr}}} \end{bmatrix}, \qquad d\mathbf{x}_i^j = \begin{bmatrix} dx_i^j \\ dy_i^j \end{bmatrix} \tag{7.14}$$

where $dx_i^j$ and $dy_i^j$ are the drifts of the $j^{\mathrm{th}}$ corner of the $i^{\mathrm{th}}$ floor in the $x$ and $y$–directions, respectively. The absolute acceleration vector is $\ddot{\mathbf{x}}^{\mathrm{abs}} = [\ddot{x}_{\mathrm{b}}^{\mathrm{abs}} \quad \ddot{y}_{\mathrm{b}}^{\mathrm{abs}} \quad \ddot{x}_1^{\mathrm{abs}} \quad \ddot{y}_1^{\mathrm{abs}} \ \ldots \ \ddot{x}_8^{\mathrm{abs}} \quad \ddot{x}_8^{\mathrm{abs}}]^{\mathrm{T}}$.

The state-space equation matrices for this set of outputs are given by

$$\begin{gathered} \mathbf{C}_{\mathrm{z}} = \begin{bmatrix} \mathbf{T}_3\mathbf{T}_2\mathbf{T}_1 & \mathbf{0} \\ -\mathbf{T}_4\mathbf{T}_1\mathbf{M}^{-1}\mathbf{K} & -\mathbf{T}_4\mathbf{T}_1\mathbf{M}^{-1}\mathbf{C} \end{bmatrix}, \qquad \mathbf{D}_{\mathrm{z}} = \begin{bmatrix} \mathbf{0} \\ \mathbf{T}_4\mathbf{T}_1\mathbf{M}^{-1}\mathbf{S}_1\mathbf{R}_2^{\mathrm{c}} \end{bmatrix}, \\ \mathbf{E}_{\mathrm{z}} = \begin{bmatrix} \mathbf{0} \\ \mathbf{T}_4\mathbf{T}_1\mathbf{M}^{-1}\mathbf{S}_2 + \mathbf{R}_4 \end{bmatrix}, \qquad \mathbf{F}_{\mathrm{z}} = \begin{bmatrix} \mathbf{0} \\ \mathbf{T}_4\mathbf{T}_1\mathbf{M}^{-1}\mathbf{S}_3\mathbf{R}_2^{\mathrm{is}} \end{bmatrix} \end{gathered} \tag{7.15}$$

where

$$\mathbf{R}_4 = \begin{bmatrix} \mathbf{I}_{2\times 2} \\ \vdots \\ \mathbf{I}_{2\times 2} \end{bmatrix}_{18\times 2}, \qquad \mathbf{T}_1 = \begin{bmatrix} \mathbf{0} & \mathbf{I} \\ \mathbf{R}_5\Phi & \mathbf{R}_1 \end{bmatrix}, \qquad \mathbf{R}_5 = \begin{bmatrix} & & \mathbf{r}_1^{\mathrm{COM}} \\ & \iddots & \\ \mathbf{r}_8^{\mathrm{COM}} & & \end{bmatrix}_{24\times 24} \tag{7.16}$$

and

$$\mathbf{T}_2 = \begin{bmatrix} \mathbf{I}_{3\times 3} & & & & & \\ -\mathbf{I}_{3\times 3} & \mathbf{I}_{3\times 3} & & & & \\ & -\mathbf{I}_{3\times 3} & \mathbf{I}_{3\times 3} & & & \\ & & \ddots & \ddots & & \\ & & & -\mathbf{I}_{3\times 3} & \mathbf{I}_{3\times 3} \end{bmatrix}_{27\times 27}, \qquad \mathbf{T}_4 = \begin{bmatrix} \mathbf{R}_3^{\mathrm{T}} & & \\ & \ddots & \\ & & \mathbf{R}_3^{\mathrm{T}} \end{bmatrix}_{18\times 27} \tag{7.17}$$

where

$$\mathbf{r}_i^{\mathrm{COM}} = \begin{bmatrix} 1 & 0 & -Y_i^{\mathrm{COM}} \\ 0 & 1 & X_i^{\mathrm{COM}} \\ 0 & 0 & 1 \end{bmatrix} \tag{7.18}$$

and $(X_i^{\mathrm{COM}}, Y_i^{\mathrm{COM}})$ are the offset coordinates of the center of mass of the $i^{\mathrm{th}}$ floor with respect to the center of mass of the base. Also,

$$\mathbf{T}_3 = \begin{bmatrix} \mathbf{P}_{\mathrm{b}} & & & \\ & \mathbf{P}_1 & & \\ & & \ddots & \\ & & & \mathbf{P}_8 \end{bmatrix}, \qquad \mathbf{P}_i = \begin{bmatrix} \mathbf{p}_i^1 \\ \vdots \\ \mathbf{p}_i^{n_{\mathrm{cr}}} \end{bmatrix}, \qquad \mathbf{p}_i^j = \begin{bmatrix} 1 & 0 & -Y_i^j \\ 0 & 1 & X_i^j \end{bmatrix} \tag{7.19}$$

where $(X_i^j, Y_i^j)$ are the coordinates of the $j^{\mathrm{th}}$ corner of the $i^{\mathrm{th}}$ floor in the $x$ and $y$–directions, respectively. Here, it is assumed that number of corners for all floors are same and equal to $n_{\mathrm{cr}}$. If they are not equal, $\mathbf{T}_3$ should be modified appropriately. Other state-space matrices, such as matrices of the measurement equation, can easily be derived using above information.

### 7.2.3 Isolation Elements

As mentioned before, two types of the benchmark structure are considered in this dissertation: linear and nonlinear. The major difference between these two structures is the isolation layer elements.

The linear benchmark structure has a linear isolation layer, which consist of 91 linear elastic rubber bearings. Linear bearings have linear stiffness and linear damping. The locations of the isolators are given in the benchmark definition paper (Narasimhan *et al*., 2006).

The nonlinear benchmark structure has a nonlinear isolation layer, where the nonlinear isolators are selected as 31 linear elastomeric rubber bearings and 61 lead-rubber bearings. The locations of the lead-rubber bearings are the same as the locations of the sliding friction bearings in the definition paper (Narasimhan *et al*., 2006). The linear elastomeric bearings are modelled with a linear stiffness and a linear viscous damping. The lead-rubber bearings are modelled with a bilinear hysteretic stiffness and a linear viscous damping.

A simplification in the modelling of the isolators is used as follows (see Figure 7.2): Let the linear stiffness of the elastomeric rubber bearings be $k$. Let the preyield and the postyield stiffness of the lead-rubber element be $k_1$ and $k_2$, respectively. The lead-rubber bearing can be considered as a combination of two elements: (1) the rubber, which can be modelled as a linear stiffness element with stiffness $k_2$, and (2) the lead that can be modelled as an elastic-perfectly-plastic stiffness element with a preyield stiffness $(k_1 - k_2)$ and a zero postyield stiffness. In this paper, it is assumed that the stiffness of the rubber in the lead-rubber bearings is equal to the stiffness of the elastomeric rubber bearings, that is $k_2 = k$. Finally, this simplification leads to a total of 92 linear stiffness elements with stiffness $k$ and 61 elastic-perfectly-plastic elements with preyield stiffness $(k_1 - k_2)$ and zero postyield stiffness (Figure 7.3). The 92 linear elements are represented in the matrix $\mathbf{K}_\mathrm{b}$ and 61 elastic-perfectly-plastic elements are represented in $\mathbf{F}_\mathrm{is}$ of equation (7.4). Similarly, 92 linear viscous damping elements for rubber bearings are represented in $\mathbf{C}_\mathrm{b}$.

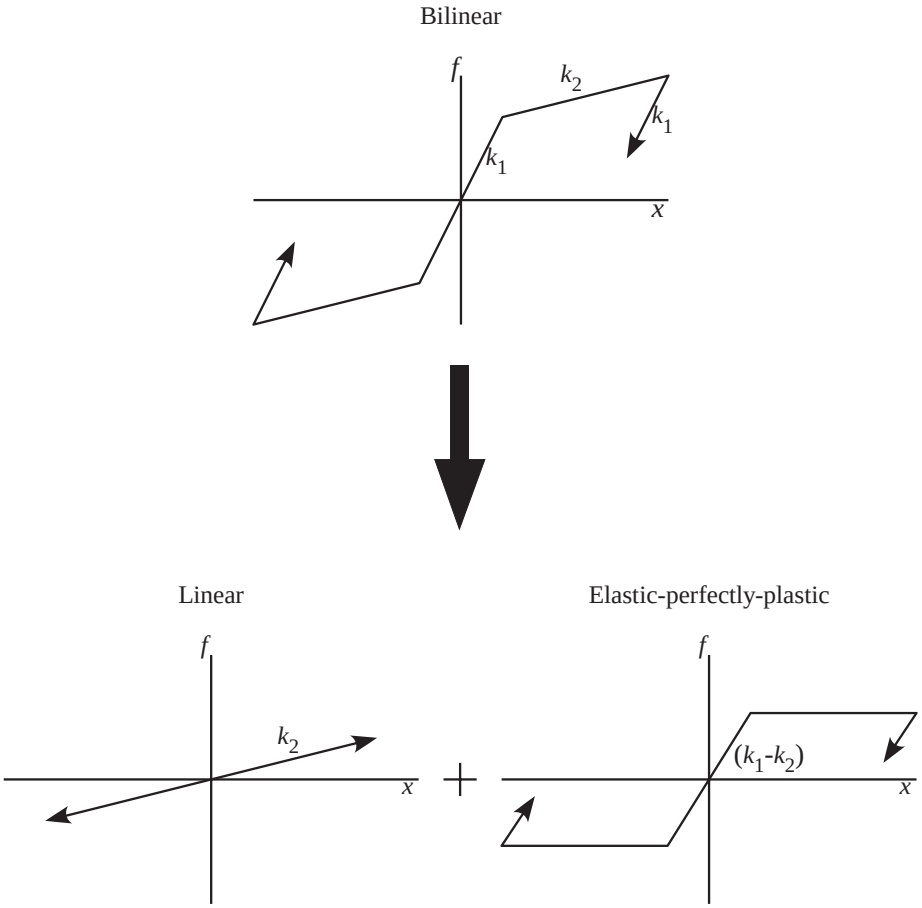


**Figure 7.2** Simplification of the bilinear model

The stiffness and damping values for the isolators are given in the benchmark problem definition paper and are as follows: the yield displacement, the preyield and postyield stiffness of the lead-rubber bearings are given as 2.388cm, 6466.100 kN/m and 919.422 kN/m, respectively. The stiffness of the elastomeric rubber bearings are given as 919.422 kN/m. The damping for both of the elements is taken as 101.439 kN·s/m. Therefore, the analysis and the design stages use 92 linear rubber elements with a stiffness of 919.422 kN/m and a damping of 101.439 kN·s/m, and 61 lead-plugs with a preyield stiffness of 5546.678 kN/m and zero postyield stiffness.

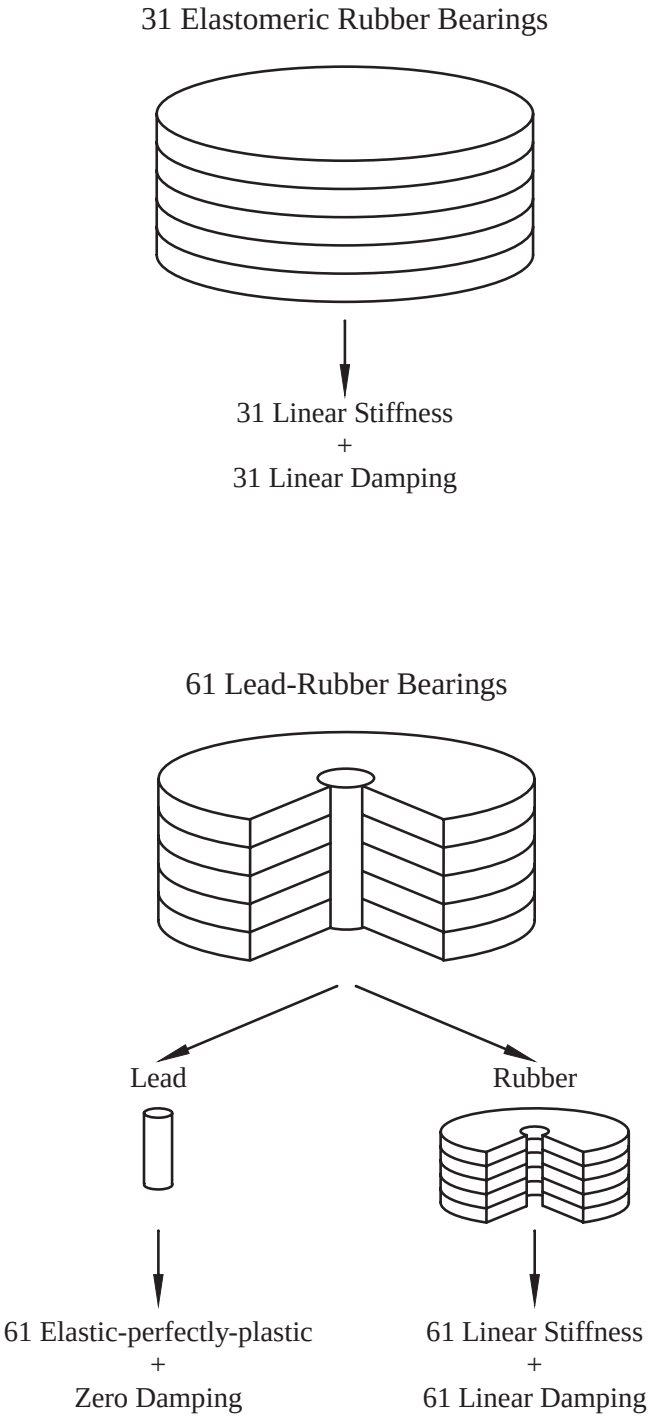


**Figure 7.3** Modelling of the rubber and LRB bearings

### 7.2.4 Controller Design

In the study of the benchmark structure, an LQR control strategy is utilized along with a Kanai-Tajimi filter and a Kalman estimator, which results in a linear quadratic Gaussian (LQG) controller. For the sake of completeness, the overall control strategy is reviewed here. Please note that the control strategy given below is based on a linear structure, yet it will also be used in the control of the nonlinear benchmark structure, where an equivalent linear model of the structure is obtained through an iterative method.

Let the state-space representation of the equation of motion, the measurements and the evaluation output to be minimized of a linear benchmark structure be given as

$$\begin{aligned} \dot{\mathbf{q}} &= \mathbf{A}\mathbf{q} + \mathbf{B}\mathbf{u} + \mathbf{E}\ddot{\mathbf{x}}_{\mathrm{g}}^{\mathrm{abs}} \\ \mathbf{y} &= \mathbf{C}_{\mathrm{y}}\mathbf{q} + \mathbf{D}_{\mathrm{y}}\mathbf{u} + \mathbf{E}_{\mathrm{y}}\ddot{\mathbf{x}}_{\mathrm{g}}^{\mathrm{abs}} + \mathbf{v} \\ \mathbf{z} &= \mathbf{C}_{\mathrm{z}}\mathbf{q} + \mathbf{D}_{\mathrm{z}}\mathbf{u} + \mathbf{E}_{\mathrm{z}}\ddot{\mathbf{x}}_{\mathrm{g}}^{\mathrm{abs}} \end{aligned} \tag{7.20}$$

where $\mathbf{q}$ is the state vector and $\mathbf{u}$ is the control force. The measurements are absolute floor accelerations, absolute ground accelerations and controller drifts. The outputs to be minimized are drifts of the isolators at the corners and absolute floor accelerations. As a first step to obtain a system to be used in the LQG design, a Kanai-Tajimi filter (Soong and Grigoriu, 1993) given by

$$G_{\mathrm{KT}}(s) = \frac{2\zeta_{\mathrm{g}}\omega_{\mathrm{g}}s + \omega_{\mathrm{g}}^2}{s^2 + 2\zeta_{\mathrm{g}}\omega_{\mathrm{g}}s + \omega_{\mathrm{g}}^2} \tag{7.21}$$

is concatenated to the system (7.34) as shown in Figure 7.4 in both $x$ and $y$–directions to model the ground motion as

$$\ddot{\mathbf{X}}_{\mathrm{g}}^{\mathrm{abs}}(s) = \begin{bmatrix} G_{\mathrm{KT}}(s) & 0 \\ 0 & G_{\mathrm{KT}}(s) \end{bmatrix} \underset{\sim}{\mathbf{W}}(s) \tag{7.22}$$

to obtain an augmented system given by

$$\begin{aligned} \dot{\underset{\sim}{\mathbf{q}}} &= \underset{\sim}{\mathbf{A}}\underset{\sim}{\mathbf{q}} + \underset{\sim}{\mathbf{B}}\underset{\sim}{\mathbf{u}} + \underset{\sim}{\mathbf{E}}\underset{\sim}{\mathbf{w}} \\ \underset{\sim}{\mathbf{y}}_{\mathrm{v}} &= \underset{\sim}{\mathbf{C}}_{\mathrm{y}}\underset{\sim}{\mathbf{q}} + \underset{\sim}{\mathbf{D}}_{\mathrm{y}}\underset{\sim}{\mathbf{u}} + \underset{\sim}{\mathbf{E}}_{\mathrm{y}}\underset{\sim}{\mathbf{w}} + \underset{\sim}{\mathbf{v}} \\ \underset{\sim}{\mathbf{z}} &= \underset{\sim}{\mathbf{C}}_{\mathrm{z}}\underset{\sim}{\mathbf{q}} + \underset{\sim}{\mathbf{D}}_{\mathrm{z}}\underset{\sim}{\mathbf{u}} + \underset{\sim}{\mathbf{E}}_{\mathrm{z}}\underset{\sim}{\mathbf{w}} \end{aligned} \tag{7.23}$$

to be used in the LQG design. In this equation, $\underset{\sim}{\mathbf{w}}$ and $\underset{\sim}{\mathbf{v}}$ are band-limited white noise stochastic vector processes modelled as discrete-time Gaussian pulse processes with disturbance covariance given by $E[\underset{\sim}{\mathbf{w}}(k\Delta t)\underset{\sim}{\mathbf{w}}^{\mathrm{T}}(l\Delta t)] = \mathbf{I}_{2\times 2}\delta_{kl}$ . Based on a previous study by Ramallo *et al*. (2002), the parameters in (7.21) are selected as $\zeta_{\mathrm{g}} = 0.3$ and $\omega_{\mathrm{g}} = 17$ rad/sec, for which the Kanai-Tajimi filter represents the ground motion of some commonly-used near- and far-source earthquake records. In the design of the LQ controller and Kalman filter, the augmented system is used as the plant.

The goal of a standard LQG controller is to find a control gain $\mathbf{K}$ that satisfies the following optimization problem:

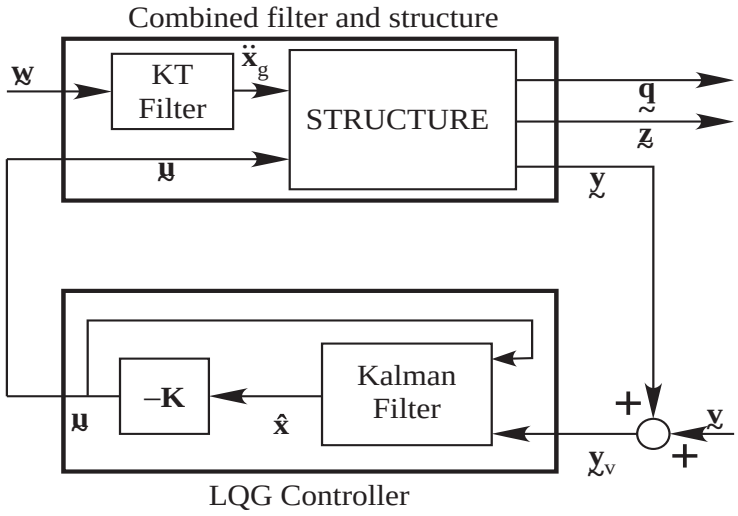


**Figure 7.4** The augmented plant and the LQG controller

$$\begin{aligned} &\min_{\mathbf{K}} E[\underset{\sim}{\mathbf{z}}^{\mathrm{T}}\mathbf{Q}\underset{\sim}{\mathbf{z}} + \underset{\sim}{\mathbf{u}}^{\mathrm{T}}\mathbf{R}\underset{\sim}{\mathbf{u}} + \underset{\sim}{\mathbf{z}}^{\mathrm{T}}\mathbf{N}\underset{\sim}{\mathbf{u}} + \underset{\sim}{\mathbf{u}}^{\mathrm{T}}\mathbf{N}^{\mathrm{T}}\underset{\sim}{\mathbf{z}}] \\ &\text{subject to} \quad (7.34) \quad \text{and} \quad \underset{\sim}{\mathbf{u}} = -\mathbf{K}\hat{\underset{\sim}{\mathbf{q}}} \end{aligned} \tag{7.24}$$

where $\mathbf{Q} = \mathbf{Q}^{\mathrm{T}} > 0$, $\mathbf{R} = \mathbf{R}^{\mathrm{T}} > 0$ and $\mathbf{N}$ are weighting matrices, and $\hat{\underset{\sim}{\mathbf{q}}}$ is the Kalman estimate of the states.

Two sets of weighting matrices are selected for the linear and nonlinear benchmark structure:

1. Weighting matrices for the linear benchmark structure: The control design parameters $\mathbf{Q}$, $\mathbf{R}$ and $\mathbf{N}$ are selected as follows:

$$\mathbf{Q} = b\begin{bmatrix} a\alpha & \\ & \beta \end{bmatrix}, \qquad \mathbf{R} = r\mathbf{I}, \qquad \mathbf{N} = \mathbf{0} \tag{7.25}$$

where

$$\alpha = [\alpha_{\mathrm{b}}], \qquad \alpha_{\mathrm{b}} = \begin{bmatrix} \alpha_{\mathrm{b}}^{1} & & \\ & \ddots & \\ & & \alpha_{\mathrm{b}}^{n_{\mathrm{cr}}} \end{bmatrix}, \qquad \alpha_{\mathrm{b}}^{j} = \begin{bmatrix} (\alpha_{x,\mathrm{b}}^{j})^2 & \\ & (\alpha_{y,\mathrm{b}}^{j})^2 \end{bmatrix} \tag{7.26}$$

and

$$\beta = \begin{bmatrix} \beta_{\mathrm{b}} & & \\ & \ddots & \\ & & \beta_{8} \end{bmatrix}, \qquad \beta_{i} = \begin{bmatrix} (\beta_{x,i}/\omega_x^2)^2 & \\ & (\beta_{y,i}/\omega_y^2)^2 \end{bmatrix} \tag{7.27}$$

where $\alpha_{x,\mathrm{b}}^{j}$ and $\alpha_{y,\mathrm{b}}^{j}$ are the relative importance of the drifts of the $j^{\mathrm{th}}$ corner of the base in the $x-$ and $y-$directions, respectively; $\beta_{x,i}$ and $\beta_{y,i}$ are the relative importance of the absolute accelerations of the mass-center of the $i^{\mathrm{th}}$ floor in the $x-$ and $y-$directions, respectively; $n_{\mathrm{cr}}$ is the number of corners considered at the base; and $\omega_x$ and $\omega_y$

are the frequencies of the dominant modes in the $x-$ and $y-$directions, respectively. The frequencies are included in the weights to normalize the acceleration weights to be compatible with the displacement weights in units and of similar magnitude. This set of parameters reduces the control design problem to a choice of the parameters $a$ and $b$, which determine the relative importance of the corner drifts and absolute floor accelerations.

2. Weighting matrices for the nonlinear benchmark structure: The control design parameter $\mathbf{Q}$ is given as

$$\mathbf{Q} = \begin{bmatrix} a\alpha & \\ & b\beta \end{bmatrix} \tag{7.28}$$

and, $\alpha$, $\beta$, $\mathbf{R}$ and $\mathbf{N}$ are same as the values given in the linear case. While a different $\mathbf{Q}$ is used for the nonlinear structure, it is clear that any control design represented by (7.25) can also be represented by (7.28).

The states are estimated using a Kalman filter. Given that $E[\underset{\sim}{\mathbf{w}}\underset{\sim}{\mathbf{w}}^{\mathrm{T}}] = \mathbf{I}_{2\times 2}$, $E[\underset{\sim}{\mathbf{v}}\underset{\sim}{\mathbf{v}}^{\mathrm{T}}] = \mathbf{R}_{\mathrm{n}}$ and $E[\underset{\sim}{\mathbf{w}}\underset{\sim}{\mathbf{v}}^{\mathrm{T}}] = \mathbf{N}_{\mathrm{n}}$, the Kalman filter finds an estimate of the states $\hat{\underset{\sim}{\mathbf{q}}}$ that minimizes the covariance of the steady state error in the states given by

$$\lim_{t\to\infty} E[(\underset{\sim}{\mathbf{q}} - \hat{\underset{\sim}{\mathbf{q}}})(\underset{\sim}{\mathbf{q}} - \hat{\underset{\sim}{\mathbf{q}}})^{\mathrm{T}}] \tag{7.29}$$

Let the magnitude of the sensor noises be on the order of $100\xi$ percent of the measurements without noise. Then,

$$\mathbf{R}_{\mathrm{n}} = E[\underset{\sim}{\mathbf{v}}\underset{\sim}{\mathbf{v}}^{\mathrm{T}}] = E[(\xi\underset{\sim}{\mathbf{y}})(\xi\underset{\sim}{\mathbf{y}})^{\mathrm{T}}] = \xi^2 E[\underset{\sim}{\mathbf{y}}\underset{\sim}{\mathbf{y}}^{\mathrm{T}}] = \xi^2 \underset{\sim}{\mathbf{C}}_{\mathrm{y}}\mathbf{X}\underset{\sim}{\mathbf{C}}_{\mathrm{y}}^{\mathrm{T}} \tag{7.30}$$

where state covariance matrix $\mathbf{X}$ is the solution of the following Lyapunov equation

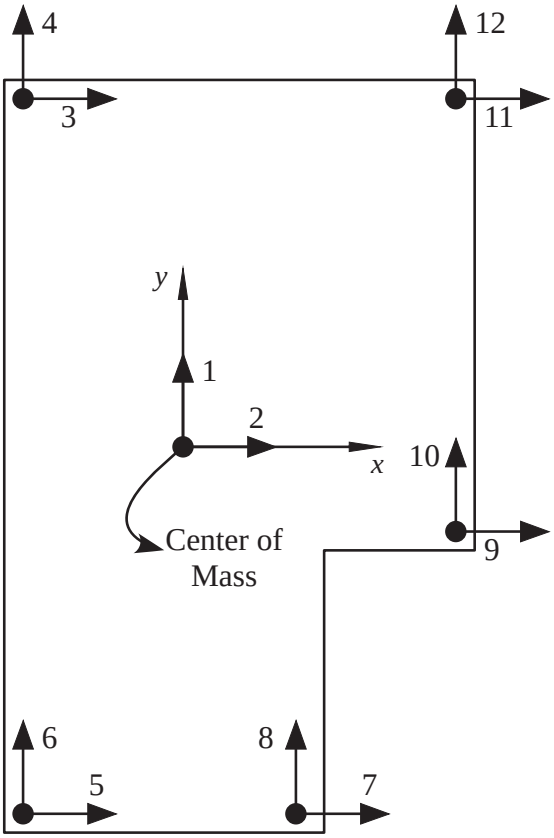


**Figure 7.5** Locations of the controllers; at each point there are two controllers.

$$(\underset{\sim}{\mathbf{A}} - \underset{\sim}{\mathbf{B}}\mathbf{K})\mathbf{X} + \mathbf{X}(\underset{\sim}{\mathbf{A}} - \underset{\sim}{\mathbf{B}}\mathbf{K})^{\mathrm{T}} + \underset{\sim}{\mathbf{E}}\underset{\sim}{\mathbf{E}}^{\mathrm{T}} = \mathbf{0} \tag{7.31}$$

In this study, the common assumption of uncorrelated excitation and sensor noise, *i.e.*, $\mathbf{N}_{\mathrm{n}} = \mathbf{0}$, is held. The schematic representation of the controlled structure is given by Figure 7.4.

In this study, controllers are placed at the corners and center of mass of the base as shown in Figure 7.5. At each location, there are two controllers — in the $x$– and $y$–directions.

### 7.2.5 Performance Indices and Earthquake Ground Motion Data

There are various performance indices defined in the benchmark problem definition paper (Narasimhan *et al*., 2006). In addition to these indices, two new indices are introduced in this

**Table 7.1:** Definitions of the performance indices

| *J* | Definition |
|---|---|
| $J_1$ | Peak Base Shear |
| $J_2$ | Peak First Floor Shear |
| $J_3$ | Peak Base Drift |
| $J_4$ | Peak Interstory Drift |
| $J_5$ | Peak Absolute Floor Acceleration |
| $J_6$ | Peak Controller Force |
| $J_7$ | RMS Base Drift |
| $J_8$ | RMS Absolute Floor Acceleration |
| $J_9$ | Energy Absorbed by the Control Devices |
| $J_{10}$ | Peak Controller Force[a] |
| $J_{11}$ | RMS Floor Drifts |

a. This index is different than $J_6$. Please see Section 7.2.5.

study. These are summarized in Table 7.1. All indices are normalized with the corresponding uncontrolled system indices, except indices $J_6$, $J_9$ and $J_{10}$. In both linear and nonlinear benchmark structures, the uncontrolled structure is the uncontrolled nonlinear benchmark structure as this will allow comparison to a realistic isolation system used in engineering practice. Index $J_6$ is the peak control force that is transferred to the center of mass of the base and normalized by peak base shear, while index $J_{10}$ is the peak control force normalized by the weight of the structure. $J_9$ is the total energy absorbed by control devices normalized by the energy input into the structure by the ground motion.

**Table 7.2:** Earthquake ground motion data used in the numerical simulations

| Earthquake | Location |
|---|---|
| Northridge, California (1994) | Newhall |
| | Sylmar |
| | Rinaldi |
| Imperial Valley, California (1940) | El Centro |
| Kobe, Japan (1995) | Kobe |
| Jiji, Taiwan (1999) | Jiji |
| Erzincan, Turkey (1992) | Erzincan |

The performance index $J_9$, the energy absorbed by the control devices, is important in this study since it can be considered as another type of deterministic dissipativity index. In the numerical studies, similarity of $J_9$ to the other dissipativity indices is also investigated.

Seven earthquake ground motion data with two components — fault-normal and fault-parallel — are used in the numerical simulations. These are summarized in Table 7.2. Details of these data can be found in the benchmark definition paper (Narasimhan *et al*., 2006).

### 7.2.6 Design Considerations

As in any control design, control of the benchmark building is also a trade-off problem. Since it would be impractical to concentrate on all of these indices, two major indices are considered to be important in this study: $J_3$ and $J_5$, *i.e.*, the peak base drift and the peak absolute floor acceleration. In a real-life control problem, other indices, such as $J_4$, the peak interstory drift may have to be taken into account. Therefore, the performance indices given in the dissipativity analysis should not be considered as a final design.

## 7.3 Benchmark Structure with Linear Isolation

In this section, the linear benchmark structure is investigated. As discussed before, the linear structure is exactly the same as the nonlinear structure that is given in the previous section except that nonlinear lead-rubber bearings are replaced with linear rubber bearings. A clipped optimal control strategy is applied to the benchmark structure, where a conventional approach for the design of the primary controller is utilized. In this approach, an active controller is designed assuming the damper is a fully active device; *i.e.,* it can apply dissipative forces as well as non-dissipative forces to the structure. This controller is selected such that it yields the best performance according to a predefined design goal for several earthquake ground motions. Then, the selected active controller is simply used in the clipped optimal control as a primary controller. Clearly, the dissipative nature of the controller is not taken into account in the design process.

In the following, a conventional semiactive design approach is explained for two design goals and applied to the linear benchmark structure as explained above. Performance indices are presented graphically and tabularly for both active and semiactive structures. Then, a dissipativity analysis is provided based on the dissipativity indices.

### 7.3.1 Conventional Semiactive Design

As the control design parameters given in the previous sections imply, two major design goals are considered. The first design goal aims to reduce peak base drift $J_3$; the resulting design is called DES1. The second design, called DES2, aims to reduce peak absolute floor accelerations $J_5$. In the following, the parameters $a$ and $b$ are investigated to yield the best $J_3$ and $J_5$ values for both designs. Moreover, as the controllers obtained from this design will be used for semiactive control, it is also desired that $J_{10} < 0.15$, which means the peak primary control force cannot exceed 15% of the weight of the structure.

**Table 7.3:** Conditions on the performance indices for control designs

| *J* | DES1 | DES2 |
|---|---|---|
| $J_3$ | min ($J_3$) | $J_3 < 1.0$ |
| $J_4$ | $J_4 < 1.0$ | |
| $J_5$ | $J_5 < 1.0$ | min ($J_5$) |
| $J_{10}$ | $J_{10} < 0.15$ | |

Conventional semiactive design requires the selection of the best active control design that is defined by the design goal. For example, for the design DES1, the selected control design should yield the best $J_3$ value while other indices have reasonable values. Similarly, the selected control design for DES2, should yield the best $J_5$ value while other indices have reasonable values. A set of conditions are defined in Table 7.3 to achieve these goals. These values are user-dependent and can be selected in different ways. To find the control parameters ($a$, $b$) of the designs that satisfy the performance indices given in Table 7.3, a numerical search is conducted for each of the earthquake ground motion records. In this numerical study, a fully active system is analyzed for the earthquakes provided by the benchmark definition study for a wide range of control design parameters ($a$, $b$), and performance indices are computed for each controller. Then, two controllers are selected that satisfy the conditions given in Table 7.3. The control weight parameters for these designs are given in Table 7.4, along with the final LQR parameters, which are found by averaging the design parameters that are selected for the earthquakes.

The control design of the benchmark building is a very complex trade-off problem, and various design approaches may yield different performances. To illustrate this challenge and the general appearance of the performance indices of the active system, the best and the final control designs for DES1 and DES2 are graphed along with some of the performance indices for some of

the earthquakes in Figures 7.6 to 7.13. It is easy to observe that performance indices $J_1$, $J_2$ and $J_5$ show similar behavior. Likewise, $J_3$ and $J_4$ have similar behavior, and they show the trade-off compared to the former set of indices. So, any design that favors one group of indices compromises the other group of indices. Moreover, they show different behaviors for different earthquakes.

To further exploit the trade-off between DES1 and DES2, indices $J_3$ and $J_5$ are graphed in separate figures given by Figures 7.14 and 7.15. The contour graphs prove the challenge associated with the trade-off problem discussed above. For example, if a design is selected for DES1 based on a single earthquake, the design will not be optimal for other earthquakes.

Having decided on the final control design parameters for designs DES1 and DES2, semiactive control can now be simulated using these control designs as primary controllers. In the semiactive simulations, the 20-ton MR damper is used. It is required that the original damper model be modified so that its capacity is suitable for the force levels of the primary controller. A

**Table 7.4:** Best and final controller design parameters

| Earthquake | DES1 | | DES2 | |
|---|---|---|---|---|
| | log(*a*) | log(*b*) | log(*a*) | log(*b*) |
| Newhall | –2.1429 | –0.9184 | –3.9796 | –0.7143 |
| Sylmar | –2.7551 | –0.7143 | –3.3673 | –0.1020 |
| El Centro | –1.7347 | –0.5102 | –3.1633 | 1.1224 |
| Rinaldi | –2.5510 | –0.9184 | –2.7551 | –0.7143 |
| Kobe | –2.1429 | –1.3265 | –3.3673 | –0.3061 |
| Jiji | –1.3265 | –1.7347 | –2.9592 | –1.3265 |
| Erzincan | –1.9388 | –1.1224 | –2.9592 | –0.1020 |
| Final | –1.9096 | –1.0933 | –3.2216 | –0.3061 |

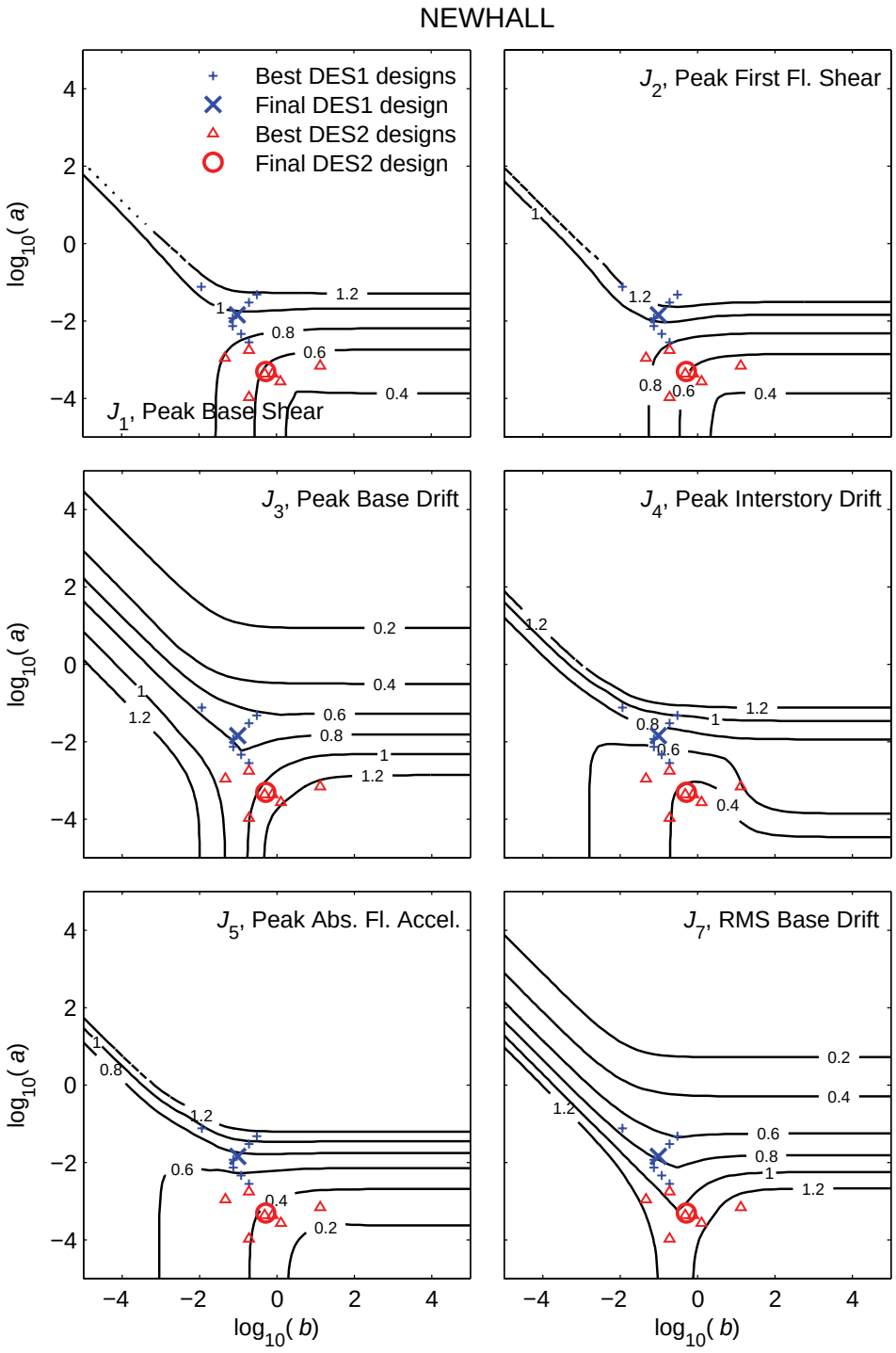


**Figure 7.6** Best and final designs and performance indices $J_1$, $J_2$, $J_3$, $J_4$, $J_5$ and $J_7$ of the linear benchmark structure for Newhall earthquake

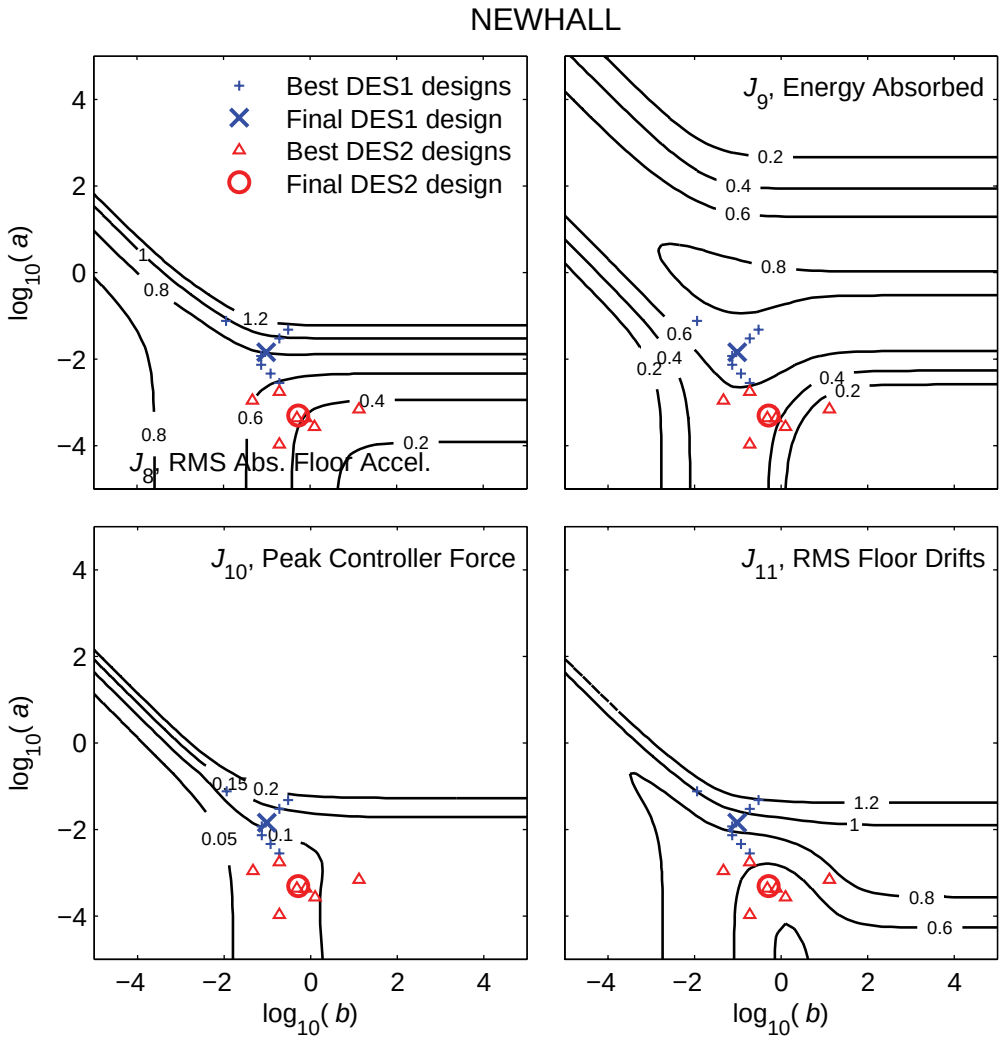


**Figure 7.7** Best and final designs and performance indices $J_8$, $J_9$, $J_{10}$ and $J_{11}$ of the linear benchmark structure for Newhall earthquake

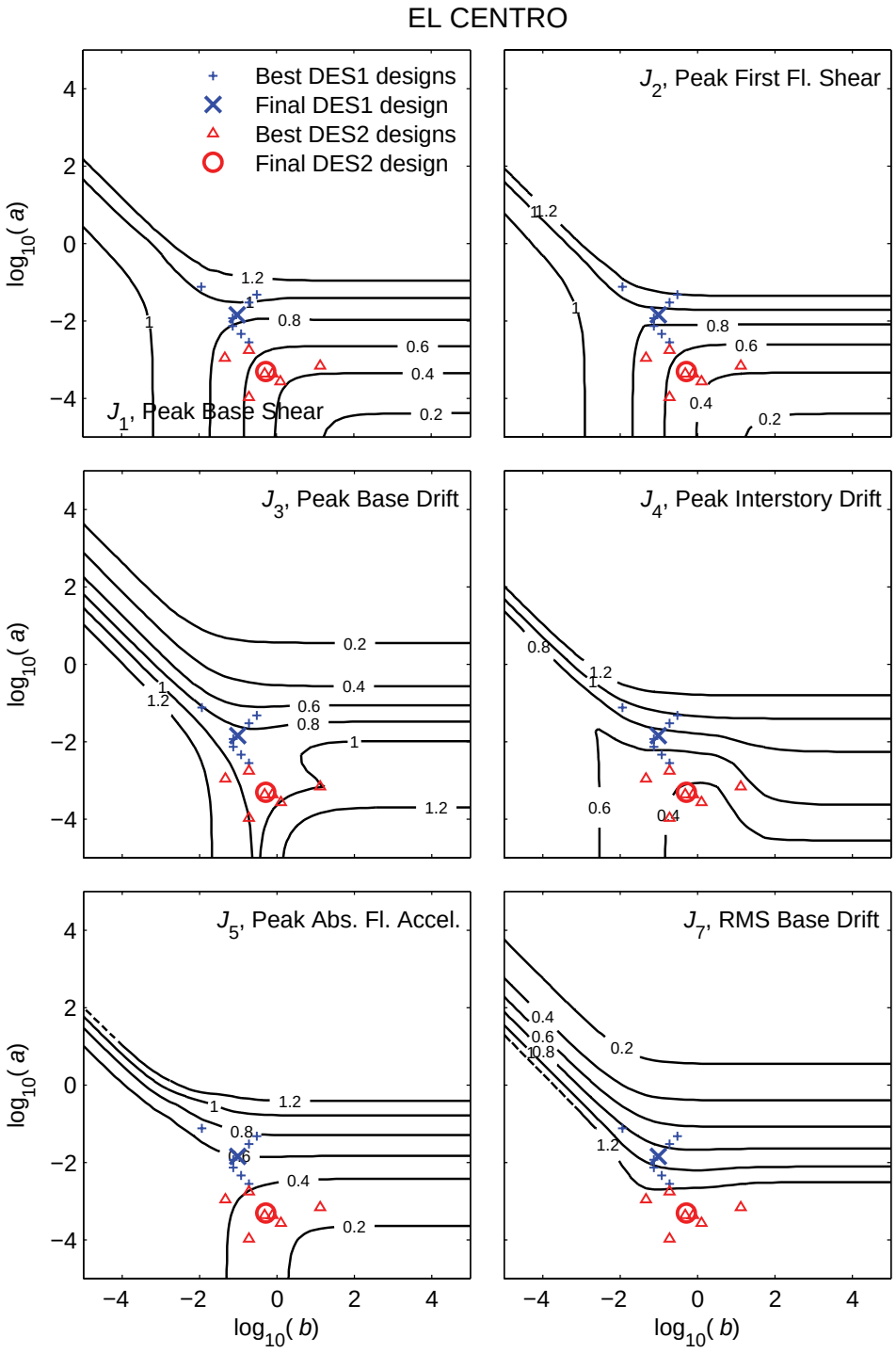


**Figure 7.8** Best and final designs and performance indices $J_1$, $J_2$, $J_3$, $J_4$, $J_5$ and $J_7$ of the linear benchmark structure for El Centro earthquake

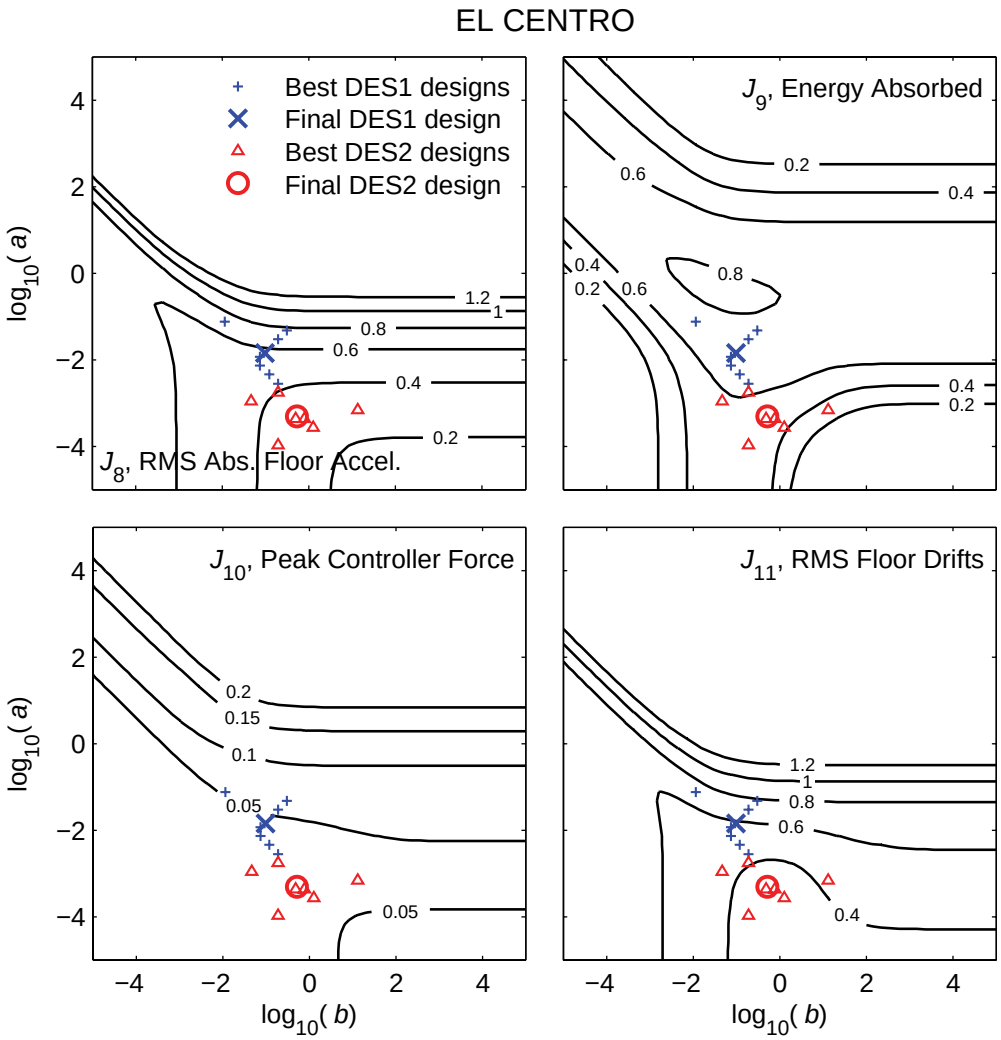


**Figure 7.9** Best and final designs and performance indices $J_8$, $J_9$, $J_{10}$ and $J_{11}$ of the linear benchmark structure for El Centro earthquake

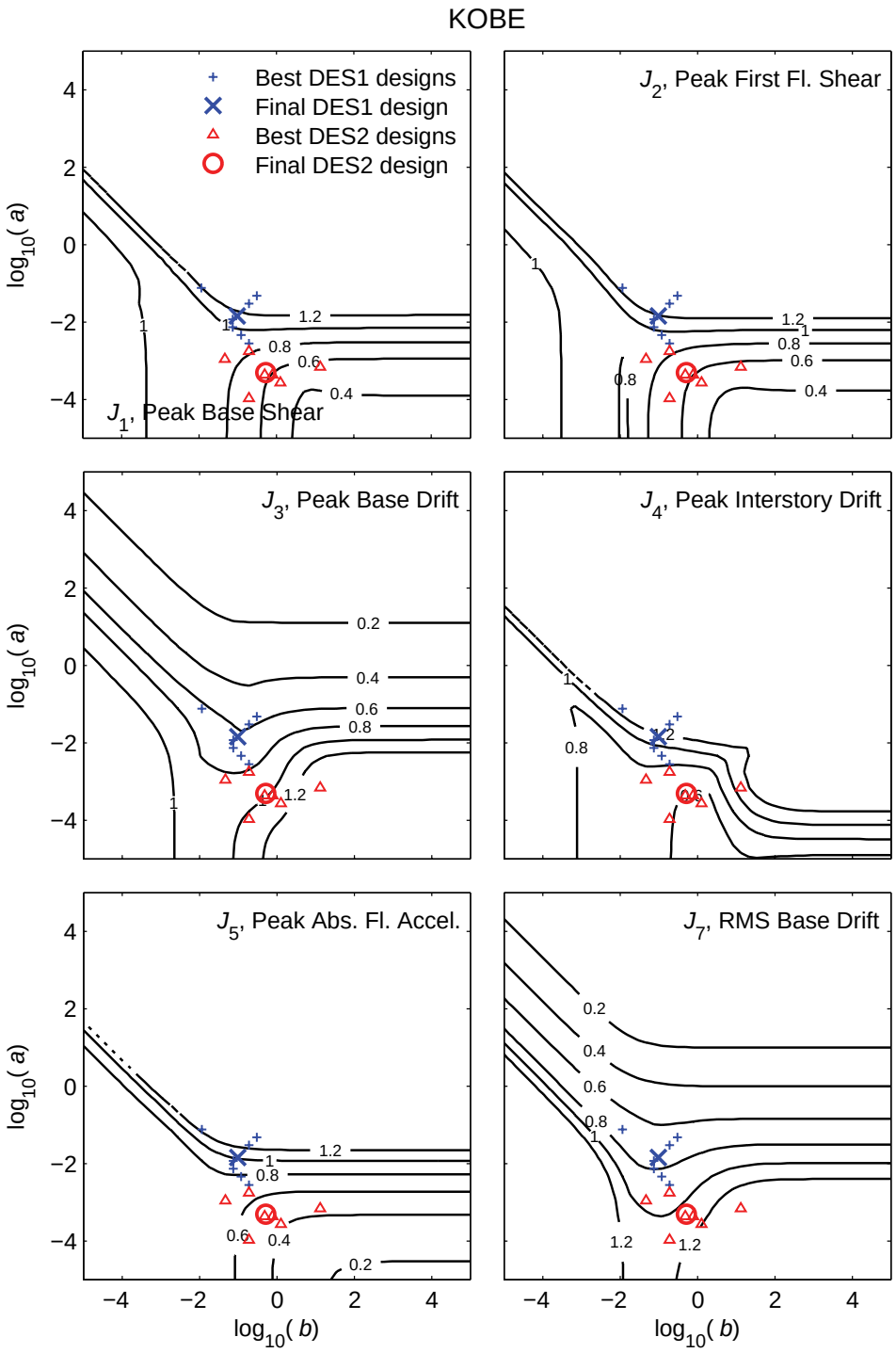


**Figure 7.10** Best and final designs and performance indices $J_1, J_2, J_3, J_4, J_5$ and $J_7$ of the linear benchmark structure for Kobe earthquake

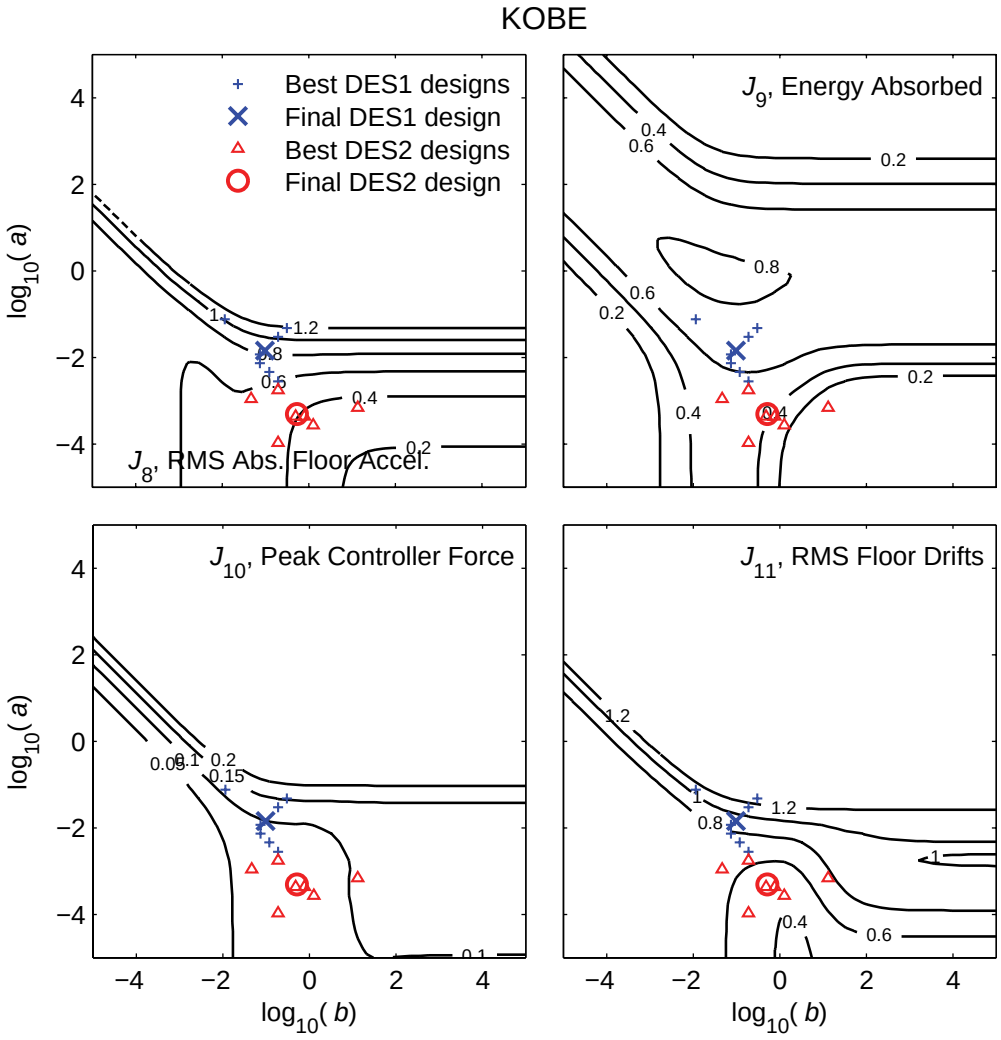


**Figure 7.11** Best and final designs and performance indices $J_8$, $J_9$, $J_{10}$ and $J_{11}$ of the linear benchmark structure for Kobe earthquake

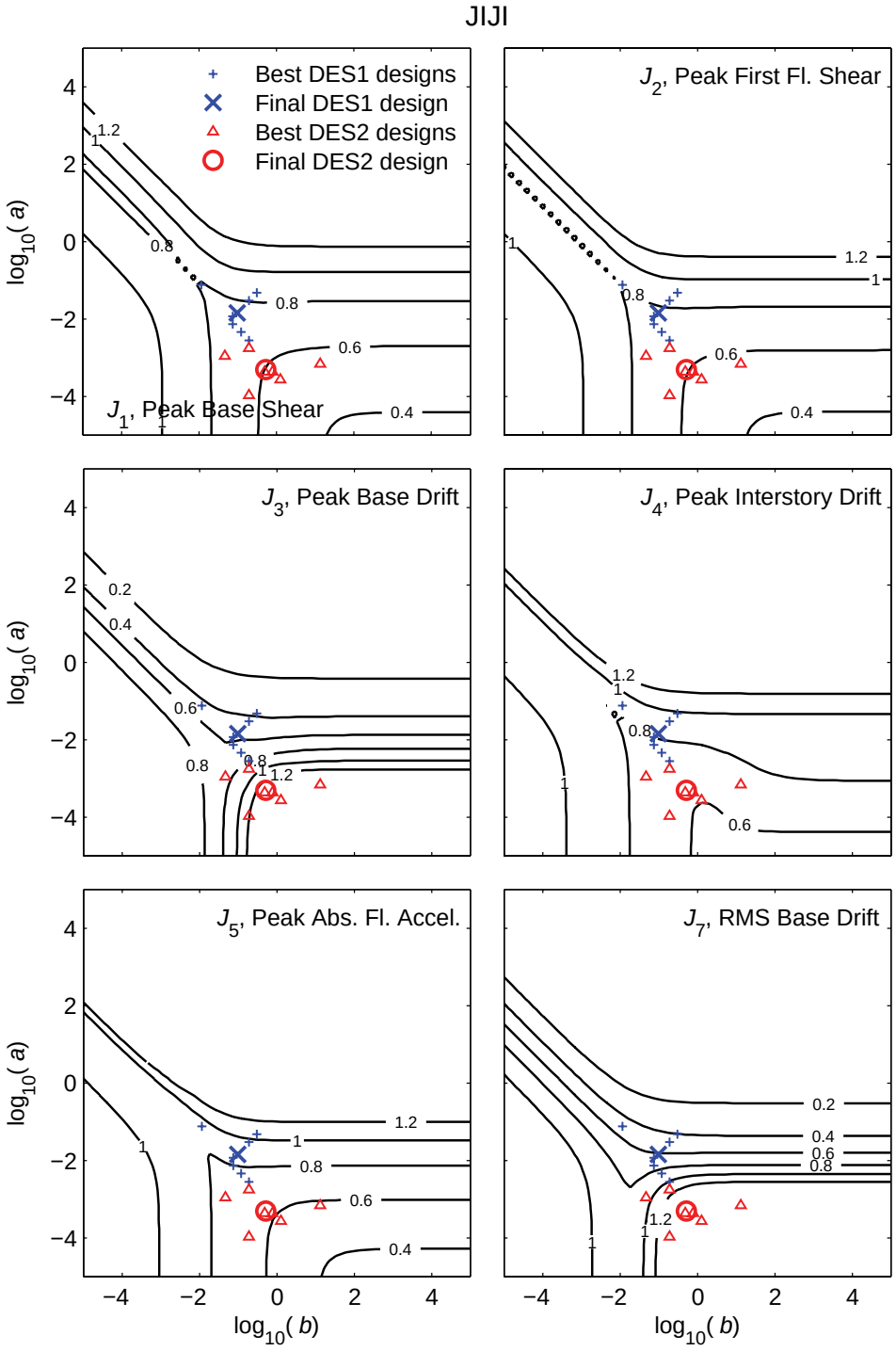


**Figure 7.12** Best and final designs and performance indices $J_1$, $J_2$, $J_3$, $J_4$, $J_5$ and $J_7$ of the linear benchmark structure for Jiji earthquake

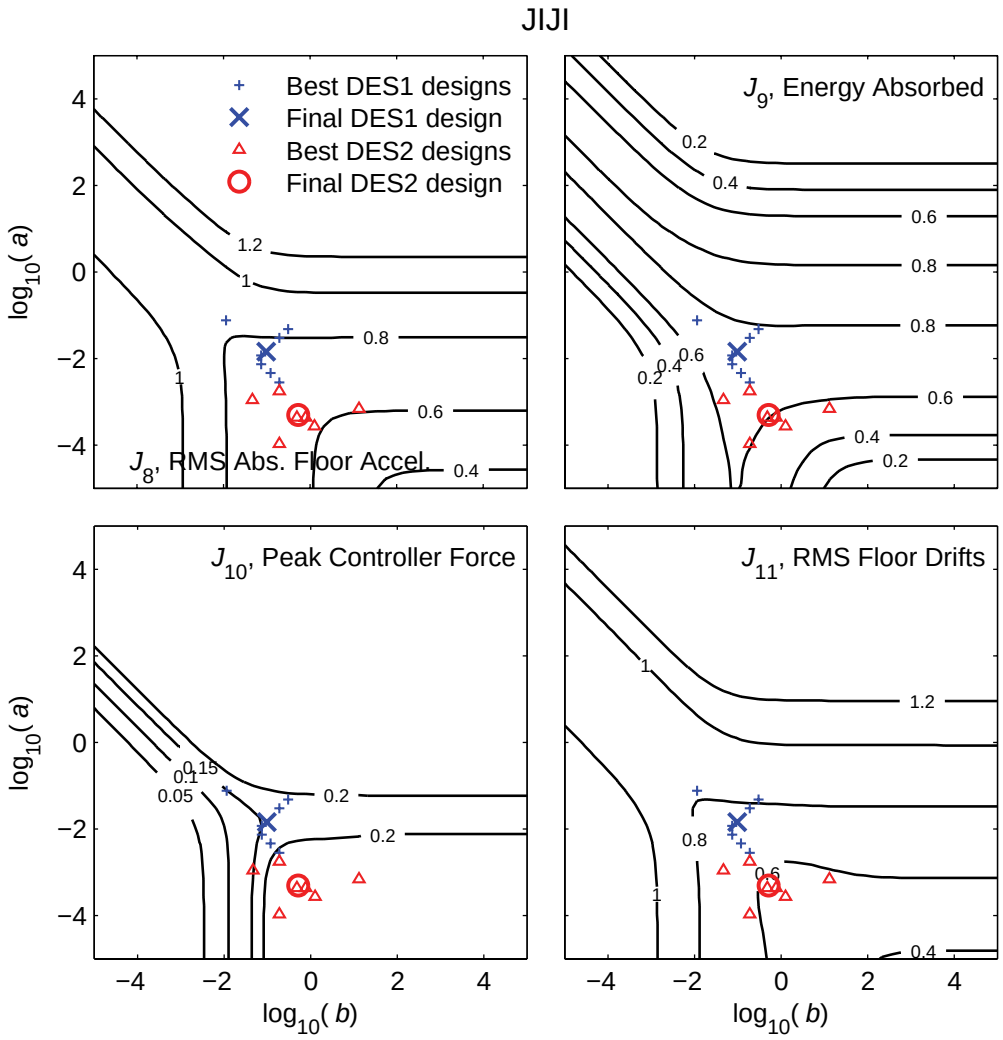


**Figure 7.13** Best and final designs and performance indices $J_8$, $J_9$, $J_{10}$ and $J_{11}$ of the linear benchmark structure for Jiji earthquake

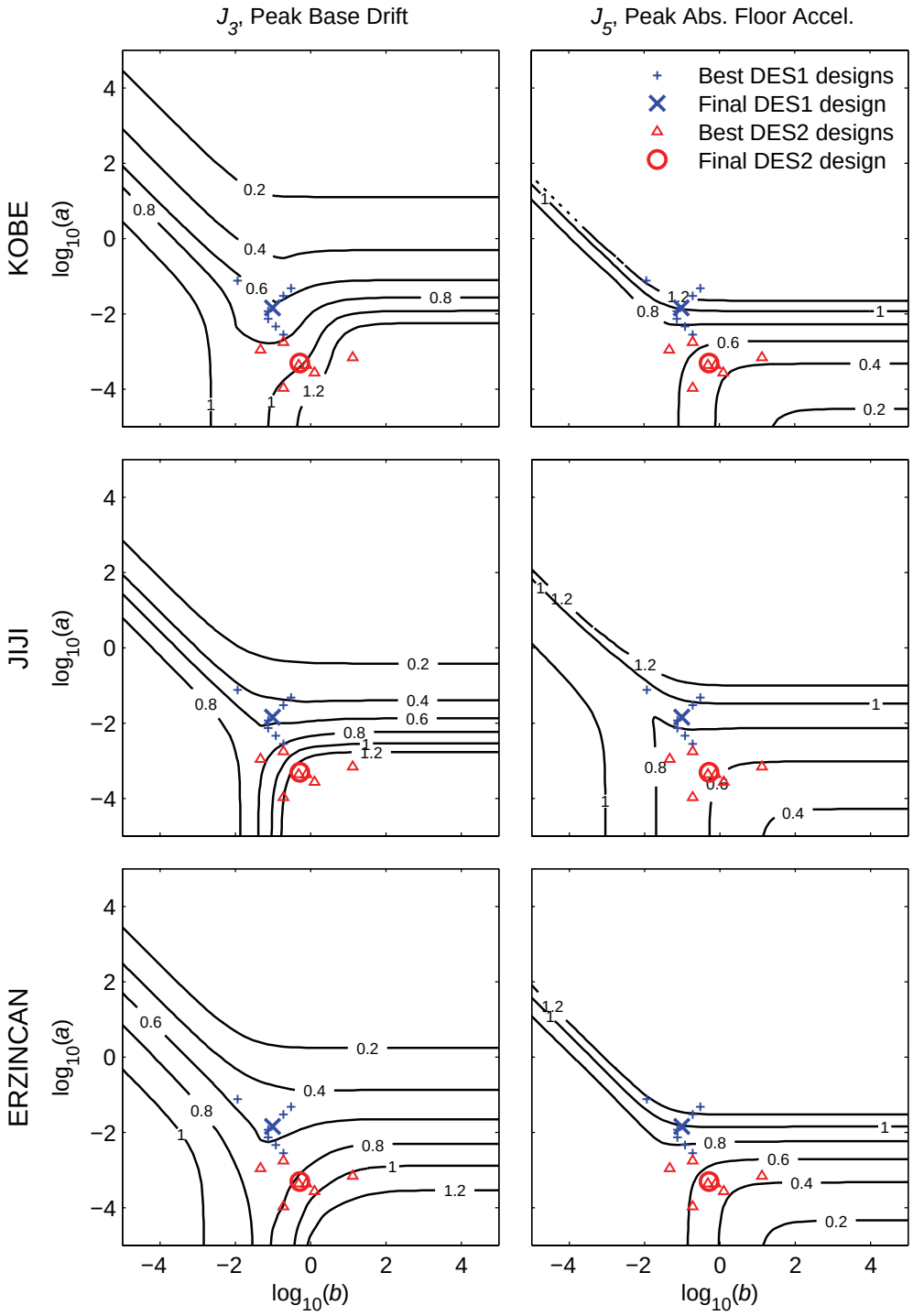


**Figure 7.14** Best and final designs and performance indices $J_3$, and $J_5$ of the linear benchmark structure for Newhall, Sylmar and El Centro earthquakes

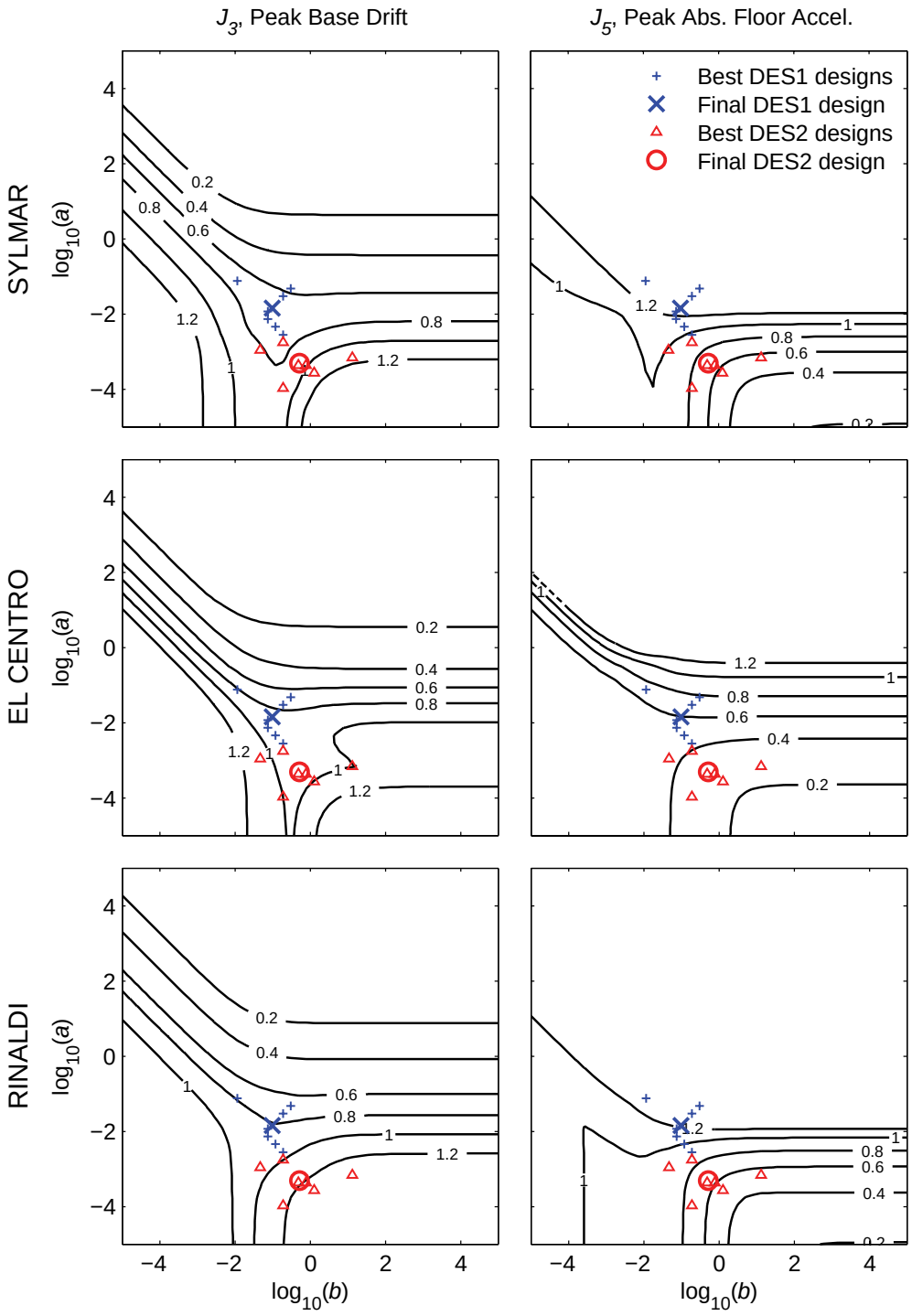


**Figure 7.15** Best and final designs and performance indices $J_3$, and $J_5$ of the linear benchmark structure for Rinaldi, Kobe and Jiji earthquakes

simple approach that is frequently employed by researchers is magnifying the damper force with a coefficient in accordance with the primary controller. To be consistent with the terminology of the previous research (Erkus *et al*. 2002), the term *magnification factor* (MF) will be used for this coefficient. Experience shows that in theoretical research, the MF should be selected for each primary control design separately to achieve the same damper and primary control force levels, so that comparison of the indices will have better physical meaning. It should be noted that this is not an approach taken in a practical problem. In practice, an engineer can select from a variety of commercial dampers with various force capacities that best fits his/her needs.

To obtain MFs suitable for the designs DES1 and DES2, several numerical studies are conducted to achieve similar $J_{10}$ indices for both active and semiactive systems using the available earthquake data. It is found that an MF = 8 and an MF = 5 are suitable for the designs DES1 and DES2, respectively. Using these MF values, semiactive systems are simulated, and performance indices for the active and semiactive systems for the final designs of DES1 and DES2 are given in Tables 7.4 and 7.6.

The results given in Tables 7.4 and 7.6 provide good information about the semiactive performance of designs DES1 and DES2. It is easily observed that DES1 reduces the $J_3$-index successfully, while DES2 is not successful in reducing the $J_5$-index. Considering the trade-off problem between DES1 and DES2, it is easily observed that a semiactive system is more suitable for DES1 than for DES2. Even in DES1, the semiactive system is not successful in reducing all of the indices. It is also observed that $J_9$ has lower values (less energy dissipated by the dampers) in DES2 when compared to DES1. This is a simple indication of the effect of the dissipative nature of the primary controller.

**Table 7.5:** Performance indices for the active and semiactive systems for DES1

| $J$ | | Newhall | | Sylmar | | El Centro | | Rinaldi | | Kobe | | Jiji | | Erzincan | |
|---|---|---|---|---|---|---|---|---|---|---|---|---|---|---|---|
| (Normalized with appropriate quantities) | | ACT | SACT | ACT | SACT | ACT | SACT | ACT | SACT | ACT | SACT | ACT | SACT | ACT | SACT |
| $J_1$ | Peak Base Shear | 0.969 | 0.979 | 0.929 | 1.019 | 0.856 | 0.943 | 1.203 | 1.295 | 1.133 | 1.150 | 0.742 | 0.806 | 1.024 | 0.983 |
| $J_2$ | Peak First Floor Shear | 1.071 | 1.188 | 1.005 | 1.087 | 0.914 | 0.965 | 1.210 | 1.302 | 1.183 | 1.160 | 0.766 | 0.802 | 1.028 | 0.994 |
| $J_3$ | Peak Base Drift | 0.764 | 0.854 | 0.656 | 0.795 | 0.862 | 0.852 | 0.809 | 0.834 | 0.620 | 0.645 | 0.549 | 0.531 | 0.552 | 0.618 |
| $J_4$ | Peak Interstory Drift | 0.689 | 1.103 | 1.169 | 1.338 | 0.725 | 0.930 | 1.204 | 1.284 | 1.139 | 1.568 | 0.821 | 0.876 | 1.006 | 1.032 |
| $J_5$ | Peak Absolute Floor Acceleration | 0.750 | 1.087 | 1.309 | 1.580 | 0.594 | 1.122 | 1.226 | 1.507 | 1.012 | 1.559 | 0.861 | 0.965 | 0.984 | 1.021 |
| $J_6$ | Peak Controller Force | 0.624 | 0.552 | 0.634 | 0.599 | 0.527 | 0.587 | 0.805 | 0.740 | 0.732 | 0.769 | 0.408 | 0.328 | 0.525 | 0.546 |
| $J_7$ | RMS Base Drift | 0.774 | 0.848 | 0.606 | 0.747 | 0.904 | 0.854 | 0.692 | 0.777 | 0.748 | 0.709 | 0.617 | 0.563 | 0.519 | 0.606 |
| $J_8$ | RMS Absolute Floor Acceleration | 0.804 | 1.110 | 0.799 | 0.996 | 0.564 | 0.929 | 1.069 | 1.240 | 0.830 | 1.232 | 0.743 | 0.820 | 0.768 | 0.840 |
| $J_9$ | Energy Absorbed by the Control Devices | 0.701 | 0.718 | 0.740 | 0.737 | 0.713 | 0.750 | 0.735 | 0.732 | 0.675 | 0.723 | 0.740 | 0.720 | 0.758 | 0.747 |
| $J_{10}$ | Normalized Peak Controller Force | 0.111 | 0.099 | 0.150 | 0.142 | 0.044 | 0.049 | 0.194 | 0.178 | 0.099 | 0.104 | 0.155 | 0.124 | 0.115 | 0.120 |
| $J_{11}$ | RMS Floor Drifts | 0.876 | 1.026 | 0.813 | 0.869 | 0.583 | 0.790 | 1.078 | 1.128 | 0.909 | 1.155 | 0.733 | 0.786 | 0.771 | 0.817 |

**Table 7.6:** Performance indices for the active and semiactive systems for DES2

| *J* | | Newhall | | Sylmar | | El Centro | | Rinaldi | | Kobe | | Jiji | | Erzincan | |
|---|---|---|---|---|---|---|---|---|---|---|---|---|---|---|---|
| (Normalized with appropriate quantities) | | ACT | SACT | ACT | SACT | ACT | SACT | ACT | SACT | ACT | SACT | ACT | SACT | ACT | SACT |
| $J_1$ | Peak Base Shear | 0.581 | 1.058 | 0.543 | 1.046 | 0.515 | 1.066 | 0.715 | 1.317 | 0.636 | 1.166 | 0.597 | 0.945 | 0.557 | 1.132 |
| $J_2$ | Peak First Floor Shear | 0.611 | 1.240 | 0.583 | 1.183 | 0.514 | 1.039 | 0.710 | 1.442 | 0.644 | 1.149 | 0.607 | 0.917 | 0.558 | 0.998 |
| $J_3$ | Peak Base Drift | 1.047 | 0.972 | 0.930 | 0.917 | 0.889 | 1.057 | 1.169 | 0.951 | 0.979 | 0.789 | 1.364 | 0.615 | 0.833 | 0.730 |
| $J_4$ | Peak Interstory Drift | 0.379 | 1.123 | 0.695 | 1.297 | 0.375 | 0.962 | 0.693 | 1.277 | 0.597 | 1.461 | 0.640 | 0.911 | 0.612 | 0.916 |
| $J_5$ | Peak Absolute Floor Acceleration | 0.372 | 1.157 | 0.699 | 1.545 | 0.292 | 1.120 | 0.653 | 1.625 | 0.504 | 1.438 | 0.636 | 1.102 | 0.527 | 1.071 |
| $J_6$ | Peak Controller Force | 0.488 | 0.473 | 0.531 | 0.504 | 0.426 | 0.423 | 0.535 | 0.624 | 0.417 | 0.677 | 1.024 | 0.328 | 0.427 | 0.379 |
| $J_7$ | RMS Base Drift | 1.034 | 1.025 | 0.755 | 0.925 | 1.444 | 1.068 | 0.969 | 0.977 | 1.060 | 0.885 | 1.674 | 0.639 | 0.704 | 0.767 |
| $J_8$ | RMS Absolute Floor Acceleration | 0.423 | 1.066 | 0.421 | 0.999 | 0.322 | 0.911 | 0.553 | 1.165 | 0.411 | 1.157 | 0.636 | 0.877 | 0.416 | 0.877 |
| $J_9$ | Energy Absorbed by the Control Devices | 0.477 | 0.651 | 0.504 | 0.649 | 0.521 | 0.678 | 0.548 | 0.650 | 0.416 | 0.656 | 0.605 | 0.649 | 0.541 | 0.655 |
| $J_{10}$ | Normalized Peak Controller Force | 0.087 | 0.084 | 0.126 | 0.120 | 0.035 | 0.035 | 0.129 | 0.150 | 0.056 | 0.091 | 0.389 | 0.125 | 0.094 | 0.083 |
| $J_{11}$ | RMS Floor Drifts | 0.502 | 1.003 | 0.514 | 0.882 | 0.327 | 0.769 | 0.594 | 1.060 | 0.502 | 1.092 | 0.580 | 0.837 | 0.503 | 0.860 |

Clearly, conventional semiactive design never takes into account the dissipativity aspects, and selected designs may yield unacceptable semiactive performance. This makes the semiactive design more challenging since, without considering the actual cause of low performances, an engineer can only do numerical simulations and vast control parameter studies to achieve primary controllers that yield better semiactive performance. This is another challenging task as a semiactive system is already very nonlinear and do not exhibit a well-defined behavior. Moreover, simulations will be very computationaly intensive and, in some cases, time-constraints will limit the number of additional simulations. In the next section, a simple dissipativity analysis is shown to provide useful information in the semiactive design process without doing extensive parametric studies.

### 7.3.2 Dissipativity Analysis

The dissipativity indices that were reviewed and introduced in Chapter 4 are for systems with a single controller and must be adapted to be used for the benchmark problem defined above since it has twelve controllers. A cumulative index is defined to represent the dissipativity characteristics of the control designs as follows:

$$D^{c} = \sum_{i=1}^{N} w_i D_i \tag{7.32}$$

where $D^{c}$ is the cumulative dissipativity index, $N$ is the number of the controllers, $D_i$ is the dissipativity of the $i^{th}$ controller, and $w_i$ is a weight associated with the $i^{th}$ controller, which is defined as follows

$$w_i = \frac{\mathrm{RMS}(u_i)}{\sum_{j=1}^{N} \mathrm{RMS}(u_j)} \tag{7.33}$$

**Table 7.7:** Dissipativity indices for DES1 for Newhall earthquake

| *i* | $D_{\%}$ | | $D_{e}$ | $D_{ne}$ |
|---|---|---|---|---|
| | **Act** | **SAct** | **Act** | **Act** |
| 1 | 0.900 | 0.878 | –1348 | –0.865 |
| 2 | 0.873 | 0.838 | –1349 | –0.853 |
| 3 | 0.900 | 0.880 | –1665 | –0.883 |
| 4 | 0.873 | 0.828 | –1504 | –0.860 |
| 5 | 0.782 | 0.800 | –934 | –0.707 |
| 6 | 0.873 | 0.828 | –1504 | –0.860 |
| 7 | 0.782 | 0.800 | –934 | –0.707 |
| 8 | 0.862 | 0.837 | –1245 | –0.837 |
| 9 | 0.875 | 0.870 | –1242 | –0.845 |
| 10 | 0.813 | 0.798 | –1090 | –0.788 |
| 11 | 0.900 | 0.880 | –1665 | –0.883 |
| 12 | 0.813 | 0.798 | –1090 | –0.788 |
| $D^{c}$ | 0.859 | 0.844 | –1324 | –0.828 |

where $u_i$ is the $i$th control force. Cumulative indices are, therefore, weighted averages of the individual indices.

Tables 7.6 and 7.8 show the dissipativity characteristics of the designs DES1 and DES2 for the Newhall earthquake. These two tables show that the proposed cumulative index is a good indicator for the overall dissipativity characteristics of the structure as the proposed cumulative index represents the individual indices successfully. Further, for other control designs selected randomly from the ($a$, $b$) parameter space, the computed cumulative dissipativity indices (not given here) also validate the proposed index. Another observation is that some controllers have (nearly) identical dissipativity indices for both active and semiactive systems such as fourth and

**Table 7.8:** Dissipativity indices for DES2 for Newhall Earthquake

| $i$ | $D_{\%}$ | | $D_{e}$ | $D_{ne}$ |
|---|---|---|---|---|
| | **Act** | **SAct** | **Act** | **Act** |
| 1 | 0.633 | 0.693 | –1101 | –0.247 |
| 2 | 0.640 | 0.723 | –1046 | –0.244 |
| 3 | 0.550 | 0.692 | –1216 | –0.237 |
| 4 | 0.617 | 0.690 | –1139 | –0.238 |
| 5 | 0.602 | 0.645 | –751 | –0.173 |
| 6 | 0.617 | 0.690 | –1139 | –0.238 |
| 7 | 0.602 | 0.645 | –751 | –0.173 |
| 8 | 0.565 | 0.717 | –962 | –0.238 |
| 9 | 0.648 | 0.700 | –1038 | –0.240 |
| 10 | 0.545 | 0.702 | –794 | –0.205 |
| 11 | 0.550 | 0.692 | –1216 | –0.237 |
| 12 | 0.545 | 0.702 | –794 | –0.205 |
| $D^{c}$ | 0.588 | 0.688 | –1012 | –0.225 |

sixth controller. This is a natural consequence of the symmetry in the control oriented mathematical model. It is also observed in both designs that the fifth and seventh controllers are the least suitable for a damper as both controllers have the lowest dissipativity indices. So, a designer may choose to remove or relocate these dampers to obtain better dissipativity characteristics, or active or passive devices may be used instead of the dampers.

The most important observation in Tables 7.6 and 7.8 is the difference in the dissipativity indices of DES1 and DES2. It is observed that DES1 is by nature more dissipative than DES2. This is true for both active and semiactive systems. This information is very important in under-

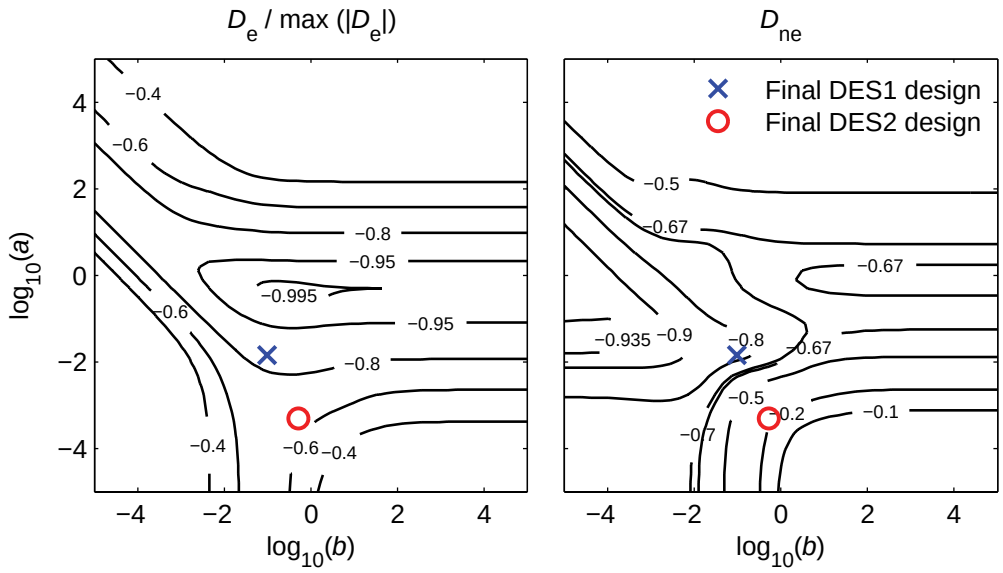


**Figure 7.16** $D_e$ and $D_{ne}$ plots for the active linear benchmark structure

standing the performance indices of DES1 and DES2 given in Tables 7.4 and 7.6. As noted before, semiactive dampers are more successful in imitating the active primary control force in DES1 than they do in DES2. The dissipative nature of the primary controller of DES2 shows that this design is not expected to be successful in imitating the active controller. Thus, if the design goal, for this or a similar structure, is to reduce the absolute accelerations of the structure, the semiactive system may not be successful in reaching this goal due to the low dissipative nature of the controller.

The results and observations given above suggest that the dissipativity of all controllers would be useful in understanding the performance indices provided. In this respect, cumulative dissipativity indices are shown in Figures 7.16 and 7.17 as a function of the control weights ($a$, $b$). Note that $D_e$ is normalized by its maximum absolute value for better visualization.

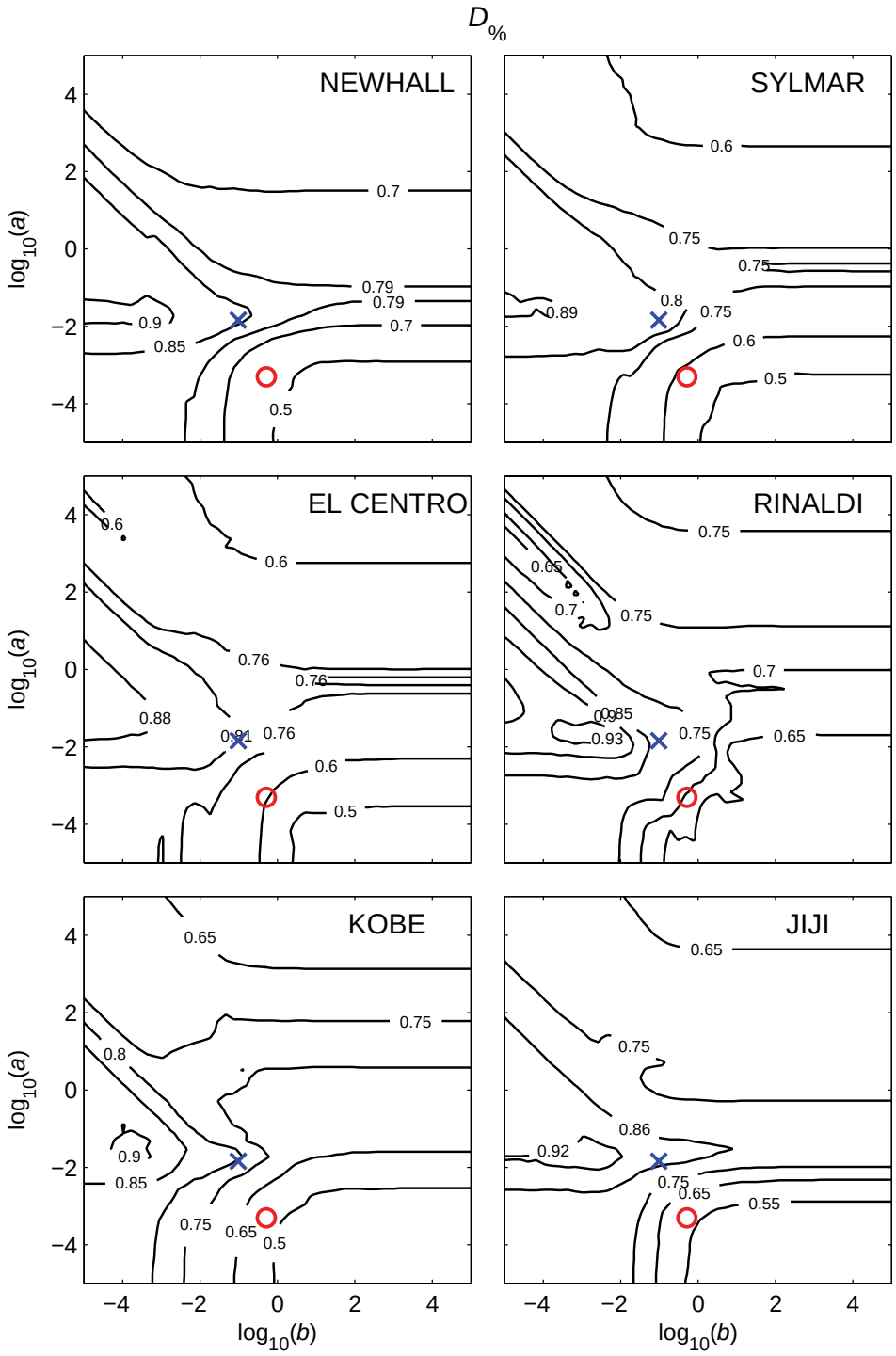


**Figure 7.17** $D_{\%}$ plots for the active linear benchmark structure for various earthquakes

**Table 7.9:** A Classification of dissipativity indices

| | Characteristics of the Control Force | Dissipativity Index |
|---|---|---|
| **GROUP 1** | Normalized mean energy dissipation rate | $D_{ne}$ |
| | Percentage of dissipative forces | $D_{\%}$ |
| | Probability of dissipative forces | $D_p$ |
| **GROUP 2** | Energy dissipation rate | $D_e$ |
| | Energy dissipated by the device | $J_9$ |

An interesting observation in the dissipativity indices are the similarities between them. For example, $D_{ne}$ has a very similar pattern to $D_{\%}$, and $D_e$ has a very similar pattern to $J_9$. The justification for these observations comes from the definitions of the indices. For example, $D_{ne}$ is the correlation coefficient between the control force and the velocity. Considering the relation between $D_p$, $D_{ne}$, and $D_{\%}$, it is quite expected to have a $D_{\%}$ index similar to the $D_{ne}$ index. Also noting that $J_9$ represents the time integral of energy flow rate, it is clear that $D_e$ is proportional to the mean of $J_9$ for a white-noise excitation. Based on these relations, a classification of the indices is provided in Table 7.9.

Another observation is the variation of dissipativity indices of the active system for various values of $J_3$ and $J_5$. For example, all of the dissipativity indices have their peak values for control designs that have either very large $J_3$ or very large $J_5$. Therefore, these controllers are not suitable for the semiactive system that would most probably result in unacceptable semiactive performance indices. This shows that high dissipativity values do not necessarily mean better semiactive performance, which can be explained by the fact that theoretically, semiactive system performance is always bounded by the corresponding active system performance. It is also

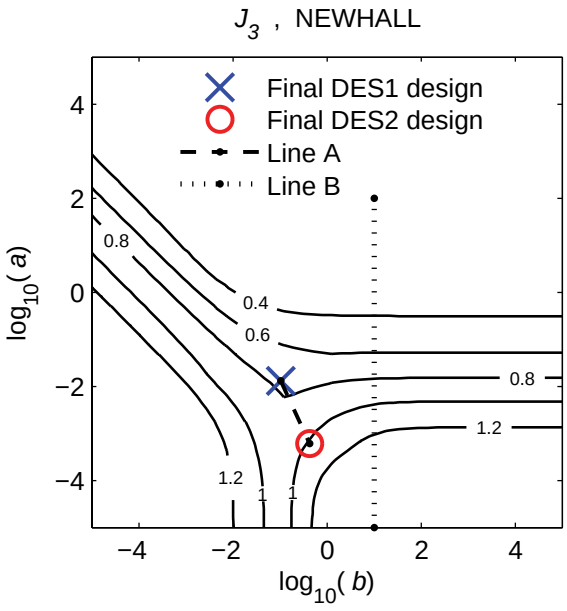


**Figure 7.18** Locations of Lines A and B

observed that control designs with high $D_{ne}$ values do not necessarily have the best $J_3$, yet they have acceptable $J_5$ performance in contrast with the 2-DOF problem considered. These simulations, therefore, show that a control design for a semiactive system should be selected both considering the active performance and the dissipativity of the controller.

To clarify the results given above, performance and dissipativity characteristics of the control designs in between the designs DES1 and DES2 in the ($a$, $b$) parameter space, and control designs not located close to DES1 and DES2 are investigated. For that purpose, two sets of control designs, which are defined by 'Line A' and 'Line B' in Figure 7.8, are considered. Control designs on Line A represent the transition between DES1 and DES2, while designs on Line B are selected because along this line $J_3$ and $J_5$ change in a uniform manner. An important issue here is the magnitudes of the control forces and MR damper forces. A standard way to investigate this

type of problem would be by comparing performances of the systems for the same force levels. Therefore, during the simulations of the Line A, the MF of the dampers are modified in a manner that damper force levels are close to the control force levels. This is done by a linearly distributed MF values between DES1 (MF = 8) and DES2 (MF = 5) values. For line B, MF is taken as 5 for all of the controllers to observe the effect of control force levels on the semiactive performance. In general, a unique MF that is valid for all earthquakes cannot be found as the control force levels may be very different from each other for various earthquakes as shown by performance index $J_{10}$ in Tables 7.4 and 7.6. The dissipativity and performance characteristics of the controllers on Lines A and B are given in Figure 7.19 for the Newhall earthquake. Note that dissipativity index $D_e$ is normalized by its maximum absolute value, and $D_{\%}$ is negated for better visualization. There are various observations that can be drawn from Figure 7.19.

- Observations for Line A: All dissipativities along Line A show similar behavior: high dissipativity for best DES1 and lower dissipativity for best DES2. The transitions of active $J_3$ and $J_5$ indices from DES1 to DES2 are easily observed: Better active $J_5$ values are achieved by controllers with low dissipativity values. The semiactive system has a good $J_3$ for DES1, yet it increases with the decreasing dissipativities. $J_5$ of the semiactive system is always larger than 1 and does not show a particular trend. (This is a good example that shows how complex a semiactive control design can be. For example, it is very likely that $J_5$ will show a different behavior for another earthquake, which does not allow the designer to pick a control design that is efficient for all earthquakes. Again, this is a consequence of the dissipative nature of the semiactive system. While the challenge explained here is a disadvantage from a performance point of view compared to the active system, it does not jeopardize the robust-

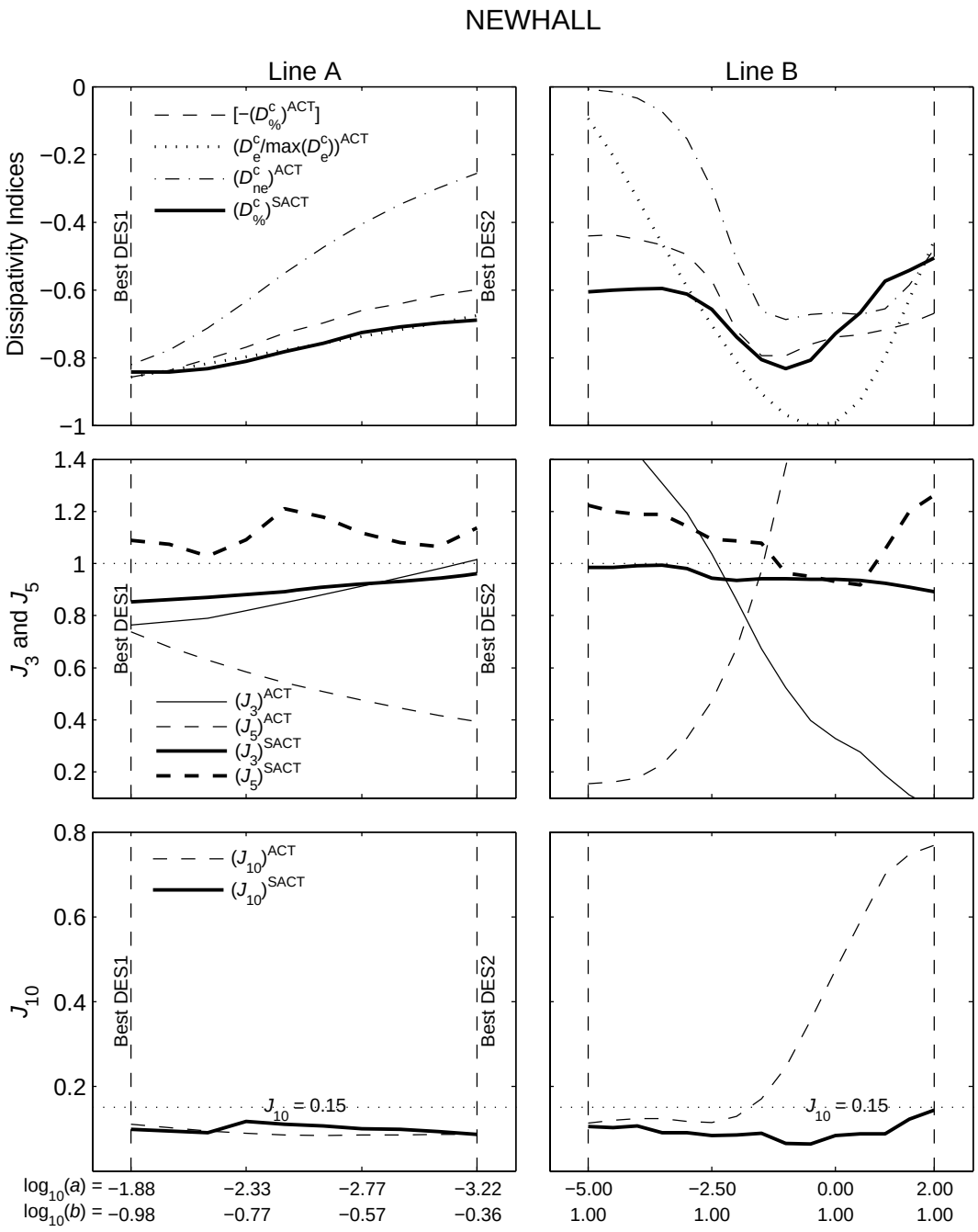


**Figure 7.19** Dissipativity and performance characteristics of the active and semiactive control designs along Lines A and B

ness of the system. Moreover, compared to a passive system, which has fixed properties, it will have a wider range of applicability for various earthquakes.)

- Observations for Line B: The dissipativity plots are more complex, which is due to the controllers selected. One observation along Line B is the similarity between $D_{\%}$ and $D_{\text{ne}}$. The trend of the performance indices are more evident in Line B. However, the effect of large control forces is evident as well. Therefore, to predict the performance of a semiactive system, it is suggested to have controllers with force levels suitable for the practical damper model.

## 7.4 Benchmark Structure with Nonlinear Isolation

A major challenge in the control of the benchmark structure with a nonlinear isolation system is that there is no general well-defined analytical method developed particularly for a system with the various types of nonlinearities that are common in civil engineering. One approach for utilizing linear control theory for the nonlinear structure is to use an equivalent linear model (ELM) of the nonlinear structure. However, the selection of an ELM is not a trivial task. A "good" ELM should behave "similarly" to the nonlinear structure when both are controlled. Therefore, the response characteristics of the controlled nonlinear structure should be known *a priori* to be compared with the controlled ELM response. To find the response of the controlled nonlinear structure, numerical simulations should be carried out. However, the controller that will be used in the simulations can only be designed by linear control theory if an ELM is available. Therefore, to design an ELM, a controller is required, and to design a controller an ELM is required. This creates a circular dependency problem in the design process, which can only be solved with an iterative procedure (Figure 7.20).

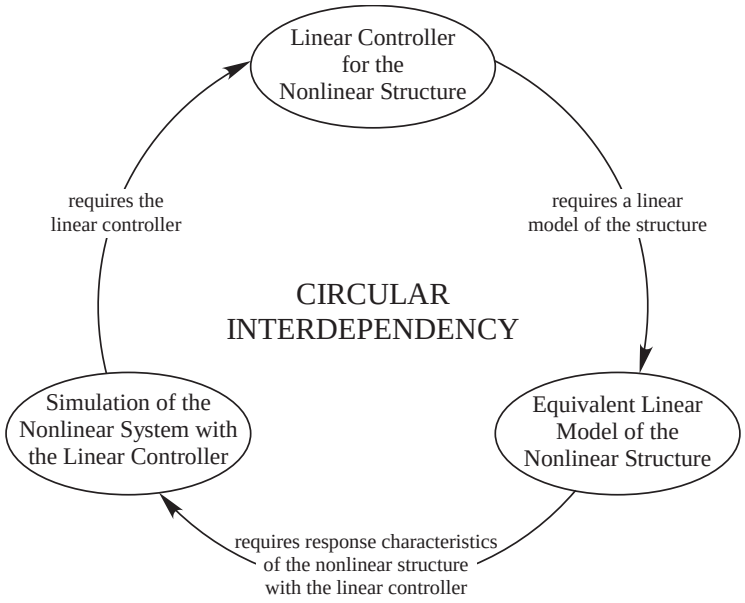


**Figure 7.20** Circular interdependency in the linear control design of a nonlinear structure

Another challenge is the time-efficiency considerations of the numerical analysis of the nonlinear benchmark structure. The active control simulations of the nonlinear structure requires considerable amount of time. If, further, a semiactive control scheme with smart dampers is utilized, the simulations become so computationaly expensive that they are not practical. Therefore, it is not possible to cover a wide variety of control design parameters to investigate the dissipativity and performance relations.

Due to these challenges as well as those discussed in the linear benchmark problem, it is evident that a complete analysis and investigation of the nonlinear problem is not feasible for this study. Therefore, the scope of the dissipativity-performance analysis is concentrated on the active control design performance and the verification of the dissipativity results for the nonlinear structure.

In this section, first, the equivalent linear model and the LQG controller design used in the nonlinear analyses are explained. For this purpose, a new set of state-space equations is defined for the ELM and used in the LQG control design. Then, the iterative method is used to obtain an ELM for the base isolated benchmark structure. This model is used in the active and semiactive control of the nonlinear benchmark structure. Finally, a dissipativity analysis similar to the linear case is given.

### 7.4.1 Controller Design

Let the state space representation of an ELM, including the measurements and the evaluation output to be minimized, be given as

$$\begin{aligned} \dot{\mathbf{q}}^{\mathrm{ELM}} &= \mathbf{A}^{\mathrm{ELM}}\mathbf{q}^{\mathrm{ELM}} + \mathbf{B}^{\mathrm{ELM}}\mathbf{u}^{\mathrm{ELM}} + \mathbf{E}^{\mathrm{ELM}}\ddot{\mathbf{x}}_{\mathrm{g}}^{\mathrm{abs}} \\ \mathbf{y}^{\mathrm{ELM}} &= \mathbf{C}_{\mathrm{y}}^{\mathrm{ELM}}\mathbf{q}^{\mathrm{ELM}} + \mathbf{D}_{\mathrm{y}}^{\mathrm{ELM}}\mathbf{u}^{\mathrm{ELM}} + \mathbf{E}_{\mathrm{y}}^{\mathrm{ELM}}\ddot{\mathbf{x}}_{\mathrm{g}}^{\mathrm{abs}} \\ \mathbf{z}^{\mathrm{ELM}} &= \mathbf{C}_{\mathrm{z}}^{\mathrm{ELM}}\mathbf{q}^{\mathrm{ELM}} + \mathbf{D}_{\mathrm{z}}^{\mathrm{ELM}}\mathbf{u}^{\mathrm{ELM}} + \mathbf{E}_{\mathrm{z}}^{\mathrm{ELM}}\ddot{\mathbf{x}}_{\mathrm{g}}^{\mathrm{abs}} \end{aligned} \tag{7.34}$$

where $\mathbf{q}^{\mathrm{ELM}}$ is the state vector, $\mathbf{u}^{\mathrm{ELM}}$ is the control force. As in the linear benchmark problem, the measured quantities in $\mathbf{y}^{\mathrm{ELM}}$ are absolute floor accelerations, absolute ground accelerations and controller drifts, and the outputs to be minimized are absolute floor accelerations and the drifts of the corner isolators. The system is augmented by a the Kanai-Tajimi filter (as described in the linear benchmark building design), giving the state-space form

$$\begin{aligned} \dot{\underset{\sim}{\mathbf{q}}} &= \underset{\sim}{\mathbf{A}}\underset{\sim}{\mathbf{q}} + \underset{\sim}{\mathbf{B}}\underset{\sim}{\mathbf{u}} + \underset{\sim}{\mathbf{E}}\underset{\sim}{\mathbf{w}} \\ \mathbf{y}_{\mathrm{v}}^{\mathrm{ELM}} &= \underset{\sim}{\mathbf{C}}_{\mathrm{y}}\underset{\sim}{\mathbf{q}} + \underset{\sim}{\mathbf{D}}_{\mathrm{y}}\mathbf{u}^{\mathrm{ELM}} + \underset{\sim}{\mathbf{E}}_{\mathrm{y}}\underset{\sim}{\mathbf{w}} + \underset{\sim}{\mathbf{y}} \\ \mathbf{z}^{\mathrm{ELM}} &= \underset{\sim}{\mathbf{C}}_{\mathrm{z}}\underset{\sim}{\mathbf{q}} + \underset{\sim}{\mathbf{D}}_{\mathrm{z}}\mathbf{u}^{\mathrm{ELM}} + \underset{\sim}{\mathbf{E}}_{\mathrm{z}}\underset{\sim}{\mathbf{w}} \end{aligned} \tag{7.35}$$

The goal of a standard LQG controller is to find a control gain $\mathbf{K}$ that satisfies the following optimization problem:

$$\min_{\mathbf{K}} E[(\mathbf{z}^{\mathrm{ELM}})^{\mathrm{T}}\mathbf{Q}\mathbf{z}^{\mathrm{ELM}} + (\mathbf{u}^{\mathrm{ELM}})^{\mathrm{T}}\mathbf{R}\mathbf{u}^{\mathrm{ELM}} + (\mathbf{z}^{\mathrm{ELM}})^{\mathrm{T}}\mathbf{N}\mathbf{u}^{\mathrm{ELM}} + (\mathbf{u}^{\mathrm{ELM}})^{\mathrm{T}}\mathbf{N}^{\mathrm{T}}\mathbf{z}^{\mathrm{ELM}}]$$
$$\text{subject to (7.35) and} \quad \underset{\sim}{\mathbf{u}} = -\mathbf{K}\hat{\underset{\sim}{\mathbf{q}}} \tag{7.36}$$

### 7.4.2 ELM Design

The ELM is obtained through an iterative method, which is explained below. Although the steps given are for the bilinear nonlinearity, they can be modified for other types of nonlinearities.

1. An initial guess for the ELM is obtained by replacing the 61 elastic-perfectly-plastic elements with 61 linear stiffness elements, where the linear stiffnesses are set to the preyield stiffness of the elastic-perfectly-plastic elements. Therefore, the lead plugs in the ELM are modelled with linear stiffness $k_{\mathrm{lead}}^{1} = k_1 - k_2$. Here, the superscript 1 in $k_{\mathrm{lead}}^{1}$ represents the iteration number.

2. An LQG controller is designed for the ELM obtained in the previous step as explained in the LQG design section.

3. Numerical simulations are carried out for both the controlled nonlinear model and the controlled ELM using an historical earthquake ground acceleration record. Then, the following ratio is obtained:

$$\gamma^{i} = \frac{RMS[F_{\mathrm{lead}}^{\mathrm{nonlin}}]}{RMS[F_{\mathrm{lead}}^{\mathrm{ELM}}]} \tag{7.37}$$

where $F_{\mathrm{lead}}^{\mathrm{nonlin}}$ and $F_{\mathrm{lead}}^{\mathrm{ELM}}$ are the resultant lead-plug forces acting on the mass-center of the base obtained from simulations of the controlled nonlinear model and controlled ELM, respectively. Here, $i$ represents the iteration number.

4. The linear stiffness of the lead plugs in the ELM are updated as

$$k_{\text{lead}}^{i+1} = \gamma^i k_{\text{lead}}^i \tag{7.38}$$

and a new ELM is obtained.

5. Steps 2–4 are repeated until convergence, and a $k_{\text{lead}}^{\text{final}}$ is obtained.

The iterative procedure is carried out for seven historical ground motion records until $|1 - \gamma^i| < 1 \times 10^{-3}$ is satisfied. The same controller is used in step 2 in every iteration. After some parametric studies, the control parameters are selected as $a = 3.548 \times 10^{-5}$, $b = 2.279 \times 10^{-2}$ and $r = 1 \times 10^{-12}\,\text{m}^2/\text{N}^2$ for equal weights on displacements and accelerations, *i.e.,* $\alpha_{x,\text{b}}^j = 1$, $\alpha_{y,\text{b}}^j = 1$, $\beta_{x,\text{b}}^j = 1$ and $\beta_{y,\text{b}}^j = 1$. In the Kalman filter design $\xi = 1 \times 10^{-2}$ is used. The energy dissipation by the lead plugs in the nonlinear model is represented in the ELM by an assumed linear damping of 207 kN·s/m, which is obtained based on some test simulations. The results of the iterative procedure are given in Table 7.10. Considering the results of the iterative study, the ELM is obtained by taking $\tilde{k}_{\text{lead}} \approx 0.18$, which is the average of the normalized stiffness obtained for the earthquakes.

It may be useful to first investigate the variation of $\gamma$ with $k_{\text{lead}}$ to check the convergence of the iterative method explained above. This can be done by simply plotting $\gamma$ for several normalized $k_{\text{lead}}$ values given by

$$\tilde{k}_{\text{lead}} = \frac{k_{\text{lead}}}{k_1 - k_2} \tag{7.39}$$

It should be noted that if the method converges, $\gamma$ goes to 1 and $RMS[F_{\text{lead}}^{\text{nonlin}}] = RMS[F_{\text{lead}}^{\text{ELM}}]$. Seven sets of numerical simulations are carried out, one per

**Table 7.10:** Results of the final iteration.

| Earthquake | Iterations | $\tilde{k}_{\text{lead}}$ | $k_{\text{lead}}$ (kN/m) |
|---|---|---|---|
| Newhall | 7 | 0.225 | 1250.297 |
| Sylmar | 10 | 0.107 | 595.733 |
| El Centro | 7 | 0.409 | 2268.341 |
| Rinaldi | 12 | 0.098 | 545.731 |
| Kobe | 8 | 0.204 | 1129.667 |
| Jiji | 15 | 0.051 | 280.826 |
| Erzincan | 8 | 0.134 | 743.401 |
| Final | - | 0.175 | 973.428 |

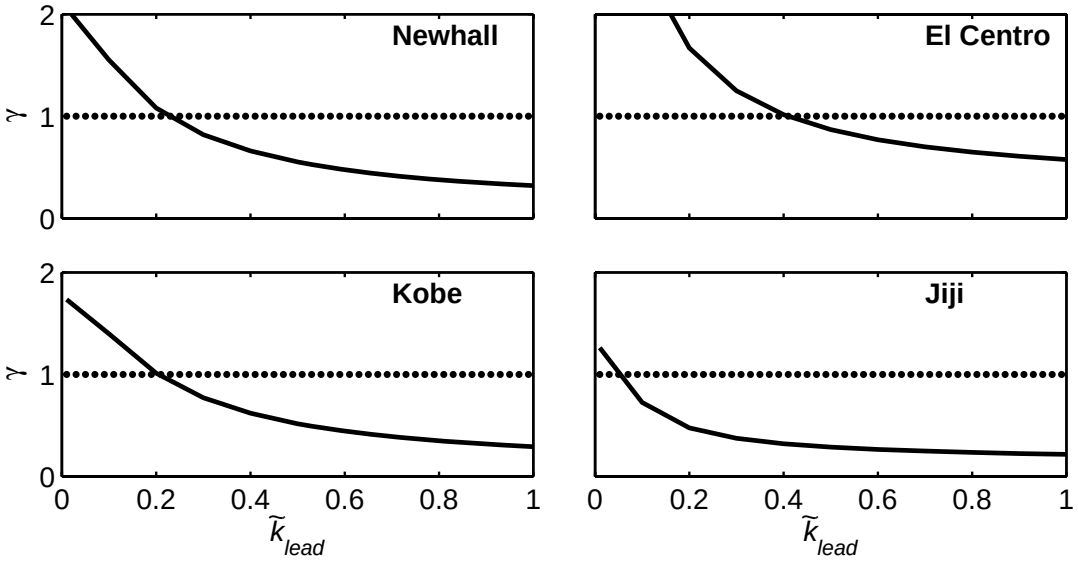


**Figure 7.21** Relation between normalized stiffness and $\gamma$

earthquake, to investigate the variation of $\gamma$ for various $\tilde{k}_{\text{lead}}$. The results of four sets of simulations are shown in Figure 7.21; those for the other three earthquakes are similar. As shown in Figure 7.21, one can easily judge that the iterative procedure will converge. For example, consider the curve for the Newhall earthquake. The first iteration starts with $\tilde{k}_{\text{lead}}^{1} = 1$, and it gives

$\gamma^1 \approx 0.3$ . In the second step, $\tilde{k}_{\text{lead}}^2 \approx 0.30$ is used, which gives $\gamma^2 \approx 0.8$ . Similarly, one can easily show that for both $\gamma < 1$ and $\gamma > 1$ , the method converges to $\tilde{k}_{\text{lead}} \approx 0.22$ . This observation is valid for other earthquakes due to the monotonically decreasing function, $\gamma$ (Figure 7.21).

The controlled nonlinear model and the converged ELM are simulated for the seven earthquake ground accelerations defined in the benchmark problem. The purpose here is to compare the responses to verify that the controlled ELM responses are indeed approximately replicating those of the original controlled nonlinear structure. For each earthquake, two ELMs are studied — one with lead stiffness optimal for the particular earthquake (*e.g.*, $\tilde{k}_{\text{lead}} = 0.410$ for El Centro) and one using the average lead stiffness ($\tilde{k}_{\text{lead}} = 0.178$ ). Figures 7.22, 7.23 and 7.24 show representative comparisons for three particular earthquakes — El Centro, Kobe and Jiji. For each of the earthquakes, the displacement of the mass-center of the base of both ELM and nonlinear model in the $x$ –direction and the hysteretic behavior, and the absolute acceleration of the mass-center of base and $8^{\text{th}}$ floor are shown.

The ELMs are able to efficiently represent the nonlinear behavior of the isolated structure when the earthquake-specific $\tilde{k}_{\text{lead}}$ are used. While the lead force peaks of the ELMs are somewhat larger, they are approximated fairly well for most of the duration of the earthquake. Further, the base drifts and the superstructure absolute accelerations of the ELM are quite similar to those of the nonlinear model. For the final ELM design, the isolation-layer stiffness is an average of the seven earthquake-specific ELMs. Consequently, the final stiffness is smaller than the optimal stiffness for smaller earthquakes, but larger than optimal for the strong records. This trade-off is expected in this type of linearization problem when excitation characteristics vary significantly. Nevertheless, the final design is a good balance in designing for the more frequent moderate earthquakes as well as the more severe strong ground motions.

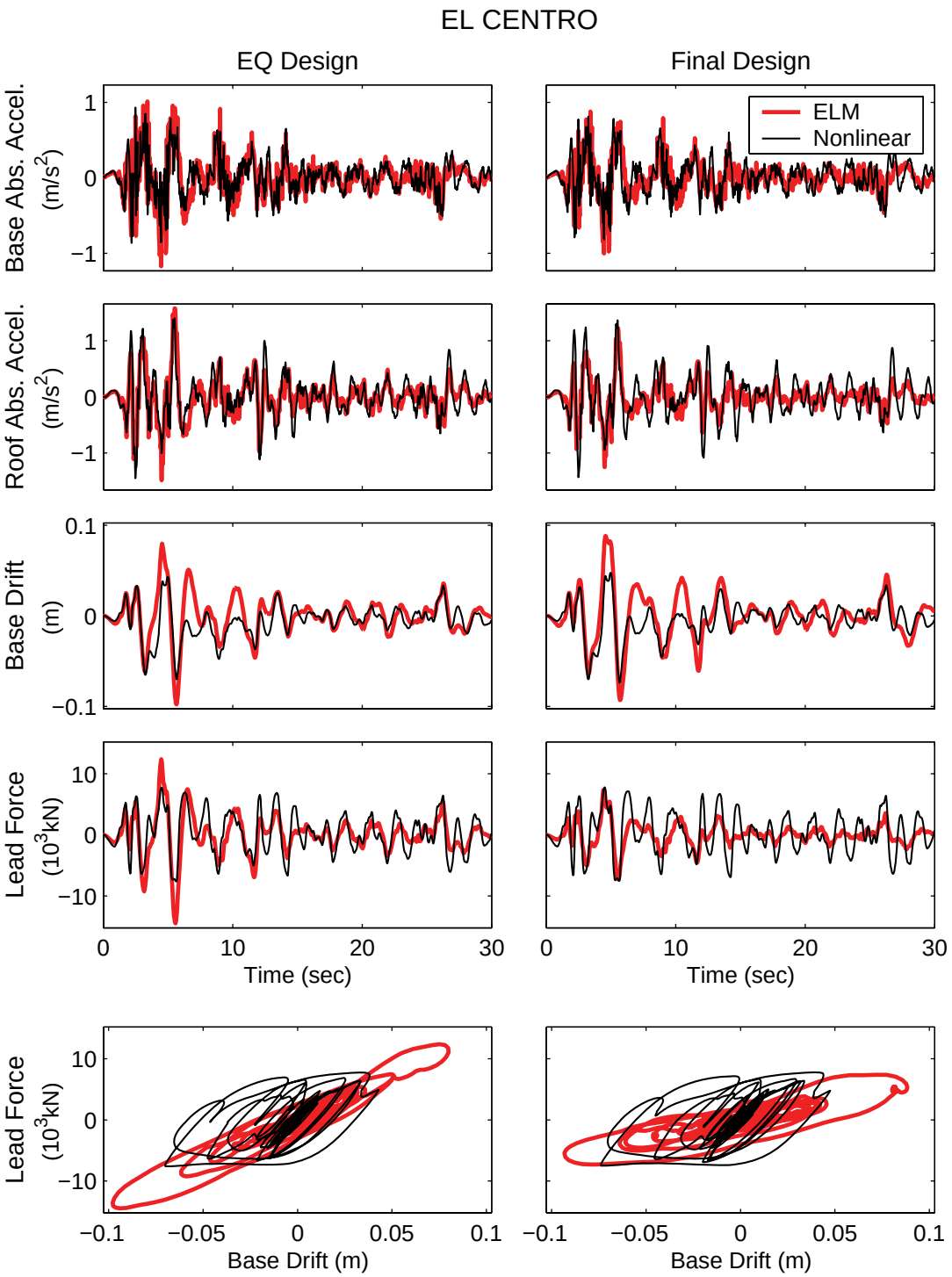


**Figure 7.22** Comparison of the ELM and nonlinear structure responses: Absolute accelerations of the base and 8th floor, base displacements and nonlinear isolator force transferred to the center of mass of the base in the $x$–direction for El Centro earthquake

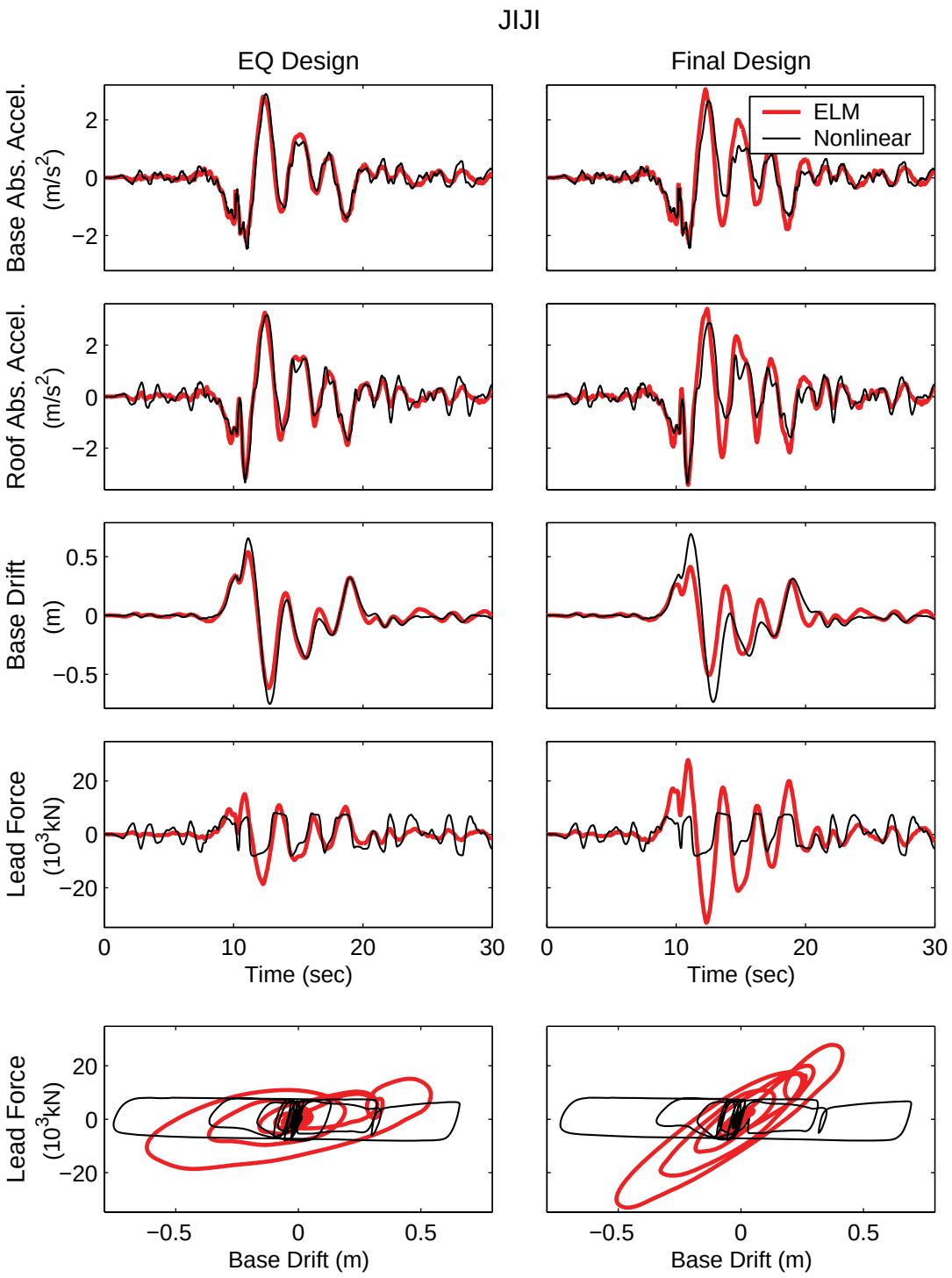


**Figure 7.23** Comparison of the ELM and nonlinear structure responses: Absolute accelerations of the base and 8th floor, base displacements and nonlinear isolator force transferred to the center of mass of the base in the $x$–direction for Jiji earthquake

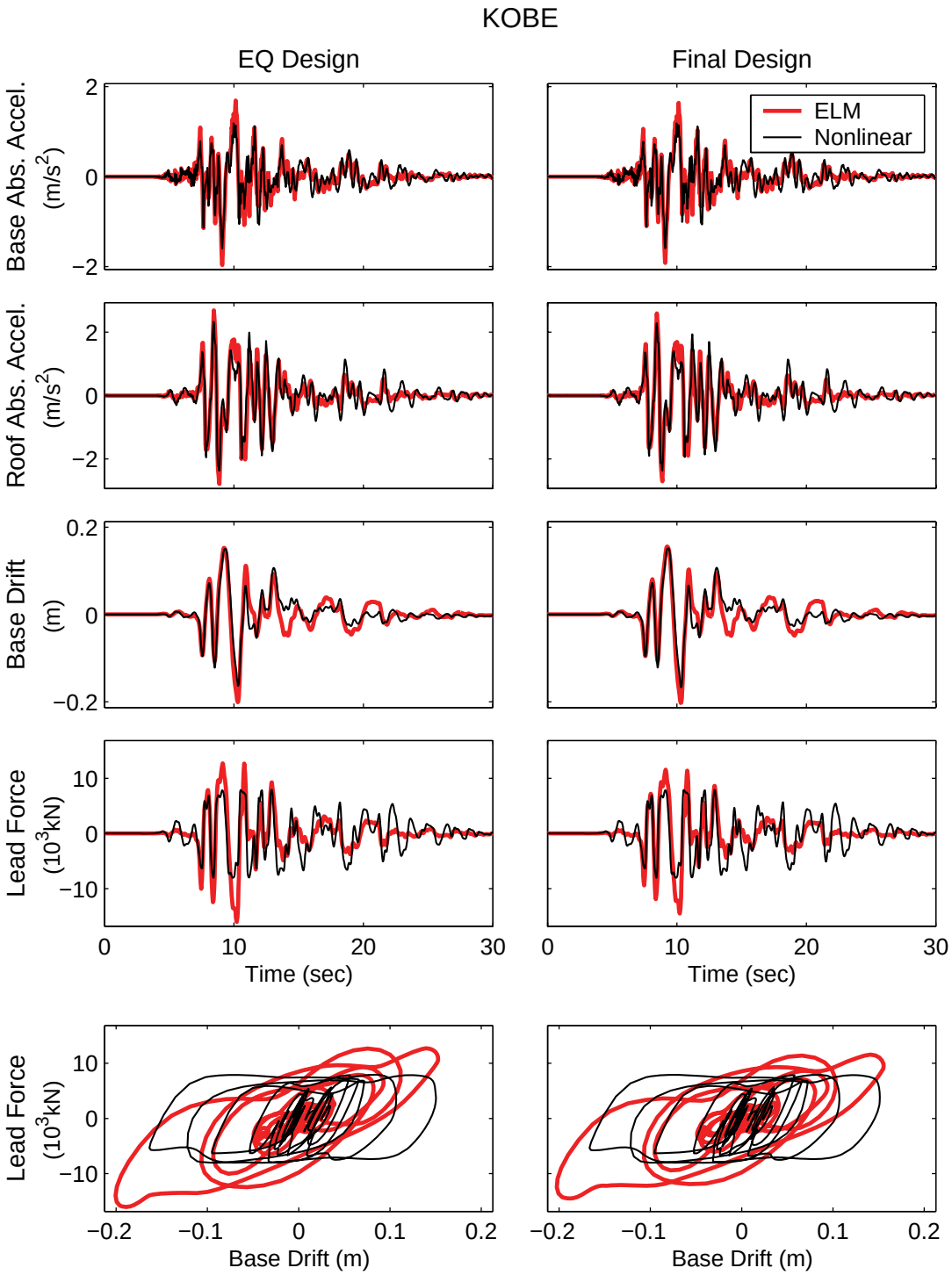


**Figure 7.24** Comparison of the ELM and nonlinear structure responses: Absolute accelerations of the base and 8th floor, base displacements and nonlinear isolator force transferred to the center of mass of the base in the *x*–direction for Kobe earthquake

The ELMs and the controller parameters are investigated by obtaining the performance indices defined in the benchmark problem definition paper. As in the ELM-nonlinear structure comparison plots, two types of ELM are investigated: earthquake specific ELMs and the final ELM. The results are shown in Table 7.11. The performance indices show that the sample controller designed here behaves satisfactorily for several earthquake ground acceleration data.

The challenges in the semiactive control of the nonlinear structure are now better clarified as the performance is also dependent on the efficiency of the ELM. Normally, the iterative procedure must be redone if a different set of control design parameters are selected. However, from the perspective of this research, it is acceptable to use the ELM given above. Therefore, the ELM given in this section is used in the dissipativity analysis.

### 7.4.3 Dissipativity Analysis

Similar to the dissipativity study of the linear structure, two design goals are considered. These goals are same as those of DES1 and DES2, which are given in Table 7.3. However, the search domain for the variables $a$ and $b$ are restricted to $[10^{-5}, 10^{-2}]$ and $[10^{-3}, 10^{0}]$ to avoid designs with unacceptable performance indices. Several test simulations are used to determine that a suitable magnification factor for the MR damper is 3. The resulting designs, along with the ELM design, are noted on the contour plots of performance indices in Figures 7.25 and 7.26 for the Newhall earthquake. Moreover, to observe the trends of indices $J_3$ (peak base drift) and $J_5$ (peak absolute floor acceleration), these indices are graphed for the earthquakes other than Newhall in Figures 7.27 and 7.28. Note that due to the difference in the definitions of the LQR control parameters, the appearance of the performance indices is shifted from the ones given previously for the linear structure. However, it is very clear that the main challenge in the design remains the same: a trade-off between various indices.

**Table 7.11:** Performance indices for the EQ and final active controller designs

| $J$ | | Newhall | | Sylmar | | El Centro | | Rinaldi | | Kobe | | Jiji | | Erzincan | |
|---|---|---|---|---|---|---|---|---|---|---|---|---|---|---|---|
| (Normalized with appropriate quantities) | | EQ | Final | EQ | Final | EQ | Final | EQ | Final | EQ | Final | EQ | Final | EQ | Final |
| $J_1$ | Peak Base Shear | 0.892 | 0.902 | 0.803 | 0.766 | 0.900 | 0.960 | 0.850 | 0.857 | 0.844 | 0.846 | 0.812 | 0.741 | 0.835 | 0.821 |
| $J_2$ | Peak First Floor Shear | 1.069 | 1.070 | 0.824 | 0.792 | 0.978 | 1.029 | 0.837 | 0.841 | 0.872 | 0.869 | 0.808 | 0.736 | 0.816 | 0.804 |
| $J_3$ | Peak Base Drift | 0.949 | 0.949 | 0.814 | 0.778 | 0.922 | 0.941 | 1.018 | 1.010 | 0.812 | 0.812 | 0.976 | 0.989 | 0.805 | 0.797 |
| $J_4$ | Peak Interstory Drift | 0.853 | 0.869 | 0.924 | 0.910 | 0.912 | 0.944 | 0.961 | 0.949 | 0.910 | 0.899 | 0.927 | 0.907 | 0.927 | 0.906 |
| $J_5$ | Peak Absolute Floor Acceleration | 0.760 | 0.734 | 0.993 | 1.006 | 0.835 | 0.830 | 0.839 | 0.848 | 0.953 | 0.939 | 0.818 | 0.826 | 0.768 | 0.768 |
| $J_6$ | Peak Controller Force | 0.363 | 0.341 | 0.303 | 0.356 | 0.415 | 0.385 | 0.286 | 0.298 | 0.335 | 0.327 | 0.258 | 0.329 | 0.275 | 0.290 |
| $J_7$ | RMS Base Displacement | 0.918 | 0.926 | 0.697 | 0.678 | 0.896 | 0.882 | 0.921 | 0.909 | 0.915 | 0.918 | 0.977 | 1.025 | 0.726 | 0.711 |
| $J_8$ | RMS Absolute Floor Acceleration | 0.815 | 0.818 | 0.774 | 0.750 | 0.891 | 0.919 | 0.856 | 0.849 | 0.867 | 0.864 | 0.792 | 0.740 | 0.744 | 0.728 |
| $J_9$ | Energy Absorbed by the Control Devices | 0.207 | 0.190 | 0.230 | 0.248 | 0.230 | 0.168 | 0.204 | 0.234 | 0.144 | 0.129 | 0.250 | 0.277 | 0.239 | 0.247 |
| $J_{10}$ | Normalized Peak Controller Force | 0.065 | 0.061 | 0.072 | 0.084 | 0.034 | 0.032 | 0.069 | 0.072 | 0.046 | 0.045 | 0.098 | 0.125 | 0.061 | 0.064 |
| $J_{11}$ | RMS Floor Drifts | 0.848 | 0.865 | 0.910 | 0.896 | 0.885 | 0.921 | 0.934 | 0.920 | 0.913 | 0.900 | 0.918 | 0.899 | 0.905 | 0.883 |

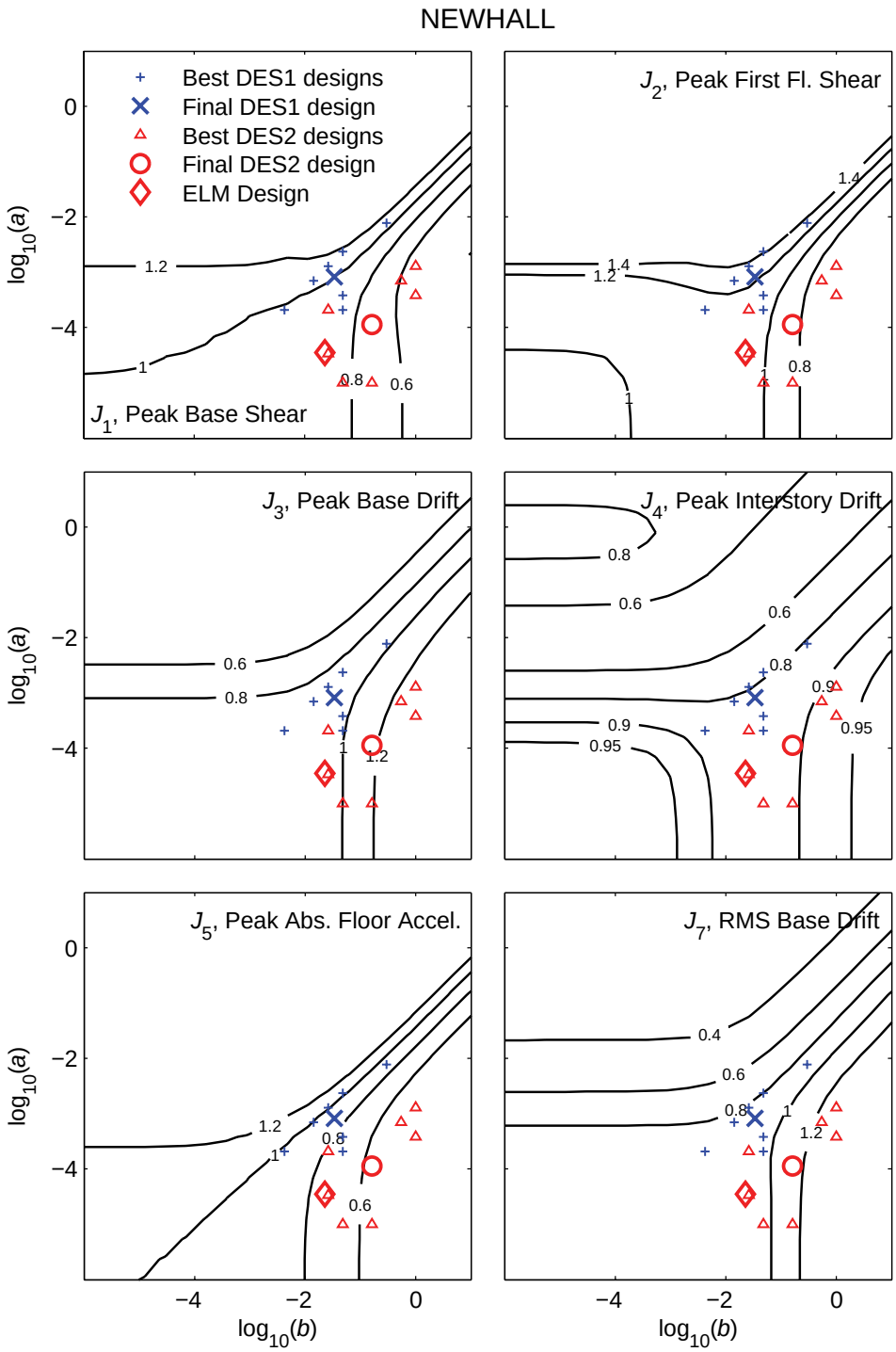


**Figure 7.25** Best and final designs and performance indices $J_1$, $J_2$, $J_3$, $J_4$, $J_5$ and $J_7$ of the non-linear structure for Newhall earthquake

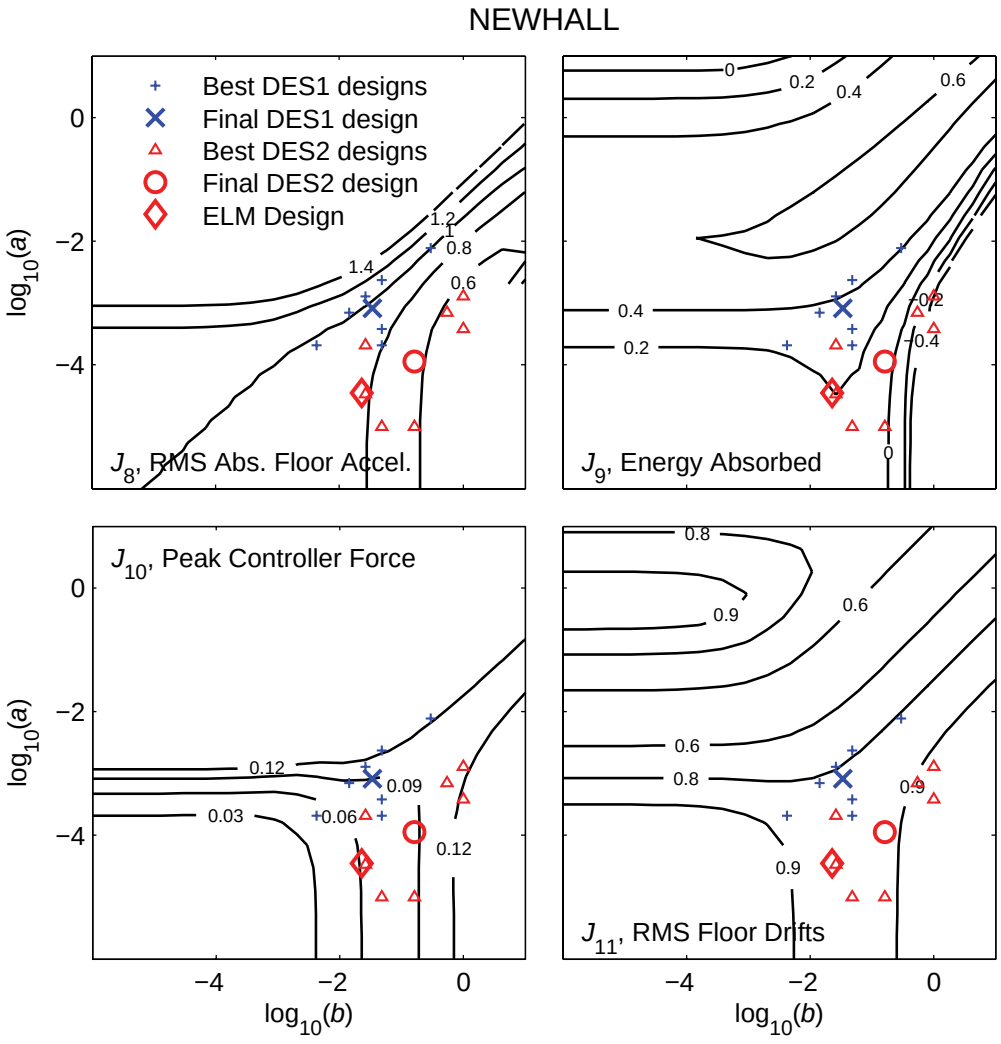


**Figure 7.26** Best and final designs and performance indices $J_8$, $J_9$, $J_{10}$ and $J_{11}$ of the nonlinear structure Newhall earthquake

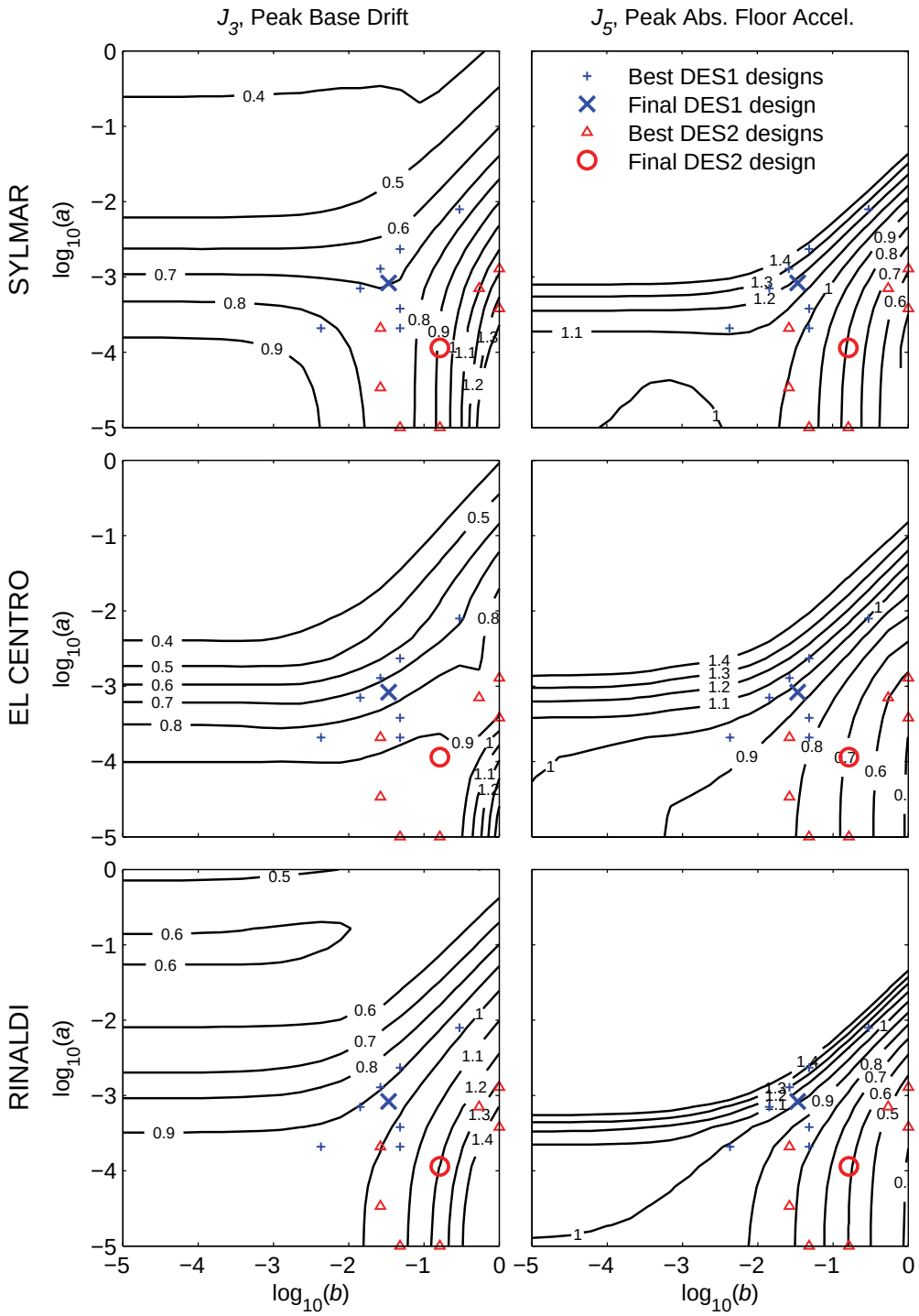


**Figure 7.27** Best and final designs and performance indices $J_3$, and $J_5$ of the nonlinear structure for Sylmar and El Centro and Rinaldi earthquakes

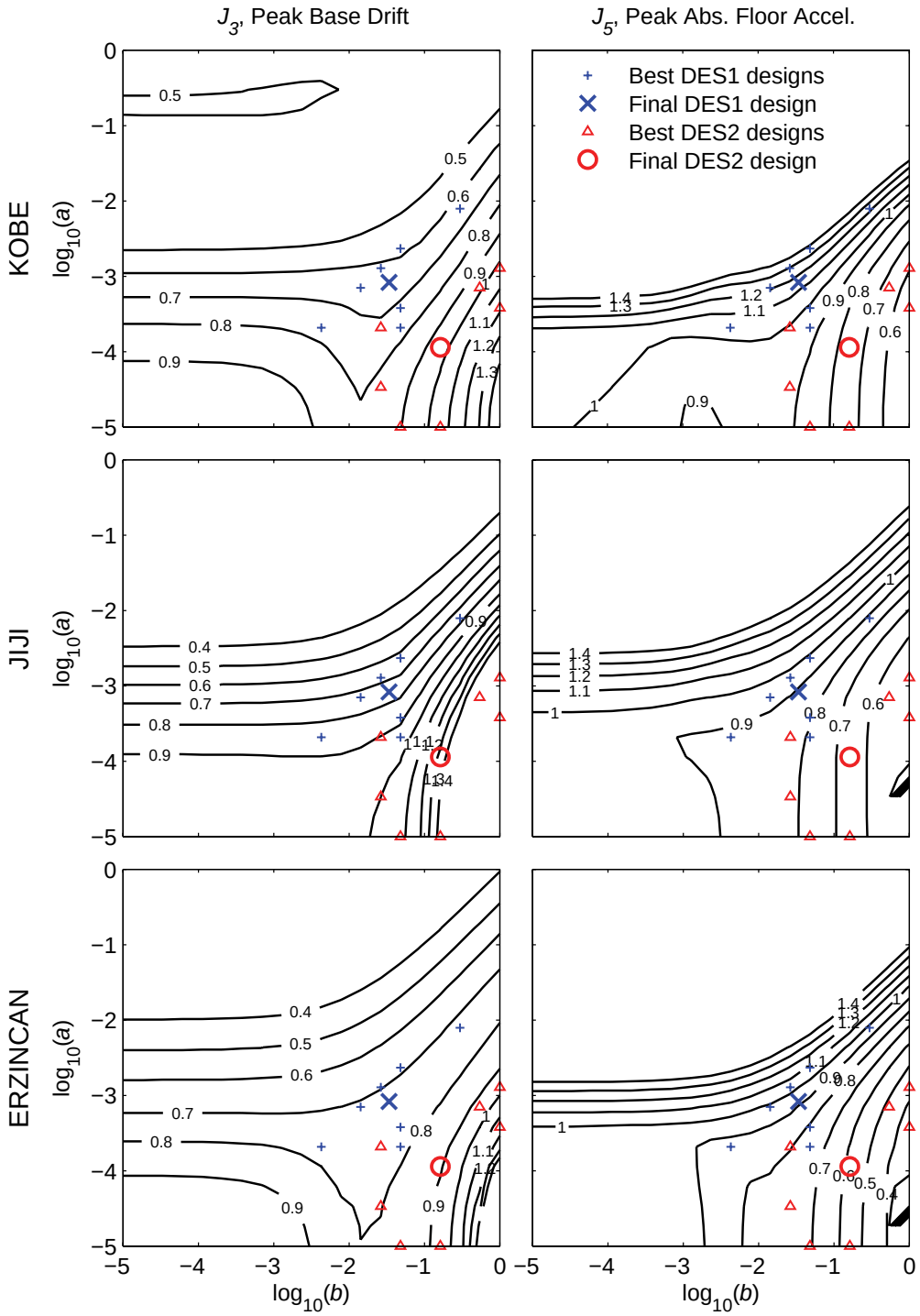


**Figure 7.28** Best and final designs and performance indices $J_3$, and $J_5$ of the nonlinear structure for Rinaldi, Kobe and Jiji earthquakes

A very important observation in the performance plots is the $J_9$ index. Some of the controllers have negative $J_9$ values, which means that the controller must add energy to the system to achieve that design objective. However, the linear benchmark structure does not have control designs with negative $J_9$ values. This result shows that for a more realistic structure, *i.e.* a structure with a nonlinear behavior, it is more likely that a controller inject energy to the structure to achieve its design goals. Therefore, robustness characteristics of semiactive devices are very important for civil structures and are more desirable than active devices for seismic protection.

It is also observed that the final ELM design selected for the nonlinear structure shows an overall performance somewhat in between DES1 and DES2 performances. For example, for almost all of the performance indices given for the Newhall earthquake (Figures 7.25 and 7.26), ELM design has an index that is between the indices of DES1 and DES2. This is also true for the $J_3$ and $J_5$ indices given for the other earthquakes (Figures 7.27 and 7.28). This result shows that the selected ELM and the corresponding design provide a good model and controller for the nonlinear benchmark structure in overall sense.

The dissipativity indices of the primary controller for the nonlinear benchmark structure are shown in Figures 7.29 and 7.30. The variation of dissipativities is similar to that of the linear benchmark structure in the sense that controllers with lower $J_3$ values have higher dissipativity characteristics than the controllers with lower $J_5$ values. The similarities between $J_9$ (in Figure 7.26) and $D_{\mathrm{e}}$ (in Figure 7.29) and between $D_{\mathrm{ne}}$ (in Figure 7.29) and $D_{\%}$ (in Figure 7.30) are observed as in the linear benchmark case.

Dissipativity and performance indices for DES1, DES2 and the final ELM controller design are given in Tables 7.12–7.17. As in the linear structure, the proposed cumulative index successfully represents the dissipativity indices of the controllers. Also, controllers 5 and 7 again have

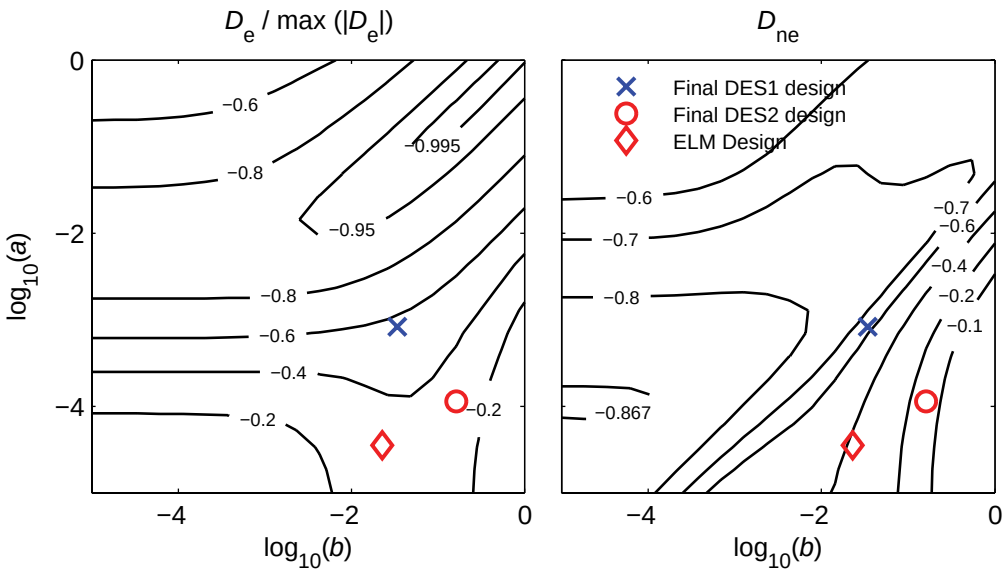


**Figure 7.29** $D_e$ and $D_{ne}$ plots for the active nonlinear structure

the lowest dissipativity indices, which shows that these controllers are the least effective in the semiactive system.

While the dissipativity tables for the Newhall earthquake (Tables 7.12–7.14) give a good idea of the behavior of the dissipativities of the designs for various earthquakes, the difference in the dissipativities of the active and semiactive system is more clear in the performance index tables (Tables 7.15–7.17). For example, the index $J_9$ has a negative value for the DES2 active design subject to the Kobe earthquake in Table 7.16. Also, the difference between the dissipativities of the active and semiactive systems is more clear in the same table. In fact, this table is a very good example of how a semiactive system with a clipped optimal control that has a low dissipativity primary controller behaves. In this case, the semiactive system behaves like a passive system as it is not efficient in reproducing the active control forces. For example, the semiactive system has better $J_3$ indices than the active system in Table 7.16, even tough DES2 is not a controller that aims to reduce $J_3$.

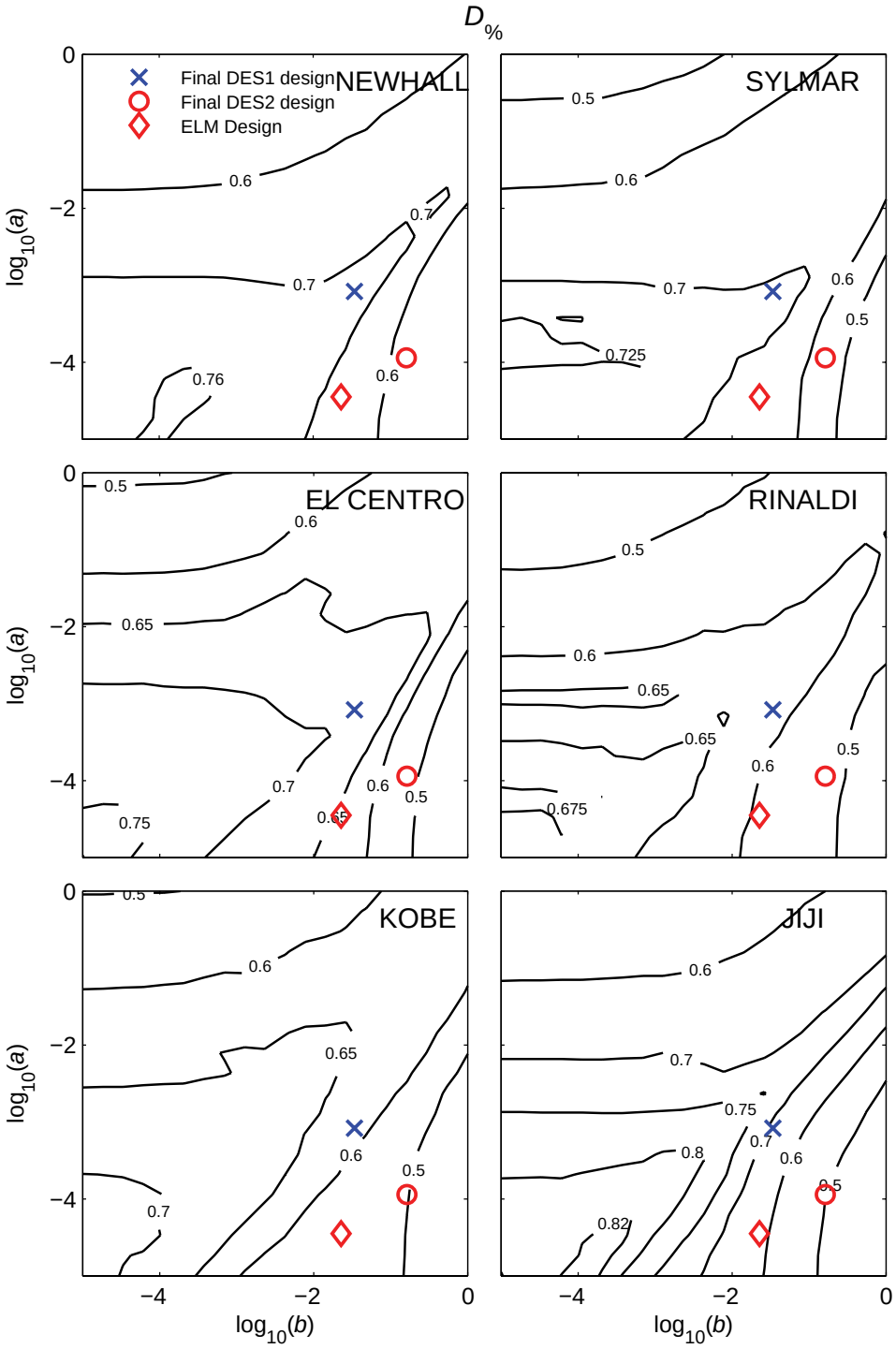


**Figure 7.30** $D_{\%}$ plots for the active nonlinear structure for various earthquakes

**Table 7.12:** Dissipativity indices of the nonlinear system for DES1 for Newhall earthquake

| $i$ | $D_{\%}$ | | $D_{e}$ | $D_{ne}$ |
|---|---|---|---|---|
| | Act | SAct | Act | Act |
| 1 | 0.730 | 0.817 | –772 | –0.672 |
| 2 | 0.777 | 0.783 | –760 | –0.670 |
| 3 | 0.680 | 0.812 | –1008 | –0.735 |
| 4 | 0.757 | 0.797 | –884 | –0.709 |
| 5 | 0.762 | 0.802 | –509 | –0.501 |
| 6 | 0.757 | 0.797 | –884 | –0.709 |
| 7 | 0.762 | 0.802 | –509 | –0.501 |
| 8 | 0.725 | 0.777 | –680 | –0.635 |
| 9 | 0.748 | 0.827 | –699 | –0.639 |
| 10 | 0.683 | 0.747 | –568 | –0.563 |
| 11 | 0.680 | 0.812 | –1008 | –0.735 |
| 12 | 0.683 | 0.747 | –568 | –0.563 |
| $D^{c}$ | 0.727 | 0.798 | –750 | –0.641 |

The differences in the performance indices of the linear and nonlinear semiactive systems are also significant. It is observed that the nonlinear semiactive structure has lower interstory drift indices ($J_4$ and $J_{11}$) compared to the linear semiactive structure for both DES1 and DES2. On the other hand, absolute floor acceleration indices ($J_5$ and $J_8$) of the nonlinear semiactive structure are quite large compared to the linear semiactive structure for both DES1 and DES2. Due to the complexity of the benchmark structure, it is difficult to reach a strict conclusion for this behavior, yet it is clear that a final semiactive controller has to be designed carefully considering the overall performance. Note that the designs DES1 and DES2 are selected for the investigation of dissipativity and cannot be used as final designs.

**Table 7.13:** Dissipativity indices of the nonlinear system for DES2 for Newhall earthquake

| $i$ | $D_{\%}$ | | $D_{\mathrm{e}}$ | $D_{\mathrm{ne}}$ |
|---|---|---|---|---|
| | **Act** | **SAct** | **Act** | **Act** |
| 1 | 0.578 | 0.680 | –525 | –0.172 |
| 2 | 0.647 | 0.702 | –429 | –0.148 |
| 3 | 0.538 | 0.722 | –669 | –0.193 |
| 4 | 0.628 | 0.688 | –432 | –0.126 |
| 5 | 0.462 | 0.522 | –135 | –0.042 |
| 6 | 0.628 | 0.688 | –432 | –0.126 |
| 7 | 0.462 | 0.522 | –135 | –0.042 |
| 8 | 0.587 | 0.677 | –411 | –0.157 |
| 9 | 0.560 | 0.652 | –452 | –0.151 |
| 10 | 0.522 | 0.660 | –352 | –0.153 |
| 11 | 0.538 | 0.722 | –669 | –0.193 |
| 12 | 0.522 | 0.660 | –352 | –0.153 |
| $D^{\mathrm{c}}$ | 0.550 | 0.661 | –428 | –0.140 |

There is a very important benefit of the proposed dissipativity indices from a numerical point of view. To compute the indices $J_9$ and $D_{\%}$, the active system (linear or nonlinear) has to be simulated for an excitation, which may take around 10 minutes on a moderate Pentium computer (*e.g.* with a Pentium 4, 2.4 GHz processor). On the other hand, computation of the $D_{\mathrm{e}}$ and $D_{\mathrm{ne}}$ indices take less than a second since they only require the solution of a Lyapunov equation. Moreover, consider the nonlinear semiactive benchmark structure with twelve MR dampers, which is a computationaly expensive process. For example, one simulation of the nonlinear semiactive system with the dampers for a 30 sec earthquake record can take about 1.5 hours on a high-end, dual processor G5 Macintosh server with a high-end, Unix-based operating system.

**Table 7.14:** Dissipativity indices of the nonlinear system for the final ELM design for Newhall Earthquake

| *i* | $D_{\%}$ | | $D_{e}$ | $D_{ne}$ |
|---|---|---|---|---|
| | **Act** | **SAct** | **Act** | **Act** |
| 1 | 0.707 | 0.747 | –504 | –0.431 |
| 2 | 0.775 | 0.735 | –430 | –0.395 |
| 3 | 0.650 | 0.757 | –626 | –0.430 |
| 4 | 0.742 | 0.738 | –471 | –0.364 |
| 5 | 0.633 | 0.682 | –309 | –0.277 |
| 6 | 0.742 | 0.738 | –471 | –0.364 |
| 7 | 0.633 | 0.682 | –309 | –0.277 |
| 8 | 0.733 | 0.718 | –400 | –0.408 |
| 9 | 0.717 | 0.735 | –459 | –0.411 |
| 10 | 0.655 | 0.713 | –351 | –0.404 |
| 11 | 0.650 | 0.757 | –626 | –0.430 |
| 12 | 0.655 | 0.713 | –351 | –0.404 |
| $D^{c}$ | 0.684 | 0.728 | –451 | –0.384 |

Simulation times can reach 4 hours on a Pentium 4-based PC with an WinXP operating system. These are very good examples to show how active and semiactive, linear and nonlinear simulations can be very time consuming and impractical. From this perspective, dissipativity analysis with the proposed indices provides an essential tool to investigate control designs that are more suitable for smart dampers.

## 7.5 Design Considerations

The results given in this chapter show that the controllers with the best dissipativity characteristics are not necessarily the best primary controllers for smart dampers, which is very evident

**Table 7.15:** Performance indices for the nonlinear active and nonlinear semiactive systems for DES1

| $J$ | | Newhall | | Sylmar | | El Centro | | Rinaldi | | Kobe | | Jiji | | Erzincan | |
|---|---|---|---|---|---|---|---|---|---|---|---|---|---|---|---|
| (Normalized with appropriate quantities) | | ACT | SACT | ACT | SACT | ACT | SACT | ACT | SACT | ACT | SACT | ACT | SACT | ACT | SACT |
| $J_1$ | Peak Base Shear | 0.984 | 1.169 | 0.814 | 1.171 | 1.067 | 1.168 | 0.944 | 1.348 | 1.026 | 1.413 | 0.746 | 0.918 | 0.917 | 1.098 |
| $J_2$ | Peak First Floor Shear | 1.190 | 1.358 | 0.914 | 1.246 | 1.172 | 1.264 | 0.954 | 1.306 | 1.076 | 1.403 | 0.768 | 0.921 | 0.896 | 1.126 |
| $J_3$ | Peak Base Drift | 0.925 | 0.880 | 0.689 | 0.776 | 0.757 | 0.599 | 0.947 | 0.749 | 0.636 | 0.567 | 0.753 | 0.576 | 0.728 | 0.693 |
| $J_4$ | Peak Interstory Drift | 0.860 | 0.791 | 0.646 | 0.732 | 0.764 | 0.598 | 0.903 | 0.785 | 0.650 | 0.674 | 0.787 | 0.660 | 0.742 | 0.774 |
| $J_5$ | Peak Absolute Floor Acceleration | 0.841 | 1.543 | 1.173 | 1.978 | 0.955 | 1.383 | 1.006 | 1.643 | 1.151 | 1.991 | 0.888 | 1.122 | 0.922 | 1.335 |
| $J_6$ | Peak Controller Force | 0.490 | 0.527 | 0.457 | 0.578 | 0.401 | 0.477 | 0.474 | 0.578 | 0.519 | 0.738 | 0.373 | 0.290 | 0.407 | 0.405 |
| $J_7$ | RMS Base Drift | 0.885 | 0.770 | 0.627 | 0.734 | 0.728 | 0.609 | 0.811 | 0.700 | 0.740 | 0.682 | 0.823 | 0.605 | 0.593 | 0.624 |
| $J_8$ | RMS Absolute Floor Acceleration | 0.953 | 1.431 | 0.801 | 1.152 | 1.072 | 1.366 | 1.008 | 1.455 | 1.037 | 1.553 | 0.744 | 0.919 | 0.781 | 1.040 |
| $J_9$ | Energy Absorbed by the Control Devices | 0.348 | 0.418 | 0.401 | 0.433 | 0.319 | 0.469 | 0.404 | 0.461 | 0.303 | 0.470 | 0.421 | 0.407 | 0.410 | 0.415 |
| $J_{10}$ | Normalized Peak Controller Force | 0.087 | 0.094 | 0.108 | 0.137 | 0.033 | 0.040 | 0.114 | 0.139 | 0.070 | 0.100 | 0.142 | 0.110 | 0.089 | 0.089 |
| $J_{11}$ | RMS Floor Drifts | 0.790 | 0.744 | 0.564 | 0.660 | 0.762 | 0.627 | 0.740 | 0.742 | 0.829 | 0.830 | 0.914 | 0.639 | 0.568 | 0.700 |

**Table 7.16:** Performance indices for the nonlinear active and nonlinear semiactive systems for DES2

| *J* | | Newhall | | Sylmar | | El Centro | | Rinaldi | | Kobe | | Jiji | | Erzincan | |
|---|---|---|---|---|---|---|---|---|---|---|---|---|---|---|---|
| (Normalized with appropriate quantities) | | ACT | SACT | ACT | SACT | ACT | SACT | ACT | SACT | ACT | SACT | ACT | SACT | ACT | SACT |
| $J_1$ | Peak Base Shear | 0.704 | 1.138 | 0.569 | 1.130 | 0.817 | 1.172 | 0.658 | 1.340 | 0.721 | 1.286 | 0.621 | 0.885 | 0.595 | 1.175 |
| $J_2$ | Peak First Floor Shear | 0.829 | 1.228 | 0.632 | 1.261 | 0.893 | 1.366 | 0.658 | 1.297 | 0.752 | 1.397 | 0.623 | 0.888 | 0.588 | 1.208 |
| $J_3$ | Peak Base Drift | 1.153 | 0.783 | 0.913 | 0.800 | 0.926 | 0.579 | 1.200 | 0.726 | 0.957 | 0.595 | 1.328 | 0.561 | 0.890 | 0.657 |
| $J_4$ | Peak Interstory Drift | 0.958 | 0.734 | 0.807 | 0.744 | 0.877 | 0.582 | 1.024 | 0.773 | 0.698 | 0.708 | 1.454 | 0.627 | 0.743 | 0.721 |
| $J_5$ | Peak Absolute Floor Acceleration | 0.548 | 1.444 | 0.788 | 1.914 | 0.688 | 1.369 | 0.617 | 1.602 | 0.755 | 1.863 | 0.654 | 1.114 | 0.579 | 1.298 |
| $J_6$ | Peak Controller Force | 0.479 | 0.522 | 0.579 | 0.570 | 0.487 | 0.452 | 0.418 | 0.552 | 0.493 | 0.645 | 0.844 | 0.323 | 0.417 | 0.493 |
| $J_7$ | RMS Base Drift | 1.127 | 0.716 | 0.772 | 0.687 | 0.993 | 0.600 | 1.038 | 0.753 | 1.008 | 0.663 | 1.634 | 0.567 | 0.755 | 0.568 |
| $J_8$ | RMS Absolute Floor Acceleration | 0.643 | 1.399 | 0.556 | 1.184 | 0.743 | 1.359 | 0.673 | 1.383 | 0.706 | 1.473 | 0.677 | 0.907 | 0.535 | 1.059 |
| $J_9$ | Energy Absorbed by the Control Devices | 0.082 | 0.421 | 0.117 | 0.440 | 0.073 | 0.437 | 0.132 | 0.455 | –0.028 | 0.465 | 0.238 | 0.419 | 0.094 | 0.440 |
| $J_{10}$ | Normalized Peak Controller Force | 0.085 | 0.093 | 0.137 | 0.135 | 0.040 | 0.037 | 0.101 | 0.133 | 0.067 | 0.087 | 0.320 | 0.123 | 0.092 | 0.108 |
| $J_{11}$ | RMS Floor Drifts | 0.982 | 0.709 | 0.610 | 0.642 | 1.004 | 0.629 | 0.847 | 0.761 | 0.873 | 0.844 | 1.823 | 0.618 | 0.593 | 0.654 |

**Table 7.17:** Performance indices of the nonlinear active and nonlinear semiactive systems for the final ELM design

| $J$ | | Newhall | | Sylmar | | El Centro | | Rinaldi | | Kobe | | Jiji | | Erzincan | |
|---|---|---|---|---|---|---|---|---|---|---|---|---|---|---|---|
| (Normalized with appropriate quantities) | | ACT | SACT | ACT | SACT | ACT | SACT | ACT | SACT | ACT | SACT | ACT | SACT | ACT | SACT |
| $J_1$ | Peak Base Shear | 0.902 | 1.129 | 0.766 | 1.128 | 0.960 | 1.192 | 0.857 | 1.331 | 0.846 | 1.459 | 0.741 | 0.845 | 0.821 | 1.139 |
| $J_2$ | Peak First Floor Shear | 1.070 | 1.312 | 0.792 | 1.288 | 1.029 | 1.364 | 0.841 | 1.284 | 0.869 | 1.392 | 0.736 | 0.837 | 0.804 | 1.188 |
| $J_3$ | Peak Base Drift | 0.949 | 0.762 | 0.778 | 0.744 | 0.941 | 0.520 | 1.010 | 0.721 | 0.812 | 0.550 | 0.989 | 0.542 | 0.797 | 0.597 |
| $J_4$ | Peak Interstory Drift | 0.869 | 0.724 | 0.910 | 0.711 | 0.944 | 0.553 | 0.949 | 0.761 | 0.899 | 0.606 | 0.907 | 0.585 | 0.906 | 0.692 |
| $J_5$ | Peak Absolute Floor Acceleration | 0.734 | 1.485 | 1.006 | 2.519 | 0.830 | 1.357 | 0.848 | 1.755 | 0.939 | 1.833 | 0.826 | 1.210 | 0.768 | 1.357 |
| $J_6$ | Peak Controller Force | 0.341 | 0.575 | 0.356 | 0.662 | 0.385 | 0.489 | 0.298 | 0.589 | 0.327 | 0.753 | 0.329 | 0.327 | 0.290 | 0.497 |
| $J_7$ | RMS Base Drift | 0.926 | 0.709 | 0.678 | 0.625 | 0.882 | 0.527 | 0.909 | 0.657 | 0.918 | 0.644 | 1.025 | 0.565 | 0.711 | 0.526 |
| $J_8$ | RMS Absolute Floor Acceleration | 0.818 | 1.450 | 0.750 | 1.204 | 0.919 | 1.400 | 0.849 | 1.446 | 0.864 | 1.578 | 0.740 | 0.917 | 0.728 | 1.059 |
| $J_9$ | Energy Absorbed by the Control Devices | 0.190 | 0.472 | 0.248 | 0.501 | 0.168 | 0.509 | 0.234 | 0.512 | 0.129 | 0.501 | 0.277 | 0.445 | 0.247 | 0.479 |
| $J_{10}$ | Normalized Peak Controller Force | 0.061 | 0.103 | 0.084 | 0.157 | 0.032 | 0.041 | 0.072 | 0.142 | 0.045 | 0.102 | 0.125 | 0.124 | 0.064 | 0.109 |
| $J_{11}$ | RMS Floor Drifts | 0.865 | 0.696 | 0.896 | 0.587 | 0.921 | 0.556 | 0.920 | 0.697 | 0.900 | 0.765 | 0.899 | 0.601 | 0.883 | 0.612 |

from the dissipativity graphs shown herein. This was also the case for the 2-DOF examples. Then the question one might pose is “What exactly is the benefit of a dissipativity analysis?”. There are several answers to this question. First, dissipativity indices identify control designs that are *more suitable* for smart dampers. This is very beneficial information that is acquired without doing any semiactive simulations. Second, dissipativity indices can be used as an index for robustness of the controller. This information is very critical for nonlinear structures. It is desirable to avoid controllers that may input energy to the system as in the nonlinear benchmark building. Another practical application is the identification of the controllers with low dissipativities. In this chapter, while cumulative indices are used for dissipativities, the dissipativity indices for the individual controllers give important information when deciding the locations of the dampers. For example, in the benchmark structure, the fifth and seventh controllers yield low dissipativities for both linear and nonlinear structures, which allows the designer to rearrange the locations of these dampers.

It should be noted that the design goals selected in this study serve completely the investigation of dissipativity. A real-life control design procedure should be based on the customized needs of the problem. For example, in the benchmark problem, the control design should aim to reduce absolute accelerations of the floors, drift of the base and floors, control force required etc. Neither DES1 nor DES2 serve realistic control design goals; rather, they were chosen to demonstrate particular dissipativity characteristics.

As discussed before, most of the civil structures experience nonlinearity during a major earthquake. In fact, in real-life conditions, the nonlinearity of the structure may be more complicated than the one considered here, which may result controllers that input more energy to the structure. If not well-designed, no matter what control theory is used, an active system may yield

very unexpected results due to the extreme changes in the characteristics of the structure. Semiactive devices simply eliminates this issue, which is desirable in structural engineering.

## 7.6 Summary

In this chapter, the smart base isolated benchmark structure is investigated in the context of dissipativity and performance. As the benchmark structure resembles a realistic structure, it possess various facets of a practical control problem. For this structure, it is verified that particular design goals are easier to achieve with smart dampers through a dissipativity study. While research on semiactive control of buildings with smart dampers shows that semiactive control is very efficient compared to passive systems and it is robust and reliable compared to active systems, selection of the control design must be done carefully; a dissipativity analysis serves this purpose.

# CHAPTER 8

# CONCLUSIONS AND DIRECTIONS FOR FUTURE RESEARCH

In this dissertation, the dissipativity and performance of semiactive systems with smart dampers are investigated. First, two new indices are defined in addition to those previously defined in the literature. The statistical and physical relations among these dissipativity indices are discussed. Then, a method based on LMI control design is proposed to modify the dissipativity characteristics of the primary control force in clipped optimal control. The method converts an LQR problem into a multiobjective EVP form, where new inequality constraints can be imposed on the controller. Based on the indices defined, possible inequality constraints are derived. Third, the proposed indices and the proposed LMI-based control theory are employed for two simple 2-DOF systems. In the last part, the smart base isolated benchmark structure is investigated for dissipativity and performance relations. Two types of isolation systems are considered: linear and nonlinear. An iterative procedure is proposed to be able to utilize a linear control theory for the nonlinear structure. The conclusions derived from this study are listed below:

- Both proposed and previously used dissipativity indices provide an efficient way of identifying the dissipativity characteristics of a force. Dissipativity indices are classified into two categories, which are summarized in Table 7.9.
- The proposed LMI-based controller successfully improves the dissipativity characteristics of a controller. This has two practical uses for simple 2-DOF structural systems with theoretical smart dampers. First, controllers with higher dissipativity characteristics can be located with

a numerical study, which reduces the semiactive design effort considerably. Second, in some cases, dissipativity is improved that also improved the semiactive performance. For complex and high-order systems, as in the case of the benchmark study, the LMI solver is not practical and the accuracy may not be in the levels of acceptable engineering limits.

- Primary controllers with low dissipativity characteristics are not adequate for smart dampers. In some cases, due to the dynamical characteristics of a smart damper, such controllers may result in further reduction in the dissipativity, which may considerably reduce the efficiency of the damper.
- The semiactive design procedure for complex, high-order structures should include a dissipativity analysis to reveal control designs that are more suitable for MR dampers.
- A study of the proposed dissipativity indices computed via an inexpensive Lyapunov solution for the active primary controller, preliminary to the semiactive design, has the potential for significant savings of the time and computational effort.

While this research gives an important insight into the concept of dissipativity in the semiactive control of structures with smart dampers, it also exposes some other related topics to be investigated. These are summarized below:

- $D_{ne}$-based dissipativity constraint and equality constraint: The dissipativity constraint used efficiently has been based on the mean energy flow rate ($D_e$). The problem with the dissipativity constraint based on $D_{ne}$, which is given by

$$\begin{aligned} \min_{\mathbf{Y},\,\mathbf{S},\,\mathbf{X}} \quad & Tr(\mathbf{Q}^{1/2}\mathbf{S}\mathbf{Q}^{1/2}) + Tr(\mathbf{X}) - Tr(\mathbf{Y}\mathbf{N}) - Tr(\mathbf{N}^{\mathrm{T}}\mathbf{Y}^{\mathrm{T}}) \\ \text{subject to} \quad & \mathbf{A}\mathbf{S} - \mathbf{B}\mathbf{Y} + \mathbf{S}\mathbf{A}^{\mathrm{T}} - \mathbf{Y}^{\mathrm{T}}\mathbf{B}^{\mathrm{T}} + \mathbf{E}\mathbf{E}^{\mathrm{T}} < 0, \qquad \begin{bmatrix} \mathbf{X} & \mathbf{R}^{1/2}\mathbf{Y} \\ \mathbf{Y}^{\mathrm{T}}\mathbf{R}^{1/2} & \mathbf{S} \end{bmatrix} > 0, \\ & \mathbf{S} > 0, \qquad \frac{-\mathbf{F}\mathbf{S}\mathbf{C}_{\mathrm{v}}^{\mathrm{T}}}{\sqrt{\mathbf{F}\mathbf{S}\mathbf{F}^{\mathrm{T}}}\sqrt{\mathbf{C}_{\mathrm{v}}\mathbf{S}\mathbf{C}_{\mathrm{v}}^{\mathrm{T}}}} < \gamma_{\mathrm{ne}}^{\mathrm{L}} \end{aligned} \tag{8.1}$$

has been implemented with an iterative method. While the iterative method solves (8.1), it does not provide an improvement in the dissipativity from a practical point of view. Clearly, the dissipativity constraint based on $D_{\mathrm{ne}}$ is a nonlinear constraint. Therefore, available software can be used to seek the solution of (8.1). It is also important whether the dissipativity constraint in (8.1) can be represented as a BMI constraint or not. Of course, even if a BMI constraint can be obtained, the BMI version of the problem given by (8.1) is not guaranteed to be solvable by the available methods and software due to the complexity of BMI problems. It should also be noted that the dissipativity constraints based on $D_{\mathrm{e}}$ and $D_{\mathrm{ne}}$ use the Lyapunov matrix instead of the state covariance matrix. To impose the actual $D_{\mathrm{e}}$ and $D_{\mathrm{ne}}$ constraints, which are based on the state covariance matrix, the equality conditions given by (5.23) must be used in the EVP. This results in a different optimization problem given by

$$\begin{aligned}
&\min_{\mathbf{Y},\,\mathbf{S},\,\mathbf{X}} \; Tr(\mathbf{Q}^{1/2}\mathbf{S}\mathbf{Q}^{1/2}) + Tr(\mathbf{X}) - Tr(\mathbf{Y}\mathbf{N}) - Tr(\mathbf{N}^{\mathrm{T}}\mathbf{Y}^{\mathrm{T}}) \\
&\qquad \mathbf{A}\mathbf{S} - \mathbf{B}\mathbf{Y} + \mathbf{S}\mathbf{A}^{\mathrm{T}} - \mathbf{Y}^{\mathrm{T}}\mathbf{B}^{\mathrm{T}} + \mathbf{E}\mathbf{E}^{\mathrm{T}} = 0, \quad \begin{bmatrix} \mathbf{X} & \mathbf{R}^{1/2}\mathbf{Y} \\ \mathbf{Y}^{\mathrm{T}}\mathbf{R}^{1/2} & \mathbf{S} \end{bmatrix} > 0, \\
&\text{subject to} \\
&\qquad \mathbf{S} > 0, \qquad \frac{-\mathbf{F}\mathbf{S}\mathbf{C}_{\mathrm{v}}^{\mathrm{T}}}{\sqrt{\mathbf{F}\mathbf{S}\mathbf{F}^{\mathrm{T}}}\sqrt{\mathbf{C}_{\mathrm{v}}\mathbf{S}\mathbf{C}_{\mathrm{v}}^{\mathrm{T}}}} < \gamma_{\mathrm{ne}}^{\mathrm{L}}
\end{aligned} \tag{8.2}$$

Both of the problems defined above are very complex nonlinear matrix inequality problems without and with equality constraints. A literature survey on this topic revealed that this is a major area of numerical optimal control. It is known that some software is available for this type of problem (*e.g.*, Michal and Michael 2004). However, an initial investigation on this topic and available software shows that these are quite challenging problems, which may require specialized code development.

- Time-Domain Dissipativity Constraint (Hard Dissipativity Constraint): The nonlinear time-domain dissipativity constraint $u_a v_d < 0$ is a *hard constraint*. Due to the nature of a hard constraint, an LQR problem is defined in a different form as follows: consider the linear system given by (3.7). A linear quadratic control problem can be defined to find a piecewise smooth control law $\mathbf{u}$ that brings the system from a known initial state $\mathbf{q}_0$ at time $t_0$ to a desired final state $\mathbf{q}_f$ at time $t_f$ such that

$$\min_{\mathbf{K}} \int_{t_0}^{t_f} (\mathbf{q}^T\mathbf{Q}\mathbf{q} + \mathbf{u}^T\mathbf{R}\mathbf{u} + \mathbf{q}^T\mathbf{N}\mathbf{u} + \mathbf{u}^T\mathbf{N}^T\mathbf{q})dt \quad \text{subject to } \dot{\mathbf{q}} = \mathbf{A}\mathbf{q} + \mathbf{B}\mathbf{u} + \mathbf{E}\mathbf{w}, \quad \mathbf{u} = -\mathbf{K}\mathbf{q} \tag{8.3}$$

Clearly, this problem is quite different than the standard infinite time horizon LQR problem defined in this dissertation. Now, consider that the control law $\mathbf{u}$ is also constrained by a set of inequalities

$$h_i(\mathbf{q}, \mathbf{u}, t) < 0 \qquad i = 1,\ldots,n \tag{8.4}$$

where $n$ is the length of the control vector $\mathbf{u}$. While there is no analytical solution to this problem, there are some numerical techniques proposed (Denham and Bryson 1964; Lasdon *et al*. 1967; Ma and Levine 1993; Pytlak and Vinter 1993; Ma and Levine 1995; Zefran and Kumar 1995). These techniques should be investigated for a possible solution of an LQR problem with a deterministic dissipativity constraint.

# BIBLIOGRAPHY

Boyd, S., Ghaoui, L. E., Feron, E., and Balakrishnan, V. (1994). *Linear Matrix Inequalities in System and Control Theory*, Studies in Applied Mathematics, **15**, SIAM, Philadelphia, Pennsylvania.

Carstairs, N., Powell, D., and Samaras, S. (2005). "Gatwick's long haul: A unique air bridge." *The Arup Journal*, **40**(3), 30–36 (on the web: http://www.arup.com/journal.cfm).

Chen, C.-T. (1999). *Linear System Theory and Design*, Oxford University, New York.

Christenson, R. E. (2003). "Probabilistic approach to assess the applicability of smart damping technology." *CD-ROM Proceedings of 16th ASCE Engineering Mechanics Conference*, Seattle, Washington.

Christenson, R.E. (2004). "A Probabilistic Method to Assess the Efficacy of Smart Damping Technology." *Proceedings of the Second International Conference on Structural Engineering, Mechanics and Computation*, Cape Town, South Africa.

Dallard, P., Fitzpatrick, A. J., Flint, A., Le Bourva, S., Low, A., Ridsdill Smith, R. M., Willford, M. (2001). "The London Millennium Footbridge." *Structural Engineer*, **79**(22), 17–35 (on the web: http://www.arup.com/millenniumbridge).

Den Hartog, J. P. (1956). *Mechanical Vibrations*, Dover Publications, New York.

Denham, W. F., and Bryson, A. E., Jr. (1964). "Optimal programming problems with inequality constraints II: Solution by steepest-ascent." *AIAA Journal*, **2**(1), p25–34.

Dullerud, G. E., and Paganini, F. (2000). *A Course in Robust Control Theory: A Convex Approach*, Springer, New York.

Dyke, S. J., Spencer, B. F., Jr., Sain, M. K., and Carlson J. D. (1996). "Modeling and control of magnetorheological dampers for seismic response reduction." *Smart Materials & Structures*, **5**(5), 565–575.

Dyke, S. J., Spencer, B. F., Jr., Sain, M. K., and Carlson J. D. (1998). "An experimental study of MR dampers for seismic protection." *Smart Materials and Structures*, **7**(5), 693–703.

Erkus, B., Abé, M., and Fujino, Y. (2002). "Investigation of semi-active control for seismic protection of elevated highway bridges." *Engineering Structures*, **24**(3), 281–293.

Erkus, B., and Johnson, E. A. (2006). "Smart base isolated benchmark building part III: a sample controller for bilinear isolation." *Journal of Structural Control and Health Monitoring*, *in press.*

Feron, E., Balakrishnan, V., Boyd, S., and El Ghaoui, L. (1992). "Numerical methods for $H_2$ related problems." *Proceedings of American Control Conference*, Chicago, Illinois, 2921–2922.

Fujioka, H., and Hoshijima, K. (1997). "Bounds for the BMI Eigenvalue Problem – A Good Lower Bound and a Cheap Upper Bound." *Transactions of the Society of Instrument and Control Engineers*, **33**, 616–621.

Gahinet, P., Nemirovski, A., Laub, A. J., and Chilali, M. (1995). *LMI Control Toolbox*. MathWorks, Natick, Massachusetts.

Goh, K. C., Turan, L., Safonov, M. G., Papavassilopoulos, G.P., and Ly, J. H. (1994) "Biaffine Matrix Inequality Properties and Computational Methods." *Proceedings of American Control Conference*, Baltimore, Maryland, 850–855.

Gurtin, M. E., and Herrera, I. (1964). "On dissipation inequalities and linear viscoelasticity." *Division of Applied Mathematics Technical Report Nonr-562(25)/27*, Brown University, Providence, Rhode Island.

Housner, G. W., Bergman, L. A., Caughey, T. K., Chassiakos, A. G., Claus, R. O., Masri, S. F., Skelton, R. E., Soong, T. T., Spencer, B. F., Jr., and Yao, J. T. P. (1997). "Structural control: past, present, and future." *Journal of Engineering Mechanics*, ASCE, **123**(9), 897–971.

Inaudi, J. A. (2000). "Performance of variable-damping systems: Theoretical Analysis and Simulation." *Proceedings of 3rd International Workshop on Structural Control*, Paris, France, 301–316.

Ioannou, P. A., and Tao, G. (1987). “Frequency domain conditions for strictly positive functions.” *IEEE Transactions on Automatic Control*, 32(**1**), 53–54.

Johnson, E. A., Baker, G. A., Spencer, B. F., Jr., and Fujino, Y. (2006). “Semiactive damping of stay cables.” *Journal of Engineering Mechanics*, ASCE, *in press.*

Johnson, E. A. (2000). “Nonlinear seismic benchmark problem: Dissipativity and the 9-Story benchmark building.” *Proceedings of 2nd European Conference on Structural Control*, Champs-sur-Marne, France.

Kelly, J. M., Skinner, R. I., and Heine, A. J. (1972). “Mechanisms of Energy Absorption in Special Devices for Use in Earthquake-Resistant Structures.” *Bulletin of the New Zealand National Society for Earthquake Engineering*, **5**(3), 63–88.

Kenneth, H., Anders, O. G., and Marcus, M. E. (2004) *TOMLAB*, TOMLAB Optimization, San Diego, CA, *http://tomlab.biz*.

Kawanishi, M., Sugie, T., and Kanki, H., (1997) “BMI Global Optimisation Based on Branch and Bound Method Taking Account of the Property of Local Minima.” *Proceedings Of the 36th Conference on Decision and Control*, San Diego, California.

Khargonekar, P. P., and Rotea, M. A. (1991). “Mixed $H_2/H_\infty$ control: A convex optimization approach.” *IEEE Transactions on Automatic Control*, **36**(7), 824–837.

Lasdon, L. S., Waren, A. D., and Rice, R. K. (1967). “An interior penalty method for inequality constraint optimal control problems.” *IEEE Transactions on Automatic Control*, **AC-12**(4), 388–395.

Ma, B., and Levine, W. S. (1993). “An algorithm for solving control constrained optimal control problems.” *Proceedings of the 32nd Conference on Decision and Control*, San Antonio, Texas, 3784–3790.

Ma, B., and Levine, W. S. (1995). “A new algorithm for solving optimal control problems with hard control constraints, end-point inequality constraints, and a variable initial state.” *Proceedings of the American Control Conference*, Seattle, Washington, 2086–2092.

Michal, K., and Michael, S. (2004). *PENOPT*, PENOPT GbR, Stöckach, Germany, *http://www.penopt.com*.

Masubuchi, I., Ohara, A., and Suda, N. (1998). "LMI-based controller synthesis: A unified formulation and solution." *International Journal of Robust Nonlinear Control*, **8**(8), 669–686.

Narasimhan, S., Nagarajaiah S., Gavin, H. P., and Johnson, E. A. (2006). "Smart base isolated building part I: problem definition." *Journal of Structural Control and Health Monitoring*, *in press.*

Nagarajaiah, S., and Narasimhan, S., (2006). "Smart base-isolated benchmark building part II: phase I sample controllers for linear isolation systems." *Journal of Structural Control and Health Monitoring*, *in press.*

Nesterov, Y., and Nemirovskii, A. (1994). *Interior-point Polynomial Algorithms in Convex Programming*, Studies in Applied Mathematics, **13**, SIAM, Philadelphia, Pennsylvania.

Nishitani, A., and Inoue, Y. (2001). "Overview of the application of active/semiactive control to building structures in Japan." *Earthquake Engineering and Structural Dynamics*, **30**(11), 1565–1574.

Ormondroyd, J., and Den Hartog, J. P. (1928). "The theory of dynamic vibration absorber." *Transactions of the ASME*, **APM-50-7**, 9–22.

Patten, W. N., Kuo, C. C., He, Q., Liu, L., and Sack, R. L. (1994a). "Seismic structural control via hydraulic semiactive vibration dampers (SAVD)." *Proceedings of 1st World Conference on Structural Control*, Los Angeles, California, FA2:83–92.

Patten, W. N., Kuo, C. C., He, Q., Liu, L., and Sack, R. L. (1994b). "Suppression of vehicle-induced bridge vibration via hydraulic semiactive vibration dampers." *Proceedings of 1st World Conference on Structural Control*, Los Angeles, California, FA1:30–38.

Peres, P. L. D., Souza, S. R., and Geromel, J. C. (1992). "Optimal $H_2$ control for uncertain linear systems." *Proceedings of American Control Conference*, Chicago, Illinois, 2916–2920.

Pytlak, R., and Vinter, R. B. (1993). “A feasible directions type algorithm for optimal control problems with hard state and control constraints.” *Proceedings of the 32nd Conference on Decision and Control*, San Antonio, Texas, 3335–3340.

Ramallo, J. C., Johnson, E. A., and Spencer, B. F., Jr. (2002). “‘Smart’ base isolation systems.” *Journal of Engineering Mechanics*, ASCE, **128**(10), 1088–1099.

Safonov, M. G., Goh, K. C., and Ly, J. H. (1994). “Control system synthesis via bilinear matrix inequalities.” *Proceedings of American Control Conference*, Baltimore, Maryland, 45–49.

Scherer, C., Gahinet, P., and Chilali, M. (1997). “Multiobjective output-feedback control via LMI optimization.” *IEEE Transactions on Automatic Control*, **42**(7), 896–911.

Shen, K. L., and Soong, T. T. (1995). “Modelling of viscoelastic dampers for structural application.” *Journal of Engineering Mechanics*, ASCE, **121**(6), 694–701

Slotine, J.-J. E., and Li, W. (1991). *Applied Nonlinear Control*. Prentice-Hall, Englewood Cliffs, New Jersey.

Soong, T. T., and Spencer, B. F., Jr. (2002). “Supplemental energy dissipation: State-of-the-art and state-of-the-practice.” *Engineering Structures*, **24**(3), 243–259.

Soong, T. T., and Grigoriu, M. (1993). *Random Vibration of Mechanical and Structural Systems*. Prentice-Hall, Englewood Cliffs, New Jersey.

Spencer, B. F., Jr., and Sain, M. K. (1997). “Controlling buildings: A new frontier in feedback.” *IEEE Control Systems Magazine*, **17(**6), 19–35.

Spencer, B. F., Jr., Johnson, E. A., and Ramallo, J. C. (2000). “‘Smart’ isolation for seismic control.” *JSME International Journal*, Series C, **43**(3), 704–711.

Spencer, B. F., Jr., and Nagarajaiah, S. (2003). “State of the art of structural control.” *Journal of Structural Engineering*, **129**(7), 845–856.

Symans, M. D., and Constantinou, M. C. (1999). "Semi-active control systems for seismic protection of structures: A state-of-the-art review." *Engineering Structures*, **21**(6), 469–487.

Taylor, J. H. (1974). "Strictly positive-real functions and the Lefschetz-Kalman-Yakubovich Lemma." *IEEE Transactions on Circuits and Systems*, **21**(2), 310–311.

Toker, O., and Özbay, H. (1995). "On the $\mathcal{NP}$-hardness of solving bilinear matrix inequalities and simultaneous stabilization with static output feedback." *Proceedings of American Control Conference*, Seattle, Washington, 2525–2526.

Tuan, D. H., Apkarian, P., and Nakashima, Y., (1999). "A new Lagrangian dual global optimization algorithm for solving bilinear matrix inequalities." *Proceedings of the American Control Conference*, **3**(3), San Diego, 1851–1855.

Turan, L., Safonov, M. G., and Huang, C. H. (1997). "Synthesis of positive real feedback systems: A simple derivation via Parrott's theorem." *IEEE Transactions on Automatic Control*, **42**(8), 1154–1157.

Wen, J. T. (1988). "Time domain and frequency domain conditions for strict positive realness." *IEEE Transactions on Automatic Control*, **33**(10), 988–992.

Willems, J. C. (1971). "Least squares stationary optimal control and the algebraic Ricatti equation." *IEEE Transactions on Automatic Control*, **AC-16**(6), 621–634.

Willems, J. C. (1972a). "Dissipative dynamical systems – Part I: General theory." *Archive for Rational Mechanics and Analysis*, **45**(5), 321–351.

Willems, J. C. (1972b). "Dissipative dynamical systems – Part II: Linear systems with quadratic supply rates." *Archive for Rational Mechanics and Analysis*, **45**(5), 352–393.

Yamazaki, S., Nagata, N., and Abiru, H. (1995). "Full scale investigation of performance of tuned active dampers installed in Landmark Tower in Yokohama." *Proceedings of the Third International Conference on Wind Engineering*, 1631–1642.

Yang, G., Spencer, B. F., Jr., Carlson, J. D., and Sain, M. K. (2002). "Large-scale MR fluid dampers: modeling and dynamic performance considerations." *Engineering Structures*, **24**(3), 309–323.

Yang, J. N., Lin, S., and Jabbari, F. (2003). "$H_2$-based control strategies for civil engineering structures." *Journal of Structural Control and Health Monitoring*, **10**(3–4), 205–230.

Yang, J. N., Lin, S., and Jabbari, F. (2004). "Linear Multiobjective Control Strategies for Wind-Excited Buildings." *Journal of Engineering Mechanics*, ASCE, **130**(4), 471–477.

Yao J. T. P. (1972). "Concept of Structural Control." *Journal of Structural Division*, ASCE, **98**(ST7), 1567–1574.

Zefran, M., and Kumar, V. (1995). "Optimal control of systems with unilateral constraints." *IEEE International Conference on Robotics and Automation*, Nagoya, Japan, 2695–2700.

# APPENDIX

## A.1 Dissipativity and Dissipative Systems

There are several definitions of dissipativity in the field of systems and control. In fact, dissipativity is one of the key concepts in control theory, and there is a vast body of literature regarding dissipative systems. However, one should note that these definitions in the controls literature are used to characterize the input–output relations of dynamical systems and are different from the mechanical definition used herein. Rather, dissipativity is associated with the control force in this study, and the concept of a dissipative force is introduced based on mechanical dissipation of energy. Although a connection between these two interpretations can be found, it is beyond the scope of this study. Interested readers are directed to the works by Gurtin and Herrera (1964), Willems (1972a,b), Taylor (1974), Ioannou and Tao (1987) and Wen (1988) for further details.

## A.2 Convex Multiobjective Optimization via LMIs

Convex optimization techniques became very popular in the control field since it has been shown that important control problems, such as robust $H_2$ and $H_\infty$ control problems, can be represented in terms of LMIs. These techniques allow numerical solution of complex problems with multiobjective goals that have no analytical solution. In fact, the LQR problem defined herein can be represented as an $H_2$ problem, and an available LMI representation of an $H_2$ problem can be used. However, robust $H_2$ control theory is quite involved and requires a good knowledge of frequency and time domain analysis. In contrast, LQR is well known and widely applied within the structural control community; therefore, LQR is used in this dissertation. Interested readers are directed to the works by Willems (1971), Khargonekar and Rotea (1991), Feron *et al*. (1992),

Peres *et al.* (1992), Boyd *et al*. (1994), Safonov *et al*. (1994), Scherer *et al*. (1997), Turan *et al*. (1997), Masubuchi *et al*. (1998), and Dullerud and Paganini (2000) for further details.

Application of LMI techniques to structural control problems is very recent. Some examples are Yang *et al*. (2003) and Yang *et al*. (2004).

## A.3 Algorithms for BMI Problems

As discussed previously, the existence of a solution of a problem with BMIs is not guaranteed in most cases since such problems are known to be $\mathcal{NP}$–hard (Toker and Özbay 1995), and no efficient algorithm exists to solve such problems as they do not have the convexity property. However, there has been some effort to find local (Goh *et al*. 1994; Fujioka and Hoshijima 1997; Kawanishi *et al*. 1997) and global (Goh *et al*. 1994; Tuan et al. 1999) solutions for BMI problems, and there has been some software developed for this purpose (Kenneth *et al*. 2004; Michal and Michael 2004). Some of these software packages are also designed to analyze optimization problems with nonlinear constraints.

## A.4 Numerical Considerations

From an engineering and computational point of view, a strict LMI is not different from its nonstrict version. For example, the dissipativity constraint is herein represented as a strict LMI in numerical computations for consistency. However, there are also situations where the computations are quite sensitive to the inequality condition. For example, during numerical simulations, it is observed that, for some specific values of the weighting matrices, the corresponding LQR problem turns out to be ill-conditioned even though the conditions for the well-posedness given by (3.11) are satisfied. It is found that some of the eigenvalues of $\mathbf{W}$ are very close to zero (in the range of $10^{-10}$) for these weighting matrices. Therefore, it is highly recommended that the

LQR weighting matrices be selected such that the smallest eigenvalue of **W** is large enough to guarantee the well-posedness of the LQR.

## A.5 MATLAB® Codes

The codes used in this research can be obtained by contacting Mr. Erkus at bariserkus@gmail.com. Benchmark problem codes are available at http://www.usc.edu/dept/civil_eng/johnsone/baseisobench/.

### A.5.1 LMI-EVP Representation of an LQR Problem

```
function [Kdis, Sopt] =  lqrlmidis (sys, lq, gamma, options)

% LQRLMIDIS solves the standard LQR problem (type "help lqr" for more info)
%   with a Lyapunov dissipativity constraint, using LMI techniques.
%
%   The problem statement is as follows:
%
%   Consider a LTI system with a state-space representation given by
%       .
%       q = A q + B u + E w
%       zv= Cvq
%
%   where zv is the velocity of the controller
%
%   Standard LQR problem calculates a optimal gain matrix K, such
%   that the state-feedback law u = -Kq minimizes the cost function
%
%        J = Integral {q'Qq + u'Ru + 2*q'Nu} dt
%                                  .
%    subject to the state dynamics  x = Aq + Bu + Ew.
%
%   This problem is equivalent to the following eigenvalue problem:
%
%      min   Tr(SQ) + Tr(X) - Tr(YN) - Tr(N'Y')
%    (Y,S,X)
%
%   subject to  AS - BY + SA' - Y'B' + EE' < 0
%
%               [ X         Sqrt(R)Y ]
%               [                    ]  > 0
%               [Y'Sqrt(R)      S    ]
%
%   The dissipativity constraint is given as -YCv' < gamma (< 0).
%   With the addition of the dissipativity constraint, the eigenvalue
%   problem defined above is no longer equivalent to the LQR problem.
%
%   LMILQR solves the above eigenvalue problem with the dissipativity
%   constraint to compute the optimal gain matrix given by K = Y inv(S).
%   It uses the "mincx" function of the LMI Control Toolbox.
```

```
%
%   SYNTAX
%
%   K = lqrlmidis (sys, lq, gamma, options)
%       where sys is a structure with sys.A, sys.B, sys.E and sys.Cv
%       matrices and lq is a structure with lq.Q, lq.R and lq.N matrices.
%
%       gamma (< 0) is the dissipativity parameter
%
%       options is defined by the options of "mincx" function. If ignored
%       it is assumed as [1e-20, 100, -1, 5, 1]
%
%   written by Baris Erkus
%   ver 1.1


% Resolve the inputs
A = sys.A; B = sys.B; E = sys.E; Cv = sys.Cv;
Q = lq.Q; R = lq.R; N = lq.N;

nstate = size(A,1);

% Enforce symmetry of Q and R in case they are different due to numerical
% roundoff in computation
Q = (Q+Q.')/2;
R = (R+R.')/2;
R_half = R^(1/2);
R_half=(R_half+R_half.')/2;

%%
%% Defintion of LMIs
%%

setlmis([]);
S=lmivar(1, [nstate,1]);
X=lmivar(2, [1,1]);
Y=lmivar(2, [1,nstate]);

% Subject function, LMI #1
%               AS - BY + SA' - Y'B' + EE' < 0

lmiterm([1 1 1 S], A,  1, 's');                % LMI #1:  AS + SA'
lmiterm([1 1 1 Y], B, -1, 's');                % LMI #1: -BY - Y'B'
lmiterm([1 1 1 0], E*E');                      % LMI #1:  EE'

% Subject function, LMI #1a additional test constraint
%               AS - BY + SA' - Y'B' + EE' - a I > 0

%a = 1e5;
%lmiterm([-1 1 1 S], A,  1, 's');                  % LMI #1a:  AS + SA'
%lmiterm([-1 1 1 Y], B, -1, 's');                  % LMI #1a: -BY - Y'B'
%lmiterm([-1 1 1 0], E*E');                        % LMI #1a:  EE'
%lmiterm([-1 1 1 0], -a * eye(nstate));            % LMI #1a:  - a I

% Subject function, LMI #2:
%               [ X         Sqrt(R)Y ]
%               [                    ]  > 0
%               [Y'Sqrt(R)      S    ]

lmiterm([-2 1 1  X], 1, 1);                    % LMI #2: X
lmiterm([-2 2 1 -Y], 1, R_half);               % LMI #2: Y'*sqrt(R)
```

```
lmiterm([-2 2 2  S], 1, 1);                      % LMI #2: S

% Subject function, LMI #3:
%               YCv' + gamma > 0 or -YCv' < gamma

lmiterm([-3 1 1 Y], 1, Cv');                     % LMI #3: YCv'
lmiterm([-3 1 1 0], gamma);                      % LMI #3: gamma

% Create the LMI system
lmisys = getlmis;

% Defining vector "c"
n = decnbr(lmisys);
c = zeros(n,1);
for i=1:n
   [Sj, Xj, Yj] = defcx(lmisys, i, S, X, Y);
   c(i) = trace(Q*Sj) + trace(Xj) - trace(Yj*N) - trace(N'*Yj');
end

% Solving LMIs
if (nargin == 2);
    options = [1e-30, 100, -1, 10, 1];
end;
[copt, xopt] = mincx (lmisys, c, options);

% Results
Xopt = dec2mat(lmisys, xopt, X);
Yopt = dec2mat(lmisys, xopt, Y);
Sopt = dec2mat(lmisys, xopt, S);

Kdis = Yopt*inv(Sopt);
```

### A.5.2 Model Creation for *N*-DOF Structure

```
function [s]  = nstory2(n, m, T, mdr)

% NSTORY Creates a SS models of a simple n-story structure with an
%   equation of motion of
%
%       M a + C v + K x = Sc Fc + Sg ag
%
%   in the form of
%       .
%       q = A q + B u + E w
%       z = Czq + Dzu + Ezw
%
%   It also returns three SS LTI object:
%
%        all_sys, lqr_sys, meas_sys
%
%
% SYNTAX
%
%   [sysmat] = nstory (n)
%       creates an SS model of a n-story shear frame structure where
%
%       n           is the number of story
%
```

```
%   and mass of the each story is 1e5 kgs, the period is 1 sec and the modal
%   damping ratio is 2 % of the critical damping
%
%   [sysmat] = nstory (n, mass, period, modal_damping_ratio)
%       creates an SS model of a n-story shear frame structure where
%
%       n           is the number of story
%       mass        is the mass of each story
%       period      is the period of each story
%       modal_damping_ratio
%                   is the modal damping ratio of each story
%
%       All units should be SI units (N, m, sec, kg)
%
%   sysmat is a cell array containing the matrices
%
%        A, B, E, Cz, Dz, Ez, Cv, M, C, K, Sc, Sg, eigvec, eigval
%
%   for the SS model
%       .
%       q = A q + B u + E w
%       z = Czq + Dzu + Ezw
%       v = Cvq    (velocity among the control device
%
%   where the states are the displacements and velocities wrt to the ground.
%   A controller is placed on the first floor by default. The outputs (4n+4)
%   are given as follows:
%
%       Displacements : n x 1
%       Velocities : n x 1
%       Drifts : n x 1
%       Absolute Accelerations : n x 1
%       Controller Displacement : 1 x 1
%       Controller Velocity : 1 x 1
%       Controller Force : 1 x 1
%       Ground Acceleration : 1 x 1
%
%   sysmat also contains the following LTI objects:
%
%   ALL_SYS
%   -------
%   Inputs :
%      1. Control Force : 1 x 1,        'u'
%      2. Ground Acceleration : 1 x 1,  'ag'
%
%   Outputs :
%      1. Displacements : n x 1,           'disp'
%      2. Velocities : n x 1,              'vel'
%      3. Drifts : n x 1,                  'drift'
%      4. Absolute Accelerations : n x 1,  'absacc'
%      5. Controller Displacement : 1 x 1, 'udisp'
%      6. Controller Velocity : 1 x 1,     'uvel'
%      7. Controller Force : 1 x 1,        'u'
%      8. Ground Acceleration : 1 x 1,     'ag'
%
%   LQR_SYS
%   -------
%   Inputs :
%      1. Control Force :1 x 1
%
%   Outputs :
```

```
%      3. Drifts : n x 1
%      4. Absolute Accelerations : n x 1
%
%   MEAS_SYS
%   --------
%   Inputs :
%      1. Control Force :1 x 1
%      2. Ground Acceleration : 1 x 1
%
%   Outputs :
%      3. Drifts : n x 1
%      4. Absolute Accelerations : n x 1
%      8. Ground Acceleration : 1 x 1
%
%
%   written by Baris Erkus
%   ver 2.0 (beta)

if (nargin == 1);
    m = 1e5;
    T = 0.5;
    mdr = 0.02;
end;

% Compute the story stiffness from period
w = 2*pi/T;   k = m*w^2;

% Mass, stiffness and damping matrices
M = m * eye(n);
K = diag(-k*ones(n-1,1), -1) + diag([2*k*ones(n-1,1);k]) + diag(-k*ones(n-1,1), 1);

if n == 1
    [mods, eigvals] = eig(inv(M)*K);
    C = real(M * mods * (2 * mdr * sqrt(eigvals)) * mods');
else
    [mods, eigvals] = eigs(inv(M)*K, n, 0);
    C = real(M * mods * (2 * mdr * sqrt(eigvals)) * mods');
end

% Coefficent matrices for the SS representation
R = ones (n,1);

Sc = [1;  zeros(n-1, 1)];
Sg = - M * R;

T1 = eye(n) + diag(-1*ones(n-1,1), -1);
T2 = [1 , zeros(1, 2*n-1); zeros(1, n), 1, zeros(1, n-1); zeros(1, 2*n)];
T3 = [0;  0;  1];

% State-Space Matrices : Eqn of Motion

A = [zeros(n)  eye(n); -inv(M)*K,  -inv(M)*C];
B = [zeros(n,1);  inv(M)*Sc];
E = [zeros(n,1);  inv(M)*Sg];

%State-Space Matrices : Outputs
%    Disp & Vel    | Drift         |  Abs. Accel          |Cont. D,V,F  | Ground. Accel |;
%=============================================================================================
====

Cz = [eye(2*n)     ;  T1, zeros(n) ; -inv(M)*K, -inv(M)*C ;  T2         ;  zeros(1, 2*n)];
```

```
Dz = [zeros(2*n,1) ;  zeros(n,1)   ;  inv(M)*Sc          ;  T3         ;  0           ];
Ez = [zeros(2*n,1) ;  zeros(n,1)   ;  zeros(n,1)         ;  zeros(3,1) ;  1           ];

Cv = Cz(4*n+2, :);

%%%%%%%%%%%%%%%%%   SS MODELS   %%%%%%%%%%%%%%%%%%
%%%%%%%%%%%%%%%%%%%%%%%%%%%%%%%%%%%%%%%%%%%%%%%%%

%%%  1. ALL INPUTS and OUTPUTS  %%%

% Create an SS system with
%
% Inputs :
%     1. Control Force :1 x 1
%     2. Ground Acceleration : 1 x 1
%
% Outputs :
%     1. Displacements : n x 1
%     2. Velocities : n x 1
%     3. Drifts : n x 1
%     4. Absolute Accelerations : n x 1
%     5. Controller Displacement : 1 x 1
%     6. Controller Velocity : 1 x 1
%     7. Controller Force : 1 x 1
%     8. Ground Acceleration : 1 x 1

output_name_all_sys = {...
    [1     : n   ],  'disp'   ;
    [n+1   : 2*n ],  'vel'    ;
    [2*n+1 : 3*n ],  'drift'  ;
    [3*n+1 : 4*n ],  'absacc' ;
    [4*n+1       ],  'udisp'  ;
    [4*n+2       ],  'uvel'   ;
    [4*n+3       ],  'u'      ;
    [4*n+4       ],  'ag'      };

input_name_all_sys = {...
    [1           ],  'u'     ;
    [2           ],  'ag'     };

all_sys = ss(A, [B, E], Cz, [Dz Ez],...
    'InputGroup', input_name_all_sys,  'OutputGroup', output_name_all_sys  );


%%%  2. FOR LQR  %%%

% Create an SS system with
%
% Inputs :
%     1. Control Force :1 x 1
%
% Outputs :
%     3. Drifts : n x 1
%     4. Absolute Accelerations : n x 1

lqr_sys = all_sys({'drift', 'absacc'}, {'u'});


%%%  3. FOR MEASUREMENTS  %%%

% Create an SS system with
```

```
%
% Inputs :
%     1. Control Force :1 x 1
%     2. Ground Acceleration : 1 x 1
%
% Outputs :
%     3. Drifts : n x 1
%     4. Absolute Accelerations : n x 1
%     8. Ground Acceleration : 1 x 1

meas_sys = all_sys({'drift', 'absacc', 'ag'}, {'u', 'ag'});


%%%%%%%%%    OUTPUTS    %%%%%%%%%%

s.all_sys = all_sys;
s.lqr_sys = lqr_sys;
s.meas_sys = meas_sys;

s.M = M;
s.K = K;
s.C = C;

s.Sc = Sc;
s.Sg = Sg;

s.eigvec = mods;
s.eigval = eigvals;

s.A = A;
s.B = B;
s.E = E;

s.Cz = Cz;
s.Dz = Dz;
s.Ez = Ez;

s.Cv = Cv;
```

### A.5.3 Base Isolated Benchmark Code Sample Simulation and Controller

a) Initialization file

```
%%%%%%%%%%%%%%%%%%%%%%%%%%%%%%%%%%%%%%%%%%%%%%%%%%%%%%%%%%%%%%%%%%%%%%%%%%%%%%%%
%
%               Smart Base-Isolated Benchmark Building
%       Part III: A Sample Controller for Bilinear Isolation
%
%             Baris Erkus      and      Erik A. Johnson
%           (erkus@usc.edu)            (JohnsonE@usc.edu)
%
% This file loads the variabeles that will be used in the control design
% and simulation into the workspace.
%
%%%%%%%%%%%%%%%%%%%%%%%%%%%%%%%%%%%%%%%%%%%%%%%%%%%%%%%%%%%%%%%%%%%%%%%%%%%%%%%%
%
% File name          : part_III_initialization.m
% Version            : 2.2
% Release Date       : **/**/****
```

```
% Report Bugs        : JohnsonE@usc.edu
%
% MATLAB Version     : 6.5.0.180913a (R13)
% Simulink Version   : 5.0 (R13)
% Control System
%  Toolbox Version   : 5.12 (R13)
% Windows Version    : MS Windows XP 5.1
%
%  Units             : tons, kN, m, sec.
%
% Abbrevations:
%       obv   : obvious
%       ELM   : equivalent linearized model
%       wrt   : with respect to
%       SS    : state-space
%       COM   : center of mass
%       EQ    : earthquake
%
% Needs:
%       nplace.m
%       cleaner.m
%%%%%%%%%%%%%%%%%%%%%%%%%%%%%%%%%%%%%%%%%%%%%%%%%%%%%%%%%%%%%%%%%%%%%%%%%%%%%%%%
%
% Modifications
%    Version         Date                          Details
%  ___________   ____________   ____________________________________________
%      2.2        02/01/2005      Corrected the comments, version numbers
%  and contact information, etc...
%      2.2        02/16/2005      Corrected units to tons, kN, m, sec
%
%
%


%%                                  %%
%%  PART I : Structural Paremeters  %%
%%                                  %%

nmodes = 24;
% Number of the modes of the superstructure.
% There are 8 stories. Each story has 3 DOFs.
% Totol DOFs is 24. Therefore,
% we have 24 modes.

nfloors = 8;
% obv

ncontrollers = 12;
% Number of control devices.

nrubber = 92; nlead = 61;
nelements = nrubber + nlead;
% Number of the linear rubber bearings,
% bilinear lead plugs.

contr_coor = [0,      0;
              0,      0;
         -17.25,  30.69;
         -17.25,  30.69;
         -17.25, -47.79;
         -17.25, -47.79;
```

```
          12.53, -47.79;
          12.53, -47.79;
          32.83, -11.16;
          32.83, -11.16;
          32.83,  30.69;
          32.83,  30.69];
% Coordinates of the controllers. The origin of
% the coordinate system is the COM
% of the base.

rubber_bearing_coor = ...
[1.82 , -47.79 ;            % Coordinates of the linear rubber bearings.
 -7.32 , -47.79 ;           % The origin of the coordinate system
 -17.25 , -47.79 ;          % is the COM of the base.
 -17.25 , -39.93 ;          % Note that the size is 92 x 2.
 -17.25 , -31.88 ;
 -17.25 , -24.05 ;
 -17.25 , -16.18 ;
 -17.25 , -8.35 ;
 -17.25 , -0.49 ;
 -17.25 , 7.35 ;
 -17.25 , 15.00 ;
 -17.25 , 22.83 ;
 -17.25 , 30.69 ;
 -7.32 , 30.69 ;
 1.82 , 30.69 ;
 10.21 , 30.69 ;
 18.17 , 30.69 ;
 25.97 , 30.69 ;
 32.83 , 30.69 ;
 32.83 , 23.04 ;
 32.83 , 15.21 ;
 32.83 , 7.35 ;
 32.83 , -0.49 ;
 32.83 , -11.16 ;
 25.97 , -11.16 ;
 18.17 , -11.16 ;
 12.53 , -16.18 ;
 12.53 , -24.05 ;
 12.53 , -31.88 ;
 12.53 , -39.75 ;
 12.53 , -47.79 ;
 -7.32 , 23.04 ;
 -7.32 , 15.21 ;
 -7.32 , 7.35 ;
 -7.32 , -0.49 ;
 -7.32 , -8.35 ;
 -7.32 , -16.18 ;
 -7.32 , -24.05 ;
 -7.32 , -31.88 ;
 -7.32 , -39.75 ;
 1.82 , 23.04 ;
 1.82 , 15.21 ;
 1.82 , 7.35 ;
 1.82 , -0.50 ;
 1.82 , -8.35 ;
 1.82 , -16.18 ;
 1.82 , -24.05 ;
 1.82 , -31.88 ;
 1.82 , -39.75 ;
 10.21 , 23.04 ;
```

```
 10.21 , 15.21 ;
 10.21 , 7.35 ;
 10.21 , -0.49 ;
 18.17 , 23.04 ;
 18.17 , 15.21 ;
 18.17 , 7.35 ;
 18.17 , -0.49 ;
 25.97 , 23.04 ;
 25.97 , 15.21 ;
 25.97 , 7.35 ;
 25.97 , -0.49 ;
 -12.28 , -47.79 ;
 -2.80 , -47.79 ;
 7.10 , -47.79 ;
 -17.25 , -43.86 ;
 -17.25 , -36.03 ;
 -17.25 , -28.16 ;
 -17.25 , -20.33 ;
 -17.25 , -12.47 ;
 -17.25 , -4.63 ;
 -17.25 , 3.23 ;
 -17.25 , 11.06 ;
 -17.25 , 18.93 ;
 -17.25 , 26.76 ;
 -12.28 , 30.69 ;
 -2.41 , 30.69 ;
 6.00 , 30.69 ;
 14.17 , 30.69 ;
 22.07 , 30.69 ;
 29.41 , 30.69 ;
 32.83 , 26.88 ;
 32.83 , 19.11 ;
 32.83 , 11.28 ;
 32.83 , 3.41 ;
 32.83 , -5.82 ;
 29.35 , -11.16 ;
 22.07 , -11.16 ;
 12.53 , -11.16 ;
 12.53 , -20.12 ;
 12.53 , -27.95 ;
 12.53 , -35.81 ;
 12.53 , -43.65 ];

lead_plug_coor = ...
[ 1.82 , -47.79 ;
 -7.32 , -47.79 ;
 -17.25 , -47.79 ;          % Coordinates of the bilinear lead plugs.
 -17.25 , -39.93 ;          % The origin of the coordinate system
 -17.25 , -31.88 ;          % is the COM of the base.
 -17.25 , -24.05 ;          % Note that the size is 61 x 2.
 -17.25 , -16.18 ;
 -17.25 , -8.35 ;
 -17.25 , -0.49 ;
 -17.25 , 7.35 ;
 -17.25 , 15.00 ;
 -17.25 , 22.83 ;
 -17.25 , 30.69 ;
 -7.32 , 30.69 ;
 1.82 , 30.69 ;
 10.21 , 30.69 ;
 18.17 , 30.69 ;
```

```
 25.97 , 30.69 ;
 32.83 , 30.69 ;
 32.83 , 23.04 ;
 32.83 , 15.21 ;
 32.83 , 7.35 ;
 32.83 , -0.49 ;
 32.83 , -11.16 ;
 25.97 , -11.16 ;
 18.17 , -11.16 ;
 12.53 , -16.18 ;
 12.53 , -24.05 ;
 12.53 , -31.88 ;
 12.53 , -39.75 ;
 12.53 , -47.79 ;
 -7.32 , 23.04 ;
 -7.32 , 15.21 ;
 -7.32 , 7.35 ;
 -7.32 , -0.49 ;
 -7.32 , -8.35 ;
 -7.32 , -16.18 ;
 -7.32 , -24.05 ;
 -7.32 , -31.88 ;
 -7.32 , -39.75 ;
 1.82 , 23.04 ;
 1.82 , 15.21 ;
 1.82 , 7.35 ;
 1.82 , -0.50 ;
 1.82 , -8.35 ;
 1.82 , -16.18 ;
 1.82 , -24.05 ;
 1.82 , -31.88 ;
 1.82 , -39.75 ;
 10.21 , 23.04 ;
 10.21 , 15.21 ;
 10.21 , 7.35 ;
 10.21 , -0.49 ;
 18.17 , 23.04 ;
 18.17 , 15.21 ;
 18.17 , 7.35 ;
 18.17 , -0.49 ;
 25.97 , 23.04 ;
 25.97 , 15.21 ;
 25.97 , 7.35 ;
 25.97 , -0.49 ];

contr_direc = nplace ([1, 2], ncontrollers/2, 'row');
% This is a vector of size "ncontroller". If
% the enrty is
% 1 : controller is in the x-direction
% 2 : controller is in the y-direction

elem_type = [ones(1, nrubber), 3 * ones(1, nlead)];
% This is a vector of size "nelements". If
% the enrty is
% 1 : isolation element is linear rubber
% bearing
% 3 : isolation element is bilinear lead plug

corner_coor1 = [-17.25,  30.69;
               -17.25, -47.79;
                12.53, -47.79;
```

```
               32.83,  30.69];
% Corner coordinates of the base and
% 1st to 6th floors
% The origin of the coordinate system is the
% COM of the base. These values may
% differ the actual corner coordinate values.

corner_coor2 = [-17.25,  30.69;
               -17.25, -47.79;
                12.53, -47.79;
                12.53,  30.69];
% Corner coordinates of the 7th and
% 8th floors
% The origin of the coordinate system is the
% COM of the base. These values may
% differ the actual corner coordinate values.

for i = 1:7;    corner_coor{i} = corner_coor1; end;
for i = 8:9;    corner_coor{i} = corner_coor2; end;
% obv

ncorners = [size(corner_coor1,1)*ones(1,7),size(corner_coor2,1)*ones(1,2)];
% A vector of size 9 and entries are the number
% of corners.

max_ncorners = max(ncorners);
% obv

mass_basex = 3565.73;    mass_basey = mass_basex;   mass_baser = 2706868;
% Mass of the base, in the x, y-directions and
% rotational.

mass_superstr = ...
    [2051,  2051,  1560994;
    2051,  2051,  1560994;
    2051,  2051,  1560994;
    2051,  2051,  1560994;
    2051,  2051,  1560994;
    2057,  2057,  1560994;
    2247,  2247,  1705017;
    2580,  2580,  1957503];
% Mass of the superstructure, 8th floor to 1st
% floor, in the x, y-directions and rotational.

total_mass = sum([mass_superstr(:,1);  mass_basex]);
total_weight = 9.81 * total_mass;
% obv

rubber_stiff = 919.422;
lead_preyield_stiff = 5546.678;
lead_postyield_stiff = 1e-4;
lead_yield_disp = 0.023882523;
lead_yield_force = lead_yield_disp * lead_preyield_stiff;
% Stiffness values of the rubber
% bearings and lead plugs. Here in the
% ELM, the lead will have
% a linear stiffness equal to the preyield
% stiffness of the lead. Note that these values
% are obtained after the simplification
% in the models explained in the paper.
```

```
rubber_damp = 101.439;
lead_damp = 207.0;
% Damping values of the rubber bearings and
% lead plugs. Note that these values are
% obtained after the simplification of the
% models explained in the paper.

eigenval = [49.6265.6691.05496.42557.82860.451674.41...
    1793.832858.653292.803511.065583.475743.955958.467453.32...
    7928.589248.479702.5010431.0811673.9412011.94...
    12912.8315828.7717720.57];
% Eigenvalues. 24 x 1

eigenvec = [Eigenvalue matrix wrt the base. 24 x 24. is not given here];

damp_rat = 0.05 * ones(1, 24);
% Modal damping ratios.

modal_freqs = eigenval.^0.5;
% Modal frequencies.

com_offset =[...
    0,         0
   -0.3500,   -1.4200
   -0.3200,   -5.8000
    0.1100,   -7.2000
    0.1600,   -9.2000
    0.1600,   -9.2000
    0.1600,   -9.2000
    0.1600,   -9.2000];
% Offset of the COMs wrt the COM of base. From 1st floor to the 8th floor.
```

b) Simulation File

```
%%%%%%%%%%%%%%%%%%%%%%%%%%%%%%%%%%%%%%%%%%%%%%%%%%%%%%%%%%%%%%%%%%%%%%%%%%%%%%%
%
%               Smart Base-Isolated Benchmark Building
%       Part III: A Sample Controller for Bilinear Isolation
%
%             Baris Erkus      and      Erik A. Johnson
%           (erkus@usc.edu)            (JohnsonE@usc.edu)
%
% Simulation of the sample LQG controller%
%
%%%%%%%%%%%%%%%%%%%%%%%%%%%%%%%%%%%%%%%%%%%%%%%%%%%%%%%%%%%%%%%%%%%%%%%%%%%%%%%
%
% File name          : part_III_sample.m
% Version            : 2.2
% Release Date       : 05/06/2005
% Report Bugs        : JohnsonE@usc.edu
%
% MATLAB Version     : 6.5.0.180913a (R13)
% Simulink Version   : 5.0 (R13)
% Control System
%    Toolbox Version : 5.12 (R13)
% Windows Version    : MS Windows XP 5.1
%
%  Units             : ton, kN, m, sec.
%
```

```
% Abbrevations:
%       obv   : obvious
%       ELM   : equivalent linear(ized) model
%       wrt   : with respect to
%       SS    : state-space
%       COM   : center of mass
%       EQ    : earthquake
%
% Needs:
%       nplace.m, gamma_vals.mat
%%%%%%%%%%%%%%%%%%%%%%%%%%%%%%%%%%%%%%%%%%%%%%%%%%%%%%%%%%%%%%%%%%%%%%%%%%%%%%%%
%
% Modifications
%    Version         Date                         Details
%  ___________   ___________   ____________________________________________
%      2.1        02/24/2004      Updated according to the recent benchmark
%  problem. The COM offsets are added. S-function parameters are updated.
%      2.2        02/01/2005      Corrected the comments, version numbers
%  and contact information, etc...

clear all;  close all;
% obv

start_time = clock;


% PART I : Structural Parameters
%%%%%%%%%%%%%%%%%%%%%%%%%%%%%%%%%%%%%%%%%%%%%%%%%%%%%%%%%%%%%%%%%%%%%%%%%%%%%%%%


initialization;
load gamma_vals;

% PART II : Earthquake and Gamma Information
%%%%%%%%%%%%%%%%%%%%%%%%%%%%%%%%%%%%%%%%%%%%%%%%%%%%%%%%%%%%%%%%%%%%%%%%%%%%%%%%

act_integ_dt = 0.001;
unc_integ_dt = 0.001;
sa_integ_dt = 1e-5;
integ_dt = 0.001;
meas_dt  = 0.001;
data_dt  = 0.05;



eq_files = {...
        'newhall.txt',...
        'sylmar.txt',...
        'elcentro.txt',...
        'rinaldi.txt',...
        'kobe.txt',...
        'jiji.txt',...
        'erzincan.txt' };


eq_names ={
    'Newhall',...
    'Sylmar',...
    'El Centro',...
    'Rinaldi',...
    'Kobe',...
```

```
    'Jiji',...
    'Erzincan'};
% EQ data files. Herein, Jiji EQ data is modified. The
% original data is more than 30 secs. The file provided here is 30 secs.


eq_index = [1:7];
% Vector of the EQs that will be simulated. E.g., if you want to simulate
% Newhall, Kobe and Jiji, Erzincan set
% eq_index = [1, 5:7];


eq_scale = 0.01;
% This is immeditely applied to the EQ data.
% Original data is in cm/sec^2. The eq_scale
% parameter converts it to m/sec^2.


eq_dt = 0.005;
% obv.

aa = [10^(-3.0827), 10^(-3.9474), 3.548e-5];
bb = [10^(-1.4662), 10^(-0.7895), 2.279e-2];


for eq_i = 1:length(eq_index)


disp(['**************   Earthquake : ', eq_names{eq_index(eq_i)}, ' (',...
        num2str(eq_i), ' of ', num2str(length(eq_index)),...
        ')   **************' ]);
disp(' ');

eq_data = eq_scale * load(eq_files{eq_index(eq_i)}, '-ascii');
neq_data = max(size(eq_data));
eq_dim = min(size(eq_data));
eq_t = [0 : eq_dt : (neq_data - 1)*eq_dt]';
% Load the EQ data and form the time array.


EQ.time = eq_t;
EQ.signals.values = eq_data;
EQ.signals.dimensions = eq_dim;
% Create a cell object for the Simulink.


for gam_i = 2:2

if gam_i == 1;
    gamma_val = gamma_stiff_eq(eq_i);
    disp (['Gamma (', eq_names{eq_i}, ') = ', num2str(gamma_val),...
            '    (1 of 2)',]);
elseif gam_i==2;
    gamma_val = gamma_stiff_final;
    disp (['Gamma (final) = ', num2str(gamma_val),...
            '    (2 of 2)',]);
end

lead_stiff_ELM = lead_preyield_stiff*gamma_val;
lead_damp_ELM = lead_damp;
% Compute the ELM lead stiffness and specify the lead damping.
```

```
% PART III : Transformation Matrices
%%%%%%%%%%%%%%%%%%%%%%%%%%%%%%%%%%%%%%%%%%%%%%%%%%%%%%%%%%%%%%%%%%%%%%%%%%%%%%%
% Details of these matrices are given in the paper.


for i = 1:ncontrollers;
    if contr_direc(i) == 1;
        rc{i} = [1; 0; -contr_coor(i,2)];
    elseif contr_direc(i) == 2;
        rc{i} = [0; 1; contr_coor(i,1)] ;
    end;
end;
% Forming the matrices rc_i

for i = 1:nelements;
    if elem_type(i) == 1;
        ris{i} = [1  0  0;
            0  1  0;
            -rubber_bearing_coor(i,2),  rubber_bearing_coor(i,1),   1];
    elseif elem_type(i) == 3;
        ris{i} = [1  0  0;
            0  1  0;
            -lead_plug_coor(i-nrubber,2),  lead_plug_coor(i-nrubber,1), 1];
    end;
end;
% Forming the matrices ris_i

bloc = [3 8 13 19 24 26 31 45]; % = output_loc_bearing
nbloc = length(bloc);
for i = 1:nbloc
    bx = rubber_bearing_coor(bloc(i), 1);
    by = rubber_bearing_coor(bloc(i), 2);
    rb{i} = [1  0  -by; 0  1  bx];
end

for i = 1:nfloors+1
    for j = 1:ncorners(i)
        p{i,j} = [1 0 -corner_coor{i}(j,2);  0  1  corner_coor{i}(j,1)];
    end
    if ncorners(i) < max_ncorners
        for j = cor(i)+1:max_corners
            p{i,j} = zeros (2,3);
        end
    end
    P{i} = cat(1, p{i,:});
end
% Forming the matrices P_i.

for i = 1:nfloors;
    r5i{i} = [1 0 -com_offset(i,2); 0 1 com_offset(i,1); 0 0 1];
end

for i = 1:nfloors;
    r5i_flip{i} = fliplr(r5i{i});
end


R1 = nplace(eye(3), nfloors, 'col');
R2 = nplace(eye(3), nfloors+1, 'col');
```

```
R2c = cat(2, rc{:});
R2is = cat(2, ris{:});
R3 = [eye(2); zeros(1, 2)];
R4 = nplace(eye(2), nfloors+1, 'col');
R5 = fliplr(blkdiag(r5i_flip{:}));
R6 = [eye(2); 0, 0];        %Note: T4 * R2 * R6 = R4
R7 = cat(1, rb{:});
T1 = [zeros(3, nmodes), eye(3); R5*eigenvec , R1];
T2 = diag(ones(3*(nfloors+1), 1)) - diag(ones(3*nfloors, 1),-3);
T3 = blkdiag(P{:});
T4 = nplace(R6', nfloors+1, 'diag');
T5 = cat(1, r5i{nfloors:-1:1}, eye(3));
T6 = [[eigenvec; zeros(3, 3*nfloors)], T5 ];
% Transformation matrices. See the paper for
% the details. (Some of these matrices do not appear in the paper.
% These are used in the nonlinear analysis block. See the Simulink
% files to explore these matrices.)



% PART IV : Mass, Stiffness and Damping Matrices
%%%%%%%%%%%%%%%%%%%%%%%%%%%%%%%%%%%%%%%%%%%%%%%%%%%%%%%%%%%%%%%%%%%%%%%%%%%


Mb = diag([mass_basex, mass_basey, mass_baser]);
% Mass matrix of the base.


Ms = diag( mass_superstr(1,:) );
for i = 2:nfloors; Ms = blkdiag( Ms, diag(mass_superstr(i,:)) ); end;
% Mass matrix of the superstructure. From 8th floor to 1st floor.


M = [eye(nmodes), eigenvec'*Ms*R1;  R1'*Ms*eigenvec,  R1'*Ms*R1 + Mb];
% Mass matrix for the whole structure.
% This is not a 100% 'mass' matrix. See the paper for details.



% Stiffness matrices includes
%   a. stiffness provided by rubber,
%   b. stiffness provided by lead.
% In the nonlinear structure the stiffness matrices include
% only (a). Below we compute (a) and (b) and the total stiffness matrices.


Ks = diag(eigenval);
% Modal stiffness matrix of the superstructure.


Kis_rubber = [rubber_stiff 0 0; 0 rubber_stiff 0 ; 0 0 0];
Kis_lead = [lead_stiff_ELM 0 0; 0 lead_stiff_ELM 0 ; 0 0 0];
% obv


%%% a. Stiffness for rubber only %%%
for i = 1:nelements;
    if elem_type(i) == 1;
        kis_rubber{i} = Kis_rubber;
    elseif elem_type(i) == 3;
        kis_rubber{i} = zeros(3);
```

```
    end;
end;
% Forming the kis matrices for rubber only.


Kis_rubber_base = blkdiag(kis_rubber{:});
Kb_rubber =  R2is * Kis_rubber_base * R2is';
% Forming the base stiffness matrix for rubber.


K_rubber = blkdiag (Ks, Kb_rubber);
% Stiffness matrix that includes rubber stiffness only.
% See the paper for the details


%%% a. Stiffness for lead only %%%
for i = 1:nelements;
    if elem_type(i) == 1;
        kis_lead{i} = zeros(3);
    elseif elem_type(i) == 3;
        kis_lead{i} = Kis_lead;
    end;
end;
% Forming the kis matrices for lead only.


Kis_lead_base = blkdiag(kis_lead{:});
Kb_lead =  R2is * Kis_lead_base * R2is';
% Forming the base stiffness matrix for lead.


K_lead = blkdiag (Ks, Kb_lead);
% Stiffness matrix that includes lead stiffness only.
% See the paper for the details


%%% Stiffness for rubber and lead %%%
for i = 1:nelements;
    if elem_type(i) == 1;
        kis{i} = Kis_rubber;
    elseif elem_type(i) == 3;
        kis{i} = Kis_lead;
    end;
end;
% Forming the kis matrices.


Kis = blkdiag(kis{:});
Kb =  R2is * Kis * R2is';
% Forming the base stiffness matrix.


K = blkdiag (Ks, Kb);
% Stiffness matrix that includes both lead and rubber stiffness only.
% See the paper for the details
% Note that Kb = Kb_rubber + Kb_lead.



% Damping matrices includes
%   a. damping from rubber,
```

```
%   b. damping from lead.
% In the nonlinear structure the damping matrices include
% only (a). Below we compute (a) and (b) and the total damping matrices.


Cs = diag(2 * damp_rat .* modal_freqs);
% Modal damping matrix for the superstructure.


Cis_rubber = [rubber_damp 0 0; 0 rubber_damp 0 ; 0 0 0];
Cis_lead = [lead_damp_ELM 0 0; 0 lead_damp_ELM 0 ; 0 0 0];
% obv


%%% a. Damping for rubber only %%%
for i = 1:nelements;
    if elem_type(i) == 1;
        cis_rubber{i} = Cis_rubber;
    elseif elem_type(i) == 3;
        cis_rubber{i} = zeros(3);
    end;
end;
% Forming the cis matrices for rubber only.


Cis_rubber_base = blkdiag(cis_rubber{:});
Cb_rubber =  R2is * Cis_rubber_base * R2is';
% Forming the base damping matrix for rubber.


C_rubber = blkdiag (Cs, Cb_rubber);
% Damping matrix that includes rubber stiffness only.
% See the paper for the details


%%% b. Damping for lead only %%%
for i = 1:nelements;
    if elem_type(i) == 1;
        cis_lead{i} = zeros(3);
    elseif elem_type(i) == 3;
        cis_lead{i} = Cis_lead;
    end;
end;
% Forming the cis matrices for rubber only.


Cis_lead_base = blkdiag(cis_lead{:});
Cb_lead =  R2is * Cis_lead_base * R2is';
% Forming the base damping matrix for rubber.


C_lead = blkdiag (Cs, Cb_lead);
% Damping matrix that includes lead stiffness only.
% See the paper for the details


%%% Damping for rubber and lead %%%
for i = 1:nelements;
    if elem_type(i) == 1;
        cis{i} = Cis_rubber;
    elseif elem_type(i) == 3;
```

```
        cis{i} = Cis_lead;
    end;
end;
% Forming the cis matrices.


Cis = blkdiag(cis{:});
Cb =  R2is * Cis * R2is';
% Forming the base damping matrix.


C = blkdiag (Cs, Cb);
% Damping matrix that includes both lead and rubber stiffness only.
% See the paper for the details
% Note that Cb = Cb_rubber + Cb_lead.



% PART V : Influence Matrices
%%%%%%%%%%%%%%%%%%%%%%%%%%%%%%%%%%%%%%%%%%%%%%%%%%%%%%%%%%%%%%%%%%%%%%%%%%%%%%%

S1 =  [zeros(nmodes, 3);  eye(3)];
S2 = -[eigenvec' * Ms * R1;   R1' * Ms * R1 + Mb] * R3;
S3 =  [zeros(nmodes, 3);  eye(3)];
% Influence matrices.
% See the paper for the details



% PART VI : State-space Matrices
%%%%%%%%%%%%%%%%%%%%%%%%%%%%%%%%%%%%%%%%%%%%%%%%%%%%%%%%%%%%%%%%%%%%%%%%%%%%%%%

A = [zeros(nmodes+3), eye(nmodes+3);   -inv(M)*K,   -inv(M)*C];
B = [zeros(nmodes+3, ncontrollers); inv(M)*S1*R2c];
E = [zeros(nmodes+3, 2);  inv(M)*S2];
% SS-matrices of the equation of motion of the ELM.


% Here, we give several outputs to be used in the controller and Kalman
% estimator design:


Cout{1} = [T1,  zeros(nmodes+3)];
Dout{1} = zeros (3+3*nfloors, ncontrollers);
Eout{1} = zeros (3+3*nfloors, 2);
% Displacements of the floor COMs wrt the ground including the base.


Cout{2} = T1 * [-inv(M)*K, -inv(M)*C];
Dout{2} = T1 * [inv(M)*S1*R2c];
Eout{2} = T1 * [inv(M)*S2] + R2*R6;
% Absolute accelerations of the floor COMs including the base.


Cout{3} = T1 * [-inv(M)*K, -inv(M)*C];
Dout{3} = T1 * [inv(M)*S1*R2c];
Eout{3} = T1 * [inv(M)*S2];
% Acceleration of the floor COMs wrt the ground including the base.


Cout{4} = T2 * [T1,  zeros(nmodes+3)];
```

```
Dout{4} = T2 * zeros (3+3*nfloors, ncontrollers);
Eout{4} = T2 * zeros (3+3*nfloors, 2);
% Drifts of the COMs of each story including the base.


Cout{5} = T3 * T2 * [T1,  zeros(nmodes+3)];
Dout{5} = T3 * T2 * zeros (3+3*nfloors, ncontrollers);
Eout{5} = T3 * T2 * zeros (3+3*nfloors, 2);
% Drifts of the corners of each story including the base.


Cout{6} = [zeros(3, nmodes),  eye(3), zeros(3, nmodes+3)];
Dout{6} = zeros (3, ncontrollers);
Eout{6} = zeros (3, 2);
% Drifts of the COM of the base.


Cout{7} = zeros(2, 2*(nmodes+3) );
Dout{7} = zeros(2, ncontrollers);
Eout{7} = eye(2);
% Absolute ground accelerations.


Cout{8} = (R2c)' * [zeros(3, nmodes),  eye(3), zeros(3, nmodes+3)];
Dout{8} = (R2c)' * zeros (3, ncontrollers);
Eout{8} = (R2c)' * zeros (3, 2);
% Drifts of the controllers.


Cout{9} = T4 * T1 * [-inv(M)*K, -inv(M)*C];
Dout{9} = T4 * T1 * [inv(M)*S1*R2c];
Eout{9} = T4 * T1 * [inv(M)*S2] + T4*R2*R6;   % Note that T4*R2*R6 = R4
% Absolute accelerations of the floor COMs in the x and y-directions
% only, including the base.


Cout{10} = Kb_lead * [zeros(3, nmodes),  eye(3), zeros(3, nmodes+3)];
Dout{10} = zeros (3, ncontrollers);
Eout{10} = zeros (3, 2);
% Lead plug forces due to the stiffness.


Cout{11} = Cb_lead * [zeros(3, 2*nmodes+3),  eye(3)];
Dout{11} = zeros (3, ncontrollers);
Eout{11} = zeros (3, 2);
% Lead plug forces due to the damping.


Cout{12} = Kb_lead * [zeros(3, nmodes),  eye(3), zeros(3, nmodes+3)] +...
    Cb_lead * [zeros(3, 2*nmodes+3),  eye(3)];
Dout{12} = zeros (3, ncontrollers);
Eout{12} = zeros (3, 2);
% Lead plug forces.


Cout{13} = [zeros(3, 2*nmodes+3),  eye(3)];
Dout{13} = zeros (3, ncontrollers);
Eout{13} = zeros (3, 2);
% Velocity of the COM of the base wrt the ground.
```

```
out_floor = [0,  5,  8];    % Zero is the base.
% This is an index for optional floor response outputs. For example
% if you want to get the response of the base, 3rd 4th and 5th floors
% use
% out_floor = [0, 3:5];
% below we compute the optional floor displacements and absolute
% accelerations.


for i = 1:length(out_floor)
    out_floor_index_temp1{i} = [out_floor(i)*3+1 : (out_floor(i)+1)*3];
    out_floor_index_temp2{i} = [out_floor(i)*2+1 : (out_floor(i)+1)*2];
end
out_floor_index = cat(2, out_floor_index_temp1{:});
out_floor_index_xy = cat(2, out_floor_index_temp2{:});
special_out_size = length(out_floor_index);
special_out_size_xy = length(out_floor_index_xy);


% Special output index.
Cout{14} = Cout{1}(out_floor_index, :);
Dout{14} = Dout{1}(out_floor_index, :);
Eout{14} = Eout{1}(out_floor_index, :);
% Special output : Displacements of the desired floors wrt the ground.


Cout{15} = Cout{2}(out_floor_index, :);
Dout{15} = Dout{2}(out_floor_index, :);
Eout{15} = Eout{2}(out_floor_index, :);
% Special output : Absolute accelerations of the desired floors
% wrt the ground.

Cout{16} = [zeros(ncontrollers, nmodes*2+3), R2c'];
Dout{16} = [zeros(ncontrollers, ncontrollers)];
Eout{16} = [zeros(ncontrollers, 2)];
% Velocities of the control devices

Cout{17} = [zeros(2*nbloc, nmodes), R7, zeros(2*nbloc, nmodes+3)];
Dout{17} = [zeros(2*nbloc, ncontrollers)];
Eout{17} = [zeros(2*nbloc, 2)];
% Drifts of the specified rubber bearings

fl_xy = [4:(nfloors+1)*3];
temp = [3:3:nfloors*3];
fl_xy(temp) = [];

Cout{18} = Cout{4}(fl_xy, :);
Dout{18} = Dout{4}(fl_xy, :);
Eout{18} = Eout{4}(fl_xy, :);
%Drifts of the COM of the floors in the x&y-directions only without base

Cout{19} = eye(size(A,1));
Dout{19} = zeros(size(B));
Eout{19} = zeros(size(E));
%States

epsilon =  1e-14;
for i = 1 : length(Cout)
    Cout{i} = Cout{i} .* (abs(Cout{i}) > epsilon);
    Dout{i} = Dout{i} .* (abs(Dout{i}) > epsilon);
    Eout{i} = Eout{i} .* (abs(Eout{i}) > epsilon);
```

```
end
% We round very small numbers to zero to avoid
% additional numerical errors. These numbers
% are in fact zero, but during the computation
% of SS matrices, they appear to be a number very close to
% zero due to the multiplication of the
% influence and transformation matrices.


% PART VII : Controller Design
%%%%%%%%%%%%%%%%%%%%%%%%%%%%%%%%%%%%%%%%%%%%%%%%%%%%%%%%%%%%%%%%%%%%%%%%%%%

% This section is devoted to the controller design. At the end of this
% section, the user must provide a LTI-SS object called 'rlqg'. (In the
% simulink file, the default controller object is 'rlqg'. If you want to
% use another name for this object, you have to modify the controller
% blocks in the simulink file.) This object
% must be formed such that it takes the measurements as input and gives the
% control force vector as output. The user should carefully understand how
% the controller force is then attached to the nonlinear analysis block
% (s-function) in the 'part_III_nonlinear_simulation.mdl' simulink file.
% It is user's responsibility to arrange the object 'rlqg' and the
% connection between the controller and the nonlinear analysis block in the
% simulink file correctly.
% In our sample controller, we provide a function that outputs the object
% 'rlqg'.

%%%%%%%%%%%%%%%%%%%%%%%%%%%%%%%%%%%%%%%%%%%%%%%%%%%%%%%%%%%%%%%%%%%%%%%%%%%
%%%%%%%%%%%          SAMPLE CONTROLLER          %%%%%%%%%%%%%%%%%%%%%%%%%


%aa = 3.5e-5;
%bb = 2.3e-2;

% a. LQ Design system.
% The outputs to be minimized are
% 5. Corner drifts of each floor,
% 9. Absolute accelerations of each floor in the x and y-directions.

sys_LQ.A = A;
sys_LQ.B = B;
sys_LQ.E = E;

sys_LQ.Cz = cat ( 1, Cout{ [5, 9] } );
sys_LQ.Dz = cat ( 1, Dout{ [5, 9] } );
sys_LQ.Ez = cat ( 1, Eout{ [5, 9] } );
% SS matrices for the output equation.


% b. Kalman Filter system
% The measurements are
% 8. Controller drifts,
% 9. Absolute accelerations of each floor in the x and y-direc,
% 7. Absolute ground accelerations.

sys_Kalman.A = A;
sys_Kalman.B = B;
sys_Kalman.E = E;

sys_Kalman.Cv = cat ( 1, Cout{ [8, 9, 7] } );
sys_Kalman.Dv = cat ( 1, Dout{ [8, 9, 7] } );
```

```
sys_Kalman.Ev = cat ( 1, Eout{ [8, 9, 7] } );
% SS matrices for the measurement equation.

for iii = 1:length(aa);
%for bi = 1:length(bb);
ai = iii; bi = iii;
a = aa(ai);
b = bb(bi);

disp(' ');
disp(['a & b are ', num2str(iii), ' of ', num2str(length(aa))]);
disp('************************************************************* ');


[rlqg, sys_closed_dis, Kc_act] = controller(a, b, sys_LQ, sys_Kalman,...
    nfloors, max_ncorners, modal_freqs);

temp_sys_LQ = ss (sys_LQ.A, [sys_LQ.B, sys_LQ.E],...
    sys_LQ.Cz, [sys_LQ.Dz, sys_LQ.Ez]);

nu = size(sys_LQ.Dz, 2);
nw = size(sys_LQ.Ez, 2);
nout = size(sys_LQ.Dz, 1);
% Size of the controller and the excitation.
% Note that nu = ncontrollers.


wg=17; zg=0.3; Gkt=tf([0  2*zg*wg  wg^2], [1  2*zg*wg  wg^2]);
KT = [eye(nu),  zeros(nu, nw);  zeros(nw, nu),  Gkt*eye(nw)];

%%%%%% COMPUTATION OF Cv FOR DISSIPATIVITY ANALYSIS %%%%%%%%
sys_Cv = ss(A, [B, E], Cout{16}, [Dout{16}, Eout{16}]) * KT;
Cv = sys_Cv.C;


%%%%%%%%%%%       This concludes the controller design.     %%%%%%%%%%%



% PART IX : Parameters for Nonlinear Simulations
%%%%%%%%%%%%%%%%%%%%%%%%%%%%%%%%%%%%%%%%%%%%%%%%%%%%%%%%%%%%%%%%%%%%%%%%%%%


K_nonlin = K_rubber;
C_nonlin = C_rubber;
% Stiffness matrix for the whole structure.
% This is not the actual stiffness matrix. See
% the paper for the details. Stiffness of the
% lead is not included. Lead force is a
% nonlinear force.


yield_dis = [lead_yield_disp*ones(nlead, 2); zeros(nrubber,2) ];
post_preyield_ratio = lead_postyield_stiff / lead_preyield_stiff;
post_preyield_stiff = [post_preyield_ratio*ones(nlead, 2);...
    zeros(nrubber,2) ];
yield_force = [lead_yield_force*ones(nlead, 2); zeros(nrubber,2) ];
% Lead plug properties.


%integ_dt = 0.005;
```

```
%meas_dt = 0.005;
tol_nonlin = 1e-3;
norm_nonlin = 1e4;
newmark_beta = 0.25;
newmark_gamma = 0.5;
angle_inci = 0;
A1 = 1 / (newmark_beta * (integ_dt^2));
A2 = 1 / (newmark_beta * integ_dt);
A3 = 1 / (2 * newmark_beta);
A4 = newmark_gamma / (newmark_beta * integ_dt);
A5 = newmark_gamma / newmark_beta;
A6 = integ_dt * (newmark_gamma / (2 * newmark_beta) - 1);
sk = A1*(T6' * blkdiag(Ms, Mb) * T6) + A4*C_nonlin + K_nonlin;
% Nonlinear analysis parameters.


output_loc_bearing = [3 8 13 19 24 26 31 45];
% obv.


%%%%%%%%%%  Transfer functions for the Simulink  %%%%%%%%%
for i = 1:ncontrollers;
    if contr_direc(i) == 1;
        sim_T1(i,i) = 1;
    elseif contr_direc(i) == 2;
        sim_T1(i, ncontrollers+i) = 1;
    end;
end;


temp1 = nplace (eye(3), (nfloors+1), 'xdiag');
temp2 = [zeros((nfloors)*3,(nfloors+1)*3);
    [zeros(3), nplace(eye(3), (nfloors), 'row') ]];

sim_T2 = temp1 + temp2;
sim_T3 = nplace(R6, nfloors+1, 'xdiag');;
sim_T4 = nplace(eye(2),nfloors+1, 'row');
sim_T5 = R2c;
sim_T6 = T2;   sim_T6([3:3:3*(nfloors+1)], :) = [];

% Transfer functions for the simulation.
% sim_T1 : Rearranges the force vector to be fed
% into the s-function box,
% sim_T2 : Finds displacements wrt ground from
% displacements wrt base,
% sim_T3 : Finds accelerations wrt ground from
% accelerations wrt base,
% sim_T4 : Rearranges the ground accelerations,
% sim_T5 : Finds the controller displacements
% from the base displacements.
% sim_T6 : finds drifts in the x and
% y-directions from the displacements



% Inputs to the nonlinear analysis S-function box %

%INPUT                  VALUE
%========               ================
integ_time           =  integ_dt;
BET                  =  newmark_beta;
```

```
GAM                 =  newmark_gamma;
n_acc_records       =  eq_dim;
transf_matrix       =  T6;
assembled_mass      =  blkdiag(Ms, Mb);
R                   =  T5;
loadmult            =  1;   % Note that EQ data is already scaled!
tolerance           =  tol_nonlin;
transf_mass         =  T6' * blkdiag(Ms, Mb) * T6;
assembled_damping   =  C_nonlin;
assembled_stiff     =  K_nonlin;
SK                  =  sk;
bearingloc_x        =  [lead_plug_coor(:,1)',  rubber_bearing_coor(:,1)'];
bearingloc_y        =  [lead_plug_coor(:,2)',  rubber_bearing_coor(:,2)'];
element_type        =  [3*ones(nelements,1),...
    [3*ones(nlead,1); ones(nrubber,1)]];
diff_max_min_fric   =  zeros(nelements, 2);
trans_coeff_fric    =  zeros(nelements, 2);
coeff_fric          =  zeros(nelements, 2);
normalizer          =  norm_nonlin;
angle_inci          =  angle_inci;
yield_dis           =  yield_dis;
post_preyield_stiff =  post_preyield_stiff;
yield_force         =  yield_force;
retained_modes      =  nmodes;
nfloors             =  nfloors;
nbearings           =  nelements;
normalforce_sliding =  zeros(nelements, 1);
output_loc_bearing  =  output_loc_bearing;
output_num          =  length(output_loc_bearing);
ndevices            =  ncontrollers;
deviceloc_x         =  contr_coor(:,1)';
deviceloc_y         =  contr_coor(:,2)';
recen_stiff         =  zeros(nelements, 1);
viscous_fric        =  zeros(nelements, 1);
viscous_lrb         =  zeros(nelements, 1);


% PART XI : Simulations
%%%%%%%%%%%%%%%%%%%%%%%%%%%%%%%%%%%%%%%%%%%%%%%%%%%%%%%%%%%%%%%%%%%%%%%%%%%%


disp('    Uncontrolled Simulation in progress...');
sim('uncontrolled');
disp('    Uncontrolled Simulation finished.');
disp(' ');

disp('    Active Nonlinear Simulation in progress...');
sim('active');
disp('    Active Nonlinear Simulation finished.');
disp(' ');

disp('    Semiactive Nonlinear Simulation in progress...');
sim('semiactive');
disp('    Semiactive Nonlinear Simulation finished.');
disp(' ');

ndata_t = length(u_act(:,1));
% PART XI : Performance Indices
%%%%%%%%%%%%%%%%%%%%%%%%%%%%%%%%%%%%%%%%%%%%%%%%%%%%%%%%%%%%%%%%%%%%%%%%%%%%

%%% J1 : Peak isolation shear normalized by the uncontrolled
```

```
R_temp = nplace(eye(2), nfloors+1, 'row');
Ms_temp = mass_superstr(nfloors:-1:1,1:2)'; Ms_temp=diag(Ms_temp(:));
M_temp = blkdiag(Mb(1:2, 1:2), Ms_temp);

iso_shear_unc  = (R_temp * M_temp * abs_acc_unc' )';
iso_shear_act  = (R_temp * M_temp * abs_acc_act' )';
iso_shear_sact = (R_temp * M_temp * abs_acc_sact')';

max_iso_shear_unc  = max(max(abs(iso_shear_unc (:, 1:2))));
max_iso_shear_act  = max(max(abs(iso_shear_act (:, 1:2))));
max_iso_shear_sact = max(max(abs(iso_shear_sact(:, 1:2))));


J_act {1,eq_i}(ai, bi) = max_iso_shear_act /max_iso_shear_unc;
J_sact{1,eq_i}(ai, bi) = max_iso_shear_sact/max_iso_shear_unc;



%%% J2 : Peak base shear normalized by the uncontrolled

R_temp = nplace(eye(2), nfloors, 'row');

base_shear_unc  = (R_temp * Ms_temp * (abs_acc_unc(:, 3:2*(nfloors+1))'))';
base_shear_act  = (R_temp * Ms_temp *...
    (abs_acc_act (:, 3:2*(nfloors+1))'))';
base_shear_sact = (R_temp * Ms_temp *...
    (abs_acc_sact(:, 3:2*(nfloors+1))'))';

max_base_shear_unc  = max(max(abs(base_shear_unc )));
max_base_shear_act  = max(max(abs(base_shear_act )));
max_base_shear_sact = max(max(abs(base_shear_sact)));

J_act {2,eq_i}(ai, bi) = max_base_shear_act /max_base_shear_unc;
J_sact{2,eq_i}(ai, bi) = max_base_shear_sact/max_base_shear_unc;

%%% J3 : Peak base displacement normalized by the uncontrolled disp

max_iso_disp_unc  = max(max(abs(iso_disp_unc )));
max_iso_disp_act  = max(max(abs(iso_disp_act )));
max_iso_disp_sact = max(max(abs(iso_disp_sact)));

J_act {3,eq_i}(ai, bi) = max_iso_disp_act /max_iso_disp_unc;
J_sact{3,eq_i}(ai, bi) = max_iso_disp_sact/max_iso_disp_unc;


%%% J4 : Peak drifts normalized by the uncontrolled

max_drift_unc  = max(max(abs(drift_unc )));
max_drift_act  = max(max(abs(drift_act )));
max_drift_sact = max(max(abs(drift_sact)));

J_act {4,eq_i}(ai, bi) = max_drift_act /max_drift_unc;
J_sact{4,eq_i}(ai, bi) = max_drift_sact/max_drift_unc;

%%% J5 : Peak abs accelerations normalized by the uncontrolled

max_abs_acc_unc  = max(max(abs(abs_acc_unc )));
max_abs_acc_act  = max(max(abs(abs_acc_act )));
max_abs_acc_sact = max(max(abs(abs_acc_sact)));
```

```
J_act {5,eq_i}(ai, bi) = max_abs_acc_act /max_abs_acc_unc;
J_sact{5,eq_i}(ai, bi) = max_abs_acc_sact/max_abs_acc_unc;


%%% J6 : Peak controller force normalized by the peak controlled base
%%% shear

total_contr_force_act  = u_act *R2c'; %assuming u_act is N x ncontroller
total_contr_force_sact = u_sact*R2c'; %assuming u_act is N x ncontroller

max_total_contr_force_act  = ...
    max(max(abs(total_contr_force_act (:, 1:2))));
max_total_contr_force_sact = ...
    max(max(abs(total_contr_force_sact(:, 1:2))));


J_act {6,eq_i}(ai, bi) = max_total_contr_force_act /max_iso_shear_unc;
J_sact{6,eq_i}(ai, bi) = max_total_contr_force_sact/max_iso_shear_unc;


%%% J7 : RMS base disp normalized by the uncontrolled

max_rms_iso_disp_unc  = max(sqrt(sum(iso_disp_unc .^2)/ndata_t));
max_rms_iso_disp_act  = max(sqrt(sum(iso_disp_act .^2)/ndata_t));
max_rms_iso_disp_sact = max(sqrt(sum(iso_disp_sact.^2)/ndata_t));

J_act {7,eq_i}(ai, bi) = max_rms_iso_disp_act /max_rms_iso_disp_unc;
J_sact{7,eq_i}(ai, bi) = max_rms_iso_disp_sact/max_rms_iso_disp_unc;


%%% J8 : RMS absolute floor acc normalized with the uncontrolled

max_rms_acc_unc  = max(sqrt(sum(abs_acc_unc .^2)/ndata_t));
max_rms_acc_act  = max(sqrt(sum(abs_acc_act .^2)/ndata_t));
max_rms_acc_sact = max(sqrt(sum(abs_acc_sact.^2)/ndata_t));

J_act {8,eq_i}(ai, bi) = max_rms_acc_act /max_rms_acc_unc;
J_sact{8,eq_i}(ai, bi) = max_rms_acc_sact/max_rms_acc_unc;


%%% J9 : Energy absorbed by all control devices normalized by energy
%%% input into the controlled structure

energy_input_act      = sum(sum( iso_shear_act .* ground_vel * data_dt));
energy_abs_contr_act  = sum(sum(-u_act  .* u_vel_act  * data_dt));
energy_input_sact     = sum(sum(iso_shear_sact .* ground_vel * data_dt));
energy_abs_contr_sact = sum(sum(-u_sact .* u_vel_sact * data_dt));

J_act {9,eq_i}(ai, bi) = energy_abs_contr_act /energy_input_act;
J_sact{9,eq_i}(ai, bi) = energy_abs_contr_sact/energy_input_sact;


%%% J10 : Peak controller force normalized by total weight of the
%%% structure

J_act {10,eq_i}(ai, bi) = max_total_contr_force_act /total_weight;
J_sact{10,eq_i}(ai, bi) = max_total_contr_force_sact/total_weight;


%%% J11 : RMS Floor Drifts normalized with the uncontrolled
```

```
max_rms_drift_unc  = ...
    max(sqrt(sum( drift_unc .^2)/ndata_t ));
max_rms_drift_act  =...
    max(sqrt(sum( drift_act .^2)/ndata_t ));
max_rms_drift_sact =...
    max(sqrt(sum( drift_sact.^2)/ndata_t ));

J_act {11,eq_i}(ai, bi) = max_rms_drift_act /max_rms_drift_unc;
J_sact{11,eq_i}(ai, bi) = max_rms_drift_sact/max_rms_drift_unc;


%%% D1 : Dissiptivity (D%)

D_act    {1, eq_i}{ai, bi} = sum((u_act    .*u_vel_act  < 0), 1)'/ndata_t;
D_sact_lq{1, eq_i}{ai, bi} = sum((u_sact_lq.*u_vel_sact < 0), 1)'/ndata_t;

rms_u_act     = sqrt(sum(u_act     .^2))/ndata_t;
rms_u_sact_lq = sqrt(sum(u_sact_lq .^2))/ndata_t;

w_norm_act     = rms_u_act    /sum(rms_u_act);
w_norm_sact_lq = rms_u_sact_lq/sum(rms_u_sact_lq);


D_norm_act    {1, eq_i}(ai,bi) = ...
    sum(D_act    {1, eq_i}{ai, bi}.*w_norm_act'    );
D_norm_sact_lq{1, eq_i}(ai,bi) = ...
    sum(D_sact_lq{1, eq_i}{ai, bi}.*w_norm_sact_lq');


%%% D2 : Dissipativity (De)

cov_states = covar(sys_closed_dis, eye(2));

D_act{2, eq_i}{ai, bi} = diag(-Kc_act * cov_states * Cv');

rms_u_cov_act{ai, bi} = sqrt(diag(Kc_act * cov_states * Kc_act'));
rms_v_cov_act{ai, bi} = sqrt(diag(Cv * cov_states * Cv'));

w_norm_cov_act = rms_u_cov_act{ai,bi}/sum(rms_u_cov_act{ai,bi});

D_norm_act{2, eq_i}(ai,bi) = sum(D_act{2, eq_i}{ai, bi}.*w_norm_cov_act);


%%% J14 : Dissipativity (Dne)

D_act{3, eq_i}{ai, bi} = D_act{2, eq_i}{ai, bi}./...
    (rms_u_cov_act{ai, bi}.*rms_v_cov_act{ai, bi});

D_norm_act{3, eq_i}(ai,bi) = sum(D_act{3, eq_i}{ai, bi}.*w_norm_cov_act);

end %iii

end %gamma
end %eqi

end_time = clock;
convtime = [0, 0, 24*60*60, 60*60, 60, 1]';
time_passed = end_time - start_time;
run_time = [num2str(time_passed * convtime), 'secs'];
disp(['Total running time = ', run_time]);
```

```
save('mbestJs', 'J_act', 'D_act', 'D_norm_act', ...
    'J_sact', 'D_sact_lq', 'D_norm_sact_lq', ...
    'aa', 'bb', ...
    'eq_names', 'eq_index');
```

### c) Sample Controller

```
function [rlqg, sys_closed_dis, Kc] = controller(a, b, sys_LQ, sys_Kalman,...
    nfloors, max_ncorners, modal_freqs)


%  A Sample Controller for the Base Isolation Prooblem - Part III
%
%  See the paper
%
%    SMART BASE ISOLATED BENCHMARK BUILDING PART III: A SAMPLE CONTROLLER
%    FOR BILINEAR ISOLATION by B. Erkus and E. A. Johnson
%
%  for the details.
%
%                                  B. Erkus (03/12/04)

%%%%%%%%%%    LQ DESIGN    %%%%%%%%%%

temp_sys_LQ = ss (sys_LQ.A, [sys_LQ.B, sys_LQ.E],...
    sys_LQ.Cz, [sys_LQ.Dz, sys_LQ.Ez]);

nu = size(sys_LQ.Dz, 2);
nw = size(sys_LQ.Ez, 2);
nout = size(sys_LQ.Dz, 1);
% Size of the controller and the excitation.
% Note that nu = ncontrollers.


wg=17; zg=0.3; Gkt=tf([0  2*zg*wg  wg^2], [1  2*zg*wg  wg^2]);
KT = [eye(nu),  zeros(nu, nw);  zeros(nw, nu),  Gkt*eye(nw)];
% Transfer function of the Kanai-Tajimi filter.


sys_KT = temp_sys_LQ * KT;
% Augmented system.


uindex = [1 : nu];
sys_LQ =  sys_KT(:, uindex);
% Form the system to be used in the LQ design.


% LQG Controller parameters
%a = 3.5e-5;
a_f = [1, 0*ones(1, nfloors)];
%b = 2.3e-2;
% a: weight on the base column drift
% b: weight on the absolute floor accelerations
% a_f : wight on the floor drifts


%% Below we compute the LQ weights %%
al = cell(nfloors+1, max_ncorners);
```

```
al(:,:) = {sqrt(1/2) * ones(1,2)};


for i =1:nfloors+1;
    for j = 1:max_ncorners;
        alp{i,j} = [(al{i,j}(1))^2  0; 0  (al{i,j}(2))^2];
    end;
    alph{i} = a_f(i) * blkdiag(alp{i,:});
end;
Alpha = blkdiag(alph{:});

wx = sqrt(modal_freqs(1)^2 + modal_freqs(4)^2 + modal_freqs(7)^2);
wy = sqrt(modal_freqs(2)^2 + modal_freqs(5)^2 + modal_freqs(8)^2);

be = sqrt(1/2) * ones(nfloors+1, 2);
for i = 1:nfloors+1;
    bet{i} = [(be(i,1)/wx)^2  0 ; 0  (be(i,2)/wy)^2];
end
Beta = blkdiag(bet{:});

Qt = blkdiag(a*Alpha, b*Beta);
Rt = 1e-12 * eye(nu);
Nt = zeros (nout, nu);
% LQ design parameters. See the paper for the
% details.



try
    Kc = lqry(sys_LQ, Qt, Rt, Nt);
    Kc_err = 0;
catch
    disp(' **** ERROR : Kc cannot be computed. Zero Kc is used. ****');
    Kc_err = 1;
    Kc = zeros(nu, nout);
end
% LQ controller gain.



%%%%%%%%%%       KALMAN FILTER DESIGN      %%%%%%%%%%%%%%%%%%

temp_sys_Kalman = ss(sys_Kalman.A, [sys_Kalman.B, sys_Kalman.E],...
    sys_Kalman.Cv, [sys_Kalman.Dv, sys_Kalman.Ev]);

nu = size(sys_Kalman.Dv, 2);
nw = size(sys_Kalman.Ev, 2);
nout = size(sys_Kalman.Dv, 1);
% Size of the controller and the excitation.
% Note that nu = ncontrollers.


KT = [eye(nu),  zeros(nu, nw);  zeros(nw, nu),  Gkt*eye(nw)];
% Transfer function of the Kanai-Tajimi filter.


sys_KT = temp_sys_Kalman * KT;
% Augmented system.


uindex = [1 : nu];  windex = [1 : nw] + nu;
```

```
A_open = sys_KT.a;
B_open = sys_KT(:, uindex).b;
E_open = sys_KT(:, windex).b;

Cv_open = sys_KT.c;
Dv_open = sys_KT(:, uindex).d;
Ev_open = sys_KT(:, windex).d;
% Open loop SS matrices of the augmented system.


A_closed = A_open - B_open * Kc;
B_closed = E_open;
C_closed = Cv_open - Dv_open * Kc;
D_closed = Ev_open;
sys_closed = ss(A_closed, B_closed, C_closed, D_closed);
% Closed loop augmented system.

A_closed_dis = A_closed;
B_closed_dis = B_closed;
C_closed_dis = eye(size(A_closed));
D_closed_dis = zeros(size(B_closed));
sys_closed_dis=ss(A_closed_dis, B_closed_dis, C_closed_dis, D_closed_dis);
% Closed loop augmented system for dissiaptivity computations
% The outputs are the the states


Qn = eye(nw);
Rn = 1e-4 * diag(  diag( covar(sys_closed, eye(nw))' )  );
Nn = zeros(nw, nout);
% Kalman filter parameters.


[kest, L, junk] = kalman (sys_KT, Qn, Rn, Nn);
rlqg = lqgreg(kest, Kc);
% LQG controller. Here "rlqg" is a SS model
% where the inputs are the measurements and the
% the outputs are the control forces.
```